LEIDSE GEOLOGISCHE MEDEDELINGEN, Vol. 42, pp. 61—130, published separately 22-1-1969

# STRUCTURAL PETROLOGY OF THE GARNET-PERIDOTITE OF ALPE ARAMI (TICINO, SWITZERLAND)

BY

J. R. MÖCKEL

## ABSTRACT

The decomposition of pyrope-rich garnet into spinel-amphibole symplektite and the alteration of the latter into chlorite indicate the presence of three successive mineral parageneses in the peridotite of Alpe Arami: a garnet-peridotite, a spinel-amphibole-peridotite, and a chlorite-peridotite association. Titanclinohumite may be a relict mineral from an older assemblage. The peridotite lens lies between gneisses of the root zone of the Pennine nappes of the Alps. The main phase of metamorphism ($F_1$) of these gneisses is of Alpine age. They have a steeply southward-dipping schistosity ($S_1$). In the peridotite, chlorite nodules deriving from altered garnets are flattened parallel to the schistosity planes of the surrounding gneisses; the formation of chlorite was contemporaneous with $F_1$. $S_1$-planes are also present as cleavage planes. Due to quantitative differences in the mineralogical composition of the peridotite, a layering plane ($S_L$) can be observed; it may show a mineral lineation ($l_0$). In the southern part of the peridotite lens, $S_L$ is subparallel to $S_1$ and $l_0$ pitches steeply to the west, whereas in the northern part $S_L$ dips moderately to the north, with $l_0$ plunging to the north.

Petrofabric analysis shows that the orientation of the garnet-peridotite minerals is dependent on the orientation of $S_L$: $\gamma$-olivine and $\beta$-orthopyroxene are perpendicular to $S_L$; the orientation of olivine is weaker than the orthopyroxene orientation. $\gamma$-orthopyroxene and $c$-clinopyroxene are parallel to $l_0$ ($= l'_0$). The alteration of garnet-peridotite into spinel-amphibole-peridotite is related to schistosity planes $S_0$ that are mostly parallel to $S_L$. $S_L/S_0$-fold axes are parallel to $l_0$-lineations. In the spinel-amphibole-peridotites, $\gamma$-olivine is perpendicular to $S_0$, and $\gamma$-orthopyroxene and $c$-amphibole are parallel to $l_0$ ($= l''_0$). The fabrics of olivine, orthopyroxene, and amphibole are not affected by the transformation of spinel-amphibole- into chlorite-peridotite, except for the olivine fabric of a chlorite-peridotite-mylonite. The garnet-peridotite fabric is inconsistent with a magmatic genesis. It may have been brought about by plastic deformation followed by recrystallization. The formation of the garnet-peridotite and its alteration into spinel-amphibole-peridotite took place before the emplacement of the peridotite into its present position, which occurred during the Alpine orogeny. The garnet-peridotite may represent a fragment of old basement material, or it may have been formed by a phase of high-pressure metamorphism of Alpine age, which antedated $F_1$.

Petrofabric analysis of biaxial minerals should preferably be done with a five-axis universal stage. Fabric diagrams can be prepared with a computer. Calculation of statistical parameters removes uncertainties from the interpretation of the diagrams.

## CONTENTS

CHAPTER I

# INTRODUCTION

## THE STRUCTURAL-PETROLOGICAL APPROACH TO PERIDOTITE PROBLEMS

The term *peridotite*, designating olivine-rich rocks carrying additional mafic minerals such as pyroxene and amphibole but little or no feldspar or other felsic constituents, dates back to Daubrée (1866) and Strüver (1874), and will be used throughout the present paper in this non-genetic sense. Rosenbusch (1877) incorporated the peridotites into the *massige Gesteine*, a term which although originally chosen as merely descriptive (its counterpart being *geschichtete Gesteine*), soon became a synonym for igneous or magmatic rocks. Due to Rosenbusch's authority, the custom of considering peridotites *a priori* as magmatic rocks became widespread. On the other hand, if we admit the possible existence of both magmatic and metamorphic peridotite varieties, it is clear that a distinction on grounds similar to those applied for granite and gneiss and for diorite and amphibolite, is more difficult to make in the case of peridotites because of the scarcity of structural indications, both in the field and under the microscope.

Petrofabric analysis, i.e. the statistical investigation of mineral orientations with use of the universal stage, seemed promising in this connection, since it could bring out structural features of a rock that cannot be detected by routine macroscopical and microscopical procedures. However, the first results of the petrofabric approach were not encouraging: shortly after Andreatta (1934) had assigned a metamorphic origin to certain peridotites on the basis of their olivine fabrics, Phillips (1938) claimed that identical fabrics could arise from magmatic processes, because gravity and flow, acting upon inequidimensional crystals in a magma, are also capable of producing planar and linear fabric patterns (for further references — mainly concerning olivine — see Collée, 1962, pp. 7—8). Consequently, unequivocal conclusions could not be drawn from petrofabric diagrams alone. Only recently has it become clear that pointless discussion can be avoided by combining petrofabric study with the analysis of other properties of the peridotite. Thus, Collée (*op. cit.*) succeeded in demonstrating the tectonite character of peridotite nodules in basalt by relating their olivine and orthopyroxene orientations to intersecting planar structures that are visible in the hand-specimen or can be brought out by the elaborate petrofabric technique of axial-distribution analysis. Additional investigations in the field enabled Raleigh (1963, 1965) and Avé Lallemant (1967) to prove for some peridotites a relation between the mineral orientations and such megascopic structures as fold axes and axial planes, thus providing strong evidence of their tectonic and metamorphic origin. On the other hand, by studying the habit of euhedral olivine and orthopyroxene crystals in a peridotite, Jackson (1961) found a correlation between the degree of anisotropism of their shape and the preferred orientation of their crystal axes, which constitutes circumstantial evidence supporting their crystallization in a magmatic environment, gravity settling probably being the most important factor in producing the preferred orientation.

In some way related to the genesis of the peridotites themselves is the problem of their emplacement. Current theories include intrusion of a magma followed by crystallization *in situ* (whether or not accompanied by magmatic differentiation); emplacement as a solid body, either tectonically or by means of gaseous explosions; and intrusion as a semi-solid "crystal mush". Avé Lallemant (1967) demonstrated the validity of the solid-emplacement hypothesis for the peridotite body of the Etang de Lers (French Pyrenees) by carrying out a comparative structural investigation of the peridotite and its country rocks in addition to a petrofabric analysis of the peridotite itself.

It may be concluded that petrofabric analysis is a powerful tool for obtaining an idea of the origin and emplacement of a peridotite, on the condition that it is used in conjunction with a structural study of the peridotite and its country rocks as well as a microscopical investigation of the peridotite for relevant mineralogical and textural properties. In this kind of

analysis, which may be said to follow a structural-petrological approach, the argumentation based on geometrical relationships is of paramount importance.

## THE PRESENT STUDY

Under the supervision of Professor E. den Tex, two theses dealing with the petrofabrics of peridotites of lherzolitic mineralogy have been completed in the Geological and Mineralogical Institute of Leiden University (Collée, 1962; Avé Lallemant, 1967). The present study may be considered to supplement the previous work, since it is concerned with the petrofabrics of garnet-peridotites and related rocks. The garnet-peridotite occurrence near Alpe Arami, on the divide between the Gorduno and Gnosca Valleys in the Swiss canton of Ticino (Grubenmann, 1908; Dal Vesco, 1953; O'Hara & Mercy, 1966), was chosen as a suitable object for this investigation.

To increase our knowledge of peridotite fabrics in general by collecting information on the fabric of another peridotite variety, was only one of the purposes of the present study. By incorporating the petrofabric investigation into the framework of a structural-petrological analysis of the peridotite of Alpe Arami and its country rocks, we also hoped to provide information relevant to its geological history, which is of some interest because of the divergent hypotheses on its genesis given by previous investigators, mainly on the basis of petrographical, mineralogical, and chemical evidence.

The close association of the peridotite with eclogite, the metamorphic origin of which seemed to be beyond doubt, and the presence of garnet, led Grubenmann (1908) to regard the peridotite of Alpe Arami as a metamorphic rock (*Granatolivinfels*); he concluded that after intrusion, crystallization, and differentiation of a basic magma, the metamorphism took place *in situ*. On textural grounds, Dal Vesco (1953) advocated a principally magmatic origin of the garnet-peridotite, especially because of the extremely lobate outline of the garnet crystals, which he attributed to magmatic corrosion. According to Dal Vesco's hypothesis, the partially crystalline magma intruded into its present position during the metamorphism of the country rocks; it finally solidified in an anisotropic stress field, thus producing the weak schistosity of the rocks. O'Hara and Mercy (1966) favoured a solid-emplacement hypothesis because of the contrast between the eclogite-facies paragenesis of the garnet-peridotite and the amphibolite-facies parageneses of the country rocks; they concluded on the basis of chemical analyses that the garnet-peridotite may represent a tectonic slice of either undifferentiated upper-mantle material or a metamorphosed accumulative igneous peridotite.

The present report comprises some remarks on the country rocks of the peridotite, chiefly concerning their structural history (Chapter II), the results of a structural (Chapter III) and petrographic (Chapter IV) investigation of the peridotite, with a detailed map of its occurrence (Enclosure I), and the results of a petrofabric analysis of the peridotite (Chapter VI). The conclusions reached in these chapters are summarized in Tables (1, 2, 5, and 6), in each of which as many data as possible from the preceding Tables are incorporated. Chapter VII gives a general discussion.

A serious disadvantage of petrofabric analysis is the amount of time required for measuring the mineral orientations and constructing the fabric diagrams, particularly when biaxial minerals are concerned. Moreover, the interpretation and mutual comparison of diagrams showing weak preferred orientation is sometimes difficult. The present author has developed some modifications and additions to the current procedures, based on the use of electronic data-processing methods and the application of the sophisticated method proposed by Watson (1966) for the statistical analysis of orientation data. The details are given in Chapter V, together with some general reflections on petrofabric analysis. All the structural and fabric diagrams in this paper are drawn in lower-hemisphere, equal-area projection, the plane of projection generally being the horizontal plane, with N indicating grid north. Geographic north (GN) and magnetic north (MN) are indicated in Fig. 2. In the captions of the structural diagrams in Chapters II and III, $A$ denotes the area of the counting circle (area of hemisphere = 1) used in the construction of the diagrams.

Although the present study has of course drawn on the publications of previous investigators listed at the end of this paper, it could not have been accomplished without the advice and information given by many others who aided in unravelling a few of the mysteries presented by the ultramagic rocks at Alpe Arami. Professor E. den Tex proposed the most intriguing subject of this thesis. While supervising my investigations, he allowed me much freedom in pursuing various aspects of it, for which I am very grateful. His critical reading of the manuscript contributed greatly to the ultimate result. Professor H. J. Zwart, now at Aarhus University, Denmark, showed me the importance of applying structural and microstructural methods to the investigation of metamorphic rocks. A most instructive excursion conducted by him together with Dr. J. A. Oele, gave me a better understanding of the geology of the Swiss Alps. Dr. P. Hartman gave his expert advice on crystallographical problems; he also read parts of the manuscript and suggested many improvements. The lectures of Professor W. R. van Zwet introduced me to statistics; I am greatly indebted to him for his help at various stages of this investigation. Without the discussions with Professor F. Rost, of Saarbrücken, Germany, the chapter dealing with the petrography of the peridotites would certainly have been less satisfactory. The petrological-geological excursion conducted by Professor E. Niggli, of Berne, Switzerland, on the occasion of the Congress of the International Union of Geodesy

and Geophysics in September 1967, offered me an excellent opportunity to visit, in the company of many experts, a number of occurrences of mafic and ultramafic rocks in Switzerland and Italy. The author also wishes to express his gratitude to Professor W. P. de Roever for his critical reading of the manuscript.
The discussions at Leiden University with my colleague Dr. H. G. Avé Lallemant were very stimulating, as were those with my fellow structural petrologists Drs. J. P. Engels and A. van Zuuren, and the experienced petrographers Drs. H. Koning and D. E. Vogel. Mr. P. Maaskant, of the Institute of Earth Sciences of the Free University, Amsterdam, performed microprobe analyses, examined opaque minerals, and translated Russian literature on behalf of the present investigation. Mr. C. F. Woensdregt helped with the X-ray identification of a number of minerals. The staff of the *Centraal Rekeninstituut* (Central Computing Institute) of Leiden University, including Mrs. L. M. J. S. Gelato and Messrs. D. Sonneveld and P. H. J. J. Terhal, instructed me on programming the IBM 360/50 computer. Mrs. I. Seeger read the English text.
In our discipline, communication with the reader through drawings and photographs is certainly as important as that accomplished by words. The skill of Mr. J. Bult can be judged from the Figures and Enclosures, all of which were prepared by him. The photographs were made by Messrs. J. Hoogendoorn and W. C. Laurijssen. The co-operation of many others should be mentioned, among them: Messrs. C. J. van Leeuwen and M. Deyn, who prepared the thin sections; Mr. A. Verhoorn, who took the X-ray photographs; and Messrs. J. G. le Rütte and F. J. L. Öry Bertha, who assisted me in searching the literature. I am also much indebted to Messrs. D. van Tol, H. Broekstra, and H. T. D. Stoppels, who ran the programs on the IBM 360/50.
A grant from the *Molengraaff-Fonds* for the field-work in Switzerland in the summer of 1964 is gratefully ackowledged.

CHAPTER II

## CHARACTERISTICS OF THE COUNTRY ROCKS

### GENERAL CONSIDERATIONS

The peridotite of Alpe Arami forms part of the Lepontine gneiss complex (Wenk, 1956) and more especially of its southernmost member, the so-called "root zone" (*Wurzelzone*), bounded in the south by an important fault-line, the Insubric line (Fig.1). The root zone consists mainly of gneisses displaying an E-W strike and a more or less vertical dip. No direct evidence is available concerning the age of these rocks, i.e. the time of crystallization of their main constituent minerals. By following the lineations in the gneisses towards the north, from the root zone across the region of flat-lying "Pennine nappes" in Central Ticino (where the lineations possess a remarkable horizontal NNW-SSE orientation) to the once again steeply dipping "frontal zone", Wenk (1955) established their continuation into definitely Mesozoic, sometimes still fossiliferous (among others: Nickel, 1960; Higgins, 1964; Bianconi, 1965), mesozonally metamorphic sediments, partly of the *Bündner Schiefer* type, as for instance in the Bedretto-Tremorgio- and Piora-Scopi-*Mulde*, south of the Gotthard Massif. This points to an Alpine (= Tertiary) age for the Lepontine gneiss complex, inclusive of the root zone. Wenk's view is also applied by Niggli & Niggli (1965) on their well-known map of the distribution of Alpine metamorphic minerals in the Swiss Alps.
Within the root zone one encounters not only gneisses but also various narrow belts consisting of marbles and lime-silicate-rocks, such as the zones of Castione and Contra-Bellinzona (Fig. 1). Although these calcareous rocks are devoid of fossils and their connection with

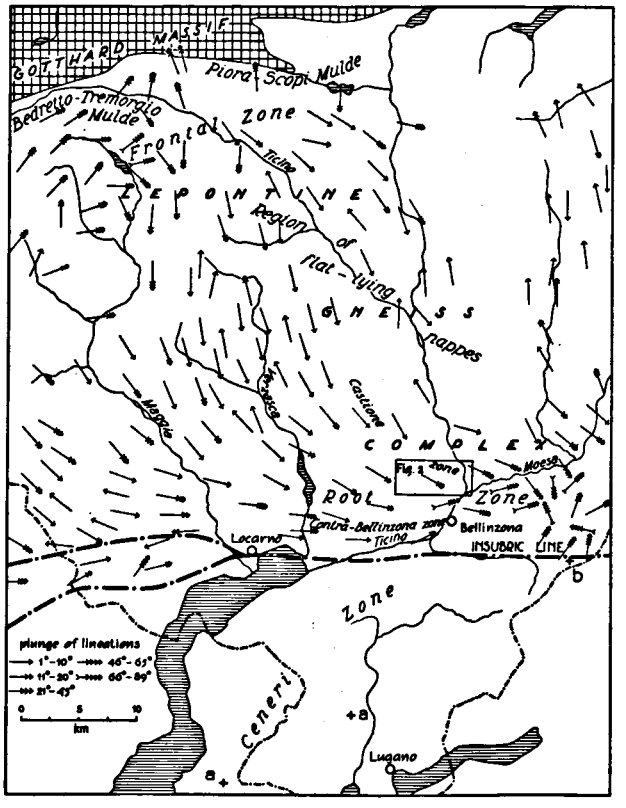


Fig. 1. The Lepontine gneiss complex and adjoining areas in Ticino (lineations of Lepontine gneisses simplified after Wenk, 1955); a: Verrucano-Servino discordant on Ceneri zone; b: Iorio Triassic.

the Mesozoic rocks in the north (e.g. the Bedretto-Tremorgio-*Mulde*) is somewhat problematic, Swiss geologists agree that the former rocks, too, most probably represent metamorphic Mesozoic. In structural analogy with their lower metamorphic equivalents in other parts of the Pennine zone of the Alps, they are considered as synclinal elements (*Muldenzonen, Deckenscheider*) separating nappes or anticlinal structures (Wenk, 1953). In this conception the latter structures (consisting chiefly of gneisses and schists) constitute the allochthonous to (par)autochthonous pre-Alpine basement, which in the Lepontine gneiss complex was strongly metamorphosed during the Alpine orogeny, along with its Mesozoic cover. The meta-sedimentary rocks of the Castione zone (and of other *Muldenzonen* too) are associated with basic and ultrabasic rocks that may be interpreted as Mesozoic ophiolites (Dal Vesco, 1953; Wenk, 1953). On Dal Vesco's map (1953, p. 237) the peridotite of Alpe Arami figures within a "zone of Arami", consisting mainly of marbles and lime-silicate-rocks and passing just south of the Castione zone. It still seems possible that this zone is a member of the Castione zone *sensu latissimo*: on the basis of the discovery of large-scale isoclinal folding of the marble-lime-silicate-rock sequence along with gneisses at the Verzasca dam site (Wenk, 1963, Fig. 4), it can also be surmised that an original *Muldenzone* split up into a number of parallel tracks as the result of later folding (and perhaps due to other tectonic complications as well). But this problem can be resolved more satisfactorily when the detailed geological map of the pertinent area becomes available (sheet Bellinzona of the 1 : 25,000 map is in preparation by the Swiss Geological Survey).

On the other hand, the age of the gneisses of the Ceneri zone, which lies directly south of the root zone, is certainly pre-Alpine, as shown by its discordant covering by unmetamorphosed Permo-triassic Verrucano-Servino (Reinhard & Bernoulli, 1964). A sliver of non-metamorphic Triassic (*Iorio-Trias*) south of the Insubric line in the Morobbia valley (Knoblauch & Reinhard, 1939) might also be an indication that south of this fault-line the influence of Alpine metamorphism was virtually nil.

Dating of micas from Lepontine gneisses in Central Ticino by Rb/Sr and K/Ar methods confirms their Alpine age (biotite: 15—20 m.y.; muscovite seems to be somewhat older; Jäger & Faul, 1959; Jäger, 1962, 1965, 1966; Jäger, Niggli, & Wenk, 1967). For hornblende crystals oriented parallel to the N-S trending main-phase Alpine lineation ($l_1$) of the southern border of the Gotthard Massif, Steiger (1964) found a K/Ar age of about 46 m.y. A distinctly later lineation ($l_2$) which is (sub)parallel to $l_1$ is connected with (re)-crystallization of biotite. Steiger supposes this lineation ($l_2$) to have the same age as the biotite from this region, for which Rb/Sr analyses (Jäger, 1962) gave ages of 15—16 m.y. Jäger, Niggli, & Wenk (1967) discussed the interpretation of radiometric age determinations in the Central Alps, and particularly the exact meaning that should be attached to the age values obtained.

Notwithstanding the structural and radiometric evidence, we must admit that there is — mainly owing to the polyphase nature of metamorphism and the

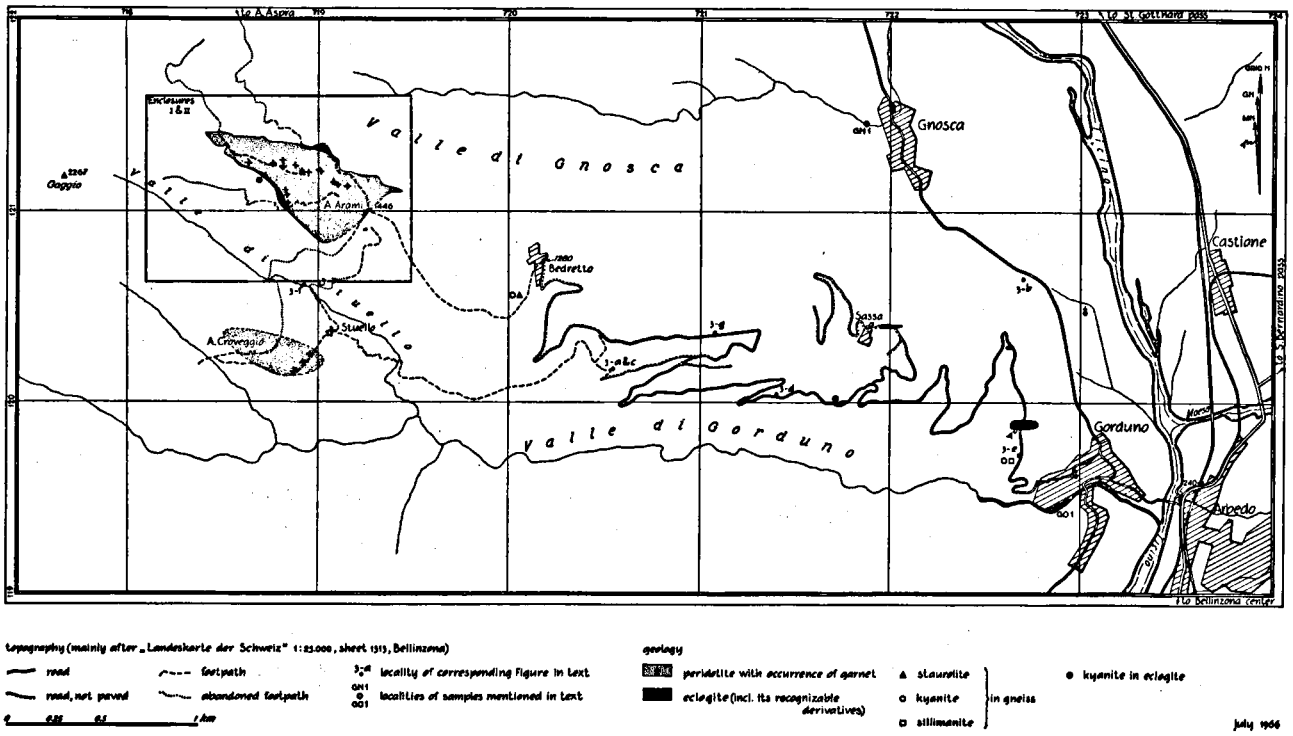


Fig. 2. Topographical and geological features of the region between Gorduno and Alpe Arami.

lack of detailed structural correlations — still some room left for the sceptics (e.g. Chatterjee, 1961) who do not entirely accept the Alpine age of the main metamorphism of the root zone in the region under consideration. In other words, they doubt the theory that the Insubric fault-line forms the exact boundary between Alpine and older metamorphic terrains.

## PETROGRAPHY

Due to a new road, passable by car, from Gorduno to Bedretto (Fig. 2)[1], the ascent to Alpe Arami is no longer as fatiguing and time consuming as in the days of Grubenmann and Dal Vesco. In addition, the fresh road cuttings offer many good exposures of the country rocks, in which we can discern mostly biotite-gneisses with local intercalations of eclogite, amphibolite, lime-silicate-rock, and marble.

Seen under the microscope, the *gneisses* often carry amphibole or muscovite in addition to biotite, and garnet, kyanite, staurolite, and fibrolitic sillimanite are sometimes present. Felsic constituents are plagioclase (oligoclase to andesine) and quartz, mostly accompanied by potash feldspar. Occurring as accessories are apatite, zircon, allanite (frequently with epidote rim), monazite (Schwander & Wenk, 1965), titanite, rutile, and opaque minerals. Chlorite is secondary after biotite.

The *amphibolites* consist of amphibole and plagioclase, which are occasionally accompanied by clinopyroxene, garnet, biotite, epidote, and quartz. The plagioclase often possesses a strong inverse zoning; in one thin section, cores of andesine composition pass into anorthite rims. Accessories are apatite, titanite, rutile, allanite, zircon, and opaque ore. Chlorite, prehnite, and potash feldspar occur as secondary minerals.

The *lime-silicate-rocks* are made up of varying amounts of clinopyroxene, amphibole, garnet, biotite, scapolite, calcite, quartz, potash feldspar, and plagioclase (bytownite-anorthite) with accessory titanite, rutile, allanite, zircon, apatite, and ore. With increasing calcite content they grade into impure *marbles* sometimes containing muscovite.

A separate section at the end of this chapter will be devoted to some properties of the *eclogitic rocks*.

In the field the gneisses typically show innumerable veins of leucocratic composition, which according to older writers originated by "injection", but which modern petrologists ascribe to anatexis (cf. Blattner, 1965). The pegmatoid leucosomes, which sometimes contain amphibole, biotite, and large titanite crystals, are mostly bordered by a narrow zone of biotite-rich melanosome. Along the road to Bedretto one also encounters several thicker pegmatites.

## STRUCTURAL ASPECTS

In the area shown in Fig. 2 the author was able to distinguish four tectonic phases in the country rocks of the peridotite. For the sake of convenience, these phases will be referred to hereafter as $F_0$, $F_1$, $F_2$, and $F_3$, in order of decreasing age. The same notation will be used for their synchronous metamorphic equivalents. Symbols for schistosity planes (S) and mineral lineations and fold axes (l) related to a particular tectonic phase, carry the same subscript as the symbol for the corresponding phase. The four phases are shown schematically in Table 1 (p. 69).

The spatial distribution of the schistosity planes (S) of the country rocks of the peridotite (for the present excluding the eclogites) is given in a diagram of poles to S-planes $\pi S$ (Fig. 3, h). It is clear that an E-W strike and a steep (75°) dip of the schistosity to the south dominate the picture. Partial diagrams of $\pi S$ from the western, central, and eastern parts of the area shown in Fig. 2 do not differ significantly (cf. Fig. 5, c).

The recognition of the two folding phases $F_1$ and $F_2$ is facilitated by a roughly horizontal outcrop of biotite- and biotite-amphibole-gneisses schematically drawn in Fig. 3, a (exact localization given in Fig. 2). The folds in biotite-amphibole-gneiss at A are very sharp. In the petrofabric diagrams (thin section no. N59, Fig. 3, i and j) there is a distinct spread of $\pi\{001\}$ of biotite in a great-circle girdle around the fold axis ($l_1$), which plunges about 40° to the east; {001} is mostly oriented in the axial plane ($S_1$), as demonstrated by the maximum within the girdle. The *c*-axis of amphibole parallels the fold axis, whereas $\pi\{100\}$ of this mineral follows the same rule as $\pi\{001\}$ of biotite. Therefore, we consider these folds as being related to the main phase of metamorphism that we shall designate as $F_1$. In Fig. 3, a, $S_3$ stands for the original

Fig. 3. Deformational aspects of the country rocks (for localization of examples, see Fig. 2).

a. $F_1$- and $F_2$-folding in gneiss; approximately horizontal outcrop (schematic).
b. Amphibole in $F_1$-type fold in amphibolite (specimen N2A).
c. Biotite in $F_2$-type fold in biotite-gneiss (specimen N60).
d. Pegmatite folded by $F_2$, in gneiss.
e. Pegmatite boudins in gneiss.
f. Lineations $l_2$ folded by $F_3$ (seen on $S_2$-plane in biotite-muscovite-gneiss).
g. $S_3$-plane accentuated by granitic vein, in gneiss (black spots are magnetite crystals).
h. 173 poles to schistosity planes $\pi S$ (except eclogites) from area shown in Fig. 2; contours at densities 2-4-6-8-12-16-20-24/1.73 ($A = 0.01$); dots: $\pi S_0$ (eclogites); crosses: $\pi S_3$.
i. Biotite-amphibole-gneiss, thin section N59 (cf. Fig. 3, a); 200 $\pi\{001\}$ of biotite; contours at densities 1-2-3-4-5-6-7-8-9 ($A = 0.01$).
j. Same section as Fig. 3, i; 100 amphiboles, *c*-axes and $\pi\{100\}$; contours at densities 2-3-4-5-6-7-8-9 ($A = 0.02$).
k. 56 lineations $l_1$ and $l_2$ from area shown in Fig. 2; contours at densities 1-3-5-7-9-11/0.56 ($A = 0.01$); open circles: lineations $l_3$.
l. Relation between plunge of lineations $l_1$ and $l_2$ (ordinate) and position with respect to N-S trending grid lines in Fig. 2 (abscissa); crosses: boudin axes.

[1] In the summer of 1967 this road was extended up to Alpe Arami.

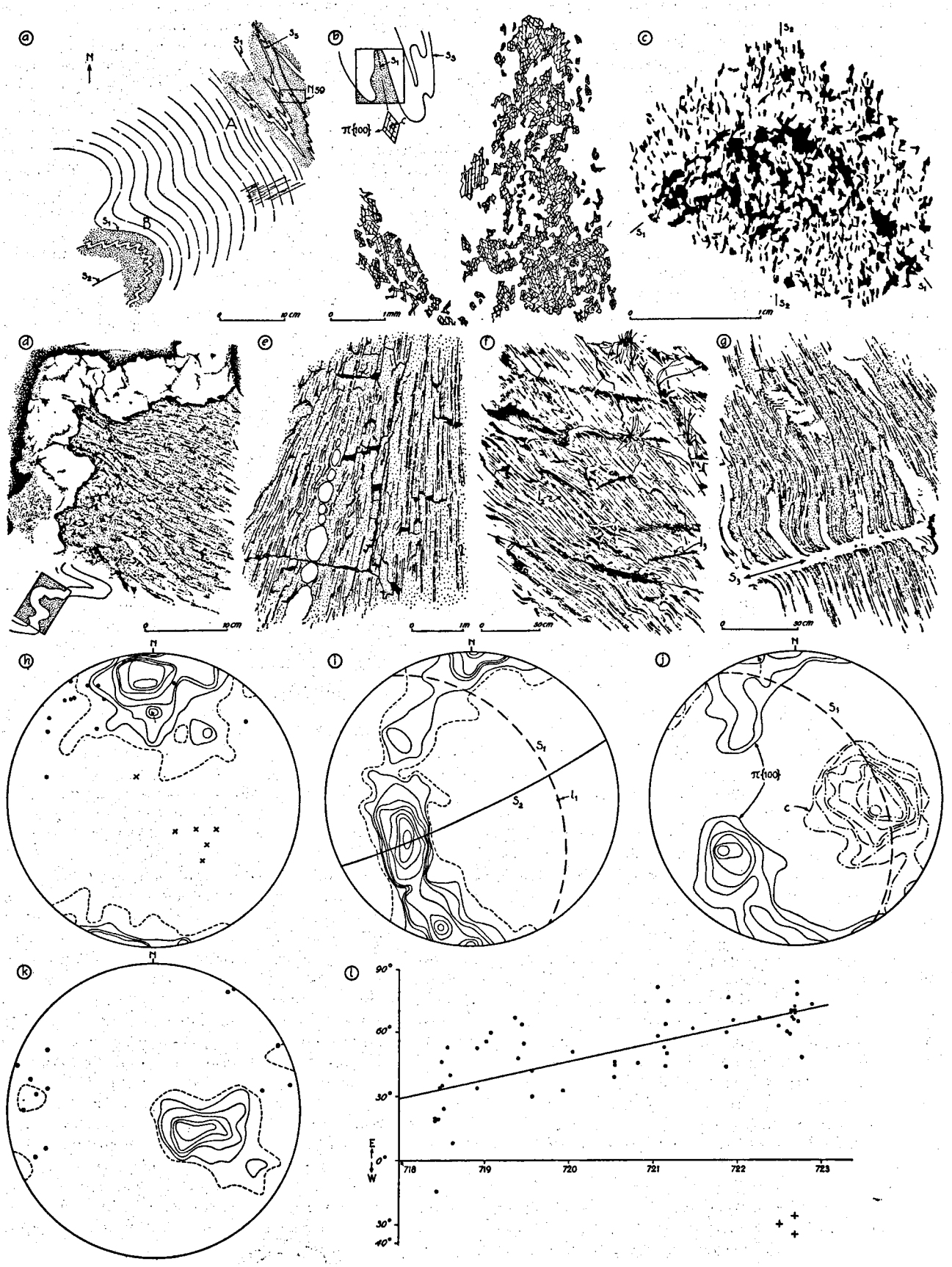
a
N
A
B
N50
10 cm
b
π{100}
1mm
c
1cm
d
10cm
e
1m
50cm
f
g
50cm
h
i
j
π{100}
c
k
l
90°
60°
30°
0°
30°
40°
E
W
718
719
720
721
722
723

layering and $S_1$ for the schistosity caused by $F_1$, i.e. the axial plane of the folds at A.

In the outcrop represented in Fig. 3, a, it is obvious that $S_1$ was folded anew during a subsequent deformation $F_2$, with axial plane $S_2$. Folds in biotite-gneiss such as those at B have a rather open and smoothly rounded character; in thin section (Fig. 3, c) it is evident that, although the minerals seem to have recrystallized, the larger flakes of biotite follow the older schistosity plane $S_1$, the axial plane $S_2$ being rather well accentuated by small biotite crystals. The orientation of the fold axis at B is about the same as at A (it plunges about 45° to the east), the parallelism of the two axes posing a problem as regards the recognition of the two deformation phases when the axial planes are also parallel or when only one of them is present.

Mineral lineations ($l_1$) on $S_1$ parallel to the fold axes at A are produced by a preferred elongation of biotite and amphibole crystals in $S_1$. Therefore, we assume that elsewhere in the region mineral lineations such as parallel amphibole prisms, elongated biotite flakes, or elliptically extended biotite spots on S, and corresponding fold axes (Fig. 3, b) are also of the same $F_1$-generation.

Not only in the outcrop of Fig. 3, a, but in the whole area shown in Fig. 2, the (sub)parallelism of these $l_1$-lineations with axes of type B folds and with lineations $l_2$ brought about by the intersection of $S_1$- and $S_2$-planes (Fig. 3, f) is striking. Very close examination of the schistosity planes of the gneisses sometimes reveals a small angle between $l_1$ and $l_2$. $l_1$ and $l_2$ are plotted together in Fig. 3, k, and display a general plunge of about 60° to the ESE. A gradual steepening of $l_1$ and $l_2$ towards the east is indicated by Fig. 3, l. This represents the approach to a region of almost vertical lineations E of Bellinzona (Fig. 1; Wenk, 1955).

The pegmatoid leucosomes were folded by $F_2$. They behaved in a more competent manner than the surrounding gneisses and produced folds which usually are called ptygmatic (Fig. 3, d). There is, however, no fundamental difference in folding style as compared, for instance, to folds of sandstone layers in slates. Another example of the more competent behaviour of the pegmatoid components of the rocks is their occurrence as boudins (Fig. 3, e), which also holds for amphibolites. Extension of the boudins is along $l_{1,2}$, from which it follows that the boudin axes (i.e. the axes of the cylindrical bodies showing in cross-section the familiar sausage-shaped appearance) lie in S perpendicular to $l_{1,2}$ (Fig. 3, l). The author was unable to determine whether the leucosomes had already been present before the $F_1$-folding. In fact, the occurrence of more than one pre-$F_2$ pegmatoid phase is likely, because leucosomes are sometimes cut discordantly by others that are also folded around $l_2$-axes.

A third folding phase, $F_3$, deformed the $l_2$-lineations (Fig. 3, f). On the schistosity planes $S_{1,2}$ this deformation is visible as minute striae and wrinkles and sometimes as somewhat larger folds with a very open character and grading into flexures. The spatial orientation of some $l_3$-lineations is depicted in Fig. 3, k. They are nearly horizontal E-W over the whole area shown in Fig. 2. The axial plane ($S_3$) of the $F_3$-folds has an almost horizontal attitude (Fig. 3, h). Frequently, veins of granitic composition, often carrying large magnetite crystals, can be seen to follow this axial plane (Fig. 3, g). Apart from sharply bounded cross-cutting dykes of aplitic composition, these sub-horizontal veins (including their apophyses that branch off preferably along $S_{1,2}$ into adjacent rocks) may be the only representatives of post-$F_2$ pegmaplitoid activity.

## ECLOGITES

Where noticed in the present study, outcropping eclogites and their recognizable derivatives are indicated on the map in Fig. 2. It is very likely, however, that more localities are to be found within the area. The rocks are composed chiefly of garnet and clinopyroxene, accompanied in some places by kyanite, amphibole, quartz, and epidote-group minerals, as well as by plagioclase, biotite, chlorite, carbonate, prehnite, and potash feldspar, and accessory rutile, titanite, apatite, zircon, allanite, and opaques. Large kyanite crystals (up to several cm in length) are to be found in veins within eclogite. Various stages of symplektitization of the clinopyroxene and kelyphitization of the garnet are present. Retrogressive metamorphism of kyanite gives rise to peculiar borders of green spinel and corundum occurring in symplektitic intergrowths with plagioclase around the kyanite crystals (cf. Dal Vesco, 1953, pp. 292—293). Final feldspathization of garnet causes the retrogressive eclogite to resemble a dark amphibolite with white spots.

Chemical analyses of eclogite surrounding the peridotite body of Alpe Arami have been presented by Grubenmann (1908, p. 150) and O'Hara & Mercy (1966, p. 296). The rock and its principal components, garnet (43 mol % pyrope) and clinopyroxene, were also analysed for some trace elements by Rost & Grigel (1964, p. 1936). From a diagram by Essene & Fyfe (1967, Fig. 15) it appears that clinopyroxene from an Alpe Arami eclogite is an omphacite containing about 40 % of the jadeite molecule.

The schistosity planes S of the eclogites differ in orientation from those of the gneisses (Fig. 3, h). The relations between eclogites and country rocks can be judged along the road from Gorduno to Bedretto, where it traverses the first large eclogite body. Two zones within the steeply SE dipping (meta-)eclogite bands show conversion into amphibolites which carry some microscopically observable clinopyroxene (Fig. 4). The schistosity of the amphibolites is almost vertical, with an E-W strike on the average. There is some variation in attitude, however, which gives rise to a boudin-like structure of some of the relict eclogite. On the schistosity planes the amphibolites carry an

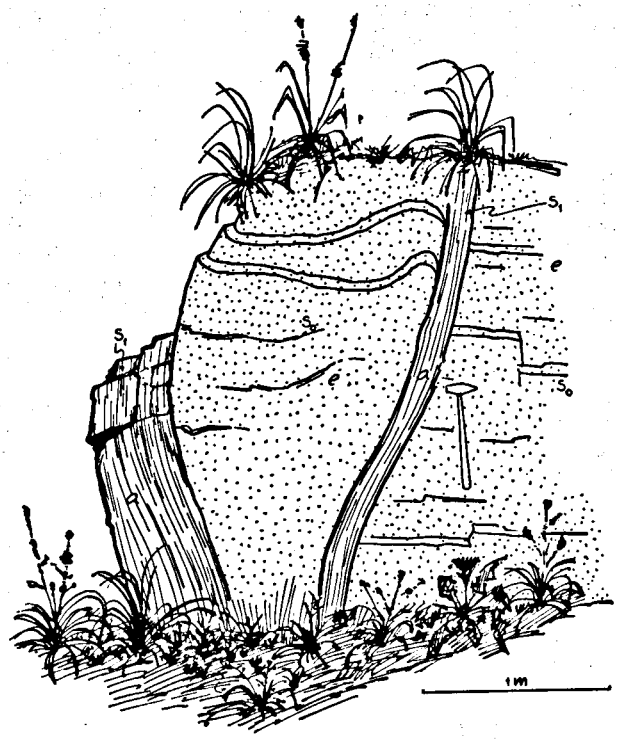


Fig. 4. Replacement of (meta-)eclogite (e) by amphibolite (a) (for locality, see Fig. 2).

amphibole lineation pitching 70° to the SE. In the light of the foregoing it is acceptable to consider this mineral lineation as $l_1$ and consequently the schistosity of the amphibolites as $S_1$. This leads to the conclusion that the schistosity of the eclogite is older than $S_1$; we shall therefore call it $S_0$, and we ascribe its formation to an older tectonic phase $F_0$. In this outcrop the intersecting line between $S_0$ and $S_1$ dips steeply to the SE and therefore lies parallel to $l_1$, as do the axes of the flexure-like folds of $S_0$ itself.

Another outcrop along the road to Bedretto, here of a much thinner eclogite layer in gneisses (co-ord. 120.0/721.8), offers a somewhat different situation. The intersecting line of $S_0$ (eclogite) and $S_1$ (gneisses), which is clearly visible as a $\delta$-lineation on $S_1$, is nearly horizontal E-W. If this line lay parallel to $l_1$ in this place, we might expect a plunge of approximately 60° E because of its geographical location in Fig. 3, l, but this is evidently not the case. We shall return to this question below (p. 74).

It is interesting to note that Wang (1939, pp. 29—32) found a similar angular discordance within a lenticular, E-W trending garnet-amphibolite body near Scalate, at the southern extremity of the Verzasca valley, where flattened lenses of feldspar originating from the replacement of garnet define a schistosity that is parallel to the schistosity of the surrounding gneisses. A layered structure in the amphibolites lies mostly parallel to this schistosity but the layering gradually deviates from it at the western and eastern margins of the amphibolite lens, along with the contact between amphibolite and country rocks. There, the local attitude of the layering plane becomes even perpendicular to the direction of elongation of the feldspar lenses. Wang supposes this layering to have a magmatic origin.

Table 1. Planar and linear components in the country rocks of the peridotite and their relative age.

| tectonic phase | eclogites | gneisses, etc. |
|---|---|---|
| $F_0$ (pre-Alpine?) | $S_0$ | ($S_3$ foliation?, bedding?) |
| $F_1$ (Alpine main phase) | $S_1$, $l_1$ amphibole | $S_1$, $l_1$ amphibole, biotite |
| $F_2$ | | $S_2$, $l_2$ biotite |
| $F_3$ | | $S_3$, $l_3$ |

## CONCLUDING REMARKS

The structural history of the area under study can be inferred from the foregoing observations as follows. There seem to have been four successive phases in the deformation and metamorphism of the country rocks of the peridotite (Table 1). For the *first* phase $F_0$ the only available evidence is that eclogites were formed with a schistosity plane $S_0$. The *second* phase $F_1$ is recognizable over the whole area and is involved in the main regional metamorphism. The now mostly E-W striking and steeply south dipping schistosity planes $S_1$ are related to $F_1$, as well as the fold axes and lineations $l_1$, which steepen gradually towards the east. Schistosity planes, lineations, and fold axes of a *third* phase of deformation $F_2$ lie in most cases approximately parallel to the corresponding structures of $F_1$. A *fourth* phase of gentle, flexure-like folding $F_3$ has a roughly horizontal axial plane and is frequently seen to be accompanied by the emplacement of some granitic material, preferably along this plane.

Because of the limited area it was impossible to ascertain the spatial orientation of the above-mentioned S-planes at their genesis. The primary attitude of $S_1$ and $S_2$ is not necessarily subvertical E-W, since it could of course have been changed by later deformations such as $F_3$ or by a possibly still later large-scale concentric folding phase that is not reflected by structures on a mesoscopic scale.

It is impossible to answer the question of which lineation ($l_1$ or $l_2$) we must correlate with the alleged single lineation of Alpine age of Wenk (cf. p. 64), since rocks of irrefutable Mesozoic origin are lacking here. Alpine radiometric ages of biotite could equally well belong to either old $F_1$- or to recrystallized $F_2$-

biotites, because we do not know whether the samples from Lepontine gneisses analysed by Jäger were acted upon only by $F_1$ or alike by $F_1$ and $F_2$. However, on the basis of the conspicuous agreement with the results of Steiger (p. 65) it is tempting to suppose an Alpine age for the two (sub)parallel lineations $l_1$ and $l_2$, in spite of the considerable distance separating the two areas concerned.

We therefore assume, as a working hypothesis, that the eclogites are pre-Alpine metamorphic rocks and that the Alpine metamorphism here comprised at least three phases (connected with $l_1$, $l_2$, and $l_3$). The latter then has a predominantly mesozonal (amphibolite-facies) character, but the position of typomorphic minerals of gneisses and schists such as garnet, kyanite, staurolite, and sillimanite in the sequence of events is rather uncertain. Bending of biotite flakes around garnet in a fold of $F_2$-type, as well as sigmoidally arranged inclusions within the latter mineral, are signs that garnet was formed relatively early with respect to the end of the $F_2$-deformation. It need hardly be said that according to the present hypothesis the kyanite in eclogite and its derivatives must be of older age than in garnet-staurolite-kyanite-gneisses.

## CHAPTER III

# MEGASCOPIC TECTONICS OF THE PERIDOTITE

## THE GEOLOGICAL MAP 1 : 5000

The topographical basis of the 1 : 5000 map (Enclosure I) consists of an enlargement of the relevant part of the "Landeskarte der Schweiz 1 : 25,000", sheet 1313 (Bellinzona), with a few simplifications, additions, and corrections. To facilitate orientation in the field, more cartographical detail has been brought into the configuration of the timber surrounding Alpe Arami, mainly with the help of aerial photographs kindly put at my disposal by Professor Dr. E. Niggli, of Berne. At present, the footpaths are generally in bad condition, and hardly continue outside the peridotite body; however, some now overgrown tracks are indicated in Fig. 2 to serve as a guide to the old descriptions of Grubenmann (1908).

The exposure of the peridotite is rather poor: an important portion of the western part lies hidden under timber and scrub, and except for a few isolated outcrops the southeastern part is concealed by moraine, scree, and alluvium.

No detailed geological map of the present area exists. The map prepared by F. Rolle (Geologische Karte der Schweiz 1 : 100,000, sheet 19, Bellinzona-Chiavenna, published in 1882) does not show any peridotite or similar rocks in the region near Gorduno. On the „Geologische Generalkarte der Schweiz", 1 : 200,000, sheet 7 (Ticino), published in 1955, the peridotite of Alpe Arami is depicted as serpentinite. The writer could not find exposures of another "serpentinite" which is marked on this map somewhat to the south, but the occurrence of much peridotite (partly garnetiferous) among the debris between the deserted huts of Stuello and Alpe Croveggio is indeed a strong indication of the presence of a second peridotite body (Fig. 2). Presumably, a substantial part of the peridotite boulders found in the torrent near the village of Gorduno derived from the latter lens and not from that at Alpe Arami, the bulk of which is exposed in the Gnosca valley. The peridotite body indicated just north of Gorduno on the 1 : 200,000 map may be identical to the eclogite body near Gorduno shown in Fig. 2 and referred to on p. 68. A geological map 1 : 50,000 by Dal Vesco (1953, p. 237) also covers Alpe Arami and its neighbourhood.

Among the country rocks indicated on the present 1 : 5000 map, only eclogites are differentiated. They are of the same type as eclogites elsewhere in the region, and as usual display various stages of alteration into amphibolites (Fig. 2 and p. 68). Other country rocks are principally biotite-gneisses (p. 66). Lime-silicate-rocks figure on the map and section given by Dal Vesco (1953, pp. 237, 245; see also our Fig. 6, c), as occurring at the outer contact of the peridotite-eclogite body, but their quantity seems to have been overestimated somewhat as compared to that of the biotite-gneisses and eclogites.

The peridotite-eclogite has a roughly lenticular shape on the map; its long axis, which lies approximately parallel to the strike of the regional schistosity, measures about 1100 m, its maximum width being about 400 m.[1] In Chapter IV it is argued that originally all the peridotite of the lens must have been present as garnet-peridotite. On the map I have marked only those localities where garnet within peridotite shows little or no retrogressive metamorphism (collectors in search of fine specimens of garnet-peridotite may find this information more useful than that provided by Gnehm (1964) who mainly paraphrases Grubenmann (1908) ).

At the western extremity of the lens, somewhat larger masses of marginal clinopyroxenite and hornblendite are present, other inhomogeneities being small bodies of amphibolite (retrogressive eclogite?) and gneiss near the northern border of the peridotite. Within eclogite (north side of lens) and between eclogite and surrounding biotite-gneiss (south side), thin peridotite layers are sometimes found.

[1] Grubenmann (1908, p. 131) mentions garnet-peridotite outcropping in a steep gully somewhere under the now largely overgrown path from Alpe Arami to Alpe Croveggio (Fig. 2). Presumably on the basis of this exposure, which could not be relocated by the present author, Grubenmann describes the dimensions of the peridotite lens as about 800 m in E-W and about 1 km in N-S direction.

## S-PLANES, FOLDS, AND LINEATIONS

The method of geometrical-statistical analysis of megascopic structures has only recently been introduced into the study of peridotites (Raleigh, 1963, 1965; Avé Lallemant, 1967), undoubtedly partly because superficial alteration and serpentinization, a phenomenon common to most peridotites, greatly hamper recognition of the structures. However, many exposures within the peridotite of Alpe Arami offer the opportunity to observe different kinds of S-planes, folds, and lineations. On the other hand, measurement of the spatial orientation of the structural features must be done critically, because especially along the steep slope towards the Gnosca valley many big rock masses may have moved in some way or other from their original positions. Furthermore, the precision of the measurements is adversely affected by the impossibility in most cases of bringing the compass into direct contact with the structure concerned, because the rocks generally do not part well along the S-planes (cf. Raleigh, 1965, p. 724); inaccuracy in the strike measurements may be caused by a slight rock magnetism when serpentinization is very advanced.

$S_L$-*planes.* — A layering ($S_L$) brought about by quantitative differences in primary mineralogical (and consequently chemical) composition of the layers is sometimes visible. The layers (varying in thickness from a few cm to some tens of cm) are either alternately rich and poor in garnet (or in its retrogressive products spinel-amphibole-symplektite or chlorite knobs—for more petrographical details *vide* Chapter IV), in clinopyroxene (or in its retrogressive product amphibole), or in orthopyroxene; or they are in turn rich and poor in combinations of these minerals (or their breakdown products), e.g. garnet-clinopyroxenite layers within normal olivine-rich peridotite (Plate I). Boudinage, preferentially limited to (garnet)pyroxenite and hornblendite layers (Fig. 5, a and b), points to a flattening of the rocks parallel to $S_L$. Discordant veins of ultramafic composition occur rarely if ever, so that $S_L$ is usually well defined.

$S_1$-*planes.* — Plate I, a and c show $S_L$-planes characterized by alternations of formerly garnet-rich and garnet-poor layers, the garnets having been converted into chlorite knobs that are flattened parallel to another plane $S_1$ which is consequently younger than $S_L$. The $S_1$-plane is also visible as a cleavage plane in these Figures. Plate I, b and d show development of $S_1$ only as a cleavage plane in rocks where garnet is still present or has been transformed into spinel-amphibole-kelyphite. In general, the intensity of development of the $S_1$-cleavage varies from place to place; it can also be absent. Locally the $S_1$-cleavage has been bent (or — to use a term borrowed from optics — "refracted") to a certain extent by (garnet)-pyroxenitic layers (Plate I, a; Fig. 5, a).
Identification of $S_1$ becomes difficult when $S_L$ parallels $S_1$. In fact, when chlorite knobs are flattened parallel to $S_L$, this may also be caused by an original flattening comparable to the boudinage in Fig. 5, a and b of primary garnet or secondary spinel-amphibole-aggregates, the external form of which may have been inherited by the chlorite aggregates. Only when the chlorite is clearly smeared out along the $S_L$-plane, with preferential orientation of the chlorite flakes in this plane, can one be sure that in the given case $S_1$ parallels the $S_L$-plane.
The spatial orientation of 91 poles of $S_1$-planes in the peridotite is depicted in Fig. 5, d, and for comparison a diagram is given of 93 $\pi S$ of country rocks in the area shown in Fig. 2 west of gridline 720 (Fig. 5, c; cf. Fig. 3, h), which are the country rocks closest to the peridotite. The similarity between the diagrams is indeed striking; in both a moderately to steeply (60°—70°) S to SSW dipping attitude of the schistosity predominates.
The diagram for 129 $\pi S_L$ of peridotite (Fig. 5, e) offers a different picture: though some concentration of poles is visible on the same spot as in the foregoing diagrams, there is also a maximum in the south-western quadrant of the projection indicating the frequent occurrence of moderately north to north-eastward dipping layering planes; other submaxima testify to almost vertical N-S striking and almost horizontal $S_L$-planes.
These data resemble the situation described on p. 68 for the eclogites. If the schistosity of the country rocks (as usual excluding eclogites) is assumed to be of Alpine age, it seems reasonable to suppose the same age for $S_1$ within the peridotite, which means that $S_L$ must be of pre-Alpine age.

$S_L/S_1$-*folds.* — We may now consider folds of $S_L$ having $S_1$ as axial plane (i. e. the axial plane of these folds dips 60°—70° to the south with an average WNW-ESE strike). They range in character from a gentle bending of $S_L$ (Plate I, a and b) to fairly tightly compressed folds (Plate II, b). Plate II, a represents an Alpine fold of parasitic type showing chlorite knobs flattened parallel to its axial plane $S_1$.
The axes of these folds show a roughly horizontal E-W strike, but because they are not very frequent, more information was obtained by measuring or constructing the intersection between $S_L$ and $S_1$ individually for each outcrop, wherever both planes are present. These lines give the same information as real fold axes. Often, however, the peridotite parts along pronounced schistosity planes without giving any clue to the nature of the S-planes present. For this case, scanty observations suggest that $S_L$ and $S_1$ may be almost parallel. Therefore, we interpreted a fine striation on such S-planes as also representing the intersection of $S_L$ and $S_1$. All 61 values (called $l_1$-lineations) are included in Fig. 5, f, demonstrating the mainly horizontal WNW-ESE attitude of the $S_L/S_1$ intersection. However, some spread within the average $S_1$-plane apparently exists. This horizontal WNW-ESE direction agrees with the pole R to the main $\pi S_L$-circle as drawn in Fig. 5, e.

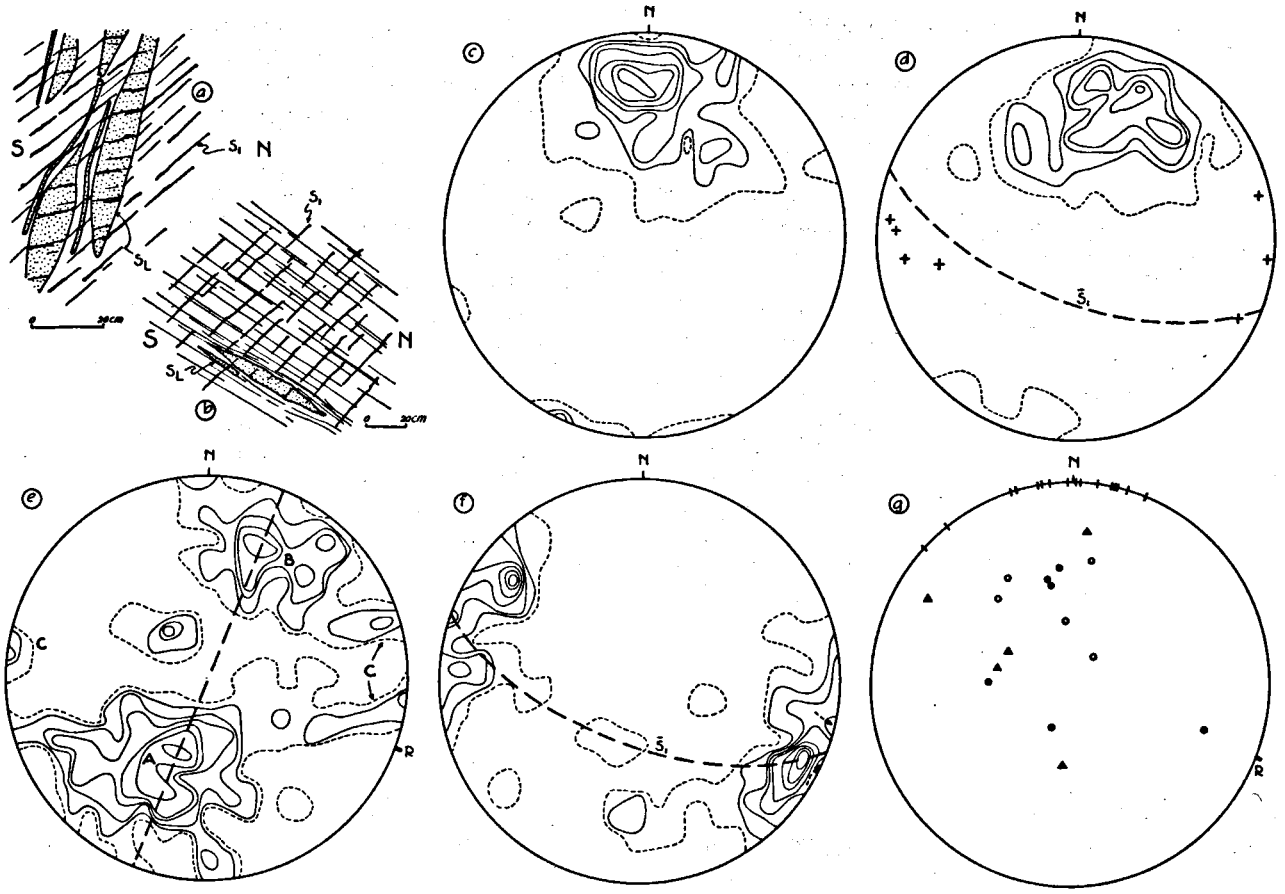


Fig. 5. Megascopic structures of the peridotite (including the orientation of S-planes in its immediate country rocks). a. and b. Boudins of garnet-pyroxenite to hornblendite (a.) and hornblendite (b.) following layering $S_L$, in peridotite (both sketches looking W). c. 93 $\pi S$ of country rocks (except eclogites) from area W of grid line 720 in Fig. 2; contours at densities 1-3-5-7-9-11-13/0.93 ($A = 0.01$). d. 91 $\pi S_1$ of peridotite; contours at densities 1-3-5-7-9-11/0.91 ($A = 0.01$); crosses: talc veins. e. 129 $\pi S_L$, $S_0$ of peridotite; contours at densities 1-2-3-4-6-8-10/1.29 ($A = 0.01$); R is pole to main $\pi$-circle; A, B, and C refer to subareas on Enclosure II. f. 61 lineations $l_1$ of peridotite; contours at densities 1-2-3-4-5-6-7-8/0.61 ($A = 0.01$). g. 16 lineations $l_0$ of peridotite; open circles: $S_L/S_0$-fold axes; dots: $S_L/S_0$-intersections; triangles: mineral lineations.

$S_L/S_0$-*folds*. — A few folds of $S_L$ show an axial plane that cannot be $S_1$. In Plate II, c (locality of AR41 in Enclosure II) $S_1$-planes are plane surfaces making a large angle with the fold axis of $S_L$. For the axial plane of these older folds, the symbol $S_0$ is introduced. A slight curvature of the axial plane of some of the folds could be observed. In the fold hinges no distinct schistosity parallel to $S_0$ is visible in the field. Another fold (Plate II, d) shows development of $S_0$ as axial plane schistosity. These folds are rather tight, so that $S_0$ almost parallels $S_L$ except in the hinges. Fold axes of this type are projected in Fig. 5, g. Lineations that are visible on $S_0$-planes due to the intersection of $S_L$ and $S_0$ are of the same kind. Obviously, these can only be identified in outcrops where the $S_0$ character of the planes concerned is clearly established by $S_L/S_0$-folds. Occasionally, when $S_0$ approximately parallels $S_1$, two lineations can be seen on the same $S_0$-plane, viz. an almost horizontal striation due to $S_0/S_1$-intersection referred to above, and a steeply pitching $\delta$-lineation caused by the intersection of $S_0$ and $S_L$.

Mineral lineations formed by prismatic pyroxene (mainly clinopyroxene), hornblende, and elongated garnet crystals, which are sometimes visible on $S_L$ ($S_0$)-planes, are treated together with the former linear components; this procedure is warranted because they fit into the picture of Fig. 5, g. For the sake of brevity, all linear elements older than $l_1$ will be described as $l_0$-lineations. A differentiation of $l_0$ into two types will be made on p. 113.

It is quite evident that the diagrams in Fig. 5, f and g are materially different, and that they illustrate the presence of at least two folding phases within the peridotite. On the assumption that the Alpine folding of $S_L$, $S_0$, and the older linear elements of Fig. 5, g was concentric in character and that the position of its axis of rotation (R) is also the axis of the main $\pi S_L$-circle of Fig. 5, e, we rotated the $l_0$-lineations in Fig. 5, g to a position at the perimeter of the diagram (keeping the angle between R and the lineations $\geqslant 90°$). Line-

ations and fold axes concentrate roughly 90° from the Alpine fold axis at R. Supposedly, therefore, before the Alpine folding the peridotite layers contained folds and lineations directed roughly perpendicular to the Alpine fold axis. It is impracticable to determine the orientation of the older folds by making a β-diagram from the $S_L$-planes; this would bring out not only the Alpine fold axis but also a number of spurious submaxima by the intersections of other groups of planes corresponding to maxima in the $\pi S_L$-diagram of Fig. 5, e (cf. Ramsay, 1964).

*Talc veins.* — Attitudes of some secondary talc veins, which are shown in Fig. 5, d, are approximately vertical with a N-S strike. These are probably the most recent structures present in the peridotite. The talc veins are not to be confounded with $S_L$-structures, although there may be a superficial similarity in the field, especially when they are closely spaced.

## OUTLINE OF THE OVER-ALL STRUCTURE OF THE PERIDOTITE. HYPOTHETICAL SECTIONS

On the structural map (Enclosure II) we observe a certain regularity in the distribution of the attitudes of the $S_L$-planes over the peridotite body. A moderate northward dip of $S_L$ preponderates in the northern part of the lens (A), although some steepening of the layering plane towards the northern contact is apparent. The southern part (B) displays predominantly steep dips to the south, whereas in the southeast a third subarea (C) can be distinguished by its principally steep, N-S striking $S_L$-planes. The most $S_L/S_0$-folds are encountered in the latter area. The areas correspond with submaxima A, B, and C on the $\pi S_L$-diagram (Fig. 5, e).

This map also gives a picture of schistosity planes $S_1$ and lineations $l_1$ within peridotite, together with some schistosity planes S and lineations $l_{1,2}$ of country rocks close to the peridotite. As expected from the abnormal position of the $S_L$-planes in subarea C, this is the only region to show important deviations from the normal attitude of the $l_1$-lineations, which causes the spread along the great-circle of $S_1$ in Fig. 5, f, already referred to (p. 71).

The geological map (Enclosure I) shows that the occurrence of unaltered garnet-peridotite seems to be restricted to two zones, with a thickness from 1 m to about 10 m (cf. map and section of Dal Vesco, 1953, pp. 237, 245), but this by no means implies that these zones represent $S_L$-structures; according to our views (cf. p. 71), their boundaries are limits of retrogressive metamorphism of garnet, whereas quantitative differences in primary mineralogical composition (as required by the definition of $S_L$ on p. 71) are probably absent. However, mainly on petrographical and petrofabric grounds to be dealt with in the next chapters, it is likely that the first retrogressive metamorphism of garnet-peridotite to spinel-amphibole-peridotite concerned S-planes lying roughly parallel to the present $S_L$ (p. 118), whereas during the second retrogressive metamorphism, which caused, for instance, the elongation of chlorite knobs along $S_1$, only already present spinel-amphibole-aggregates were affected and not the unaltered garnets. Therefore, we believe that the garnet-peridotite zones may indeed approximately follow the $S_L$-structures. A northern zone lies in subarea A, and a southern, rather incomplete, zone lies in subarea B. These zones seem to approach each other, but the absence of critical exposures made it impossible to establish a connection.

It is tempting at this point to try to construct a three-dimensional picture of the peridotite body. In considering section PQ (Fig. 6, a), we noticed that $S_L$-planes near the northern garnetiferous zone have lower dips than the topographical slope (cf. Plate I, b); we therefore combined the $S_L$-planes of subareas A

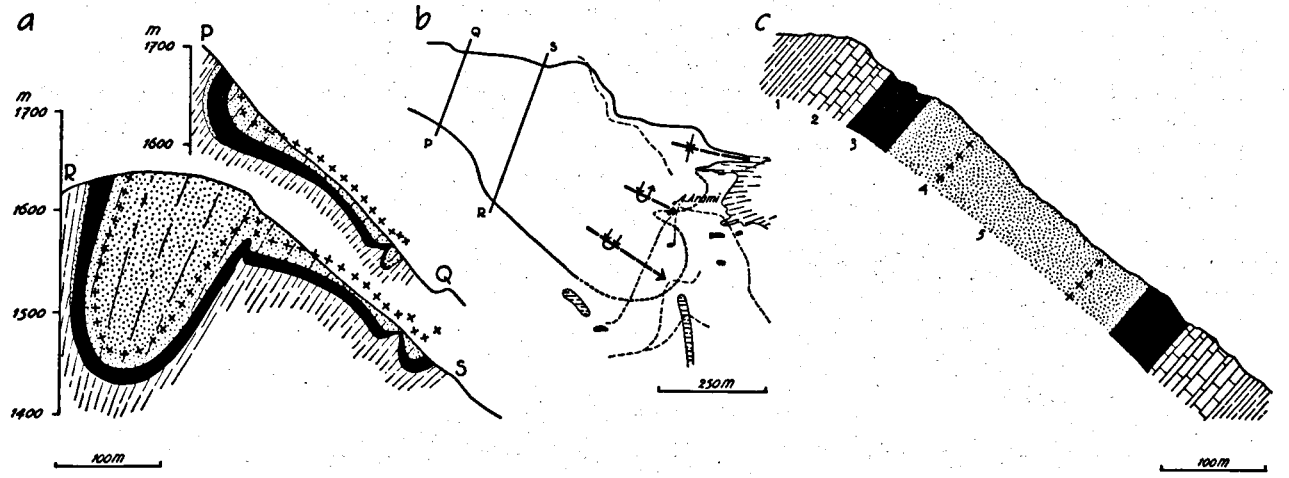


Fig. 6. a. Two hypothetical sections through the peridotite of Alpe Arami (PQ and RS on Enclosure I). b. Inferred eastern boundary of the peridotite-eclogite body. c. Schematic N-S section through the peridotite after Dal Vesco (1953, p. 245). 1 = gneiss; 2 = lime-silicate-rock, lime-silicate-gneiss; 3 = eclogite, (garnet-)amphibolite; 4 = garnet-peridotite; 5 = peridotite.

and B, including the two still garnetiferous zones, by means of a synform. We also assumed the contact between the peridotite-eclogite body and the gneisses to be generally parallel to the peridotite layering, and we accounted for the inliers of amphibolite and gneiss near the northern border (and likewise for the rather steep dips of $S_L$, including frequent sharp $S_L/S_1$ minor folds in this region, as shown in Plate II, b) by a hypothetical antiform in the north. The small offshoot of peridotite within gneiss shown on the map at the northeastern border of the massif might lie in the continuation of the synform adjoining this antiform to the north. Wedging out of eclogite in the section is not at all improbable, since the same phenomenon in a lateral sense is visible on the map. In section RS (Fig. 6, a) another subsidiary hypothetical antiform is needed to establish a connection between the two garnetiferous zones.

Cleavage ($S_1$)/layering ($S_L$) relations, including "refraction" of cleavage planes and asymmetry of parasitic folds, can be used to determine the position of synform and antiform axes. Fig. 5, a indicates a synform to the N, and refraction of $S_1$ in a pyroxenitic layer in Plate I, a points to a synform to the S. These observations were also considered in the construction of the two sections, but especially for the southern part, where $S_L$ frequently parallels $S_1$, such clues are too scarce to permit anything more than a hypothetical solution.

Comparison of sections PQ and RS shows that between them the northern portion of the synform structure plunges slightly (about 10°) to the east. Its southern part may have a moderate eastward plunge of about 40°, so that its nose would emerge south of Alpe Arami (Fig. 6, b), probably with some interference from the $S_L/S_0$-folds in subarea C. This offers a rather elegant explanation for the abrupt disappearance of the peridotite to the east, which cannot be accounted for by the section of Dal Vesco (Fig. 6, c).

However, it is reiterated that this outline is based on many assumptions, one of the important ones being that the contact between the ultramafic body and the surrounding gneisses lies primarily parallel to the peridotite layering. The exposed contacts (various outcrops at the southern side and near the lower footpath in the Gnosca valley at the northern side of the lens) lie parallel to the schistosity of the country rocks but also to the local peridotite layering and therefore neither support nor contradict the above hypothesis.

## COMPARISON WITH TECTONICS OF THE COUNTRY ROCKS

From Fig. 3, l we find an average plunge for $l_{1,2}$ of the country rocks of 30°—40° E in the region of the peridotite body. Although this may approximately agree with the general plunge of the southern part of the peridotite body (*vide supra*), it is in contrast with the almost horizontal attitude of Alpine fold axes and intersection lineations of the peridotite displayed in Fig. 5, f. We have alluded to a comparable question on p. 69 with respect to an eclogite-gneiss contact. This discrepancy may arise from an initial non-parallelism of the planes that later underwent folding. For instance, before the beginning of the Alpine folding the gneisses around Alpe Arami may have had dips of 30°—40° E, whereas the peridotite and eclogite formed almost horizontal layers. But this is only one of many possibilities.

There can be no doubt that the $S_1$-planes in the peridotite have the same age as the S-planes of the gneisses. However, a question that was ignored in the preceding paragraphs remains: is it possible to correlate $S_2$ (country rocks) with $S_1$ (peridotite), and $S_1$ and $S_3$ (country rocks) with $S_0$ and $S_L$ (peridotite)? This is not very likely, for if $S_1$ (country rocks) and $S_0$ (peridotite) were originally parallel it would be very difficult to explain the above-mentioned angular discordance between lineations originating inside and outside the peridotite during the second Alpine folding phase ($F_2$). But even supposing that for some reason the $F_2$-axis was roughly horizontal in the peridotite (and that it plunged 30°—40° E parallel to the $F_1$-axis in the gneisses), we are still faced with the steep N-S striking attitude of the axial planes of $S_L/S_0$-folds in subarea C, which constitutes another objection to the above theory. Furthermore, the average angle between the presumed horizontal $F_2$-axis (= R on Fig. 5, g) and the $l_0$-lineations is not 30°—40°, but at least some 65°.

We therefore conclude that $S_1$ (peridotite) = $S_1$ (country rocks), and that $S_2$ (and of course the weak $S_3$) are not developed within the peridotite, with the possible exclusion of some $F_2$-influence at the margins of the body (Table 2). The structure of the peridotite as a whole (Fig. 6, a) is perhaps to be conceived as an $F_1$-synform.

Table 2. Megascopically recognizable planar and linear components in peridotite and country rocks and their relative age.

| tectonic phase | peridotite | eclogites | gneisses, etc. |
|---|---|---|---|
| $F_0$ (pre-Alpine?) | $S_L$<br>$S_0, l_0$ pyroxene, amphibole | $S_0$ | ($S_3$ foliation?, bedding?) |
| $F_1$ (Alpine main phase) | $S_1, l_1$ chlorite | $S_1, l_1$ amphibole | $S_1, l_1$ amphibole, biotite |
| $F_2$ | $S_2$ ? | | $S_2, l_2$ biotite |
| $F_3$ | | | $S_3, l_3$ |
| | vertical, N-S striking talc veins | | |

CHAPTER IV

# PETROGRAPHY OF THE ULTRAMAFIC ROCKS

## INTRODUCTION: THE MINERALOGICAL CLASSIFICATION OF PERIDOTITES

The development of a workable classification of peridotites based on their mineralogical composition is fairly recent (e.g. Rost, 1961, 1963). The study of a large number of olivine-rich ultramafics occurring among the crystalline rocks of Europe showed Rost that spinel, garnet, and chlorite are mutually exclusive constituents of their mineral parageneses, and he was therefore able to distinguish three types of peridotites, viz.:

1. *spinel-peridotites:* olivine, ortho- and clinopyroxene, and primary spinel (ol + opx + cpx + sp).
2. *garnet-peridotites:* olivine, ortho- and clinopyroxene, and pyrope-rich garnet (ol + opx + cpx + gar).
3. *chlorite-peridotites:* olivine, orthopyroxene, clinopyroxene or amphibole, and chlorite (ol + opx + cpx/amph + chl).

Although the number of peridotite types may be enlarged to some extent and details of Rost's classification may require modification, the exact determination of the mineralogical composition of peridotites, with special attention to the recognition of mineral parageneses (including critical minerals and/or critical mineral associations), remains a most promising starting-point for their study. Only thorough investigation of this particular aspect might justify the application of interesting but rather vague terms such as "*Alpine-type*" *peridotites*. Rost's essentially descriptive approach is so successful because different mineral parageneses encountered in rocks of *grosso modo* isochemical composition in all probability reflect different conditions of formation (Rost, 1961, 1963). Green & Ringwood (1963) arrived at a similar conclusion by surveying the literature on ultramafic-rock mineralogy. In addition to the spinel- and garnet-peridotite assemblages mentioned above, they proposed a *spinel-amphibole-peridotite* (ol + amph (edenite, pargasite) + accessory chromian spinel ± opx ± cpx) and a *plagioclase-peridotite* (ol + opx + cpx + plagioclase + accessory chromite) paragenesis.

The precise determination of the conditions under which the various ultramafic assemblages are in equilibrium is a problem of experimental petrology that has not yet been completely solved. In the PT-diagram of Fig. 7 (based on Fig. 9 in Rost, 1961), the present author hazards a guess about the position of the stability fields of some petrographically distinguishable peridotite varieties.

The experimentally determined stability of olivine and orthopyroxene from magmatic circumstances of crystallization down to the advent of serpentinization (Rost, 1963) again points to their unsuitability for a sound classification of peridotites. The experimental results also indicate that the occurrence of spinel, garnet, and chlorite, to which we may add: plagioclase, clinopyroxene, and amphibole, provides better criteria.

The results of Kushiro & Yoder (1965, 1966), who investigated a dry mixture of forsterite and anorthite (2:1 mole) at high temperatures and pressures, justify a discrimination between *plagioclase-peridotites*, *spinel-clinopyroxene-peridotites* or *lherzolites*[1] (i.e. Rost's spinel-peridotites), and *garnet-peridotites*, which at between 1000° and 1300 °C are stable within ranges of increasing pressure (Fig. 7; see also Macgregor (1965, 1967), Ito & Kennedy (1967), and Green & Ringwood (1967)). Considerable textural and structural evidence supports the view that plagioclase-peridotites (e.g. those from the Stillwater Complex, Montana, U.S.A.; Jackson, 1961) are the shallow-level magmatic rocks that should be correlated with the gabbro facies, rather than the spinel-clinopyroxene-peridotites as suggested by Rost (1963). In many cases the spinelloid phase of plagioclase-peridotites seems to be chromite (Green & Ringwood, 1963). Concerning the application of spinel proper as a critical mineral, it should be remarked that according to the already cited papers of Kushiro & Yoder, Macgregor, Ito & Kennedy, and Green & Ringwood, the assemblage ol + (cpx and/or opx) + sp + gar may be stable over a limited interval — probably depending on the chemical composition of the rock — on the lower pressure side of the garnet-peridotite field. However, natural occurrences of *garnet-spinel-peridotites* seem to be very scarce indeed. A case in point may be the peridotite of Alpe Seefeld, Alto Adige, northern Italy[2] (Hammer, 1899; Andreatta 1936) (Plate III, a).

Recent work by Yoder (1967) partially concerns the system anorthite(an)-forsterite(fo)-water. Although the mixture used by Yoder (an : fo = 1 : 1 mole) does not appear to be very representative of ultramafic compositions, his experiments allow us to draw (Fig. 7) a stability field for chlorite in paragenesis with other mafic minerals (clinopyroxene and amphibole). These results might therefore suggest the approximate position of the *chlorite-peridotite* field. Above $P_{H_2O}$ = 7kb and T = 800 °C the amph + chl + cpx + an assemblage obtained by Yoder gives way to an amph + an + cpx + sp assemblage, changing in

[1] Spinel (picotite) is a ubiquitous constituent of lherzolite from the type locality (Lacroix, 1894); I therefore recommend that it be embodied in the definition.

[2] Unfortunately, a paper by Ladurner (1956), who like Andreatta (1934, 1936) made petrofabric analyses of these rocks, has caused some confusion, because it neither mentions the name of the country where the studied rocks are exposed nor contains a clear reference in the text to Andreatta's petrofabric work in the same region. In a classification of peridotites according to their mode of occurrence (Collée, 1962, pp. 4—8), the ultramafic rocks of Alpe Seefeld as described by Andreatta are even placed in a different group than the same rocks described by Ladurner.

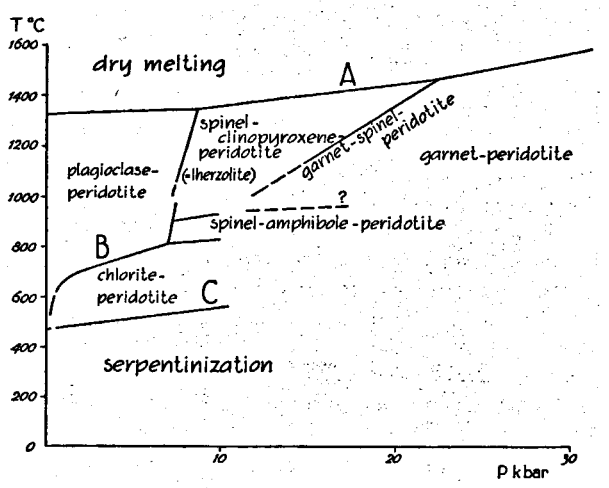


Fig. 7. Approximate stability fields of some peridotite types. A: after Kushiro & Yoder, 1966, Fig. 2 (investigated composition: forsterite + anorthite, 2 : 1 mole). B: after Yoder, 1967, Fig. 49 (investigated composition: forsterite + anorthite, 1 : 1 mole, P = $P_{H_2O}$). C: after Yoder, 1967, Fig. 50 (serpentine ⇋ forsterite + talc, strict reversibility not demonstrated, P = $P_{H_2O}$).

turn into an + cpx + opx + sp above about 900 °C (Yoder, 1967). This is suggestive of the presence of a field of clinopyroxene-bearing *spinel-amphibole-peridotites* between the chlorite-peridotite field on the one hand and the spinel-clinopyroxene- and garnet-peridotite fields on the other. However, we are still poorly informed about the situation in this region.
At its lower side the chlorite-peridotite field is bounded by a line representing the transformation of olivine into serpentine (Yoder, 1967; cf. Rost, 1961).

## PETROGRAPHY OF THE ULTRAMAFIC ROCKS AT ALPE ARAMI

The first observations on the peridotite of Alpe Arami were made by Grubenmann (1908). Dal Vesco (1953) also contributed petrographical and chemical details, and O'Hara & Mercy (1963, 1966) and Mercy & O'Hara (1965) published chemical analyses of rocks and minerals. The following account contains elements already known from previous papers about the peridotite of Alpe Arami, and is partially based on petrographical studies of comparable peridotites. However, we of course do not mean to imply that petrographical details, for instance the mineralogical composition of kelyphite rims around garnet, are identical in every peridotite mass.

### *A—Garnet-peridotites and their retrogressive products*

In the field the peridotites are easily recognizable from a distance among the gray gneisses by their typical yellowish-brown weathering colour. Garnet-peridotites have a restricted occurrence, as has already been remarked (pp. 70, 73; Enclosure I). The constituent minerals (including their decomposition products) will be described first, before the discussion of the rocks composed of them, i.e. the mineral parageneses.

#### *Mineralogy*

Crystals of dark violet-red garnet are most conspicuous in fresh hand-specimens of garnet-peridotite. They generally attain fairly large sizes (⌀ 5—10 mm), thus giving the rock a pseudoporphyritic appearance, although peridotites with small garnets (⌀ 1—2 mm) are occasionally seen. In the medium- to fine-grained matrix, which consists chiefly of olivine, ortho- and clinopyroxene, the latter mineral is also clearly visible with the naked eye because of its emerald-green colour. Orthopyroxene has a light brown colour, which is especially distinct in monomineralic layers. The macroscopic colour of olivine varies from a rather oily olive-brown — especially evident when it is enclosed by garnet — to a dull greenish-black due to incipient serpentinization.

Under the microscope, pale pink *garnet* shows a completely anhedral habit, often even with concave grain boundaries. It is a chromiferous, pyrope-rich variety, as indicated by the analyses given by Grubenmann (1908) and O'Hara & Mercy (1963) (Table 3, a and c). More or less rounded olivine, clinopyroxene, and opaque grains sometimes occur as inclusions; primary orthopyroxene is seldom wholly enclosed by garnet. Moreover, very slender yellowish-brown needles are found in parallel orientation, sometimes in three sets intersecting at about 60° angles. They are probably rutile and may account for some of the $TiO_2$-content of the garnet. Amphibole may be present in rows of tiny crystals commonly containing a spinel grain, thus showing a superficial resemblance to rows of fluid inclusions. Occasionally, even larger, isolated amphibole crystals — almost everywhere together with spinel — are found within garnet. These inclusions are probably related to kelyphitization of the garnet (see below), and are thus of a secondary nature. Only once was a possibly primary inclusion of deep brown spinel (⌀ 0.2 mm) intergrown with an opaque mineral observed. The garnets are always somewhat cracked, but owing to their optically isotropic nature, deformation of the crystals is difficult to detect.

*Kelyphitization of the garnet.* — Even the freshest hand-specimens show macroscopically the development of a narrow dark-green fringe around the garnets. This *kelyphite* rim (Schrauf, 1882) is radially[1] textured, but otherwise of a very compact nature, thus preventing the determination of its mineral composition by the naked eye. Owing to its toughness, the kelyphite substance resists weathering very well, so that wart-like nodules stand out on weathered surfaces of kelyphitized garnet-peridotite. A chemical analysis of the kelyphite was given by Grubenmann (1908) (Table 3, e).

[1] In this connection the term *radialstrahlig* is frequently encountered in the German literature; this must be considered as a fine example of tautology.

Microscopical observations and X-ray analyses demonstrate that garnet is gradually replaced inwards by a *symplektitic intergrowth* of very fine, radially arranged green to greenish-brown spinel threads and relatively coarse amphibole crystals (Plate III, d). Its replacement character is also demonstrated by the fact that the pattern of rutile needles enclosed within garnet may continue without change of orientation into the symplektite. Some orthopyroxene may also be present within the symplektite, judging from the presence of a few faint reflections of its X-ray powder pattern. It should be noted that in many cases the microscopically visible radial texture of the kelyphite arises solely from the orientation of the spinel threads; the amphiboles may lack such a preferential arrangement (which diverges from the views held by Grubenmann (1908) and Dal Vesco (1953) ). Although a centripetal penetration of the garnet by the symplektite is most common, symplektitization starting around inclusions (Plate III, d) and along internal cracks was also observed. The rows of minute amphibole crystals mentioned earlier may be considered to initiate the latter kind of symplektitization, whereas the isolated amphibole-spinel aggregates may indicate a beginning of patchy garnet alteration. At the outside, i.e. just where we would expect the oldest symplektite, a coarsening of the fabric may have taken place: spinel threads recrystallized into small grains and amphibole crystals are now better individualized. Recrystallization may continue until the whole finely textured symplektite has been replaced by amphibole crystals poikiloblastically enclosing numerous spinel grains. A radial pattern of relict spinel threads commonly remains recognizable.

In the recrystallized kelyphite, *spinel* occurs as bluish-green to greenish-brown anhedral grains (⌀ up to about 50—100 $\mu$), now and then with a dark brown core. Small octahedra may also be found. A pale green and weakly pleochroic *amphibole* at the exterior of the spinel-amphibole symplektite has $+ 2V = 80°$ to $89°$ ($r < v$ distinct) and $\gamma \wedge c = 18°$ to $20°$. Although the positive optic axial angle might suggest the presence of cummingtonite (Dal Vesco, 1953, p. 262), the X-ray powder pattern rules out this possibility: it rather points to a member of the hornblende family (cf. O'Hara & Mercy, 1963, p. 276), perhaps with pargasitic affinity on account of the positive value of its 2V.

Grubenmann (1908, p. 135) already noticed that at the outside of the kelyphite another zone may appear that is especially well developed against olivine. This zone is virtually devoid of spinel and consists mainly of small crystals of *orthopyroxene* (⌀ about 80 $\mu$, + 2V about 84°, $r > v$; Plate IV, c). To explain the nature of this orthopyroxene rim we may consider the development of spinel-amphibole symplektite around olivine inclusions within garnet. Two cases are often represented: either olivine grains in direct contact with garnet, or olivine grains with an orthopyroxene border, in contact with spinel-amphibole symplektite (Plate III, d). Therefore, it is quite clear that the development of orthopyroxene rims is closely connected with the transformation of garnet into spinel-amphibole symplektite. The original margin of the garnet can be located where recrystallization of the symplektite is virtually absent (Plate IV, c). Since orthopyroxene has grown beyond the former range of the garnet, it must have developed at the expense of olivine. Kelyphitization of garnet around inclusions of clinopyroxene or opaque grains produces only spinel-amphibole symplektite, without orthopyroxene borders.

Symplektite amphibole also grows out into the matrix: even when the kelyphite proper is narrow, the amphibole may protrude very far as subhedral crystals, sometimes speckled with spinel and optically continuous with symplektite amphibole (Plate III, c). When replacing olivine it sometimes seems to "push" before itself an orthopyroxene rim, but direct contacts between amphibole and olivine, without intermediate orthopyroxene, are also found. The birefringence of amphibole crystals increases markedly where they obviously replace olivine or clinopyroxene.

Thus, starting from the original garnet border, on the one side garnet is converted into spinel and amphibole, with perhaps some orthopyroxene, and on the other side clinopyroxene, olivine, and possibly orthopyroxene, are partly replaced by amphibole protruding from the symplektite, whereas in particular against olivine — and replacing it — an orthopyroxene rim may develop.

*Chloritization of the spinel-amphibole symplektite.* — At the exterior of the kelyphite nodules, green, silvery-shining *chlorite* scales may be visible with the naked eye. Indisputable evidence of its origin may be present when chlorite occurs within the kelyphite. Plate V, c shows a large chlorite crystal which has grown across the radial pattern of a spinel-amphibole symplektite. Since this pattern is well preserved within chlorite by the arrangement of spinel grains, it is evident that chlorite replaces the symplektite. The spinel content of chlorite is significantly lower than that of the original spinel-amphibole symplektite: chlorite seems capable of "absorbing" spinel. Chlorite (⌀ 0.5—2 mm) is colourless in thin section, and polysynthetic twins parallel to {001} are ubiquitous, yielding a superficial similarity to plagioclase. The mineral is optically positive (+ 2V small, $r < v$ weak) with negative elongation and yellowish-white interference colours between crossed polarizing prisms. In one thin section (Plate V, c) some very pale brown *phlogopite* was found in parallel intergrowth with chlorite.

More common, however, are peridotites with nodular aggregates consisting entirely of subhedral chlorite blades (⌀ about 0.5 mm) with subordinate subhedral amphibole ($-2V \approx 83°$) of about the same size. These are the chlorite knobs already referred to (p. 71). Even then, their derivation from an original spinel-amphibole symplektite is made plausible by the occasional occurrence of rows of tiny spinel grains, frequently altered into limonite or opaque ore (Plate V, d). The rows cut across variously oriented chlorite crystals and thus suggest the former presence of spinel-amphibole symplektite. Three arguments, a) the observed alteration of spinel-amphibole symplektite into chlorite, with diminution of the spinel content, b) the above-mentioned relict structures within chlorite nodules, and c) the appearance of the nodules in the field (they are generally of the same size as garnets and kelyphite nodules, and likewise help to define a layering plane), contradict the view of Dal Vesco (1953, pp. 264—265) that the chlorite knobs bear no relation to either garnet or spinel-amphibole symplektite. Dal Vesco points to the absence of spinel within the chlorite nodules, but from the foregoing it is clear that this cannot be a sound argument supporting his view. It seems better to agree with Grubenmann's (1908) opinion that chlorite knobs represent altered garnets, with the qualification (cf. Grubenmann, 1908, p. 144) that the decomposition of garnet proceeded in two separate stages, with chlorite forming at the second stage from spinel-amphibole symplektite. Direct transformation of garnet into chlorite was not observed.

*Olivine* (⌀ 0.5—2 mm) is present in colourless anhedral crystals, often, like the garnet, with very irregular grain boundaries (Plate IV, b). A {010}-cleavage is

Table 3. Chemical analyses (wt %) of minerals and rocks from the Alpe Arami peridotite mass (a—k and m) and of plagioclase-peridotite from the Lanzo Massif near Turin, Italy, (l).

| | a. | b.* | c. | d. | e. | f. | g. | h. | i. | j. | k. | l. | m. |
|---|---|---|---|---|---|---|---|---|---|---|---|---|---|
| | garnet | garnet | garnet | garnet | kelyphite | chlorite | olivine | ortho-pyroxene | clino-pyroxene | garnet-peridotite | garnet-peridotite | plagioclase-peridotite | garnet-clino-pyroxenite |
| reference | (1) p. 135 | (2) no. 554 | (3) p. 275, no. A. 2 | (4) p. 276 | (1) p. 136 | (1) p. 146 | (3) p. 268, no. A. 2 (5) Table 1, no. A. 2 | (3) p. 270, no. A. 2 (5) Table 1, no. A. 2 | (3) p. 272 no. A. 2 | (1) p. 138 | (6) Table 1, no. III | (7) Pl. I, no. 1 | (6) Table 1, no. IV |
| $SiO_2$ | 41.85 | 41.85 | 41.54 | 41.30 | 38.28 | 31.02 | 40.64*** | 56.36*** | 52.48 | 43.47 | 44.18 | 43.57 | 44.07 |
| $TiO_2$ | 0.20 | 0.20 | 0.24 | 0.19 | 0.19 | tr | 0.082 | 0.10 | 0.19 | 0.15 | 0.12 | 0.10 | 0.25 |
| $Al_2O_3$ | 24.00 | 24.78 | 21.72 | 22.10 | 21.25 | 18.93 | 0.10 | 1.39 | 2.53 | 2.97 | 3.09 | 3.59 | 16.04 |
| $Fe_2O_3$ | | 2.63 | 0.68 | 11.24** | 3.12 | 0.97 | 3.01 | 1.50 | 0.53 | 4.42 | 1.00 | 3.56 | 2.67 |
| $Cr_2O_3$ | 1.09 | | 1.70 | 0.18 | 0.39 | tr | 0.023 | 0.12 | 0.88 | 0.43 | 0.35 | | 0.121 |
| FeO | 9.80 | 7.43 | 8.98 | ** | 3.44 | 1.63 | 6.33 | 4.81 | 2.14 | 4.48 | 6.92 | 5.04 | 8.02 |
| MnO | | 0.10 | 0.32 | 0.25 | | | 0.109 | 0.124 | 0.071 | tr | 0.13 | 0.11 | 0.30 |
| NiO | | | 0.03 | | | | 0.37 | 0.080 | 0.13 | | 0.27 | 0.1375 | 0.041 |
| CuO | | | | | | | | | | | | 0.0045 | |
| CoO | | | 0.003 | | | | 0.0080 | 0.0036 | 0.003 | | | 0.0043 | |
| MgO | 18.23 | 18.23 | 20.06 | 20.02 | 23.07 | 33.78 | 49.23 | 34.90 | 18.65 | 39.44 | 38.72 | 38.54 | 17.20 |
| CaO | 5.41 | 5.41 | 4.78 | 4.66 | 8.99 | 0.12 | 0.08 | 0.51 | 20.98 | 3.30 | 2.90 | 3.29 | 10.53 |
| $Na_2O$ | | | 0.08 | | | | | 0.09 | 1.03 | | 0.23 | 0.28 | 0.14 |
| $K_2O$ | | | tr | | | | | <0.01 | 0.02 | | <0.01 | | <0.01 |
| $P_2O_5$ | | | 0.013 | | | | 0.015 | 0.006 | 0.005 | | <0.005 | 0.01 | 0.009 |
| $CO_2$ | | | | | | | | | | | | 0.35 | |
| $H_2O+$ | | | | | 1.42 | 12.70 | | | | 1.87 | 1.90 | } 2.09 | 0.88 |
| $H_2O-$ | 0.10 | 0.10 | | | 0.13 | 0.63 | | | | | | | |
| total | 100.68 | 100.73 | 100.14 | 99.94 | 100.28 | 99.78 | 100.00*** | 100.00*** | 99.64 | 100.53 | 99.81 | 100.68 | 100.27 |

* revision of a.?
** total iron calculated as $Fe_2O_3$.
*** Mercy and O'Hara (1965) calculate $SiO_2$ by subtracting the sum of the other oxides from 100.00. For h. they give $SiO_2 = 56.48$, the total thus exceeding 100.00.

(1) Grubenmann (1908)
(2) Grubenmann & Hezner (1916)
(3) O'Hara & Mercy (1963)
(4) Dal Vesco (1953)
(5) Mercy & O'Hara (1965)
(6) O'Hara & Mercy (1966)
(7) Nicolas (1966)

distinct, and sometimes {100}-cleavage can also be seen. A chemical analysis (Table 3, g, after O'Hara & Mercy, 1963, supplemented with data from Mercy & O'Hara, 1965) indicates a composition of $Fo_{91}Fa_9$ (all iron considered as bivalent), which is in good agreement with the observed value of the optic axial angle $+ 2V = 88°$ ($r < v$ very weak). Brown rutile needles enclosed in olivine are somewhat shorter and wider than the needles in garnet. They measure about $15 \times 2\ \mu$ and are oriented parallel to the *b*-axis of the olivin host crystal. The presence of Ti in the needles was confirmed by a qualitative electron-microprobe analysis done by Mr. P. Maaskant (Institute of Earth Sciences, Free University, Amsterdam). Rows of fluid(?) cavities are especially frequent in rocks that underwent local alteration into talc and carbonate. The rows continue from one olivine crystal into the other, so that they are certainly of secondary origin. Some olivine grains bear signs of mechanical deformation (undulatory extinction and lamellae approximately parallel to {100}), but most crystals exhibit only one extinction position. Serpentinization affects olivine in the usual manner: along internal cracks and grain boundaries a fibrous serpentine variety with negative elongation and pleochroism from light brown ($\alpha'$) to light green ($\gamma'$) is developed ($\alpha$-chrysotile), mostly perpendicular to the wall; the original crack is still marked by a narrow streak of magnetite. An indented front of the serpentinization (Legoux, 1960) starting from a {100}-cleavage plane may be observed. Presumably as a result of finely dispersed limonite produced by the decomposition of magnetite, the serpentine mineral sometimes shows a deep brown colour and is virtually non-pleochroic.

*Orthopyroxene*[1] grains (⌀ 0.2—1.5 mm) are only slightly smaller than olivine (we of course disregard orthopyroxene related to kelyphitization, which has already been described). Although roughly prismatic crystals may be encountered, they are almost invariably bounded by irregular surfaces. Against olivine a development of {110}, {100}, and {010} can sometimes be seen. Its composition (Table 3, h) is $En_{91}Fs_9$, which is in accordance with the normally observed value of the optic axial angle $+ 2V = 82°$ ($r > v$ weak). One thin section of garnet-peridotite (AR49-A1), however, gave constantly larger values of $+ 2V$, i.e. about 89°. Orthopyroxene has a very light brown colour in thin section, and is not pleochroic. Cleavages along {110} are well developed, some grains also show {010}- and/or {100}-cleavage, with occasional *Schiller* inclusions along one of these planes.

Often the orthopyroxene crystals exhibit narrow lamellae parallel to {100} (Plate IV, b). The extinction angle of the lamellae, measured against the trace of {100} of the orthopyroxene host in sections at right angles to $\alpha_{OPX}$, is about 13°. Accurate determination is impeded by their small size (width about 1 $\mu$), but the angle is certainly less than the extinction angle of 40° reported for clinopyroxene lamellae exsolved parallel to {100} of orthopyroxene, in sections perpendicular to $\alpha_{OPX}$ (Hess, 1960). Moreover, there is no evidence for a difference in birefringence between the lamellae and the orthopyroxene host. X-ray scanning profiles for Ca and Fe, done with an electron microprobe (Mr. P. Maaskant), and taken at right angles to the trace of the lamellae did not reveal any chemical heterogeneity. The observations confirm the results of Henry (1942), who showed, on the basis of X-ray oscillation photographs, that similar lamellae in orthopyroxene also consist of orthopyroxene, with its *c*-axis inclined at about 7° to that of the main crystal in the {010}-plane. According to Henry, there is some graduation in this angle, however, and it may amount to as much as about 15°.

Small olivine grains enclosed in orthopyroxene are met with as often as the reverse situation. In some cases deformation has given rise to a plastic bending of the grains, causing undulatory extinction and kink bands mostly subparallel to {001} (Plate IV, b). Orthopyroxene alters into serpentine or bastite. Local decomposition into talc was also observed.

Crystals of a colourless or very pale green, non-pleochroic *clinopyroxene* variety may attain rather large sizes (⌀ 0.4—5 mm). They are often somewhat elongated parallel to the *c*-axis, but generally do not show well-developed crystal faces in thin section. Results of a chemical analysis are quoted in Table 3, i. Such pyroxenes are usually called chrome diopsides. Optical properties of the clinopyroxene are: $+ 2V = 60°$ ($r > v$ weak), $\gamma \wedge c = 39°$. {110}-, {010}-, and {100}-cleavages may be observed. Frequently, a very fine striation can be seen parallel to {010}. Inclusions of olivine are quite common. Orthopyroxene rims may be present in oriented intergrowth with clinopyroxene, with $c_{OPX} // c_{CPX}$ and $b_{OPX} // b_{CPX}$.

*Alteration of the clinopyroxene into amphibole and spinel.* — Although decomposition of clinopyroxene into amphibole is a well-known phenomenon, the simultaneous separation of spinel seems to be less common. A short description is therefore of some interest, the more so because no attention has been paid to it previously in the literature about Alpe Arami. The process is clearly depicted in Plates IV, d and V, a. Greenish-brown to brown grains and threads, the latter frequently in short dendritic patterns, are developed within variously oriented colourless amphiboles penetrating from all sides into a clinopyroxene crystal. Other thin sections display alteration of clinopyroxene along laminae or in a patchy way; in these cases the secondary amphibole is optically continuous throughout the clinopyroxene host. The coloured mineral could be determined as spinel with the electron microprobe. Its chromium content is conspicuous (Plate V, b). The reason why spinel separates remains obscure; clinopyroxene is low in $Al_2O_3$ (2.53 % in Table 3; microprobe analysis of the crystal of Plate IV, d gave an even lower value: 1.9 %). This interesting point has not been elaborated because it lies somewhat outside the scope of the present investigation. The quantity of spinel

[1] The designation of the crystallographic axes is taken in accordance with Tröger (1959): $a = \beta$, $b = \alpha$, $c = \gamma$; the most prominent prismatic cleavage is referred to as {110}.

originating from the clinopyroxene-amphibole alteration is far less than that from the symplektitization of garnet. The optical properties of the amphiboles are also different. In section AR32, the values of 2V and $\gamma \wedge c$ found for amphiboles at the outside of kelyphite are: + 2V = 87.8°; 85.8°; 85.0°; 87.2°; 86.4°; $\gamma \wedge c$ = 20.5°; 18°; 18°; 16.8°. So: + $\overline{2V}$ = 86° ($r < v$ distinct) and $\overline{\gamma \wedge c}$ = 18° (cf. p. 77). Amphiboles originating from clinopyroxene in the same section (Plate IV, d) showed: — 2V = 84.5°; 79°; 80.5°; 82.2°; 79°; $\gamma \wedge c$ = 17°; 16°; 15°; 15°; 12°. Therefore: — $\overline{2V}$ = 81° ($r > v$ weak) and $\overline{\gamma \wedge c}$ = 15°. A difference in chemical composition between the two types of amphiboles may therefore be inferred. It is conceivable that amphibole developing during kelyphitization of garnet contains much more $Al_2O_3$ than amphibole originating from clinopyroxene decomposition. The former presence of clinopyroxene can still be demonstrated where we find amphibole aggregates containing spinel grains and threads in a typical dendritic fashion (see Plate V, a), the limitation of the part of the aggregate clouded by spinel often being remarkably straight; confusion with the radially textured spinel-amphibole symplektite is generally out of the question. The occurrence of amphibole beyond the margin of the original clinopyroxene again demonstrates that this mineral is also capable of replacing other constituents of the matrix.

A few notes should be added here: sometimes *orthopyroxene* with spinel inclusions also seems to have replaced clinopyroxene, and spinel may even already be developed within clinopyroxene itself. On the other hand, alteration of clinopyroxene into amphibole was also found without separation of spinel. No subsequent development of chlorite was observed within the amphibole-spinel aggregates derived from clinopyroxene.

Sparsely occurring *opaque minerals* were not studied extensively. Ilmenite, sometimes intergrown with greenish-brown spinel, and sulfides such as pentlandite were found to be present. Magnetite developing during serpentinization has already been mentioned.

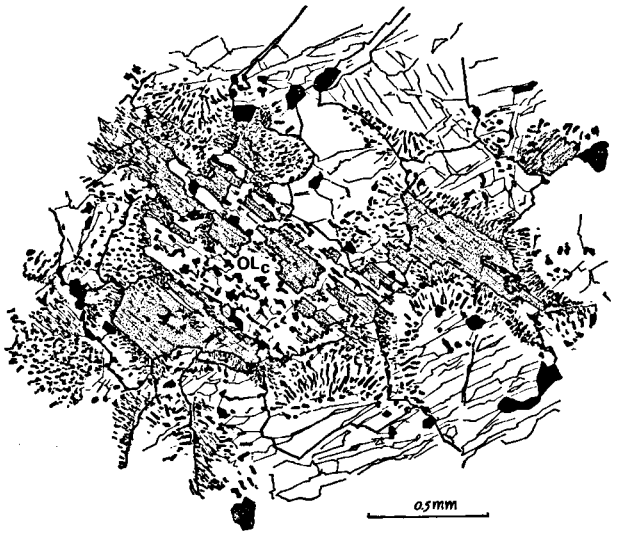


Fig. 8. A large grain of titanclinohumite (stippling) has been partially replaced by olivine and ilmenite. Central olivine grain $OL_C$ is regularly intergrown with titanclinohumite. Another small grain of titanclinohumite in the upper right corner. Thin section GO1-A.

Of special interest is the occurrence of *titanclinohumite*, which is described here for the first time from the Gorduno region. This mineral was found in a loose block of garnet-peridotite in the torrent near Gorduno (no. GO1, Fig. 2); it could therefore have originated from the garnet-peridotite lens near Stuello (p. 70). The rock was collected in collaboration with Dr. W. Grigel, Saarbrücken. It is a garnet-clinopyroxene-peridotite, with little or no orthopyroxene. In the hand-specimen, garnet (somewhat kelyphitized) is orange-red, in contrast with its dark violet-red colour in the normal orthopyroxene-bearing garnet-peridotites; clinopyroxene is greenish white. Titanclinohumite is only visible under the microscope; it occurs very sparsely in orange-yellow grains (⌀ 0.1—1.5 mm, Fig. 8). Its determination was confirmed by the X-ray powder pattern (clinohumite); strong dispersion of the optic axes and of the extinction points to the presence of a considerable amount of Ti. A universal-stage study revealed certain facts which, although they are only distantly related to the subject of this paper, are interesting enough to report.

*Optical and physical properties of titanclinohumite.* — The structure of clinohumite proper was determined by Taylor & West (1928). We shall take their monoclinic unit cell as a starting-point for the present discussion, but we shall rename its elements in accordance with Deer, Howie, & Zussman (1962, p. 49); thus $a_0$ = 13.68 Å, $b_0$ = 4.745 Å, $c_0$ = 10.27 Å, and $\beta$ = 100°50′ (Fig. 9, b). The olivine- and the $Mg(OH, F)_2$-layers of the structure are now parallel to (100). Consequently, oriented intergrowths of clinohumite and olivine can be expected to have this plane preferentially as a contact plane, and $a_0$ = 4.755 Å and $b_0$ = 10.21 Å of olivine will lie parallel to $b_0$ and $c_0$ of clinohumite respectively in that case (Fig. 9, a).

An unpleasant property of the clinohumite unit cell is that the angle between ($\bar{1}02$) and (100) is 100°48′, which within two minutes is equal to the angle between (001) and (100), i.e. $\beta$ = 100°50′. Therefore, the early crystallographers were able to describe the various crystal faces with reference to the orthorhombic system. But at present the problem is to correlate the classical orthorhombic setting (including the orientation of the optical indicatrix) with the unit cell of Taylor & West.

Lacroix (1893) used orthorhombic axes with $a:b:c$ = 1.08028 : 1 : 5.65883 (after vom Rath). It follows from the position of the optical indicatrix (Fig. 9, c) that Lacroix's $b$-axis (and $\gamma$ of the indicatrix) correspond to the $b$-axis of clinohumite chosen in Fig. 9, a and b. Lacroix's (101)- and (001)-planes include an angle of 100°48′. This angle may be equivalent to the angle between (100) and (001) in Fig. 9, a (*possibility 1*). Then, the ratio $a/\sqrt{(a^2+c^2)}$ = cos 79°12′ (Lacroix) must be related in a simple way either to $a_0/c_0$ or to $c_0/a_0$ of the unit cell of Taylor & West. It is found that $4 \times a/\sqrt{(a^2+c^2)}$ (Lacroix) $\approx c_0/a_0$ (Taylor & West). Hence, (001) and (101) of Lacroix become (100) and (001) of Fig. 9, a, respectively. The principal axes of the optical indicatrix thus obtained are depicted in Fig. 9, a as $\alpha_1$, $\beta_1$, and $\gamma_1$. However, we may also consider *possibility 2*, i.e. that Lacroix's (001) and (101) are equivalent to (100) and ($\bar{1}02$) of Fig. 9, a, respectively, because of the pseudo-symmetry of (001) and ($\bar{1}02$). For the latter case, the orientation of the indicatrix is indicated by the positions of $\alpha_2$ and $\beta_2$, $\gamma_2$ remaining parallel to $\gamma_1$.

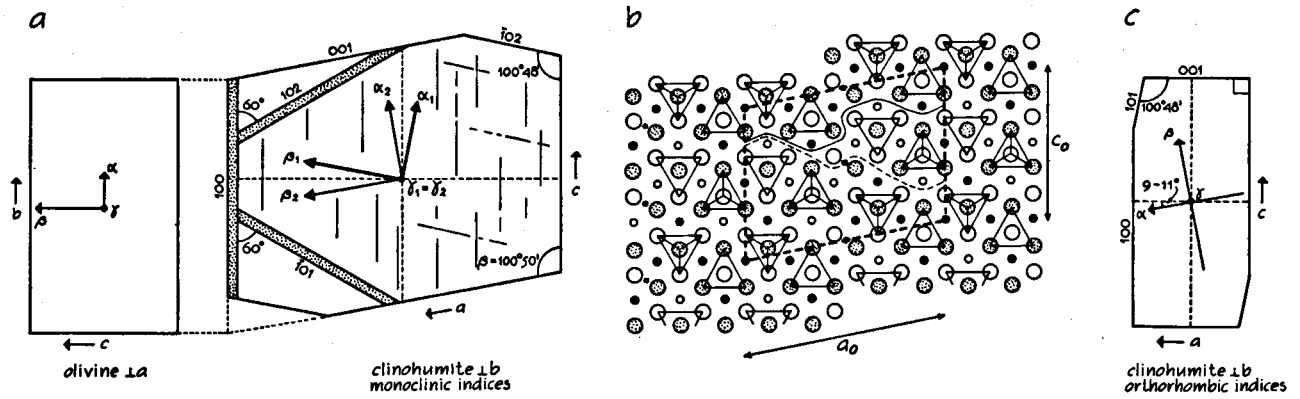


Fig. 9. a. Orientation of regular intergrowth between olivine and clinohumite. Orientation of clinohumite as in Fig. 9, b. Possible twin lamellae stippled; {$\bar{1}$02}-cleavage hypothetical. $\alpha_1$, $\beta_1$, and $\gamma_1$ indicate the correct position of the optical indicatrix according to the present author. b. Structure of clinohumite ⊥*b* (after Taylor & West, 1929, Fig. 4, e; designation of the crystallographic axes in accordance with Deer, Howie, & Zussman, 1962, p. 49). c. Clinohumite in rhombic setting after Lacroix (1893, p. 120, Fig. 2).

It is interesting to note that the textbooks of Tröger (1959, no. 126b) and Deer, Howie, & Zussman (1962, p. 49) favour position (2) of the indicatrix, whereas Winchell (1951, 4th ed., 2nd printing, Fig. 408) gives position (1), provided we interchange (001) and (100) in his Figure. Of course, only one of these representations can be the right one. The formula for the transformation from orthorhombic to monoclinic indices as given by Taylor & West (1928, Table III) leads to position (1), but because no optical study was included in their paper and the relation between the orthorhombic indices of Taylor & West and those of Lacroix is not clear *a priori*, we may consider the discussion still open.

Lacroix and others describe cleavage and polysynthetic twinning along (001), and twinning also along (103) and ($\bar{1}$03). Translated into the co-ordinates of Fig. 9, a, these planes are respectively (10$\bar{0}$), (102), and ($\bar{1}$01) for the first transformation, and (100), ($\bar{1}$01) and (102) when applying the second one. The three types of twins found in nature are in very good accordance with the possibilities provided by the crystal structure (Fig. 9, b), but they do not offer a clue for the choice between (1) and (2).

Returning now to the titanclinohumite of sample GO1, we observe (Fig. 8) that the mineral is being replaced by olivine (+ 2V = 88°), with separation of ilmenite. Within titanclinohumite ilmenite development starts with exsolution of thin lamellae along planes perpendicular to $\gamma$ of the optical indicatrix, i.e. along {010}. In Fig. 8 the orientation of most olivine grains containing an abundancy of ilmenite is unrelated to that of titanclinohumite. The only exception is the central olivine grain $OL_C$. The narrow olivine lamellae (crowded with ilmenite) within titanclinohumite, which belong to the central olivine grain, are oriented perpendicular to $\beta$-olivine and approximately perpendicular to $\beta$-titanclinohumite. The $\gamma$-axes of the two minerals are exactly parallel. This situation is in harmony with Fig. 9, a and also with the observations of Tilley (1951, Fig. 9) and others. Within the titanclinohumite grain a {100}-cleavage can be observed parallel to the olivine lamellae, but no twinning is present. The extinction angle $\alpha \wedge c = 4°$—5° is lower than is generally reported for clinohumite.

Universal-stage study reveals another imperfectly developed cleavage plane belonging to the zone [010]; this plane is almost parallel to $\beta$ and may be near either {001} or {$\bar{1}$02}. The crystal structure appears to favour a {$\bar{1}$02}- above a {001}-cleavage (Fig. 9, b), because in the latter case two more Mg-O bonds must be cut through, so that under the assumption that the observed second cleavage is indeed {$\bar{1}$02}, we may now decide that transformation (1) is more likely than (2). It would be interesting to check this point by means of a combined X-ray and optical study of a single crystal.

Titanclinohumite in sample GO1 is distinctly pleochroic with $\alpha$ orange, $\beta$ orange yellow, and $\gamma$ pale yellow; absorption $\alpha > \beta \geqslant \gamma$. Its optic axial angle is: + 2V ≈ 71°. Perpendicular to an optic axis, the isogyre shows a green rim on the concave side and a violet rim on the convex side in the 45° position. It would be imprudent to conclude that dispersion is $r > v$, because Carpanese (1933), who describes the same optic-axis figure, showed that the dispersion of titanclinohumite is a quite complicated phenomenon: the optic axial angle is smallest for green or blue-green light, larger for orange-red, and still larger for indigo light. Comparable complications arise for the extinction angle $\alpha \wedge c$ (Carpanese, *op. cit.*). The present author also noticed dispersion of the extinction in sections perpendicular to $\gamma = b$, but he did not pursue the investigation of this point, which would stringently require the use of a number of monochromatic light sources.

Apart from ilmenite lamellae along {010}, the crystals are also crowded with needles (rutile?) approximately parallel to the *c*-axis of titanclinohumite.

Titanclinohumite has been described in a pyrope-serpentinite from the Kokchetavsky Massif (Central Kazakhstan) by I.A. Efimov (1961) (after Voskresenskaya, *et al.*, 1965). It is also recorded as accessory round grains (⌀ up to 10 mm) from a Siberian kimberlite breccia, along with olivine, phlogopite, pyrope, ilmenite, magnetite, perowskite, apatite, and Cr-diopside. The main mass of the kimberlite consists of serpentine (Voskresenskaya, *et al.*, *op. cit.*). A discussion of some other occurrences of titanclinohumite in the Swiss, Italian, and Austrian Alps will be given below (p. 87).

The presence of *zircon* in the titanclinohumite-bearing sample is worth mentioning. It occurs abundantly in small rounded grains (⌀ about 70 $\mu$) enclosed in garnet, clinopyroxene, and olivine (Plate IV, a). Zr was demonstrated by microprobe analysis. The mineral was also found in some peridotite samples from the Alpe Arami mass as rounded but sometimes also as broken grains.

*Spinel*, *amphibole*, and *chlorite* have already been mentioned in previous sections pertaining to the decomposition of garnet and clinopyroxene, and a short account will suffice here.

*Spinel* is always too small to be recognized in the hand-specimen. It occurs mainly in connection with alteration of garnet and clinopyroxene, in one instance perhaps as a primary inclusion within garnet (p. 76). Furthermore, it may be sparsely dispersed in tiny crystals throughout the whole rock (except garnet) without bearing a clear-cut relation to the described mineral transformations. Its colour seems to vary rather unsystematically between green and brown.

Dark green to greenish-black *amphibole* crystals (⌀ about 3 mm) may be macroscopically visible. Their protrusion from kelyphite rims into the olivine-orthopyroxene-clinopyroxene matrix (p. 77) can often be observed with the naked eye. The macroscopic colour of amphibole may also tend to a somewhat lighter green approaching the emerald green of clinopyroxene.

We have already stated that kelyphitization of garnet and alteration of clinopyroxene both involve amphibole development, and have demonstrated for one case (p. 80) the difference in optical properties of the two amphibole types in the same thin section. Amphibole also forms from the matrix surrounding the kelyphite (see above). However, we may not ignore the fact that — as in the case of spinel — there are many crystals whose origin cannot be ascribed unequivocally to either of these processes.

A serious difficulty offered by the amphiboles is that their chemical composition cannot be determined solely from optical data. An electron-microprobe study might throw more light on the causes of variation of optical properties, such as are often displayed even by single amphibole crystals in which a zonary character can be revealed by differences in birefringence (cores generally more weakly birefringent than borders), colour and pattern of inclusions (cores may be light green and weakly pleochroic, and contain numerous parallel needle-like inclusions (rutile?, spinel?), whereas borders are colourless and free of inclusions), and optic axial angle (cores usually show a larger value of $-2V$ than borders). A chemical investigation is beyond the scope of this paper, however.

Nonetheless, although I am aware that use of the term "amphibole" certainly involves an oversimplification, I do not consider it very useful, at this stage of our knowledge, to distinguish between amphibole varieties that are neither chemically nor texturally well defined, the more so since their optical properties grade over into one another.

A subhedral to euhedral development of the amphibole crystals is quite common. Cleavages along {110} and {010}, and possibly other cleavages in the [001]-zone, are present. Twinning — partly polysynthetic — of amphibole according to {100} has been observed, as well as alteration into serpentine.

*Chlorite* has been described in some detail (p. 77). We may remark — as for spinel and amphibole — that although a direct origin from spinel-amphibole symplektite can be proved for most of the chlorite, crystals simply disseminated between other components of the rock are also found (Plate VI, a). A chemical analysis of chlorite from a chlorite-rich band in the Alpe Arami peridotite (after Grubenmann, 1908), is quoted in Table 3, f.

### *Mineral parageneses*

After having examined the constituent minerals of the peridotites we must sort out the numerous data to obtain an idea of which combinations of minerals represent stable associations. A brief review of some of the petrographical arguments may be useful: a) if a mineral A alters into B, then A and B do not belong to the same paragenesis; b) minerals occurring together in the same hand-specimen or thin section are likely to belong to the same paragenesis; c) if minerals A and B possess sharp contacts without mutual reaction phenomena they probably belong to the same paragenesis; d) if anywhere in a thin section the incompatibility of A and B can be demonstrated, the same most probably holds for all grains of compositions A and B in this section. It will be clear that there are contradictions in these arguments (which demonstrates their rather subtle character): partial decomposition of a mineral A into B leads to different parageneses within the same hand-specimen, and A and B may nonetheless show sharp contact planes. Therefore, these arguments do not have equal value; a) may override b) and c). But even a) is not as foolproof as we might wish. Consider, for instance, the partial alteration of olivine into orthopyroxene as a result of kelyphitization (p. 77); this does not imply that olivine and orthopyroxene are unstable together, as would be concluded from argument a). Classical petrography deduces from the observed phenomenon the incompatibility of the *pair* garnet + olivine at a certain moment in the evolution of the rock, not necessarily the instability of garnet and olivine individually.

The exact mechanism of the formation of such synantetic minerals is difficult to grasp without a profound knowledge of the chemical composition of all minerals involved. It is conceivable, for instance, that the $SiO_2$ liberated during decomposition of garnet into spinel-amphibole-symplektite (Vogel, 1967, p. 170), reacts with adjoining olivine to yield orthopyroxene until all the $SiO_2$ has been consumed. However, reactions involving the mobilization of other oxides can be envisaged equally well. In any case, only the

Table 4. Modal analyses (vol. %) of peridotites from Alpe Arami.

| thin section | a. garnet-peridotite 1* | b. garnet-peridotite 2* | c. garnet-peridotite GN1-E1 | d. garnet-peridotite AR37-A1 | e. garnet-peridotite AR26-B1 | f. spinel-amphibole-peridotite AR41-A1 | g. chlorite-peridotite AR17-A2 |
|---|---|---|---|---|---|---|---|
| garnet | 8.0—16.5 | 15 | 13 } 16 | 2 } 3 | 6 } 11 | | |
| kelyphite (spinel-amphibole symplektite) | 4.0— 5.0 | | 3 } | 1 } | 5 } | 5 | |
| olivine | 56.5—81.0 | 40 | 49 | 52 | 61 } 61 | 68 } 68 | 60 |
| orthopyroxene (± amphibole) rims replacing olivine | | | | | tr } | tr } | |
| orthopyroxene | 2.0—11.5 | 15 | 10 | 26 | 14 | 17 | 13 |
| clinopyroxene | } | 25 | 18 | 8 | 5 | | |
| amphibole | 3.0—11.5 | 5 | 6 | 10 | 9 | 2 | 13 |
| spinel | | | | | | tr | |
| chlorite | | | | | | tr | 6 |
| opaque minerals | 0.5— 1.0 | | 1 | tr | tr | 1 | tr |
| serpentine | | | | tr | tr | 7 | 8 |
| talc | | | | 1 | | | |

* 1: Dal Vesco (1953, p. 256)
2: O'Hara & Mercy (1963, p. 265)

proportion of olivine to orthopyroxene changes in favour of the latter mineral.

Generally speaking, the most strongly conflicting evidence arises when in one part of the thin section a mineral B develops from A and elsewhere, A and B appear to possess sharp contacts without reaction phenomena. Some subjectivity in geological reasoning thus seems unavoidable, but a qualitative study of the mineral content in a large number of thin sections (about 100) may be considered to yield sufficiently reliable results.

*Garnet-peridotites.* — Peridotites displaying a relatively slight degree of kelyphitization of garnet are comparatively rich in unaltered clinopyroxene along with olivine and orthopyroxene. The idea that ol + opx + cpx + gar constitutes a stable assemblage is corroborated by the fact that the minerals concerned may possess sharp contact planes. This means that we are dealing here with the garnet-peridotite assemblage of Rost (1963) and Green & Ringwood (1963) (p. 75). To be considered as primary accessories are : opaque ore (ilmenite, also sulfides?) and zircon. The position of the rare titanclinohumite (p. 80) and the one primary(?) brown spinel grain (p. 76) is not clear. Because of its strong decomposition (within a moderately kelyphitized garnet-peridotite) into olivine and ilmenite fitting well into the garnet-peridotite assemblage texturally and mineralogically, titanclinohumite may even belong to a paragenesis older than the garnet-peridotite association. In any case the mineral is prekelyphite, because olivine of the olivine-ilmenite aggregates representing the products of titanclinohumite transformation, may subsequently be replaced by kelyphite amphibole. The results of chemical analyses of garnet-peridotites are given in Table 3, j and k, and modal analyses (partly after Dal Vesco, 1953 and O'Hara & Mercy, 1963) in Table 4, a—e. We repeat that garnet-peridotites occur only in two narrow zones within the lens of Alpe Arami.

*Spinel-amphibole-peridotites.* — Decomposition of garnet into spinel and amphibole (together with the formation of amphibole and orthopyroxene from the matrix) seems to go hand in hand with the alteration of clinopyroxene into amphibole ± spinel ± orthopyroxene. Olivine and orthopyroxene remain present in large quantities. Therefore, we deem likely the existence of a spinel-amphibole-peridotite paragenesis: ol + opx + amph + sp (cf. Green & Ringwood, 1963). As judged from one thin section showing a large amount of unaltered clinopyroxene but only decomposed garnet, the alteration of clinopyroxene may have lagged somewhat with respect to garnet symplektitization. It is therefore reasonable to add ± clinopyroxene to the paragenesis. This is supported by the fact that some garnet-peridotites show only slightly altered clinopyroxene, whereas symplektitization of garnet has already given rise to the development of much amphibole. However, the material studied is in-

sufficient to warrant a further subdivision of the spinel-amphibole-peridotite paragenesis. The crucial point is our scanty knowledge of the amphibole compositions. It may well be that in a first stage spinel and amphibole (+ 2V) derived from garnet coexist with clinopyroxene, olivine, and orthopyroxene, and that afterwards the clinopyroxene in the latter assemblage is replaced by amphibole (— 2V) and spinel. A modal analysis of a spinel-amphibole-peridotite is given in Table 4, f.

*Chlorite-peridotites.* — In rocks in which chloritization of the spinel-amphibole symplektite is complete, olivine and orthopyroxene do still occur, together with amphibole, but clinopyroxene is no longer present. Thus, the paragenesis: ol + opx + amph + chl, i.e. the chlorite-peridotite paragenesis (without clinopyroxene) of Rost (1963), has been demonstrated. Phlogopite was found as a subordinate constituent of this paragenesis (p. 77). Table 4, g provides a modal analysis of a chlorite-peridotite from Alpe Arami. The present author has made no attempt to distinguish on the map between spinel-amphibole-peridotite and chlorite-peridotite. Amphibole aggregates may contain spinel grains in the typical pattern pointing to their derivation from clinopyroxene (p. 79). It seems probable that the spinel grains represent metastable relicts from the preceding stage.

It is remarkable indeed that the described mineral transformations may be of a very local nature: instances are even encountered in which the whole sequence from garnet- to chlorite-peridotite can be observed within the same thin section. Reaction rates were probably imperceptly slow where aqueous solutions could not penetrate, and interchange of matter between different domains must have generally been very restricted. The variations in birefringence within a single amphibole crystal, depending on which mineral it replaces (e.g. garnet or olivine) have already received attention (p. 77). One excellent example of a metastable relict was found: a small garnet (⌀ 100 $\mu$), very pale pink in thin section, and bearing no sign of symplektitization, enclosed in olivine within a chlorite-peridotite containing chlorite aggregates with only sporadically one or two spinel grains. Similar garnets (⌀ 200 $\mu$) without a kelyphite rim, within olivine, were also observed in the titanclinohumite-bearing garnet-peridotite already described (p. 80). The larger garnets in the same rock, however, are invariably surrounded by a symplektite zone of fair size (Plate IV, a). Thus, small garnet grains may survive decomposition as armoured relicts within olivine, notwithstanding the incompatibility of the two minerals under conditions of retrogressive metamorphism. The same holds in reverse for olivine enclosed within garnet: the olivine-garnet contact around an olivine inclusion may still be unaffected by mutual reaction, whereas at the outside of the garnet, spinel-amphibole symplektite and orthopyroxene are found between the garnet and the olivine (p. 77).

*Metamorphic facies*

Fortunately, the three mineral parageneses deduced from petrographical observations fit into the graph shown in Fig. 7, which was constructed by means of experimental data, so that their provisional allocation to well-known facies of metamorphism is possible, for instance by superposing den Tex's (1965, Fig. 6) graph on our Fig. 7. It then appears that the garnet-peridotite assemblage belongs to the eclogite facies, which is in accordance with the opinion of, for instance, Sobolev (1962), and O'Hara & Mercy (1963). The spinel-amphibole-peridotite assemblage may be correlated with the granulite facies (O'Hara, 1967), and the chlorite-peridotite assemblage with the amphibolite facies (Rost, 1963).

*Mylonites*

Two interesting examples of mylonitized peridotite were found. AR49 (Plate VI, c) is a garnet-peridotite with a mortar structure; in a narrow zone (width 2—3 mm) the small- to medium-grained peridotite (grain size about 1 mm) has been rubbed down to minute grains (⌀ about 100 $\mu$). The original minerals belong principally to the garnet-peridotite association: olivine, ortho-and clinopyroxene, all showing signs of mechanical deformation, and somewhat kelyphitized garnet, with development of a little green amphibole (which may also be strained) and spinel outside the area of the original garnet crystals. Within the mylonitized zone, however, the spinel-amphibole-peridotite assemblage appears to be represented, with unstrained olivine, orthopyroxene, amphibole, often in aggregates representing altered garnets, spinel (enclosed within amphibole, but also within orthopyroxene and olivine) and some clinopyroxene grains, along with a few strained porphyroclasts of orthopyroxene and olivine. It is therefore highly probable that this phase of mylonitization took place during — perhaps at the end of — the formation of spinel-amphibole-peridotite from garnet-peridotite, i.e. under granulite-facies conditions. The development of a mortar structure and narrow mylonitic bands was not found only in specimen AR49; in fact, most garnet-peridotites bear weak signs of the same type of deformation, albeit not in such a convincing manner. AR14 is a mylonite of quite another type (Plate VI, d). Porphyroclasts consist of olivine (⌀ 0.5—1 mm) with deformation lamellae and undulose extinction, orthopyroxene, and amphibole, both in single crystals and aggregates often crowded with spinel and suggesting the former presence of clinopyroxene. The schistose matrix curving around the porphyroclasts is composed of olivine (⌀ about 80$\mu$), orthopyroxene, amphibole, and chlorite (—elongation, {001}-twinning), with some opaque matter and a few spinel grains. The formation of this mylonite must therefore be correlated with the development of chlorite-peridotite; in view of the occurrence of amphibole porphyroclasts, the original rock might have been a spinel-amphibole-peridotite.

*Serpentine, carbonate, and talc*

Serpentinization is of only local importance and acts upon all peridotite varieties alike. The occurrence of almost unserpentinized chlorite-peridotite proves that, contrary to the opinions of Grubenmann (1908) and Dal Vesco (1953), no relation exists with the decomposition of garnet; the opposite impression created by Table 4 is merely accidental. Serpentinization is obviously very recent, because it affects nearly all peridotite minerals, including those of the chlorite-peridotites: olivine, ortho- and clinopyroxene, and amphibole give way to serpentine[1], whereas magnetite originating during the serpentinization may intrude into chlorite along its cleavage planes (cf. the *Chlorit-Erz-Pakete* of Rost, 1961). More details about serpentine are to be found under *olivine* in the mineralogical section (p. 79).

Strong tectonic movement does not cause serpentinization: even the matrix in chlorite-peridotite-mylonite AR14 (Plate VI, d) is only slightly serpentinized. To the contrary, serpentinization seems to proceed under static conditions. The pattern of rutile needles continues undisturbed from fresh olivine into serpentine replacing olivine, so that there was not even a large increase in volume. The different parts of an olivine crystal still retain the same optical orientation, even when large quantities of serpentine separate the various relicts.

Abundant formation of carbonate and talc occurred only in discrete veins, some of which reach a thickness of some centimetres. These veins (which are found in all peridotite varieties) are orange-brown in the field. The carbonate mineral is probably magnesite, because of the absence of Ca demonstrated by a qualitative chemical analysis (cf. Hezner, 1909). Antigorite also occurs in the carbonate-talc veins, sometimes grown on chlorite as described by Rost (1961, Fig. 4). Carbonate and talc appear sparsely in peridotites without a direct relation to veins. Carbonate develops readily parallel to the basal cleavage of chlorite (Plate V, d), and talc is often in the process of replacing orthopyroxene. Serpentinization and related phenomena took place under greenschist-facies conditions.

*B—Garnet-pyroxenites, pyroxenites, hornblendites, and garnet-rocks*

In defining the $S_L$-plane (p. 71) it was stated that the primary minerals are not homogeneously distributed throughout the peridotite: almost completely mono- and bimineralic layers are frequently encountered. From an academic point of view these may be considered as separate rock types, but we shall deal at some length with only a few of their characteristics, because most of the mineralogical and petrographical properties of these rocks can easily be deduced from the foregoing description of the peridotites.

[1] It is a matter of regret that Dal Vesco (1953) did not make a sharp distinction between serpentine and chlorite (the crystals designated as serpentine in his Figs. 17 and 18, for instance, could preferably be called chlorite).

In specimen AR30A, a *garnet-pyroxenite* layer (about 2 cm thick) differs from the surrounding garnet-peridotite by the absence of olivine and a relatively low orthopyroxene content. The garnets are a pale orange-red, contrasting with the dark violet-red of the peridotite garnets. Clinopyroxene is light green in the hand-specimen, and macroscopically visible amphibole is greenish-black. Decomposition of garnet into amphibole is attended only by a minor development of spinel, but other samples of garnet-pyroxenite show its normal alteration into spinel-amphibole symplektite and the subsequent transformation of the latter into chlorite. Amphibolization of clinopyroxene does not produce any spinel, unlike the situation in adjoining peridotite. Rather large rutile grains (⌀ about 100 $\mu$) were seen only in the garnet-pyroxenite layer of AR30A. Garnet-pyroxenites sometimes carry minor amounts of olivine; the orthopyroxene content of some samples may outweigh the quantity of clinopyroxene present. Alteration of orthopyroxene and olivine typically produces a mica-like, brown pleochroic mineral displaying at most second-order interference colours (vermiculite?). Results of the chemical analysis of a garnet-clinopyroxenite from Alpe Arami, after O'Hara & Mercy (1966, p. 296), are given in Table 3, m.

The marginal *clinopyroxenite* and *hornblendite* at the western extremity of the ultramafic lens (see geological map — Enclosure I) are somewhat larger masses of rocks also found as layers within the peridotite itself. Patchy alteration of clinopyroxene into amphibole is ubiquitous, and amphibole is often distinctly zoned with moderately birefringent green cores and more strongly birefringent colourless borders. It is not unlikely, therefore, that hornblendites are the retrogressive equivalents of (garnet)-clinopyroxenites.

Virtually monomineralic layers of garnet may be called *garnet-rocks*. AR21, from a 7 cm wide layer in spinel-amphibole-peridotite, is a typical example. Garnet is rimmed along internal cracks and/or grain boundaries (impossible to distinguish by crystal-optical methods because of the optical isotropy of garnet) by a comparatively coarse-grained spinel-amphibole symplektite with clearly individualized green spinel threads (thickness about 5 $\mu$). Abundant opaque matter (⌀ 100—300 $\mu$) was identified as ilmenohematite showing exsolution into an ilmenite- and a hematite-rich phase (P. Maaskant, personal communication). It is commonly intergrown with green spinel (⌀ 80—160 $\mu$) (Plate VI, b). Zircon and apatite occur as accessories. The ilmenohematite-spinel grains are hardly ever found in direct contact with garnet, a small intercalation of spinel-amphibole symplektite is almost always observed. This poses a problem as to the paragenetic relations: although garnet and zircon appear to belong to the primary assemblage and amphibole and at least part of the spinel to a secondary association, the observations related to the ilmenohematite-spinel grains can be explained in either of two ways: 1) the ilmenohematite-spinel forms part of the primary assemblage; the

absence of direct contacts with garnet would then be accounted for by the assumption that symplektitization of garnet started preferentially along these contact planes, and two generations of green spinel would have to be considered. 2) the ilmenohematite-spinel develops as a result of symplektitization and therefore belongs to the secondary assemblage. To decide between these two possibilities, we assume that the composition of the garnet differs little from that of the peridotite garnet. In this respect we may point to the results of a chemical analysis (Dal Vesco, 1953, p. 276; see our Table 4, d) of garnet from a garnet-rich band possibly comparable to the garnet-rock concerned here. Since the alteration of peridotite garnet causes the development of neither opaque minerals in such considerable quantities nor spinel (intergrown with opaque matter) in crystals which are relatively large in view of the low degree of symplektitization present, we are forced to assume that ilmenohematite-spinel belongs to the primary assemblage.

With admixture of ortho- and/or clinopyroxene, the garnet-rocks grade into the garnet-pyroxenites mentioned earlier. In one case (AR51) green spinel seems to be co-stable with garnet, thus suggesting a mineralogical affinity to the pyrope-ceylonite-pyroxenites (garnet-bearing ariégites) of Peters & Niggli (1964). However, the host rocks of the pyroxenites treated by Peters & Niggli are spinel-clinopyroxene-peridotites (lherzolite of Lers, French Pyrenees, and serpentinized lherzolite of Totalp, Grisons, Switzerland) without any indication that they had previously been garnet-peridotites.

*Paragenetic relations to the peridotite varieties.* — Since garnet-pyroxenites grade into garnet-peridotites, it seems natural to assume the same formational environment for both, i.e. eclogite-facies conditions. And because the same sequences of decomposition of garnet (into spinel-amphibole symplektite and then into chlorite) and of clinopyroxene (into amphibole, admittedly without the development of spinel) are present both in peridotites and garnet-pyroxenites, one is tempted to assume that these phenomena occurred simultaneously in the two rock types. However, this assumption is disproved by the observation that only partially altered garnet-pyroxenites (and garnet-rocks) are found quite often as layers within spinel-amphibole- or even in chlorite-peridotite. Evidently, the decomposition of garnet-pyroxenites and garnet-rocks is slower than the mineral transformations in the peridotites. There are several possible reasons for this retardation: 1) It takes more time to kelyphitize a rock consisting entirely of garnet than a rock containing only discrete garnet grains along with other minerals, so that at a certain moment peridotite garnets may have disappeared whereas in garnet-rocks much garnet is still left. 2) Garnet may have different compositions in the mono- or bimineralic layers and in the surrounding peridotite. This argument is invalidated by the chemical analysis of Dal Vesco (see above). 3) The garnet-pyroxenites and garnet-rocks as a whole have a different chemical composition than the peridotites. They may therefore possess other stability fields in a PT-diagram. Qualitatively, the experimental results of Kushiro & Yoder (1966) point in the same direction: a comparison of their diagrams for compositions $An_1Fo_1$ and $An_1Fo_2$ shows that with decreasing pressure and constant temperature the reaction gar $\rightarrow$ opx + cpx + an + sp takes place at a lower pressure than the reaction gar + fo $\rightarrow$ opx + cpx +sp (the transformation of garnet-peridotites into spinel-clinopyroxene-peridotites, see Fig. 7). So there may be a region in which with decreasing pressure the association of garnet + olivine is no longer stable, whereas garnet alone (of the same composition) — or garnet accompanied by ortho- and/or clinopyroxene — may still be the stable phase. As a result, under conditions of decreasing pressure, the decomposition of garnet will start first in the peridotite and only after some time in garnet-rocks and garnet-pyroxenites. Both 1) and 3) may have played a part in our case.

Chloritization of the spinel-amphibole symplektite is present wherever chlorite has been developed in the adjoining peridotite. Consequently, a gross synchronism of the evolutionary processes of the mineral parageneses still obtains.

## SOME OTHER OCCURRENCES OF GARNET-PERIDOTITE, GARNET-PYROXENITE, AND TITANCLINOHUMITE IN THE SWISS, ITALIAN, AND AUSTRIAN ALPS

To complete our petrographical survey we shall consider some occurrences in Switzerland, Italy, and Austria of typical rocks and minerals resembling those encountered in the Gorduno region. The localities a—f are indicated in Fig. 10.

### *Garnet-peridotite and garnet-pyroxenite*

a. Dal Vesco (1953, p. 321 sqq.) mentions marginally amphibolized, spinel-bearing garnet-clinopyroxenites in the Moleno Valley, just north of the Gnosca Valley. These are enclosed in a peridotite consisting of olivine, orthopyroxene (no clinopyroxene), amphibole, and chlorite, and thus show a similarity to the situation at Alpe Arami, where it could be demonstrated, however, that the two parageneses are not in equilibrium with each other (see above). The marginal amphibolization of the garnet-pyroxenites suggests the same disequilibrium in the rocks of the Moleno Valley. On the analogy of the petrographical observations presented in the preceding sections I deem it likely that garnet was also formerly present in the peridotites of the Moleno Valley.

b. Wang (1939, p. 97 sqq.) describes chlorite-peridotite with spherical masses of chlorite crystals occurring near Gordola, about 10 km west of Bellinzona, and presumes that these chlorite nodules replace garnets, as at Alpe Arami. An indication of the intermediate stage of spinel-amphibole symplektite may be the occasional presence of a dark-brown isotropic mineral within the chlorite aggregate, which according

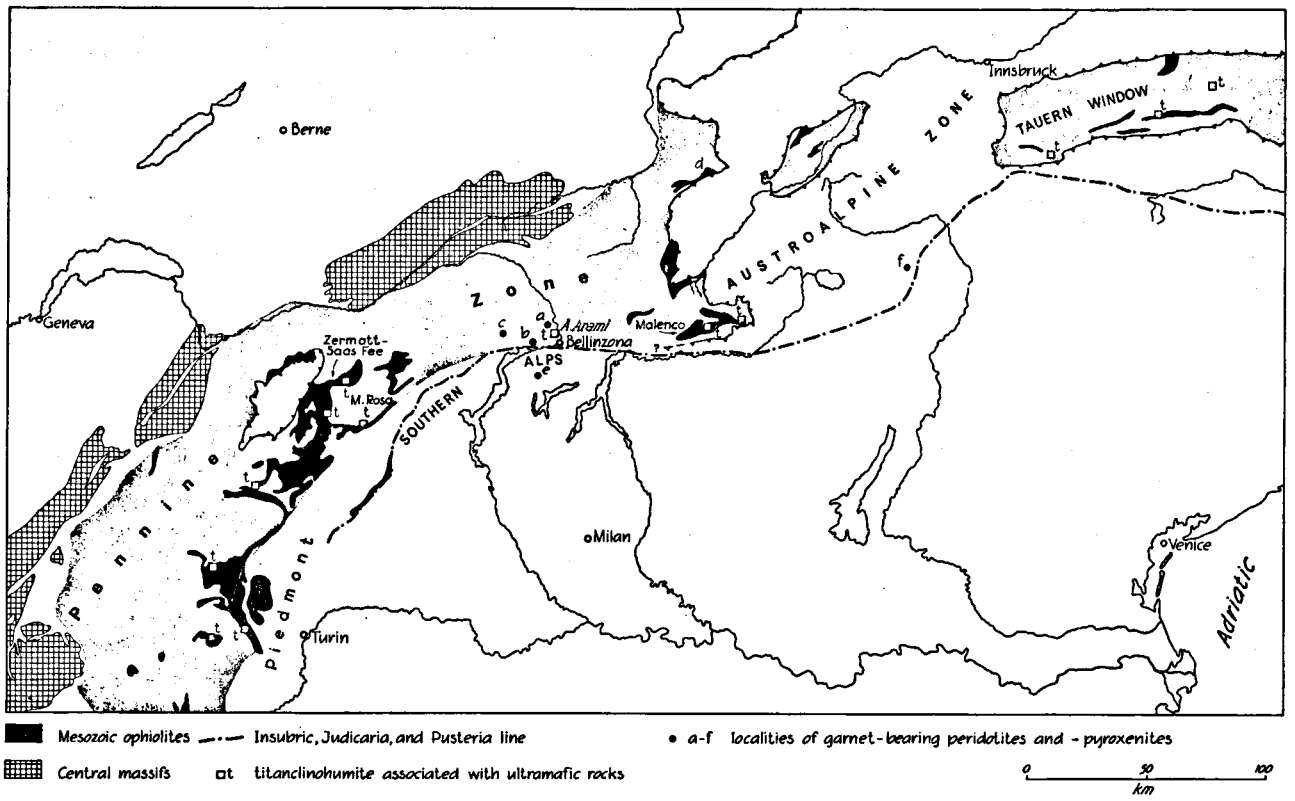


Fig. 10. The Mesozoic ophiolites of the Alps. Main sources: Carte géologique internationale de l'Europe, sheet C 5 (2nd ed., 1933) and Staub (1951, Table IV).

to Wang may be hisingerite but seems more likely to be a brown spinel.

c. According to a geological map published by Kobe (1956), garnet-peridotite is present about 8 km NW of Locarno, near Capoli and north of the Salmone. No detailed petrography is given, but the resemblance to Alpe Arami rocks is mentioned (Kobe, *op. cit.*, p. 338).

d. As mentioned above, Peters (1963, p. 645 sqq.) found garnet-spinel-pyroxenites in the Totalp serpentinite near Davos in the Grisons. According to Peters, the primary composition of the serpentinite is a spinel-clinopyroxene-peridotite (lherzolite). No relicts of an older, garnet-bearing stage seem to be present.

e. In the pre-Alpine crystalline basement of the Southern Alps, within the gneisses of the Ceneri zone, a small body of garnet-bearing serpentinite was discovered by Bächlin (1937, p. 26) 1 km NE of Arosio. It can be found on sheet 1333 (Tesserete) of the 1 : 25,000 geological map of Switzerland. Pale pink garnet frequently encloses a brown spinel, sometimes in a peculiar fashion suggesting perhaps exsolution of spinel from a still more pyrope-rich garnet (Plate III, b). But spinel is also present as separate grains unrelated to garnet. These observations warrant the opinion that spinel and garnet are co-stable. Amphibole and some almost colourless spinel(?) threads develop at the outside of decomposing garnets. However, the strong degree of serpentinization prevents a more accurate determination of the primary mineralogical composition of the rock.

f. Garnet-spinel-peridotites can be found between pre-Alpine gneisses of the Upper Austro-alpine Tirolides in the Ultimo Valley west of Bolzano, Alto Adige (Hammer, 1899; Andreatta, 1934, 1936). According to Andreatta's descriptions, there are several occurrences of these rocks, but only some easily accessible peridotite lenses near Alpe Seefeld in the valley south of San Nicolo d'Ultimo were visited by the present author. Brown spinel once again appears to belong to the primary assemblage, along with garnet, olivine, ortho- and clinopyroxene (Plate III, a). Garnet is rimmed by a narrow zone of spinel-amphibole symplektite; amphibole may protrude from the symplektite into the matrix and is also found as separate grains not directly related to garnet decomposition, but there too, in my opinion, it is secondary in nature. Clinopyroxene does not show any signs of decomposition in our samples. Andreatta also mentions uralitization of clinopyroxene and the occurrence of chlorite with properties comparable to chlorite from Alpe Arami, but the paragenetic relations cannot be deduced from his descriptions.

*Titanclinohumite*

Several occurrences of titanclinohumite associated with serpentinized peridotite have been compiled in Fig. 10. The data are taken from Carpanese (1933), de Quervain (1938), Schiener (1950), and Meixner(1960).

It is beyond the competence of the present author to discuss all localities indicated, but some points may be put forward. Titanclinohumite is frequently seen in veins or bands, together with olivine, diopside, and sometimes calcite, magnetite, and perowskite (de Quervain, 1938; Meixner, 1960). Quite often the surrounding rocks are reported to be schistose antigorite-serpentinites (antigorite-schists), sometimes microfolded. The schistosity defined by a preferential alignment of the antigorite blades curves around porphyroclastic aggregates of titanclinohumite, olivine, and diopside, so the titanclinohumite-bearing assemblage was already present when the formation of antigorite started (de Quervain, Meixner). All localities lie within ultramafic rocks that are deemed to belong to the ophiolite sequence (partially metamorphosed basic and ultrabasic intrusive and extrusive rocks) of the Pennine zone of the Alps. We find titanclinohumite in the ophiolites of the Piedmont zone in the Western Alps and in their continuation, in the zone of Zermatt-Saas Fee (Bearth, 1967) as well as its Italian counterpart south of Monte Rosa. This mineral is met again in the Malenco serpentinite mass, and in the ultrabasic rocks of the *Schieferhülle* bordering the gneisses of the Tauern window where the Pennine zone reappears to the east. Because of the generally low degree of metamorphism of the associated metasediments the ophiolites can be recognized as rocks of Mesozoic age (the exact meaning of the term "age" will be discussed in Chapter VII). However, this direct argumentation cannot of course be applied to the strongly metamorphosed areas of the Lepontine gneiss complex such as the Alpe Arami region, which also forms part of the Pennine zone of the Alps.

*Discussion*

Correlations based solely on the occurrence of identical minerals and rocks in different regions admittedly may have little value. Nevertheless, the rarer a mineral, the more one is tempted to assume that its formation took place only once in geological history, at least within a given region. Titanclinohumite is a characteristic mineral in the serpentinites of the Mesozoic ophiolite association of the Pennine region. Does this give reason to suppose that the titanclinohumite-bearing garnet-peridotite of the Gorduno Valley also is a Mesozoic ophiolite? I think the facts already presented make it impossible to give a negative answer to this question. According to Dal Vesco (1953), the peridotite of Alpe Arami is associated with calcareous rocks of a zone directly south of the Castione zone; these rocks are thought to represent metamorphic Mesozoic sediments separating different tectonic units (p. 65, Fig. 1). The same association, now with calcareous rocks of the Castione zone *s. str.*, holds for the garnet-pyroxenitebearing peridotite of the Moleno Valley (Dal Vesco, 1953). The meta-garnet-peridotite near Gordola belongs to a similar *Muldenzone*, the zone of Contra-Bellinzona (Wang, 1939), and the garnet-peridotites NW of Locarno lie within a comparable zone (Kobe, 1966, Fig. 2, zone no. 4).

In fact, the association of metamorphic calcareous rocks and ultrabasic (and basic) rocks has long been familiar to Swiss geologists, and Grubenmann (1908, p. 131) already pointed to the similarity of the basic and ultrabasic rocks of Alpe Arami to the *Pietre verdi* (= ophiolites) of the zone of Contra-Bellinzona.

However, this does not imply that the primary mineralogical composition of *all* Mesozoic serpentinites was that of a garnet-peridotite, as in the Gorduno Valley and NW of Locarno, and probably also in the Moleno Valley and near Gordola. The Totalp serpentinite — also belonging to the Mesozoic ophiolite sequence and lying between the Pennine and the Austro-alpine nappes at the base of the Austro-alpine overthrust (Streckeisen, Grauert, & Peters, 1966) — originally possessed a lherzolitic paragenesis, and among the ophiolites of Piedmont even plagioclase-peridotites (olivine, ortho- and clinopyroxene, and plagioclase, sometimes with accessory brown-red spinel) were observed (Nicolas, 1966), with a *chemical* composition closely approaching that of the garnet-peridotite of Alpe Arami (Table 3, 1).

Lastly, we may remark that the garnet-bearing peridotites mentioned as occurring within the pre-Alpine (Hercynian or older) gneisses of the Southern Alps and the Tirolides carry spinel as a stable constituent, in contrast with the garnet-peridotite of Alpe Arami. But this is not the time to venture upon further speculations.

## CONCLUDING REMARKS

The petrographical-geological approach leads to the conclusion that the ultramafic rocks of Alpe Arami are most probably members of the Mesozoic ophiolite suite in the Pennine region of the Alps. All peridotites of Alpe Arami were originally present as garnet-

Table 5. The successive mineral parageneses (a → e) of the Alpe Arami peridotite mass.

| | peridotite type | mineral paragenesis | metamorphic facies |
|---|---|---|---|
| a. | ? | titanclinohumite + . . . ? | ? |
| b. | garnet-peridotite | ol + opx + cpx + gar | eclogite facies |
| c. | spinel-amphibole-peridotite<br>spinel-amphibole-peridotite-mylonite | ol + opx + amph + sp (± cpx) | granulite facies |
| d. | chlorite-peridotite<br>chlorite-peridotite-mylonite | ol + opx + amph + chl | amphibolite facies |
| e. | serpentinite | serpentine, carbonate, and talc | greenschist facies |

peridotites, consisting essentially of olivine, ortho- and clinopyroxene, and pyrope-rich garnet, which according to experimental petrological data constitute an eclogite-facies paragenesis. Titanclinohumite may represent a relict of a pre-eclogite-facies association. Later, the garnet-peridotites underwent two successive phases of retrogradation: initially into a spinel-amphibole-peridotite paragenesis consisting of olivine, orthopyroxene, amphibole, and spinel, ± clinopyroxene, which may indicate granulite-facies conditions, and secondarily into a chlorite-peridotite paragenesis, with olivine, orthopyroxene, amphibole, and chlorite, which points to amphibolite-facies conditions. The same sequence of events holds *mutatis mutandis* for garnet-pyroxenites and related rocks, which occur as bands in the peridotites, although the decomposition of garnet and clinopyroxene seems to set in somewhat later than in the adjoining peridotites.

Two phases of mylonitization can be distinguished: the first under granulite-facies conditions, the second under amphibolite-facies conditions. Serpentinization and formation of carbonate and talc conclude the peridotite development. Table 5 shows the successive stages schematically.

CHAPTER V

# THE METHOD OF MICROSCOPICAL FABRIC ANALYSIS AS APPLIED TO ULTRAMAFIC ROCKS

## PRINCIPLES OF THE STATISTICAL ANALYSIS OF MINERAL ORIENTATIONS IN ROCKS

Measuring the direction in space of a given crystal axis of a mineral grain (such as olivine) in a rock specimen, e.g. while investigating a thin section of the rock on a universal stage, is a "random" experiment (Hodges & Lehmann, 1964, p. 4). This measurement, unlike the measurement of the axial angle of olivine, which within narrow limits will yield the same result when repeated with similar grains in the sample, is bound to produce a different result each time it is carried out with a different grain.

Since the measured directions are without polarity (compare, however, Tocher, 1960), they are most conveniently represented in the following way: suppose that parallel to each of the measured axes, lines are drawn through the center of a sphere with unit radius; along an equatorial plane the sphere is divided into two halves, only one of which is considered further. The intersections of the lines through the center with the surface of the hemisphere symbolize the measured directions. The points of intersection can be examined graphically by means of a stereographic, equal-area, or equal-interval projection on the equatorial plane — the projecting method of course causing some distortion of the real configuration of the points (Vistelius, 1966, Fig. 2) — or they can be fixed numerically by spherical or Cartesian co-ordinates. The directions can also be conceived of as vectors with unit length (Fig. 11, c).

Being especially concerned with random experiments, viz. the study of mineral orientation, petrofabric analysis must be based on arguments of a probabilistic and statistical nature. Indeed, underlying petrofabric work since its beginning about 40 years ago, is the notion that the assemblage of directions of a crystal axis, as determined on similar mineral grains in a rock, may be described in terms of some probability density distribution, albeit of a qualitative kind, on the unit hemisphere (or on its equal-area projection in a plane). In the petrofabric literature these probability models bear such names as point-maxima or great- and small-circle girdle maxima. One also encounters several combinations of these patterns.

Sometimes the spatial orientation of a mineral in a rock is described with the help of a model taking into account the joint distribution of more than one crystal axis, e.g. the joint distribution of the three mutually perpendicular axes of olivine. Other descriptions of the rock fabric also make allowance for some of its non-directional properties, for example the axial-distribution analysis, by which the joint distribution of the position of a mineral grain in a rock and the orientation of one or more of its crystal axes can be studied.

Mathematical models have been constructed for only a few distributions on the sphere, which are of interest to structural petrologists. Because the directions concerned are without sense, the models must fulfil the requirement that the probability density be equal at diametrically opposite points of the sphere. The trivial case is the uniform distribution, representing no preferred orientation. Fisher (1953) developed a model especially suitable for dealing with concentrations of palaeomagnetic directions. This model cannot, however, be fully compared with the point-maximum of petrofabrics because of the polar character of the data involved. The Fisher distribution spreads over the whole sphere, showing a maximum density at one point and a minimum at the opposite point of the sphere. Extending the work of Fisher, Watson (1966) proposed a model of bipolar and equatorial distributions resembling point-maxima and great-circle girdles, respectively. Two other models representing equatorial distributions and also related to the Fisher distribution, were investigated by Selby (1964).

Stauffer (1966) simulated fabric diagrams with a digital computer. For point-maxima he used the Fisher distribution (which according to the foregoing, however, is not entirely appropriate to fabric diagrams). Stauffer's equatorial distribution follows from his formula for the simulation experiment (Stauffer, *op. cit.*, p. 488). The density on the sphere is $f(\varphi, \varrho) = (p/4\pi \arctan p)\ (1 + p^2 \cos^2 \varrho)^{-1}$, $\varphi$ and $\varrho$ denoting azimuth and polar distance respectively, and $p$ a positive parameter of precision. Maximum density is

attained when $\varrho = \pi/2$, i. e. at the equatorial girdle. The distributions proposed by Watson ($f(\varphi, \varrho)$ proportional to $e^{\varkappa \cos^2 \varrho}$) and Selby ($f(\varphi, \varrho)$ proportional to $e^{-\gamma|\cos\varrho|}$ and to $e^{\delta \sin\varrho}$ ($\gamma$ and $\delta \geqslant 0$) ) seem to be more amenable from a mathematical point of view than Stauffer's distribution.

Analysis of the fabric of a particular mineral of a rock means the determination of a probability distribution. A definition of the population to which the probability model is to be applied must *precede* the analysis: we may, for instance, consider all the fine-grained olivine grains within mylonitic bands in a hand-specimen as a population. Of course, it is inadmissable to use the quantity to be measured, e.g. the spatial direction of the *a*-axis of an olivine grain, as a criterion to decide whether the measured item belongs to the analysed population or not. The population is usually thought to consist of distinct mineral grains; a model valid for the *c*-axis of orthopyroxene gives the probability that the *c*-axis of an orthopyroxene grain randomly chosen from the population, possesses a direction within a certain area of the hemisphere ("grain statistics"). On the other hand, a kind of "volume statistics" can also be imagined. In the latter case, a probability model ascribes more weight to the orientation of an axis of a large grain than to that of a small one. Suppose that we choose at random a point within the analysed rock specimen, repeating this until we arrive within orthopyroxene. Then the latter model can be considered adequate to yield the probability that at that particular point the direction of the considered orthopyroxene axis will be within a selected area of the hemisphere. In the following we shall adopt somewhat axiomatically the former idea about the character of the populations in which we are interested. In an inequigranular rock, with olivine occurring chiefly in two grain sizes, we can, for instance, define one population of large and another of small sized olivine grains. But after having set up a proper delimiting grain size value, we must attach the same weight — irrespective of its size — to every grain within either population.

Once the population has been properly defined, the second problem is to draw a representative sample from all grains belonging to that population, i.e. a random sample in a statistical sense. Since a rock specimen cannot be directly attacked by the customary optical universal-stage methods of mineral orientation determination, a system of two-stage sampling is inevitable. As the first step, a thin section is made from the specimen. From this thin section a number of grains are then chosen for investigation of their orientation. Sampling errors may cause an incorrect picture of the population, which may be due to the existence of a correlation between grain size and orientation. Much attention has also been paid to the influence of a correlation between the anisotropic shape of a mineral grain and the position of its crystal axes, as is generally the case with mica. Sander, Kastler, and Ladurner (1954) discussed the effect of the latter relation at the first stage of sampling (the so-called *Schnitteffekt*), and Collée (1962, pp. 15—19) commented briefly on its possible effect at the second stage. The difference between the two views can be illustrated as follows (cf. Collée, *loc. cit.*). Consider a rock containing olivine grains with their longest diameter parallel to $\gamma$ of the optical indicatrix. Whatever the spatial distribution of the orientation of $\gamma_{OL}$ in the rock, according to the *Schnitteffekt* theory the thin section will contain a relatively excessive number of olivine grains with $\gamma_{OL}$ at large angles to the plane of the section, because in the preparation of the thin section these grains have the best chance of being cut. But in Collée's reasoning, grains of this orientation would rather be underrepresented in the ultimate sample in respect of grains with a peripheral orientation of $\gamma_{OL}$, because the latter grains occupy the comparatively largest surface in the section. It will be clear that the extent to which Collée's counter-effect is operative, depends upon the method of sampling the thin section. If volume were applied instead of grain statistics, the correct procedure would consist of choosing a number of random points within the section and measuring only those olivine grains that contain such a point (which means that the thin section is sampled with a preference for grains with large cross-sections). In the case of volume statistics Collée's effect would then just counterbalance the *Schnitteffekt* of Sander *et al.* When all grains are of the same size, the sampling method of volume statistics can also be applied for grain statistics. It follows that in this case there will be no sampling errors, whether or not there is a correlation between the shape and the position of the crystal axes of the grains.

Once the information contained in the sample has been collected and represented in a numerical or graphical way, the next problem is to determine which probability model we may apply to the population from which the sample has been drawn. Statistical tests can be used if an appropriate mathematical model exists, for an assumption ("null-hypothesis", abbreviated: $H_0$) of a probability distribution is required. When testing (for instance by a $\chi^2$ goodness-of-fit test) has shown that $H_0$ cannot be rejected, it is likely that the obtained sample has been drawn from the assumed model. On the other hand, rejection of $H_0$ points to the presence of a certain distribution other than $H_0$. As a null-hypothesis the uniform distribution on the hemisphere (or on its equal-area projection on a plane) is very popular among structural petrologists, and many testing procedures based on this distribution have been proposed by them. Unfortunately, they generally lack high power against a specific alternative, so that rejecting the null-hypothesis only leads to the conclusion that the distribution is non-uniform, without any indication that a given probability model is more likely (compare, however, tests developed by such statisticians as Watson (1965) and Selby (1964): they test the uniform distribution against the alternative of an equatorial distribution). The power of most published tests seems to be small, pointing to a low probability that the null-hypothesis

will be rejected when it is in fact not true. This can be illustrated by the existence of a weak point-maximum: when we apply the test we cannot reject the null-hypothesis of no preferred orientation (Chayes, 1949, Fig. 23—4).

A proper model having been found, an estimate can be made of the parameters of the distribution, either visually (e.g. by locating the center of a point-maximum or drawing a great-circle through distinct girdle-shaped concentrations of the fabric diagram) or by computation if appropriate formulae are available. The size of the sample (the number of measurements) must be considered in relation to the accuracy wanted 1) for the determination of the type of distribution, and 2) for the estimation of the parameters of the distribution.

The reader will perhaps be disappointed when he discovers how few of the principles of fabric analysis given in the foregoing are elaborated in the next section. The initiated, however, will know which unknown country we have entered and how many pitfalls lie on our way, only a few of which we are able to explore. Nevertheless, it is an advantage to know that there are many more.

## THE PRACTICE OF MICROSCOPICAL FABRIC ANALYSIS OF ULTRAMAFIC ROCKS

We shall now concentrate on the practical problem of fabric analysis of the optically biaxial minerals olivine, ortho- and clinopyroxene, and amphibole, occurring in the ultramafic rocks at Alpe Arami.

### *The experiment: orientation measurement with the universal stage*

Orthoscopic measurement of the orientation of biaxial minerals with the *five*-axis universal stage (Emmons, 1943) proves to be the easiest and quickest procedure at present. The author employed the Leitz UT5 model as available in 1960. For, contrary to the opinion of some structural petrologists (Turner & Weiss, 1963, p. 197), the complexity of handling a universal stage does not increase proportionally with the number of its axes (nor is the working area of a five-axis stage smaller than that of a four-axis stage). The great advantage of the five-axis stage over the model with four axes is that it enables us to bring the three axes $\alpha$, $\beta$, and $\gamma$ of the optical indicatrix parallel to axes of the instrument *in one setting*. No construction is needed, even for the determination of the axial angle 2V when only one optic axis is visible.

The method of orienting a biaxial crystal on the five-axis stage has been explained by Emmons in a most lucid way, but some attention may be paid to the plotting of the measured directions into an equal-area projection. For convenience's sake we shall adopt Emmons's (1943, p. 13) notation concerning the designation of the axes of the stage. Consequently, the drum, which we normally have to the right when working with the stage on the microscope, is at the eastern end of the outer east-west (O.E-W) axis, and so on. Now, assume that after having properly oriented a crystal we make the following readings: 319° on the inner vertical (I.V.) axis (the scale at the outside of the inner stage is graduated clockwise, zero is at the eastern end of the inner east-west (I.E-W) axis); 30° on the northern arc of the I.E-W axis; 40° on the western arc of the N-S axis. We intend to make an equal-area projection of $\alpha$, $\beta$, and $\gamma$, i.e. of the N-S axis, O.E-W axis, and microscope axis, into the plane of the thin section (lower hemisphere), the index mark on the inner stage — pointing parallel to some direction on the thin section (a barbed arrow for instance) — indicating zero azimuth in the projection. With the Schmidt net the desired projections are plotted on a transparent overlay; zero of the scale of the net must be laid to the *right* (E)[1]. The mark on the overlay (Fig. 11, a) is placed at 319°, 30° are counted from N along the N-S line of the net: this is the position of the N-S axis (I). On the great circle 30° south of the E-W line the positions of the O.E-W axis (II) and the microscope axis (III) are found 40° from W and 40° eastward from the N-S line, respectively.

Two more quantities are required to determine which axis of the indicatrix, $\alpha$, $\beta$, or $\gamma$, corresponds to each of the positions I, II, and III. For this reason the N-S axis of the stage is rotated clockwise around the microscope axis over 45° to determine with the aid of the gypsum plate whether the N-S axis parallels the largest or the smallest axis of the elliptical section of the indicatrix. Moreover, the position of the plane of the optic axes, which may be either vertical N-S or vertical E-W or horizontal, should be ascertained by turning around the O.E-W and N-S axes of the stage. Given that addition with the gypsum plate occurs — meaning that $\beta$ or $\gamma$ parallels the N-S axis — and that the axial plane is vertical N-S — indicating that $\beta$ parallels the O.E-W axis — we are now able to conclude that $\alpha$ = III, $\beta$ = II, and $\gamma$ = I, and our projection is complete.

Of course a digital-computer procedure to plot the data is still more rapid. The author had the opportunity to use an IBM 360/50 computer and an on-line CALCOMP plotter (model 565) at the computing center of Leiden University. Programming for various problems arising during the present study was done in FORTRAN. The above problem consists essentially of three steps, viz. 1) converting the readings of the five-axis stage into spherical co-ordinates $\varphi$ and $\rho$ of the positions I, II, and III, 2) assigning $\alpha$, $\beta$, and $\gamma$ to the three positions mentioned, and 3) calculating the rectangular co-ordinates of the equal-area projections of $\alpha$, $\beta$, and $\gamma$, and plotting them into three separate diagrams.

A punch card of one measurement (Fig. 11, a) carries a grain number (it is practical to number measured

[1] Fairbairn (1949, pp. 280—281) proposed a rather intricate plotting procedure because he seems to have overlooked this point of difference between the five- and four-axis stages; the latter has zero to the S.

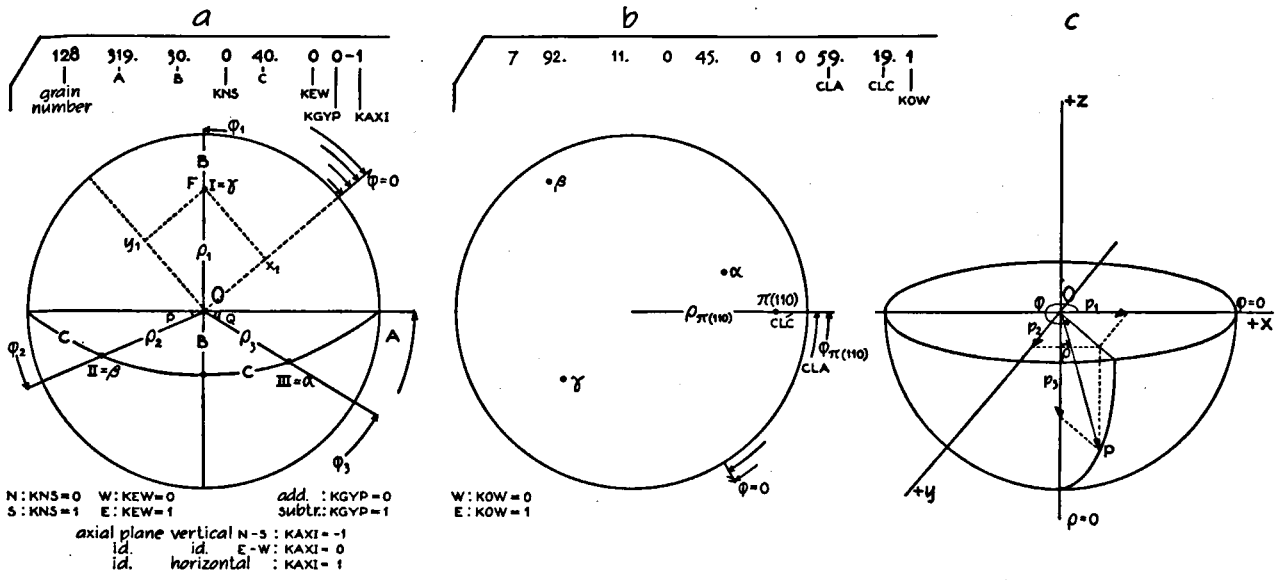


Fig. 11. a. Geometry of five-axis universal-stage measurement (equal-area projection, lower hemisphere), with format of punch card for computer input (above) and code numbers (below). b. The same as a. for additional measurement of (110)-cleavage of amphibole or clinopyroxene. c. Relation between spherical and rectangular co-ordinates of **OP**.

mineral grains on a photograph of the thin section), followed by readings of the I.V. axis ($A$) and the I.E-W axis ($B$), a code number denoting whether the angle of rotation on the I.E-W axis was read off on the N- or S-arc (KNS), a reading of the N-S axis ($C$), a similar code number referring to the latter axis (KEW), and code numbers for the reaction with the gypsum plate (KGYP) and the position of the optic axial plane (KAXI) (codes are to be found in Fig. 11, a). By application of elementary spherical trigonometry, the polar distances $\varrho$ of positions I, II, and III can be found. We have (Fig. 11, a):

$$\varrho_1 = 90° - B$$
$$\cos \varrho_2 = \cos B \sin C$$
$$\cos \varrho_3 = \cos B \cos C$$

To obtain the azimuths $\varphi_1$, $\varphi_2$, and $\varphi_3$ (measured counter-clockwise), we calculate the angles $P$ and $Q$:

$$\cos P = \frac{\cos C}{\sin \varrho_2} \text{ and } \cos Q = \frac{\sin C}{\sin \varrho_3}.$$

Dependent on the values of KNS and KEW, we get:

$$\varphi_1 = A \pm 90°$$
$$\varphi_2 = A \pm P\ (+\ 180°)$$
$$\varphi_3 = A \pm Q\ (+\ 180°)$$

Subsequently the computer assigns $\alpha$, $\beta$, and $\gamma$ to the calculated positions by selecting the pertinent combination from the values of KGYP and KAXI.

By using the formula of the azimuthal equal-area projection for position I (Fig. 11, a):

$$OF = R\sqrt{2} \cdot \sin \tfrac{1}{2}\varrho_1$$

($R$ being the radius of the projection),

we finally have $OX_1 = OF \cos \varphi_1$

and $OY_1 = OF \sin \varphi_1$,

being the rectangular co-ordinates of the equal-area projection of $\gamma$ in the case represented in Fig. 11, a. *Mutatis mutandis* the same holds for positions II and III.

*Amphibole and clinopyroxene.* — With respect to monoclinic amphibole and clinopyroxene, a study of the orientation of crystallographic directions is more productive than that of their indicatrix axes alone. Therefore, in addition to the measurement of the optical indicatrix, the orientation of at least one {110}-cleavage plane is commonly used to construct the desired crystallographical directions. Because manual construction with the Schmidt net of $c$-axes, poles to {100}, and poles to both cleavages {110} is rather tedious, it was of some interest to this study to look for a short cut by means of a computer procedure.

We measure a {110}-cleavage plane of amphibole or clinopyroxene by using the five-axis stage as a four-axis one, thus allowing no rotation on the I.E-W axis. The cleavage plane to be measured should be set vertical N-S by means of the I.V. and the N-S axis, so that its pole $\pi$ {110} is parallel to the O.E-W axis. Three additional numbers appear on the data card, viz. a reading of the I.V. (*CLA*) and of the N-S axis (*CLC*), plus a code number (KOW), denoting whether the latter reading was made on the W- or E-arc of the N-S axis (Fig. 11, b). From Fig. 11, b it is clear that $\varrho_{\pi\{110\}} = 90° - CLC$, and $\varphi_{\pi\{110\}} = CLA$ ($+180°$) dependent on the value of KOW.

To keep the following calculations as simple as possible, it is advantageous to transform the spherical

co-ordinates $\varphi$ and $\varrho$ of $\beta$, $\gamma$, and $\pi$ {110} into rectangular co-ordinates of vectors of unit length. In Fig. 11, c, P is a point on the lower unit hemisphere with spherical co-ordinates $\varphi$ and $\varrho$ ($\varphi$ is measured counterclockwise as before). However, it also represents the end-point of the vector **OP**. In the arrangement of Fig. 11, c its co-ordinates are:

$$p_1 = \sin \varrho \cos \varphi$$
$$p_2 = -\sin \varrho \sin \varphi$$
$$p_3 = -\cos \varrho$$

Returning to the measurement of amphibole and clinopyroxene, let us assume — as is the case in the present study — that $\beta$ parallels the crystallographic *b*-axis. Since there should be a definite relation in one grain between the optical indicatrix and a {110}-cleavage plane, we first check the accuracy of the measurement by calculating the angles $x$ between $\beta$ and $\pi$ {110} and $y$ between $\gamma$ and *c*. We find (for the sake of brevity putting *d* instead of $\pi$ {110})

$$\cos x = \beta_1 d_1 + \beta_2 d_2 + \beta_3 d_3,$$

the scalar product of $\boldsymbol{\beta}$ and **d**.

The *c*-axis is perpendicular to both $\boldsymbol{\beta}$ and **d**, thus equalling the vector product, brought back to unit length, of $\boldsymbol{\beta}$ and **d**. Hence

$$c_1 = (\beta_2 d_3 - \beta_3 d_2) / l \quad (1)$$
$$c_2 = (\beta_3 d_1 - \beta_1 d_3) / l \quad (2)$$
$$c_3 = (\beta_1 d_2 - \beta_2 d_1) / l \quad (3)$$

where

$$l = \sqrt{\{(\beta_2 d_3 - \beta_3 d_2)^2 + (\beta_3 d_1 - \beta_1 d_3)^2 + (\beta_1 d_2 - \beta_2 d_1)^2\}}.$$

Now $\cos y = \gamma_1 c_1 + \gamma_2 c_2 + \gamma_3 c_3$.

Of course, the angles $x$ and $y$ found in this way are not exactly equal for every measured amphibole or clinopyroxene grain in a thin section, because of manifold sources of error, but we require them to remain within reasonable limits. For instance, the actual angle $r_x$ between $\beta$ and $\pi$ {110} of amphibole should be some 62°, $r_y$ between $\gamma$ and *c* in a given section — as provisionally determined from some favourably oriented grains — may be about 18°. Assuming a tolerable deviation of $r_x$ of $\pm t_x$ (e.g. 5°) and of $r_y$ of $\pm t_y$ (e.g. 6°), we accept a measurement as being valid only if

$$\cos (r_x + t_x) < |\cos x| < \cos (r_x - t_x)$$

and if

$$\cos (r_y + t_y) < |\cos y| < \cos (r_y - t_y),$$

the absolute signs around $\cos x$ and $\cos y$ accounting for angles between 90° and 180°, which — in this case — are equivalent to their supplements. Otherwise, the measurement is rejected and must be corrected by the investigator; its number is printed by the computer together with its values of $x$ and $y$. When a series of measurements has been processed, average values for $x$ and $y$ of all grains are printed in order to alter, if necessary, the previously assumed values of $r_x$ and notably $r_y$.

The above inequalities having been satisfied, we proceed to calculate other crystallographical directions such as $\pi$ {100} and the pole to the other cleavage plane {110}. Since $\pi$ {100} is perpendicular to $\beta$ and *c*, its method of computation is identical to that for the *c*-axis as outlined. To obtain the poles to both cleavages {110}, we note that **d** is perpendicular to **c** and makes an angle $x$ or $180° - x$ with $\boldsymbol{\beta}$. Moreover, its length equals unity. Hence, we have

$$c_1 d_1 + c_2 d_2 + c_3 d_3 = 0 \quad (4)$$
$$\beta_1 d_1 + \beta_2 d_2 + \beta_3 d_3 = |\cos x| \quad (5)$$
$$d^2_1 + d^2_2 + d^2_3 = 1 \quad (6)$$

The three simultaneous equations possess two solutions for $d_1$, $d_2$, and $d_3$, constituting the two vectors **d**, one of which is perpendicular to the measured cleavage plane.

To bring the vector notation back into spherical co-ordinates, we need only consider the lower hemisphere (Fig. 11, c). Therefore, the azimuth $\varphi$ of vectors with positive values of the $z$ co-ordinate has to be incremented by 180°.

Sometimes it is very hard to locate the {110}-cleavage of clinopyroxene; the same may apply to amphibole. In that case, we recommend an alternative computer procedure. Its first object is to calculate the four possible locations of $\pi$ {110}, starting with the measurement of the optical indicatrix only. Therefore, we require previously fixed values for the angles $x$ (between $\beta$ and $\pi$ {110}) and $y$ (between $\gamma$ and *c*); $y$ can be determined from grains showing a pronounced {110}-cleavage.

To obtain the two possible locations *c* and *c'* at $y$ degrees from $\gamma$, we form *mutatis mutandis* the same equations as (4), (5), and (6) above, since **c** is perpendicular to $\boldsymbol{\beta}$, and at an angle of $y$ or $180° - y$ with $\boldsymbol{\gamma}$. The two solutions of (4), (5), and (6) yield **c** and **c'**. If (4), (5), and (6) are applied again, now with **c** and $\boldsymbol{\beta}$, we find one pair of {110}-cleavages; **c'** and $\boldsymbol{\beta}$ yield the other pair. Two possible locations of {100} (which may occur as an additional cleavage in clinopyroxene) are also calculated, either by using (1), (2), and (3) with **c** (or **c'**) and $\boldsymbol{\beta}$, or by (4), (5), and (6) with **c** (or **c'**), $\boldsymbol{\beta}$, and $|\cos x| = 0$. The poles to possible cleavages are transformed into spherical co-ordinates as before, and in each case $CLC = 90° - \varrho$ (Fig. 11, b) is calculated. For each measurement the computer produces six poles to possible cleavages, corresponding to six different settings of the universal stage, viz. three settings (two for {110} plus one for {100}) assuming *c* is true, and another three assuming *c'* is true.

Although some possible planes cannot be adjusted on the universal stage because the required tilt (*CLC*) on the N-S axis is too large, it is in most cases rather easy to find out which possibility (*c* or *c'*) pertains to the investigated mineral grain, so that we are able to complete the measurement of the optical indicatrix as in Fig. 11, b, and to process the data as explained earlier in this section.

*Mathematical rotation of the plane of projection.* — In a regional petrofabric study the need often arises to

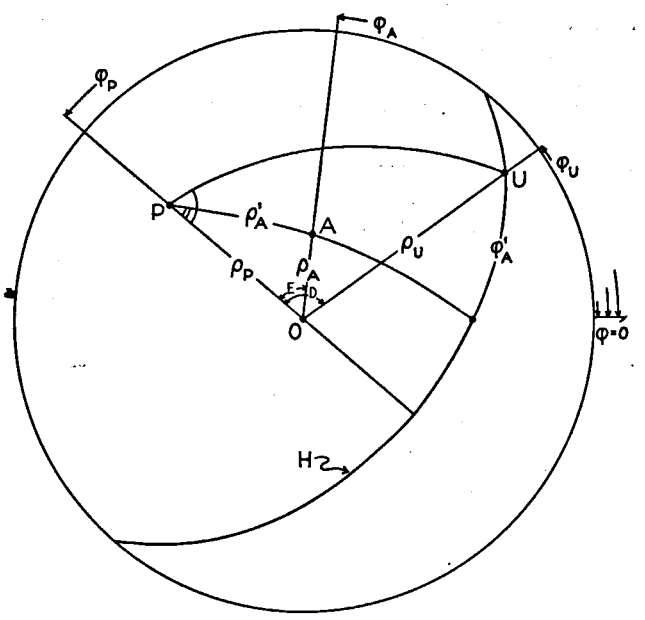


Fig. 12. Geometry underlying rotation of the plane of projection (equal-area projection, lower hemisphere).

project directional data obtained from thin sections of various orientations into one common plane, which may be the horizontal plane. This operation can be performed by a computer program, as has been shown among others by Noble (1964) and Wenk & Trommsdorff (1965). We shall follow essentially the method proposed by the latter authors. In the *lower*-hemisphere projection of Fig. 12 (cf. Wenk & Trommsdorff, 1965, Fig. 1) A is an arbitrary point with spherical coordinates $\varphi_A$ (counter-clockwise) and $\varrho_A$ . P ($\varphi_P$,$\varrho_P$) represents the pole of the horizontal plane H in the projection, U ($\varphi_U$, $\varrho_U$) is the projection of geographic N or S. First, we shall assume that P corresponds to the nadir and U is north. Now the problem is to determine the azimuth $\varphi'_A$, measured clockwise from N over E, and the polar distance $\varrho'_A$, of A in the horizontal lower-hemisphere projection. Therefore, we first calculate the angles $D$ and $UPO$, which are independent of the position of A. We have

$$D = \varphi_P - \varphi_U$$

and

$$\cos UPO = \frac{\cos \varrho_U}{\sin \varrho_P}.$$

If $D$ is negative, we add 360°.
Next we calculate

$$E = \varphi_P - \varphi_A,$$

likewise adding 360° for negative values of $E$.
Hence, in the spherical triangle APO

$$\cos \varrho'_A = \cos \varrho_P \cos \varrho_A + \sin \varrho_P \sin \varrho_A \cos E$$

and

$$\cos APO = \frac{\cos \varrho_A - \cos \varrho_P \cos \varrho'_A}{\sin \varrho_P \sin \varrho'_A}$$

We find $\varphi'_A = \pm UPO \pm APO$,
the plus- and minus signs depending on whether $D$ and/or $E$ exceed 180° or not. If $\cos \varrho'_A$ is negative, $\varrho'_A > 90°$, pointing to a position of A at the opposite side of P with respect to the arc H. Therefore, we have to take 180° — $\varrho'_A$ instead of $\varrho'_A$, at the same time adding 180° to $\varphi'_A$.
If we now assume that P is zenith (always in lower-hemisphere projection), it is immediately clear that $\varphi'_A$ should be replaced by — $\varphi'_A$ + 180°, whereas 180° should be added to $\varphi'_A$ if U is S instead of N. In both cases $\varrho'_A$ of course is left unchanged.
After having performed the rotation procedure in this way, all directions are fixed by two spherical coordinates $\varphi$ and $\varrho$, $\varphi$ denoting the azimuth measured clockwise from N over E, and $\varrho$ the angle measured from a downward directed vertical line.

*Accuracy of the measurement.* — As has been stated by Fairbairn (1949, p. 291), the possible errors arising from the measurement of the orientation of a single mineral grain are of minor importance in petrofabric work. An experienced universal-stage worker is able to keep them within limits of a few degrees deviation. In any case they are generally far under the stochastic variation between the measurements of the sampled population. Therefore, too much effort spent to obtain the most exact determination of the orientation of one grain does not pay.

*The sampling of a population of mineral grains in a thin section*

To obtain a strictly random sample of the grains of a particular mineral in a thin section, we would in theory have to number all grains of that mineral accessible to universal-stage measurement, and then draw the sample with the aid of a table of random numbers, but this is hardly feasible in practice. Moreover, in the general case it still would not render a random sample of the population contained in the whole rock specimen, because we have no control over the influence exerted by the preceding sampling stage (i.e. the thin section as a sample of the rock specimen, cf. p. 90).
Raleigh (1965) suggested the superposition of a rectangular grid on a photograph of the thin section; the grains containing the intersections constitute the sample. His method is, however, not fully in accordance with the idea of a population consisting of individual grains (p. 90): the sample will contain an excessive amount of large-sized grains. Raleigh's sampling procedure, to the contrary, is consistent with the idea of volume statistics.
For fabric analysis, I commonly used sections cut perpendicular to megascopical S-planes. On photographs of the thin sections I plotted strips perpendicular to the trace of S; within the strips I numbered and measured all grains of a given mineral. Isolated olivine grains lying within short distance of each other sometimes possess exactly the same optical orientation; because of the generally irregular, often

concave grain boundaries of olivine (Plate IV, b), these cases may be cross-sections of the same grain and were consequently counted only once. Grains that can be subdivided into zones of slightly different optical orientations on the basis of the presence of lamellae, kink bands, or undulatory extinction, were also regarded as single grains, and "average" values of their orientation were taken.

The author acknowledges a remark of Dr. P. Hartman (Leiden University), who pointed out that the method of selecting mineral grains as outlined above equally promotes the effect of the orientation of large grains. This can be explained by considering the somewhat hypothetical case of a thin section containing grains with circular cross-sections. Suppose that there are two kinds of cross-sections A and B, A with radius $r_A$, and B with radius $r_B$ ($r_A > r_B$). When we imagine a cross-section to be represented by its centre, we may define the number $n_A$ of grains A within a certain subarea of the thin section as the number of centres of A contained in that subarea. When the grains are uniformly distributed over the surface of the thin section, it is reasonable to assume that the expected values of $n_A$ and $n_B$ in a subarea will be in the same proportion as in the thin section as a whole. Therefore, when grains are selected lying with their *centre* within the subarea, the sampling method appears to be correct (van Harten, 1965). But when *all* cross-sections lying partially or completely within the subarea are selected for measurement, the area sampled for A ($S_A$) is larger than that for B ($S_B$) (Fig. 13). We have:

$$S_A = (l + 2r_A)\ (b + 2r_A)$$

and

$$S_B = (l + 2r_B)\ (b + 2r_B)\ .$$

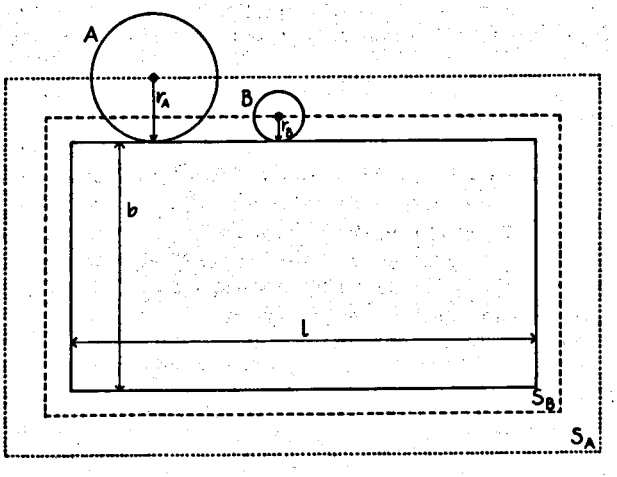


Fig. 13. The sampling of mineral grains in a rectangular subarea ($l \times b$) of a thin section.

For narrow strips with $l >> r_A$ the proportion $S_A$ to $S_B$ depends mainly on $(b + 2r_A) / (b + 2r_B)$; this proportion will therefore approach unity if $b$ is chosen large with respect to $r_A$ and $r_B$.

However, an important argument for sampling all grains of a given mineral within a certain strip lies in the fact that the procedure of determining the centre of cross-sections of an irregular shape such as we encounter in practice, introduces a rather subjective element, which is preferably avoided. We must also be aware that with methods involving sampling along strips or lines, the number of contiguous grains is greater than in a random sample. Therefore, besides the possible sources of sampling errors already mentioned, the sample may be distorted because of the frequent and significant clustering of grains of similar orientation in thin sections, as revealed by axial-distribution analysis (cf. Flinn, 1965).

*The microscopical distinction between olivine, ortho- and clinopyroxene, and amphibole.* — A prerequisite for successful fabric analysis is that the nature of *every* mineral grain within a given strip on the thin section be determinable. In the present study this was applied to the minerals olivine, ortho- and clinopyroxene, and amphibole.

*Orthopyroxene* is easily distinguished from the other minerals because of its weaker double refraction; its interference colours do not exceed first-order yellow in thin sections of the right thickness (which are, however, difficult for a grinder to prepare because of the absence of quartz). When the universal stage is rotated around one of its horizontal axes, the change of the interference colour is in general markedly slower than is the case for the other minerals mentioned; the colour attains second-order blue or green at most.

*Olivine* can be made visible without difficulty by an etching and staining method as old as the term peridotite itself (Cossa, 1874). The present author used a technique proposed for feldspathoids by Shand (1939). The uncovered thin section is exposed for about half an hour to the fumes of concentrated hydrochloric acid. To stain the silica gel thus developed on the olivine grains, the acid is first removed from the section by careful dipping into water, after which the section is held in a 0.25 wt % aqueous solution of methylene blue for a few minutes. Since the gelatinization of forsterite-rich olivine is far less intensive than that of nepheline, for instance, one or two repetitions of the treatment may improve the results. The section is then cleaned, dried, and provided with a cover glass.

The other minerals are not visibly attacked by the acid. However, the dye also enters cracks, serpentine masses and veins, and — to a lesser extent — chlorite crystals, which take on a light violet hue. If these effects hinder the optical investigations in a special case, it will suffice to only etch the olivine grains, omitting the staining procedure.

There is a wide difference in the magnitude of the axial angles of *clinopyroxene* (+ 2V about 60°) and *amphibole* (2V from + 80° through 90° to — 80°), which provides a simple way to distinguish between them. Here, Emmons's five-axis universal stage furnishes another proof of its superior quality. Half of the axial angle can easily be read off when the acute

bisectrix is parallel to the microscope axis; if the obtuse bisectrix occupies a vertical position, the same holds for amphibole, whereas in this case the rotation required to bring an optic axis of clinopyroxene parallel to the microscope axis (about 60°) may be too large to be performed by the instrument. But then Berek's (1913, 1923, 1924) ingenious method of determining the axial angle (and the optic orientation) from the extinction angle in a known position of the indicatrix may be used, the more easily since Berek's starting-position is already realized because one axis of the indicatrix has been oriented parallel to the microscope axis (Dodge, 1934; Emmons, 1943). The axial plane being horizontal, Berek's method is the only one to discriminate between clinopyroxene and amphibole on the basis of the axial angle, i.e. when other methods fail[1].

*The search for the probability distribution: the preparation of the petrofabric diagram*

According to Vistelius (1966, p. 138) "structural diagrams are graphs of probability density functions". One wishes this were true! In fact, a petrofabric diagram does not represent a probability density function on the equal-area projection of a hemisphere, as implied by Vistelius' statement, but is a special way of depicting the information contained in a sample from a population, thus contributing to the ultimate determination of its underlying probability distribution.

*The petrofabric diagram considered as a three-dimensional histogram.* — By way of example, let us suppose that we have measured the length of a hundred zircon grains constituting a random sample separated from a granite. To obtain an impression of the distribution of the length of the zircon grains (i.e. the probability distribution characterizing the population formed by the lengths of all zircon grains within the analysed granite specimen), we may group the measurements into classes (for instance 100—110 $\mu$, 110—120 $\mu$, etc.). Next we draw a *histogram* (Fig. 14) by erecting rectangles above the classes. The area of a rectangle

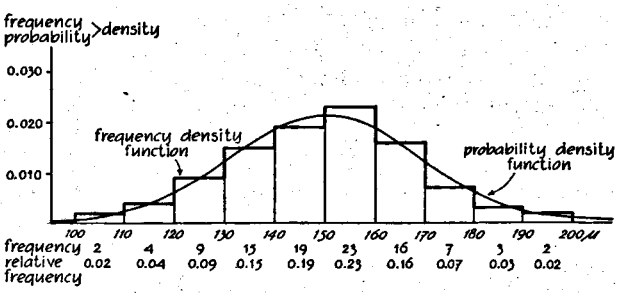


Fig. 14. Histogram and probability density function.

is made equal to the relative frequency[2] of the class to which it belongs. Hence, the total area under the step-like line of the histogram is equal to 1. It also follows that the height of the step-like line above the abscissa represents the frequency density. The frequency density function is important because it enables direct comparison with the probability density function of a distribution possibly lying at the basis of the population, perhaps the normal distribution.

In general, to calculate the frequency density $d$ (i.e. the altitude of the histogram) within a class of length $A$ containing $n$ of a total of $N$ measurements, we use the definition of frequency density: $d = n/NA$.

In petrofabrics, we try to find a probability density function of two random variables (expressed, for instance, by $\varphi$ and $\varrho$) that can be represented by a surface above the plane of the equal-area projection. The solution of the problem of approximating the position of this surface is analogous to the histogram method explained above.

Consider first the squared-grid method of constructing petrofabric diagrams (Stauffer, 1966, p. 475). We assume that the area of the equal-area projection (which will be taken as unity) contains $N$ points representing spatial directions as outlined on p. 89. We divide the unit area into non-overlapping squares (other Figures are also permitted) of area $A$. According to the number of points $n$ contained in a square, we calculate a relative frequency $n/N$ and erect a rectangular block with content $n/N$ above that square. Thus, the total content under the step-like surface of the petrofabric diagram equals unity. Above a given square, the altitude of this surface (the frequency density function) is $d = n/NA$.

However, as the representation on paper of petrofabric diagrams is necessarily restricted to two dimensions, the squared-grid method is not very satisfactory, because it is difficult to obtain an impression of the shape of the frequency density surface.

By the customary procedures of constructing petrofabric

[1] Ehlers (1966) claimed to have found a rather simple method of bringing biaxial crystals into a cardinal position with the help of the *four*-axis stage, but this method may not be entirely correct. Ehlers orients an axis of the indicatrix parallel to the E-W axis by the routine universal-stage technique, then rotates on the N-S axis causing the crystal to depart from extinction, after which he rotates on the E-W axis to attain extinction anew; at that moment, he maintains, one axis of the indicatrix is horizontal, i.e. perpendicular to the microscope axis. However, this does not hold in the general case, as shown by a construction using the Biot-Fresnel law and the plane of the N-S and E-W axes as a plane of projection. After the rotation on the N-S axis, the E-W axis is no longer parallel to an axis of the indicatrix, unlike the axis by which a second symmetry plane of the indicatrix is adjusted with the five-axis stage. The incorrectness of Ehlers's procedure has since been pointed out by D. Jerome Fisher (Ehlers, 1967).

[2] Under the *frequency* of a class is understood the number of measurements contained in that class; the *relative frequency* of a class is equal to its frequency divided by the total number of measurements, so that the sum of the relative frequencies of all classes equals 1; the *frequency density* within a certain class is found by dividing the relative frequency by the width of that class.

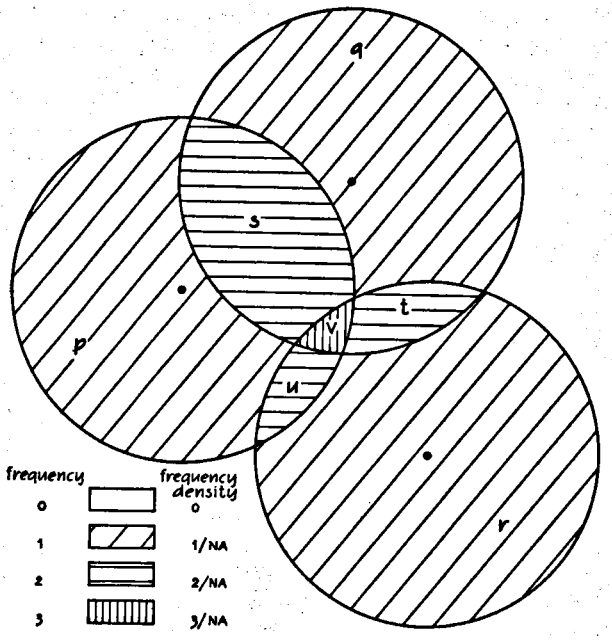


Fig. 15. Mellis's counting method.

diagrams, we move a counting circle over the point diagram. At a multitude of places (termed counting points) we center the counting circle and assign the frequency of points falling within the circle to the pertinent counting point. By contouring, equal frequencies are combined into *areas of equal frequency*. We think of them in three dimensions as surfaces above the plane of projection at altitudes proportional to these frequencies (*Höhenschichtendarstellung* of Fischer, 1960).

At first, this method seems to be rather suspect from a statistical point of view, because the points are counted more than once (Vistelius, 1966, p. 71). However, it can be demonstrated, by examining the counting method proposed by Mellis (1942) and advocated by Flinn (1958), that this objection does not invalidate the method.

In Fig. 15 three points somewhere within the circle of the projection are counted according to the Mellis method. One may imagine that the Mellis counting circle is centered at every spot in the projection, implying that we simply may draw circles equal to the size of the counting circle around each measuring point to obtain the areas of equal frequency as defined above. Obviously, the frequency (the number of points within the counting circle) of a particular area is equal to the number of circles to which it belongs. The surfaces of equal frequency in Fig. 15 are therefore at altitudes of 0, $c$, $2c$, and $3c$. To obtain the correct value of the proportionality constant $c$, so that the altitudes represent frequency densities comparable to probability densities, we calculate the content under these surfaces. We find:

$$c\,(p+q+r) + 2c\,(s+t+u) + 3c\,v\,.$$

By rearranging and putting $A$ for the area of the counting circle this equals:

$$c\{(p+s+v+u) + (q+t+v+s) + (r+u+v+t)\} = c\,.\,3A\,.$$

Of course, a similar addition holds for any total number of points $N$ within the diagram. Hence, the total content amounts to $cNA$, which must be unity. So $c = 1/NA$. Thus, to obtain the frequency density $d$ within a plane of equal frequency where $n$ points fall within the counting circle, we have to apply the same formula as above, viz.

$$d = n/NA \qquad (7)$$

A disadvantage of the Mellis counting method is that it offers a quite unrealistic approximation of the expected probability density functions (see e.g. Fischer, 1960, Fig. 10). Moreover, unsurmountable technical difficulties arise in the construction of a diagram with a large number of overlapping circles. The conventional method of preparing petrofabric diagrams (since Schmidt, 1925) therefore uses a finite instead of an infinite number of counting points, which allows some latitude in sketching the areas of equal frequency density. Although the content under the frequency density function is probably no longer equal to unity when using (7), we feel that this still must hold by approximation (see Fischer, *op. cit.*, Figs. 8, 9, and 10).

Instead of indicating the altitudes of the planes of equal density, it is convenient in the explanation of petrofabric diagrams to state the altitudes of the curves (*contours*) delimiting the density planes at the lower sides. They are of course identical to the former values. It is now evident that — taking the area of the equal-area projection as unity — contours possess *absolute* values indicating frequency density, being expressed in a measure that is independent both of the total number of measurements and of the area of the counting circle used. Therefore, in the opinion of the present author, there is no need to express contour values in percentages per percentage area.

As a further simplification, contours below 1 (the density of the uniform distribution on the circle of projection) are generally omitted to focus attention on areas of maximum density. Further, when too many contours would obscure the diagram, some are omitted, preferentially in a regular manner.

*The "significance" of the contours, the choice of the area of the counting circle, and the number of measurements.* — In the Appendix to a study on ice petrofabrics, Kamb (1959) maintains that it is possible to obtain contours of direct statistical significance. He finds that, if we draw a random sample of $N$ points from a probability distribution on the hemisphere (or on its equal-area projection), the distribution of the number of points $\underline{n}$ falling within an area $A$ of the hemisphere (or its projection), is binomial. In the case of the uniform distribution this binomial distribution has $E(\underline{n}) = NA$ and $\sigma^2(\underline{n}) = NA(1-A)$; because $N$ is generally large and $A$ small, the latter distribution may be approx-

imated by a Poisson distribution with the same expectation. For instance, the distribution of $\underline{n}$ provides the probability of finding $n$ points or more within a counting circle that is centered somewhere on the projection *before* drawing the sample of $N$ points from the uniform distribution. In this way, the probability of finding 4 points or more out of a sample of 100 points, within a 1 % counting circle ($A = 0.01$), is 0.02; so this event is expected to occur only in two out of a hundred diagrams. Kamb, however, treats the former distribution as if it would yield the probability that in any given one of the hundreds of positions occupied by the counting circle during the preparation of a petrofabric diagram from the sample, this circle contains at least 4 points. This probability is in fact larger (compare Friedman, 1964, pp. 468—469, with Flinn, 1958, Fig. 1).

Following a slightly different approach, we recall the squared-grid method of p. 96. Under the same assumptions as above, the probability of finding $n$ points within a square of area $A$ is:

$$P(\underline{n} = n) = e^{-NA}\frac{(NA)^n}{n!}$$

using the Poisson approximation of the binomial distribution. When the total number of squares containing $n$ points is $\underline{s}_n$, it appears that

$$E(\underline{s}_n) = \frac{1}{A}e^{-NA}\frac{(NA)^n}{n!}$$

(Winchell, 1937). The expectation of the total area of squares with frequency $n$ will be

$$E(A\underline{s}_n) = A\,E(\underline{s}_n) = e^{-NA}\frac{(NA)^n}{n!} = P(\underline{n} = n)$$

which is in excellent agreement with the results of Flinn (1958, Table 1) and Stauffer (1966, Fig. 6). Consequently, in the example mentioned above, the areas of frequencies $\geqslant 4$ are expected to cover about 2 % of the area of the projection.

In a somewhat modified form, Kamb's suggestion implies that we focus our attention on those areas of equal frequency of the petrofabric diagram that are expected to be of negligible size under the null-hypothesis of a uniform distribution. With samples of $N = 200$ and a 4 % counting circle, areas of frequencies $\geqslant 16$ are expected to occupy no more than 0.8 % of the diagram, areas of frequencies $\leqslant 1$ no more than 0.3 %, under $H_0$ uniform. To start contouring from frequency 16 (i.e. frequency density 2) onwards would provide contours "of direct statistical significance" (cf. Stauffer, 1966, pp. 482—483).

However, we must remember that Kamb's method is not more than a way of testing the null-hypothesis of a uniform distribution. The power of such a test against specific alternatives such as a point-maximum is small (p. 90). As a result, in cases where we cannot reject $H_0$ (i.e. where we cannot draw "significant" contours), indications for the existence of some non-uniform distribution may nevertheless be present in the configuration of the "insignificant" contours.

Although treated together by Kamb, the problem of the choice of the area of the counting circle does not seem to be directly related to that of the possible "significance" of the contours. The former problem is analogous to that of the choice of the class width in the case of the two-dimensional histogram of Fig. 14. Excessively narrow classes cause a wildly fluctuating frequency-density function, which may obscure the general pattern, whereas excessively wide classes may smooth out possibly interesting details of the distribution. The same applies to the counting circle, as has also been observed (among others) by Kamb (1959). The decrease of the variance $\sigma^2(\underline{d})$ of the frequency density with increasing area $A$ of the counting circle can easily be demonstrated for the uniform distribution:

$$\sigma^2(\underline{d}) = \sigma^2(\underline{n}/NA) = (1/N^2A^2)\,\sigma^2(\underline{n}) = 1/NA - 1/N.$$

An experimental approach is presented in Fig. 16. Fig. 16, a and b represent samples of 200 γ-axes of orthopyroxene from two parallel thin sections of a hand-specimen of garnet-peridotite originating from the Alpe Arami mass. There is no reason to assume that these samples do not originate from the same population. Therefore, the "best" counting circle would be the one producing the most perfect resemblance between the orthopyroxene fabric diagrams of the two sections. We observe that the 1 % counting circle is a rather bad choice: it is hardly possible to indicate corresponding contour details in the diagrams of GN1-B1 and GN1-B2 (cf. Kamb, 1959). On the other hand, the 5 % circle is quite satisfactory: the shape of the diagram is rather well reproduced, although the maximum densities differ to some extent. Olivine γ-axes of the same two sections and the same sample sizes are shown in Fig. 16, c and d. Here, the resemblance of two diagrams counted with the 9 % circle is still rather poor.

However, before deciding on the area of the counting circle to be used, several points must be taken into account:

1. We are not certain whether the orientation-distributions of this rock specimen are representative of all the specimens we shall investigate.
2. Although α, β, and γ of a mineral may require different counting circles, we are forced to count them by the same circle for the sake of mutual comparison of the frequency densities, because the densities obtained from a given sample also depend on the area of the counting circle, as appears from Fig. 16.
3. An excessively large counting circle prevents the detection of any closely spaced maxima of the probability density distribution (Friedman, 1964, p. 468).

To keep on the cautious side, we used a 4 % counting circle for olivine and a 2½ % one for orthopyroxene, both in connection with samples of 200 points. In the olivine diagrams the lowest contour is at density 1 (frequency = 8), whereas contours delimiting areas

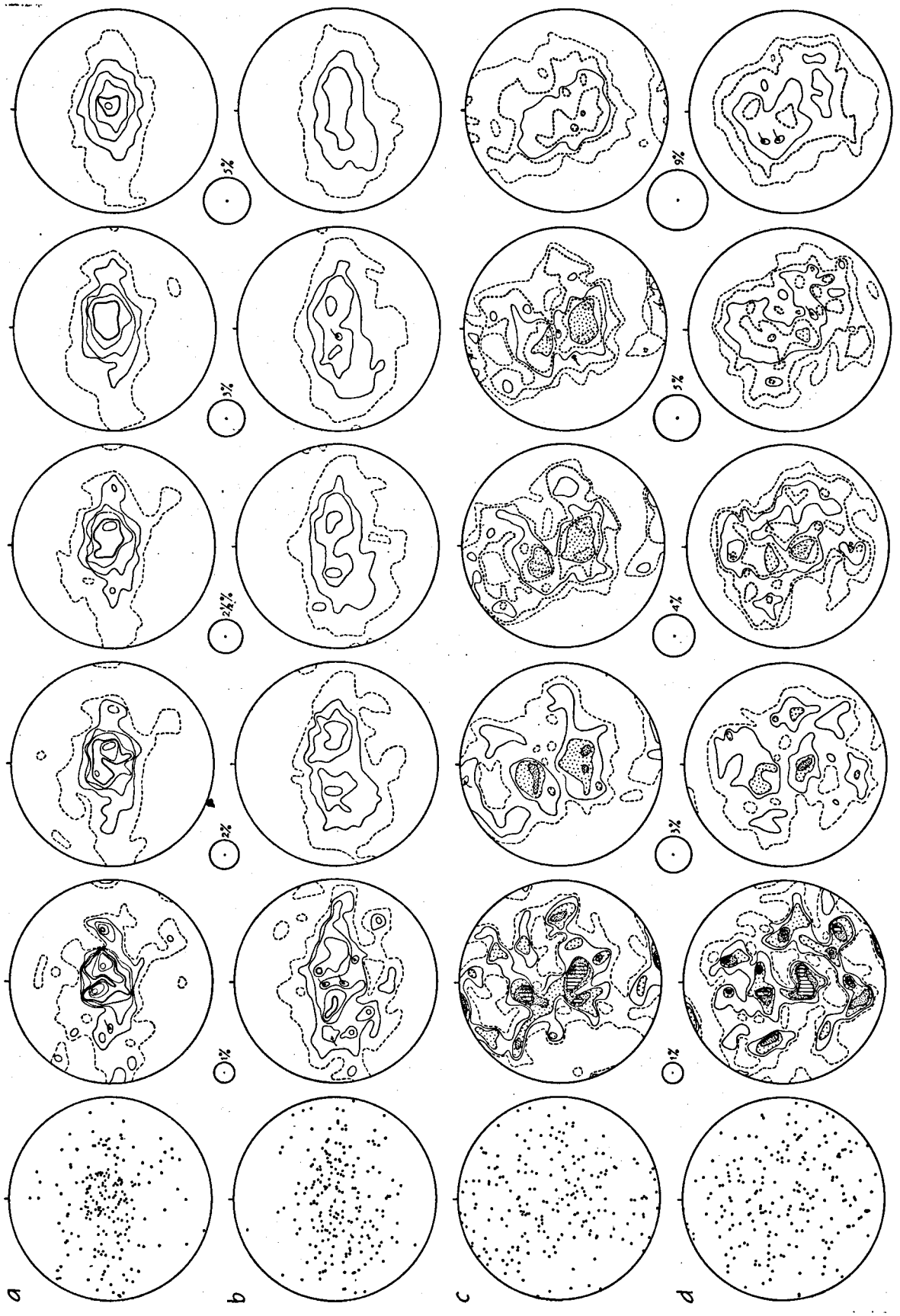


Fig. 16. Influence of the area of the counting circle on the petrofabric diagram; data from two parallel thin sections of garnet-peridotite GN1. a. 200 γ-orthopyroxene from section GN1-B1; contours at densities 1, 2, 3, . . . b. Idem for section GN1-B2. c. 200 γ-olivine from section GN1-B1, contours in diagrams counted with 1 % and 3 % circles at densities 1, 1.5, 2, . . .; contours at densities 1, 1.25, 1.50, . . . in the other diagrams. d. Idem for section GN1-B2.

N.B. Orthopyroxene and olivine have been rotated into different planes.

of frequencies 9, 11, 13, etc. are omitted, the contour interval therefore being 0.25 instead of 0.125. Contours of orthopyroxene diagrams are only drawn at densities 1, 2, 3, etc. In addition, olivine fabric diagrams are shaded above frequency density 2, thus showing more clearly the "significant areas" according to the "testing" procedure explained above.

Considering finally the question of sample size, we may state the problem of preparing petrofabric diagrams from mineral orientations again in a more generalized form: we try to find a probability density function of which neither the *type* nor the *parameters* are known. Only in the case of a *known* distribution, as in the simulation studies of Stauffer (1966), is it possible to choose a reasonable minimum sample size, together with the "best" area of the counting circle (unfortunately the latter has not been investigated by Stauffer) to obtain petrofabric diagrams reproducing the probability density function with the required precision (regarding the location of maxima, for instance).
However, when the present study was undertaken nothing whatever was known about the distributions to be encountered. Therefore, the only consideration to influence the choice of the sample size at $N = 200$ was the fact that 200 measurements of the orientation of biaxial minerals such as olivine and orthopyroxene can be performed within a reasonable period, say two or three days of universal-stage work.

*A computer procedure for counting in and representation of petrofabric diagrams.* — Once punch cards of the measurements are available, it seems logical to develop a further computer procedure to obtain the frequencies of points falling within a counting circle centered at selected spots on the hemisphere or on the equal-area projection. In this respect the hemisphere is preferable from a mathematical point of view. The following method is essentially adopted from Noble and Eberly (1964).
Assume that a direction of a certain kind (e.g. $\alpha$ of olivine) has been computed from the universal-stage measurements according to p. 92 and that the plane of projection has been rotated into the horizontal plane according to p. 94. Its position on the lower hemisphere is now characterized by the spherical co-ordinates $\varphi_\alpha$ (clockwise from N) and $\varrho_\alpha$. On the hemisphere, counting circles of area $A$ (area of hemisphere = 1) are centered on a counting grid with 351 different counting points $(\varphi_T, \varrho_T)$ falling into 12 groups possessing identical values of $\varrho_T$ (Noble & Eberly, *op. cit.*, Table 1). From Fig. 17, a it is clear that the distance $D$ to a particular counting point is given by:

$$\cos D = \cos \varrho_\alpha \cos \varrho_T + \sin \varrho_\alpha \sin \varrho_T \cos (\varphi_T - \varphi_\alpha) \quad (8)$$

The spherical radius $R_A$ of a counting circle with area $A$ can be found from: $\cos R_A = 1 - A$. Hence, the frequency belonging to the counting point $(\varphi_T, \varrho_T)$ is incremented by 1 only if: $|\cos D| \geqslant \cos R_A$, absolute signs being necessary to account for supplementary values of $D$ that may arise for counting points near the margin of the projection.
To speed computation, before applying (8) the polar distance $\varrho_\alpha$ of a measurement is compared with minimum and maximum test-values belonging to groups of counting points with identical $\varrho_T$ (Noble & Eberly, *op. cit.*). To compute these critical values for a particular group, in the case of a counting circle with area $A$, we simply have (Fig. 17, a):

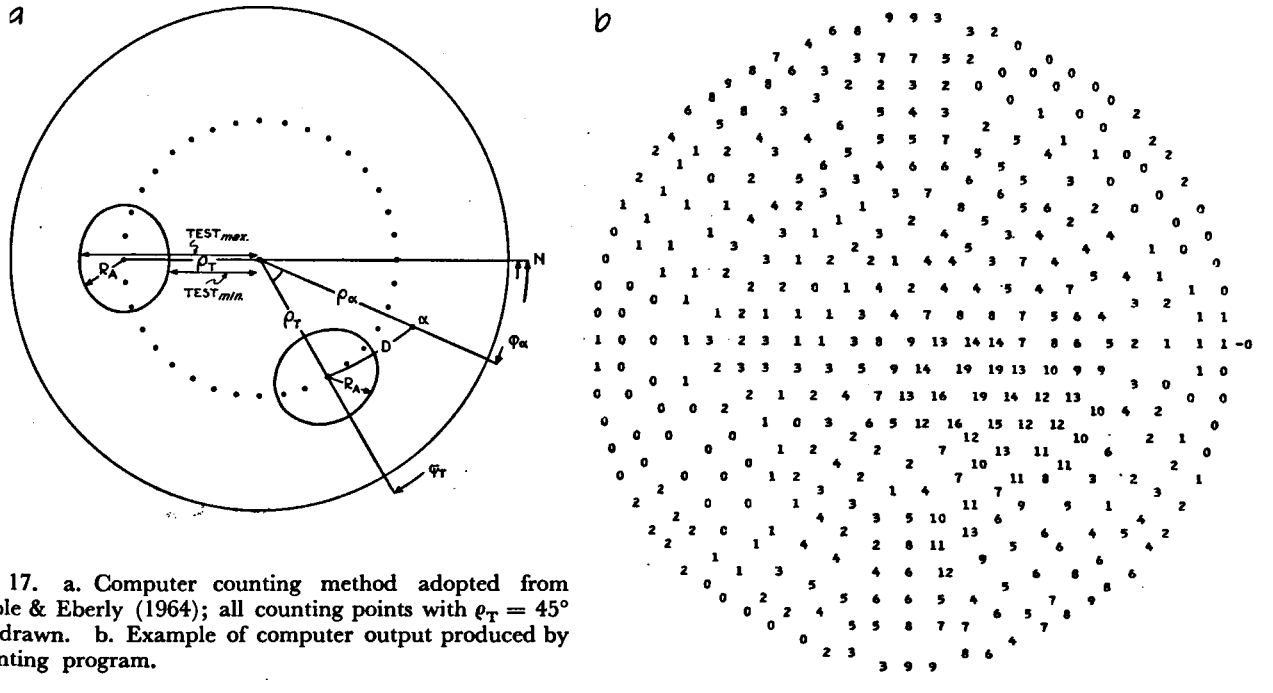


Fig. 17. a. Computer counting method adopted from Noble & Eberly (1964); all counting points with $\varrho_T = 45°$ are drawn. b. Example of computer output produced by counting program.

$TEST_{min} = \varrho_T - R_A$ and $TEST_{max} = \varrho_T + R_A$. Thus, starting with the group of counting points with smallest $\varrho_T$, we calculate $\varrho_\alpha - TEST_{min}$. If the difference is positive, we calculate $\varrho_\alpha - TEST_{max}$. If the latter difference is negative, we enter the counting subroutine (8) for all counting points of the tested group and proceed to the following group of counting points having a larger value of $\varrho_T$. If, on the contrary, $\varrho_\alpha - TEST_{max}$ is positive, we proceed without entering the subroutine to the next group. We repeat the testing procedure with pertinent values of $TEST_{min}$ and $TEST_{max}$, until $\varrho_\alpha - TEST_{min}$ becomes negative. Then we abandon the measurement and proceed to the following direction to be counted.

To present the computed frequencies in a convenient way, i.e. on the standard equal-area projection of 10 cm radius, we used a method fundamentally the the same as that proposed by Siemes (1967) for the presentation of intensity data of the X-ray texture diffractometer. First, all counting-points (including the 36 not used during the counting procedure proper because they lie diametrically opposite to identical points on the margin of the projection) are projected into an equal-area projection of $R = 10$ cm; $X$- and $Y$ co-ordinates are calculated as on p. 92. However, reproduction of the frequency values at the exact position pertaining to each counting point by means of the output printer of the computer is impossible because the distances $D1$ between the nearest two lines and $D2$ between the nearest two characters on the same line have fixed values. But by rounding the values of $X/D1$ and $Y/D2$ to the nearest integers, the assignment of the counting points to the nearest possible one and two positions on the output printer is sufficiently accurate for petrofabric work (cf. Siemes, *op. cit.*, Fig. 2). Two positions are needed if the frequency of a counting point consists of a two-digit number. Fig. 17, b is a reproduction of computer output prepared according to the foregoing. Only the drawing of contours remains to be done by hand.

An additional advantage of counting on the hemisphere is that it avoids the inaccuracy accompanying counting with a circular counter in the equal-area projection because of the distortion of the spherical surface at the margin of the projection (Mellis, 1942). However, the equal-area projection remains inevitable, from a statistical point of view, to *represent* the frequency density distribution (Schmidt, 1942).

*The quantitative analysis of the orientation data*

It is interesting to know to what extent a fabric diagram may be compared with a mathematically formulated probability density distribution. As an instance we shall consider the mathematical model of point-maxima and great-circle girdles as proposed by Watson (1965; 1966, pp. 795—796) and Scheidegger (1965). Much of the following has been adopted from Watson (1965, 1966).

The probability density on a sphere with unit radius is:

$$f(\varphi, \varrho) = ce^{\varkappa \cos^2 \varrho} \qquad (9)$$

$\varphi$ and $\varrho$ are spherical co-ordinates as before. When $\varkappa > 0$, maximum density is attained for $\varrho = 0$ and $\varrho = \pi$ (point maximum), when $\varkappa < 0$, the same happens for $\varrho = \pi/2$ (equatorial girdle). $\varkappa$ is a measure for the degree of concentration of the distribution. Since

$$\int_\varphi \int_\varrho f(\varphi, \varrho)\, d\varphi\, d\varrho = 1, \quad c = \frac{1}{4\pi \int_0^1 e^{\varkappa t^2} dt}.$$

Assuming that all directions are expressed by means of vectors of unit length (p. 93), we may indicate any point on the sphere as $(l, m, n)$ and the "true" centre of the distribution (the centre of the point-maximum or the axis of the great-circle girdle) as $(\lambda, \mu, \nu)$. Hence, the distribution can be rewritten as:

$$ce^{\varkappa(l\lambda + m\mu + n\nu)^2} \qquad (10)$$

with $\lambda^2 + \mu^2 + \nu^2 = 1$.

Suppose that we draw a random sample of size $N$ from (9), and that $(l_i, m_i, n_i)$ represents the $i$th observed direction. Estimators for $(\lambda, \mu, \nu)$ and $\varkappa$ can be found by applying the method of maximum likelihood estimation to (10). It can be shown (Watson, 1965, 1966) that the estimator of $(\lambda, \mu, \nu)$ is the eigenvector (of unit length) associated with the largest $(\varkappa > 0)$ or smallest $(\varkappa < 0)$ eigenvalue of the symmetric matrix

$$M = \begin{pmatrix} \Sigma l_i^2 & \Sigma l_i m_i & \Sigma l_i n_i \\ \Sigma m_i l_i & \Sigma m_i^2 & \Sigma m_i n_i \\ \Sigma n_i l_i & \Sigma n_i m_i & \Sigma n_i^2 \end{pmatrix}$$

The estimator of $\varkappa$, $k$, is the solution of the equation

$$\frac{\int_0^1 t^2 e^{kt^2} dt}{\int_0^1 e^{kt^2} dt} = \frac{\tau}{N} \qquad (11)$$

where $\tau$ is the largest $(\varkappa > 0)$ or smallest $(\varkappa < 0)$ eigenvalue of $M$. Watson (1965, 1966) provides Tables (together with approximative formulae for large and small values of $k$) to resolve $k$ from (11) for given values of $\tau/N$.

We shall now analyze a sample of 500 directions of β-axes of orthopyroxene from garnet-peridotite specimen no. GN1. The petrofabric diagram shows an almost circular concentration pattern. As a first approximation it seems warranted to suppose that the underlying distribution is a point-maximum $(\varkappa > 0)$. First, estimates for $(\lambda, \mu, \nu)$ and $\varkappa$ are calculated from the observed directions according to the foregoing. (All computations were made with the help of the computer.)

It is convenient to rotate the fabric diagram into a plane perpendicular to the estimated value of $(\lambda, \mu, \nu)$ (Fig. 18, b). On the assumption that the estimates for $(\lambda, \mu, \nu)$ and $\varkappa$ are sufficiently close to their actual values, a density function (9) of the distribution

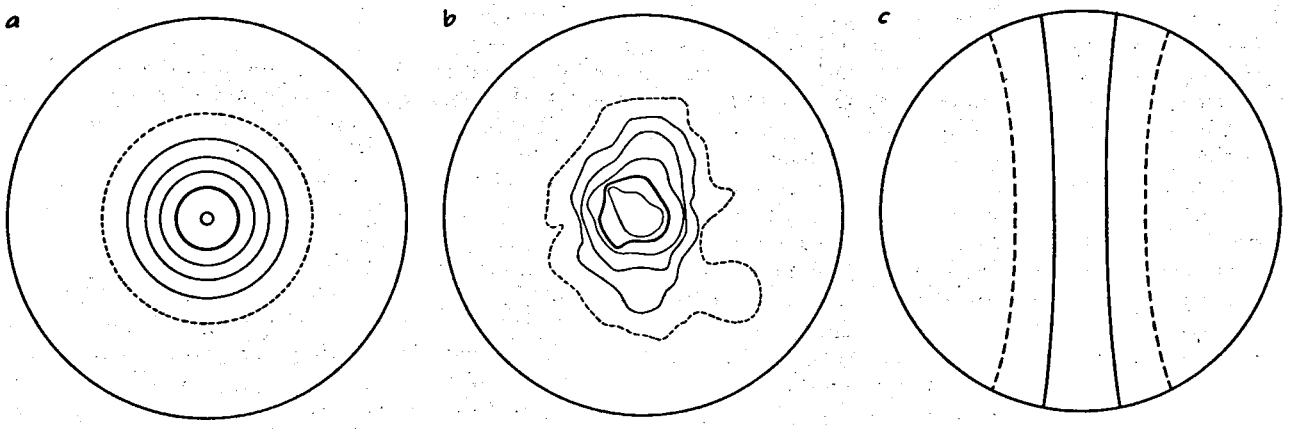


Fig. 18. Fabric diagram (b.) and probability density functions (a. and c.). b. Fabric diagram of 500 β-orthopyroxene from garnet-peridotite GN1 ($A = 0.02$). a. and c. Distribution (9) for $\varkappa$-values estimated by considering b. as a point-maximum ($k = 3.7$) and as a great-circle girdle ($k = -4.20$), respectively. Contours at densities 1, 2, 3, ....

standing for the population from which the observed directions were drawn, can be constructed, inserting for $\varkappa$ its estimate $k$ (Fig. 18, a). Two points have to be kept in mind when constructing Fig. 18:

*a*) distribution (9) refers to a sphere with unit radius (area $= 4\pi$), whereas the frequency densities indicated in fabric diagrams presuppose a hemisphere with area = 1 (p. 97). To be comparable to a fabric diagram, the right-hand side of (9) should therefore be multiplied by $4\pi$.

*b*) contours in fabric diagrams are drawn at the lower sides of planes of equal frequency density (p. 97). For the sake of comparison it seems better in this special case to draw the contours midway between the lower and higher sides of these step-like areas (cf. Fig. 14).

Watson's model gives quite satisfactory results. Comparison of Fig. 18, a and b shows that the highest concentration of points in the fabric diagram is at the same spot as in the model distribution. The contour pattern is well reproduced in Fig. 18, a, apart from the tendency of the fabric diagram to show some spread along a great-circle girdle.

If we now assume that the great-circle girdle model ($\varkappa < 0$) underlies Fig. 18, b, we obtain Fig. 18, c. The estimated point-maximum in Fig. 18, a and the estimated axis of the great-circle girdle in Fig. 18, c lie 90° from each other because the eigenvectors of $M$ are mutually perpendicular. It is evident that the computed estimate of the girdle axis lies close to the axis of the girdle yielded by visual estimation in the fabric diagram, although the latter certainly suggests more of a point-maximum-like than of a girdle-like distribution. It may therefore be warranted (cf. Watson, 1965, 1966, and Loudon, 1964, as quoted by Whitten, 1966) to extend the quantitative analysis to fabric types intermediate between a true point-maximum and a great-circle girdle, such as the elongated point-maximum of Fig. 18, b. In a number of diagrams in the next chapter the directions of the eigenvectors associated with the largest and smallest eigenvalues of $M$ are indicated; estimated values for $\varkappa$ are given in a few cases.

CHAPTER VI

## MICROSCOPICAL FABRIC ANALYSIS OF THE PERIDOTITE

### INTRODUCTION

The primary aim of the application of petrofabric analysis in the present study was to investigate the relations between the orientation patterns of the peridotite minerals and the structures that are visible in the hand-specimen and in the exposure. In this way a certain mineral can be related to a particular S-plane or lineation, and even a mineral association to a generation of megascopic structures, so that the mineralogical (Table 5) and structural (Table 2) evolution of the peridotite can be correlated. Secondly, the fabric patterns obtained for olivine and orthopyroxene were examined apart from their regional setting at Alpe Arami to find indications concerning the mode of origin of the garnet-peridotite, by comparing them with olivine and orthopyroxene fabrics from the literature as well as on the basis of theoretical and experimental arguments.

*Presentation of the diagrams.* — All fabric diagrams are in lower hemisphere, equal-area projection. Unless otherwise stated, the equatorial plane is the horizontal plane; N on the diagrams points to grid north. In the

explanatory text, $N$ is the number of grains measured, $A$ is the area of the counting circle (area of hemisphere = 1), and $k$ is the estimated value of the concentration parameter $\varkappa$ for a model point-maximum distribution (p. 101). E.P. and E.G. stand for the estimated positions of the centre of a point-maximum and the axis of a great-circle girdle, respectively, i.e. the locations of the eigenvectors associated with the largest and smallest eigenvalue of matrix $M$ (p. 101). We have seen that the application of the eigenvector technique may be extended to distributions that are intermediate between a point-maximum and a great-circle girdle (p. 102).

In the olivine diagrams contours are drawn at densities 1, 1.25, 1.50, etc., in the clinopyroxene diagrams at 1, 1.5, 2, etc., in the orthopyroxene and amphibole diagrams at 1, 2, 3, etc. Shadings are explained in Fig. 19. In the orthopyroxene and amphibole diagrams the heavy contour is at density 5; the area under the 1-contour is shaded where the interpretation becomes difficult because of a very low degree of preferred orientation. The dashed contour is at density 1 in all diagrams.

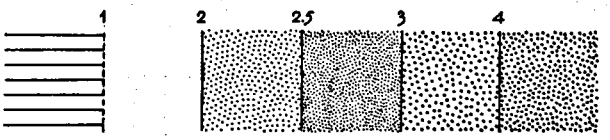


Fig. 19. Key to shading of petrofabric diagrams in Chapter VI (numbers refer to contour density values).

Megascopically observed S-planes are shown as solid lines, statistically inferred planes are dashed in the fabric diagrams. There is always some uncertainty regarding the exact localization of the megascopic structures (S-planes, lineations, fold axes) in the diagrams, in particular when they are not visible in the analysed hand-specimen. In the latter case the orientations measured in the exposure were transposed into the diagrams.

*Relation between optical and crystallographical directions of the investigated minerals.* — The axes of the optical indicatrix $\alpha$, $\beta$, and $\gamma$ correspond to crystallographical directions as follows. Olivine: $\alpha_{OL} = b_{OL}$, $\beta_{OL} = c_{OL}$, and $\gamma_{OL} = a_{OL}$; orthopyroxene: $\alpha_{OPX} = b_{OPX}$, $\beta_{OPX} = a_{OPX}$, and $\gamma_{OPX} = c_{OPX}$; clinopyroxene: $\beta_{CPX} = b_{CPX}$, $\gamma_{CPX} \wedge c_{CPX} \approx 39°$. For amphibole, only the orientation of crystallographical directions is shown.

## ORIENTATION OF THE PERIDOTITE MINERALS AND ITS RELATION TO THE MEGASCOPIC STRUCTURAL COMPONENTS

### *Garnet-peridotite fabrics*

*Specimen AR26: garnet-peridotite (Fig. 20)*[1]. — The locality is an exposure of the southern garnetiferous zone (Enclosure I). Pyroxenite streaks defining a layering plane ($S_L$) dip steeply to the southwest. On $S_L$, two lineations are visible: a mineral lineation ($l_0$), pitching steeply NW, and a fine striation ($l_1$), pitching gently SE. The rocks exhibit a schistose character; they part well along $S_L$. Although its position cannot be ascertained because of the absence of chlorite, the Alpine cleavage $S_1$ is here in all probability subparallel to $S_L$. In that case the $l_1$-lineation would be due to the intersection of $S_L$ and $S_1$ under a very low angle (cf. p. 71).

The garnet-peridotite is partly altered into spinel-amphibole-peridotite (Plate III, c; modal composition in Table 4, e). In the thin section, olivine, ortho- and clinopyroxene, and amphibole grains are markedly elongated parallel to the trace of $S_L$. A quantitative study of grain shape and grain elongation is difficult to perform, however, because of the extremely xenomorphic outline of most of the grains.

Olivine. Among the three axes of the indicatrix, $\gamma_{OL}$ shows the strongest concentration. The diagram indicates the presence of a point-maximum of $\gamma_{OL}$ perpendicular to $S_L$ ($k = 1.0$), with perhaps a tendency to spread along two great-circle girdles perpendicular to $S_L$. $\beta_{OL}$ exhibits a great-circle girdle pattern along $S_L$, with maximum concentrations near $l_0$. The diagram for $\alpha_{OL}$ does not show significant concentrations.

Orthopyroxene. $\beta_{OPX}$ has a strong maximum ($k = 3.2$) roughly perpendicular to $S_L$, with some extension along a great-circle girdle whose axis is close to $l_0$. $\gamma_{OPX}$ spreads in a partial great-circle girdle with a maximum concentration near $l_0$. The calculated axis of the $\gamma_{OPX}$-girdle does not coincide exactly with $\pi S_L$, but the angle between E.G. and $\pi S_L$ is not large (about 20°). The orientation of $\alpha_{OPX}$ is weaker than that of $\beta_{OPX}$ and $\gamma_{OPX}$, there exists a broad maximum, elongated along $S_L$, and roughly perpendicular to the maxima of $\beta_{OPX}$ and $\gamma_{OPX}$.

Clinopyroxene. The most obvious feature of the clinopyroxene fabric of AR26 is the point-maximum of $c_{CPX}$ ($k = 3.7$). E.P. is within 5° from $l_0$. The great-circle around E.G. reflects the slight extension of the maximum along $S_L$. In the $\gamma_{CPX}$-diagram a small-circle has been drawn with an angular radius of 39° (equalling the average value of $c_{CPX} \wedge \gamma_{CPX}$) around the E.P. determined for $c_{CPX}$. It can be seen that the small-circle girdle of $\gamma_{CPX}$ depends on the orientation of $c_{CPX}$. In a broad sense the same holds for the $\alpha_{CPX}$-pattern. The angular radius of the small-circle drawn in the $\alpha_{CPX}$-diagram is 51°. As could be expected from their common perpendicularity to $c_{CPX}$, the diagrams for $\beta_{CPX}$, $\pi$ {100}$_{CPX}$, and $\pi$ {110}$_{CPX}$ display about the same great-circle girdle pattern, with its axis near $l_0$. Both $\pi$ {100}$_{CPX}$ and $\pi$ {110}$_{CPX}$ are concentrated near $\pi S_L$. Within the $\pi$ {110}$_{CPX}$-girdle there is an additional maximum near $S_L$, at right angles to the main $\pi$ {110}$_{CPX}$-concentration.

It should be borne in mind that $\pi$ {110}-diagrams for

[1] Localities of hand-specimens AR are to be found on Enclosure II.

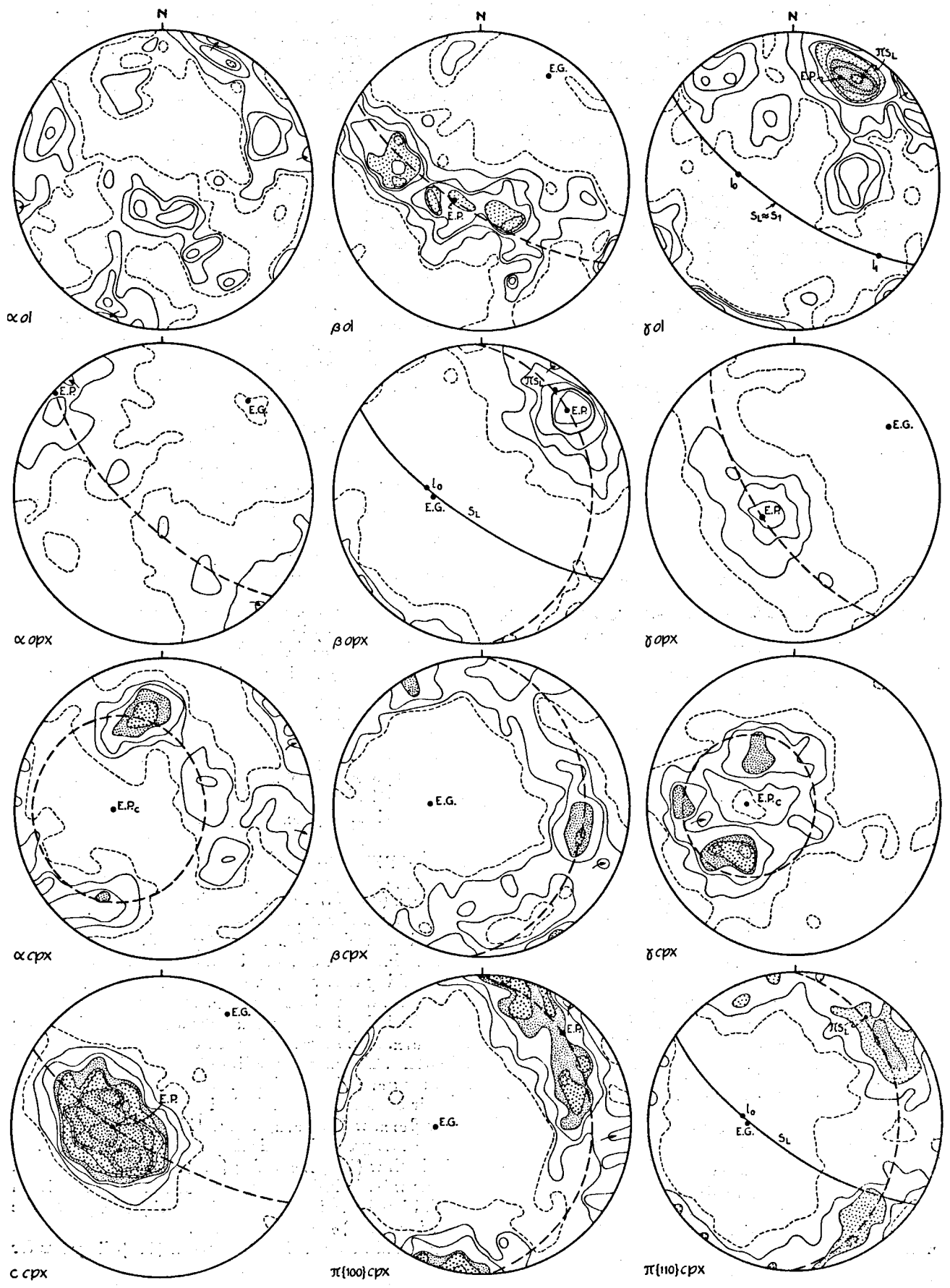


Fig. 20. Garnet-peridotite AR26 — olivine: $N = 200$, $A = 0.04$; orthopyroxene: $N = 200$, $A = 0.025$; clinopyroxene: $N = 100$, $A = 0.04$.

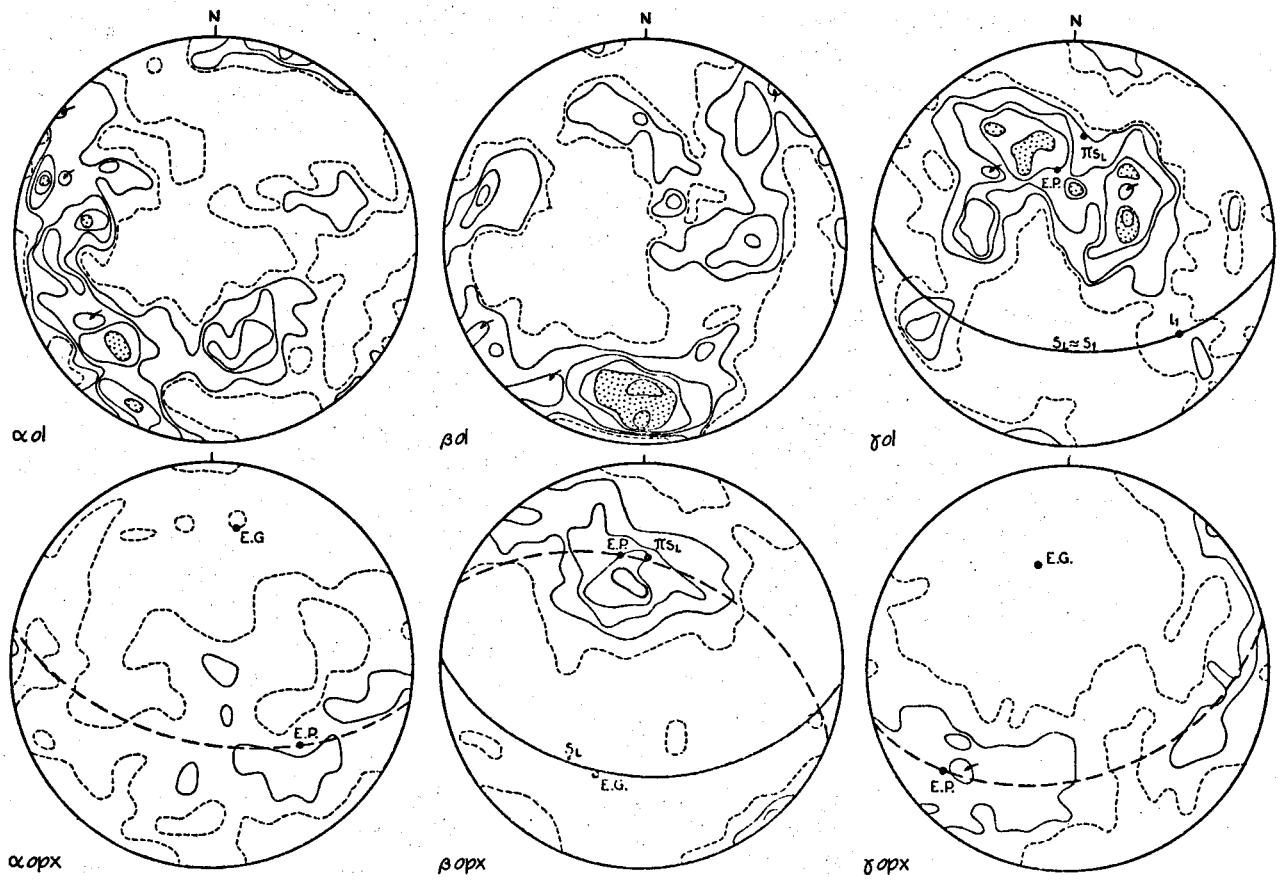


Fig. 21. Garnet-peridotite AR50 — olivine: $N = 200$, $A = 0.04$; orthopyroxene: $N = 200$, $A = 0.025$.

clinopyroxene and amphibole are constructed with a double number of directions, since both (110) and (1$\bar{1}$0) are considered. The observations are correlated, for they consist of pairs of {110}-planes enclosing a fixed angle. Therefore, the probability model underlying the $\pi$ {110}-diagrams cannot consist of a single point-maximum within a great-circle girdle. However, this does not necessarily imply that two equally well-developed $\pi$ {110}-maxima, with a distance between them of about 90° (clinopyroxene) or 60° (amphibole), should always be present.

*Specimen AR50: garnet-peridotite (Fig. 21).* — This specimen also originates from the southern garnetiferous zone of the peridotite lens. $S_L$ can be recognized in the field by the presence of garnet- and clinopyroxene-rich layers, dipping 45° to the south. A pronounced cleavage is parallel to $S_L$, and again a fine $l_1$-striation is visible; this lineation is almost parallel to the attitude of $l_1$ at the exposure of AR26, described just now. It may be inferred that $S_L$ approximately parallels $S_1$. No other lineation could be observed.
AR50 is less decomposed into spinel-amphibole-peridotite than AR26. Clinopyroxene is hardly altered, and the occurrence of amphibole is virtually limited to the kelyphitized borders of the garnets and their immediate surroundings. The grains are flattened parallel to $S_L$. Narrow mylonitized zones (cf. Plate VI, c) parallel to $S_L$ are present; grains occurring within these zones were left out in the measurement of the mineral orientations. A relatively large proportion of the olivine and orthopyroxene crystals exhibits undulatory extinction and kink bands.

Olivine. A point-maximum for $\gamma_{OL}$ ($k = 0.9$) lies near the pole of the layering plane $\pi S_L$, with possibly some extension along two great-circle girdles roughly perpendicular to $S_L$. The highest concentrations of $\beta_{OL}$ (and of $\alpha_{OL}$) occur near $S_L$, but in contrast with the $\beta_{OL}$-diagram of Fig. 20, no $\beta_{OL}$-girdle parallel to $S_L$ is visible here.

Orthopyroxene. The $\beta_{OPX}$-diagram shows a well-defined point-maximum ($k = 2.5$) close to $\pi S_L$. The great-circle drawn around E.G. reflects to some extent the elongation of the area of maximum concentration perpendicular to $S_L$. $\gamma_{OPX}$ displays a great-circle girdle pattern roughly along $S_L$, with a broad maximum in the southwestern quadrant of the diagram. The $\alpha_{OPX}$-diagram shows weak preferred orientation along $S_L$, with some concentration in the southeastern quadrant, perpendicular to the maxima of $\beta_{OPX}$ and $\gamma_{OPX}$.

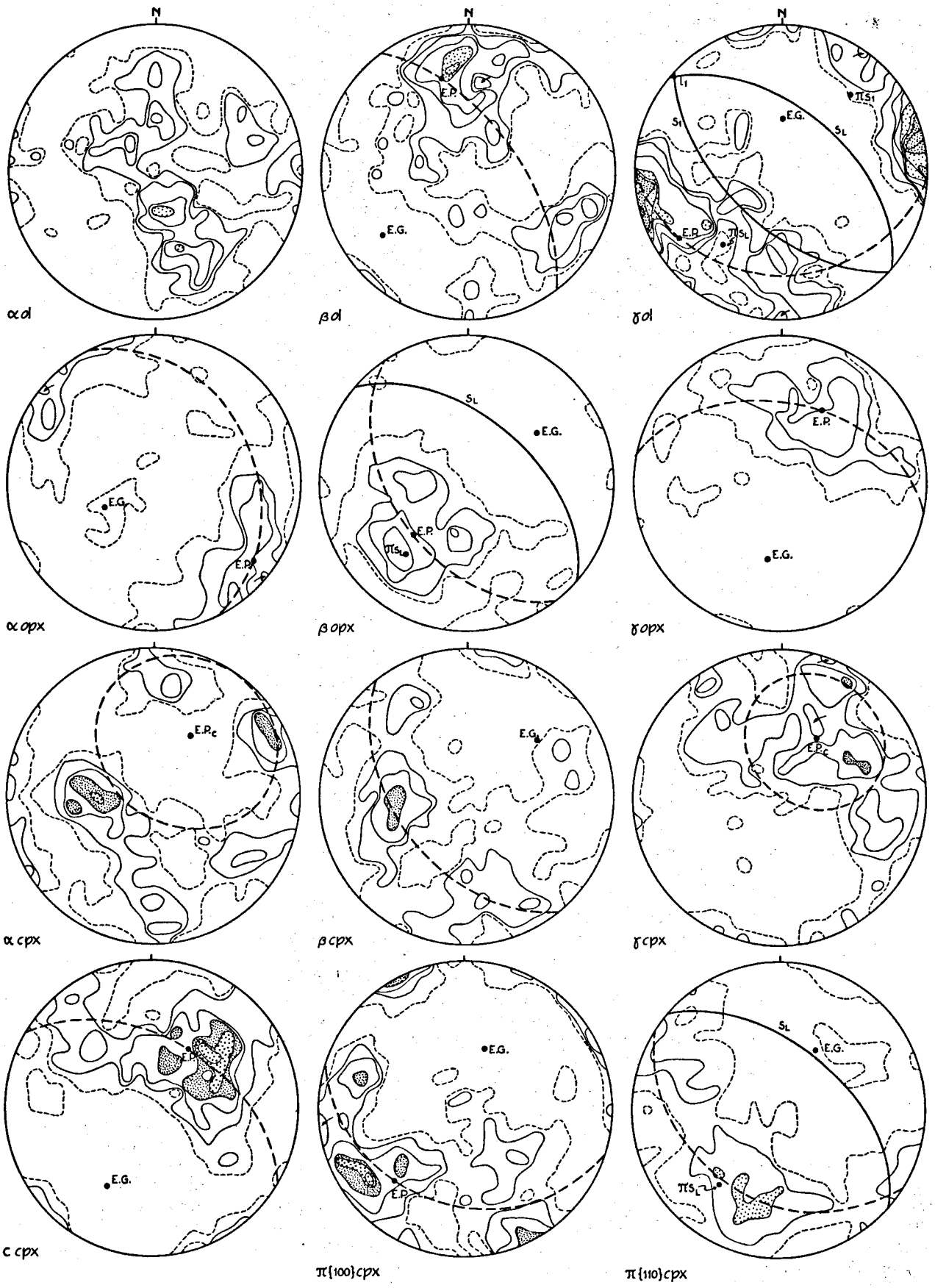


Fig. 22. Garnet-peridotite AR37 — olivine: $N = 200$, $A = 0.04$; orthopyroxene: $N = 200$, $A = 0.025$; clinopyroxene: $N = 100$, $A = 0.04$.

*Specimen AR37: garnet-peridotite (Fig. 22).* — The exposure of AR37 lies in the northern garnetiferous zone. $S_L$-planes (pyroxenite layers and layers alternately rich and poor in garnet) have somewhat varying attitudes, with an average dip of 50° to 60° to the NNE. $S_1$-planes are represented as closely spaced cleavage planes dipping steeply SW. It can be inferred that $l_1$ is almost horizontal NW-SE. The rocks do not part well along either $S_L$ or $S_1$.
The garnet-peridotite (Table 4, d) is weakly altered into spinel-amphibole-peridotite. In a thin section perpendicular to $l_1$ the long diameter of most grains is parallel to $S_L$, and narrow mylonitic bands follow the same plane. Only grains outside these zones were measured. At large angles to the trace of $S_L$, the traces of the $S_1$-cleavage planes cut across the mineral grains without disturbing their orientation; there are no signs of mylonitization along $S_1$.

Olivine. Although the highest concentration in the $\gamma_{OL}$-diagram does not coincide with $\pi S_L$, the configuration of the area above the 1-contour as a whole is still indicative of a broad point-maximum ($k = 1.1$) perpendicular to $S_L$, with a tendency to spread along a great-circle girdle. The $\alpha_{OL}$- and $\beta_{OL}$-maxima are weaker than the maximum of $\gamma_{OL}$. The $\beta_{OL}$-axes are concentrated near $S_L$, with a maximum plunging moderately northward. The $\alpha_{OL}$-axes follow a broad, incomplete girdle parallel to the great-circle drawn around E.G. in the $\beta_{OL}$-diagram, i.e. a great-circle with its axis close to E.P. in the $\gamma_{OL}$-diagram.

Orthopyroxene. A point-maximum of $\beta_{OPX}$ ($k = 2.4$) can be observed near $\pi S_L$. The great-circle drawn around E.G. in the fabric diagram indicates some spread of the maximum along a girdle perpendicular to $S_L$. Both $\alpha_{OPX}$ and $\gamma_{OPX}$ display partial great-circle girdles. The concurrence between the calculated girdle axes is not very satisfactory, but the average girdle axis for the two diagrams is still near $\pi S_L$ and near E.P. of $\beta_{OPX}$. $\gamma_{OPX}$ has a maximum concentration plunging moderately in a north- to northeastward direction, and the slightly weaker-oriented $\alpha_{OPX}$ possesses its maximum density 90° away from the $\gamma_{OPX}$-maximum.

Clinopyroxene. The $c_{CPX}$-diagram shows a point-maximum-like concentration ($k = 1.7$) that is much weaker than the $c_{CPX}$-maximum of AR26. Moreover, the extension along $S_L$ is more clearly represented in the diagram of AR37. The small-circle girdle patterns for $\gamma_{CPX}$ and $\alpha_{CPX}$ are therefore not so distinct as in Fig. 20 (in Fig. 22 small-circles with angular radii of 39° ($\gamma_{CPX}$) and 51° ($\alpha_{CPX}$) are drawn around E.P. of $c_{CPX}$). The three axes, which are crystallographically perpendicular to $c_{CPX}$, viz. $\beta_{CPX}$, $\pi$ $\{100\}_{CPX}$, and $\pi\{110\}_{CPX}$, lie in roughly coincident great-circle girdles around the $c_{CPX}$-maximum. $\pi$ $\{110\}_{CPX}$ and $\pi$ $\{100\}_{CPX}$ are notably concentrated in the neighbourhood of $\pi S_L$; in the $\pi$ $\{110\}_{CPX}$-diagram a weak, secondary maximum appears perpendicular to the main $\pi$ $\{110\}_{CPX}$-concentration.

*Specimen AR49: garnet-peridotite with mylonitic band (Fig. 23).* — In this outcrop of the northern garnetiferous zone the layering dips gently NNE, whereas the Alpine cleavage $S_1$ dips moderately to steeply towards the south (Plate I, b). On $S_L$ two lineations are visible: $l_0$, produced by a preferred orientation of pyroxene *c*-axes and even by a preferred elongation of garnets, plunging northward, and $l_1$, the intersection of $S_L$ and $S_1$, gently plunging ESE. Thin section study reveals the presence of a narrow mylonitized zone along a third plane $S_m$, lying subparallel to $S_L$ (p. 84; Plate VI, c). The minerals of the garnet-peridotite assemblage are flattened parallel to $S_L$, but the minerals within the mylonite band constituting a spinel-amphibole-peridotite paragenesis possess a nearly equant habit. There is no microscopical evidence for movement along $S_1$.

Olivine. The orientation of olivine (1) outside the mylonitic band, is characterized by a maximum of $\gamma_{OL(1)}$ ($k = 1.0$) near $\pi S_L$. The concentration parameter $k = 1.1$ for $\alpha_{OL(1)}$ is even greater than for $\gamma_{OL(1)}$ in this case. Although $\alpha_{OL(1)}$-concentrations can be observed near $S_L$, the most important $\alpha_{OL(1)}$-maximum lies about halfway between $S_L$ and $\pi S_L$ (and $\pi S_m$). The $\beta_{OL(1)}$-girdle roughly follows the $S_L$-plane.
Correlation of the fabric of fine-grained olivine(2) with megascopic structures is more difficult. Compared to the corresponding diagrams of olivine(1), the $\gamma_{OL(2)}$-point-maximum ($k = 1.2$) has shifted away from $\pi S_L$ and $\pi S_m$, and $\alpha_{OL(2)}$ has developed into a great-circle girdle with a maximum near $\pi S_m$, but with other maxima as well. Only the $\beta_{OL(2)}$-diagram, with its girdle along $S_m$, resembles the $\beta_{OL(1)}$-diagram to a certain extent. Neither the centre of the $\gamma_{OL(2)}$-point-maximum nor the axis of the $\alpha_{OL(2)}$-great-circle girdle, are represented in the megascopic fabric of the rock. Of course, it still is possible that these directions have a tectonic significance, but another explanation that seems more likely will be given below.

Orthopyroxene. $\beta_{OPX(1)}$ displays a point-maximum ($k = 2.6$) close to $\pi S_L$, with a tendency to spread in an incomplete girdle, with its estimated axis near $l_0$. A girdle of $\gamma_{OPX(1)}$ extends along $S_L$, E.P. is near $l_0$. The $\alpha_{OPX(1)}$-orientation is rather weak, the estimated girdle axis E.G. is about at the same place as E.G. for $\gamma_{OPX(1)}$, and E.P. for $\alpha_{OPX(1)}$ is perpendicular to the estimated maxima in the $\beta_{OPX(1)}$- and $\gamma_{OPX(1)}$-diagrams.
The orientation of fine-grained orthopyroxene(2) is almost uniform. Some areas of higher concentration are vaguely reminiscent of similar concentrations in the corresponding orthopyroxene(1)-diagrams.

*Discussion.* — The orientation patterns for olivine, orthopyroxene, and clinopyroxene of the garnet-peridotites are related to the megascopic $S_L$- and $l_0$-structures, and not to the $S_1$- and $l_1$-structures. This is at once clear from the fact that the positions of the significant features in the fabric diagrams move along

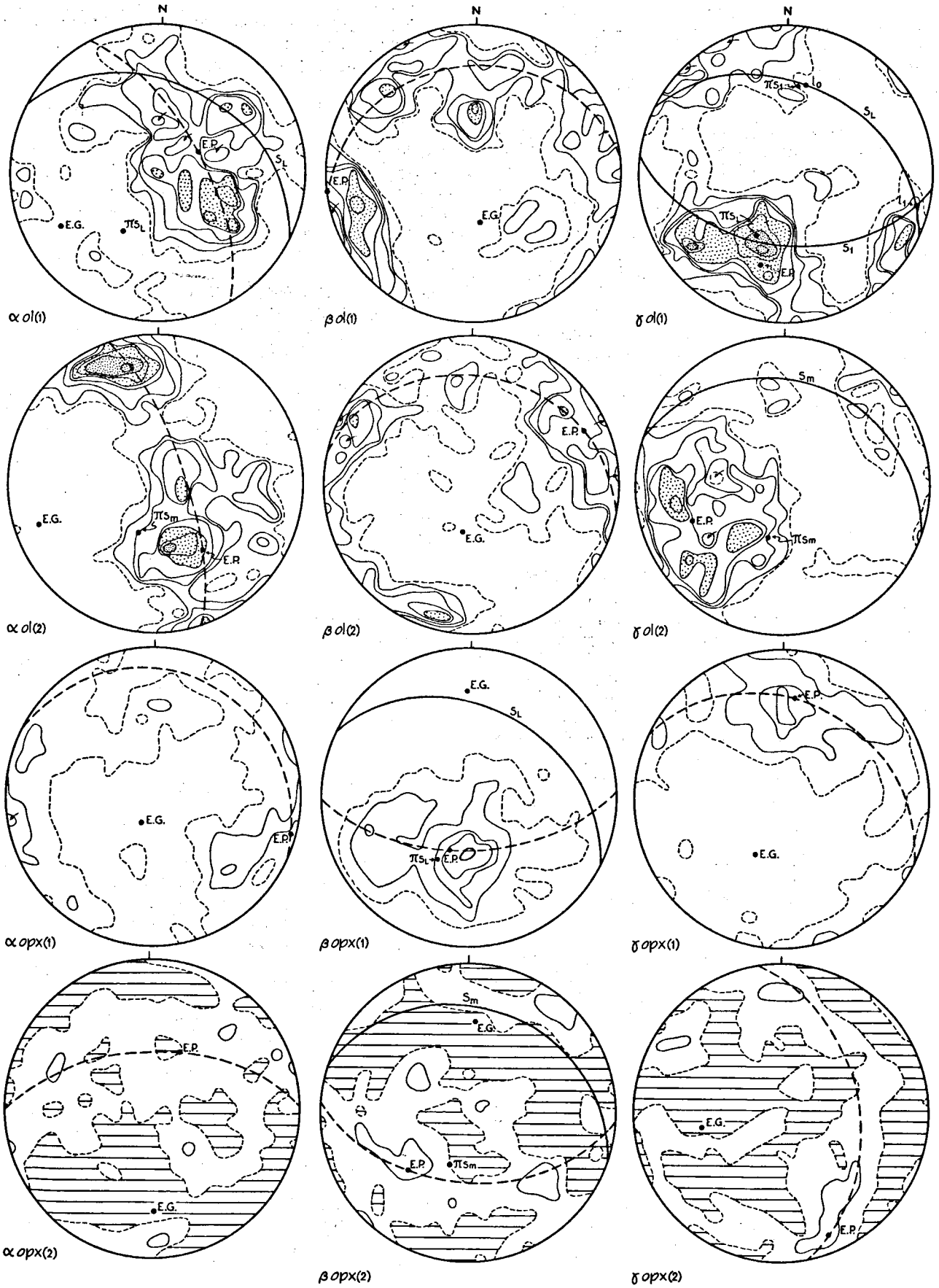


Fig. 23. Garnet-peridotite with mylonitic band AR49 — olivine (1) outside mylonitic band: $N = 200$, $A = 0.04$; fine-grained olivine (2) within mylonitic band: $N = 200$, $A = 0.04$; orthopyroxene (1) outside mylonitic band: $N = 200$, $A = 0.025$; fine-grained orthopyroxene (2) within mylonitic band: $N = 200$, $A = 0.025$.

with the change in attitude of the $S_L$-planes from the southern towards the northern garnetiferous zone, instead of remaining in the same place, as one would expect if $S_1$ governed the fabric.

The most clearly defined orientations are shown by the pyroxenes. *Orthopyroxene* possesses a rather strong orientation of $\beta$ ($= a$) perpendicular to $S_L$ ($k = 2.4$—3.2, average = 2.7) with some extension along a great-circle girdle whose axis is at $l_0$. Its *c*-axis ($= \gamma$) spreads in the layering plane, with a maximum concentration in the direction of $l_0$, as could be anticipated from the megascopical observations (AR26 and AR49). $\alpha_{OPX}$ also follows $S_L$, but its orientation is always weaker than that of the *c*-axis, and its maximum concentration lies about 90° from $l_0$. Probably the $\alpha_{OPX}$-orientation was controlled by the orientation of the two other axes.

The orientation of the *c*-axes of *clinopyroxene* confirms the field observations: $c_{CPX}$ ($k = 1.7$—3.7, average = 2.7) parallels $l_0$ (AR26) and $c_{OPX}$, like the latter with some spread within $S_L$. The estimated axes of the $\beta_{CPX}$-, $\pi$ {100}$_{CPX}$-, and $\pi$ {110}$_{CPX}$-girdles are near $l_0$. There may be a slight preferential tendency for {110}-planes of clinopyroxene to occupy attitudes parallel to the layering plane. Where no $l_0$-lineation is visible in the field (AR37 and AR50), the $l_0$-direction can now be determined from the fabric diagrams: E.P.s of $c_{OPX}$ and $c_{CPX}$ may be used, together with E.G.s of $\beta_{OPX}$, $\beta_{CPX}$, $\pi$ {100}$_{CPX}$, and $\pi$ {110}$_{CPX}$, and the direction at right angles to E.P. of $\alpha_{OPX}$ on the great-circle around E.G. of $\alpha_{OPX}$. It appears that in AR50 a moderately to steeply westward pitching $l_0$-direction is present on $S_L$, much like $l_0$ of AR26, whereas in AR37 a similar $l_0$-direction plunges moderately NNE to NE, being comparable to $l_0$ of AR49. Consequently, the hypothesis developed in Chapter III is corroborated: the $S_L$-planes were folded by the Alpine fold axis at R in Fig. 5, e and g, with $l_0$ curving from moderately to steeply westward pitching orientations at the southern side of the peridotite synform to gently to moderately north- to northeastward plunging attitudes at the northern side.

The interpretation of the *olivine* fabrics is less easy, undoubtedly because the degree of preferred orientation is rather low. A concentration of $\gamma_{OL}$ ($k = 0.9$—1.1, average = 1.0) near the pole to the layering plane recurs constantly. The orientation of the other two axes is less explicit, although a preference for directions parallel to $S_L$ is often visible. No persistent relation between $\alpha_{OL}$ or $\beta_{OL}$ and $l_0$ could be ascertained.

*Mylonitization* as in AR49 seems to exert a different influence on the pre-existing olivine- and orthopyroxene fabrics. Whereas the preferred orientation of the garnet-peridotite orthopyroxenes decreases by mylonitization to an almost isotropic fabric, the orientation of olivine within the mylonitic band is equal to or even slightly better than outside it (and likewise better than the orthopyroxene(2) orientation). Instead of considering E.P. of $\gamma_{OL(2)}$ and E.G. of $\alpha_{OL(2)}$ as a tectonic direction that is not present as a megascopic structural component, a second and perhaps more natural interpretation might be that the garnet-peridotite pattern is overprinted by a fabric of another type, the result representing the sum of two preferred orientations. One might tentatively conclude that the mylonitization of olivine in AR49, while acting upon a previously existing fabric with $\gamma_{OL}$ at right angles to $S_L \approx S_m$, itself favours the development of a fabric with $\gamma_{OL}$ rather parallel to $S_m$, and $\alpha_{OL}$ perpendicular to $S_m$. The tendency for $\gamma_{OL}$ to approach $S_L$ may also be present in other diagrams (e.g. AR37).

To summarize, it has been demonstrated that the garnet-peridotite assemblage may be correlated with the $S_L$- and $l_0$-structures. This holds even for garnet itself, since flattening of garnet parallel to $S_L$ goes together with its elongation along $l_0$ in the exposure of AR49.

### *Spinel-amphibole-peridotite and chlorite-peridotite fabrics*

*Specimen AR41: folded spinel-amphibole-peridotite (Fig. 24).* — In the outcrop (subarea C on Enclosure II), bands of garnet-pyroxenite and garnet-rock define a roughly vertical and N-S striking layering plane $S_L$. Within the peridotites the same plane can be recognized by an alternation of layers, rich and poor in small spinel-amphibole knobs, representing altered garnets. $S_L$ is folded around an axis (B) plunging moderately N; the axial plane $S_0$ is about vertical with a N-S strike, and is therefore parallel to the general attitude of $S_L$, except in the fold hinges. The hand-specimen was taken from the hinge region of the $S_L/S_0$-folds in Plate II, c. The fabric diagrams are drawn in a projection perpendicular to B. Sketches of the fold outline, as far as it is visible in the hand-specimen, in which the locations of the two analysed sections are indicated, can be found in Fig. 24. The most prominent cleavage in the hand-specimen is the Alpine $S_1$-cleavage, cutting the fold axis at a large angle. There is only a faint indication of a schistosity parallel to $S_0$.

The rock is a somewhat serpentinized spinel-amphibole-peridotite with a few chlorite crystals developing in the spinel-amphibole-symplektite aggregates (Table 4, f). The aggregates are unusually small (⌀ 0.5 mm and less) but petrographically there is no doubt that they are altered garnets. In sections at right angles to B there is no distinct elongation of the grains along $S_L$ or $S_0$, but in a section taken parallel to B and perpendicular to $S_0$, olivine and orthopyroxene are clearly elongated along the fold axis. The $S_1$-cleavage cuts across the minerals without producing changes in their orientation.

Olivine. In section AR41-A1, where $S_L$ and $S_0$ are almost at right angles, $\gamma_{OL}$ possesses a maximum ($k = 1.5$) perpendicular to $S_0$, perhaps tending to a great-circle girdle around an estimated axis that is only 24° away from the fold axis observed in the field. $\alpha_{OL}$ occupies a great-circle girdle along $S_0$, with a maximum concentration close to E.G. of $\gamma_{OL}$. Without being very distinct, the pattern of $\beta_{OL}$ is also suggestive of a broad girdle along $S_0$.

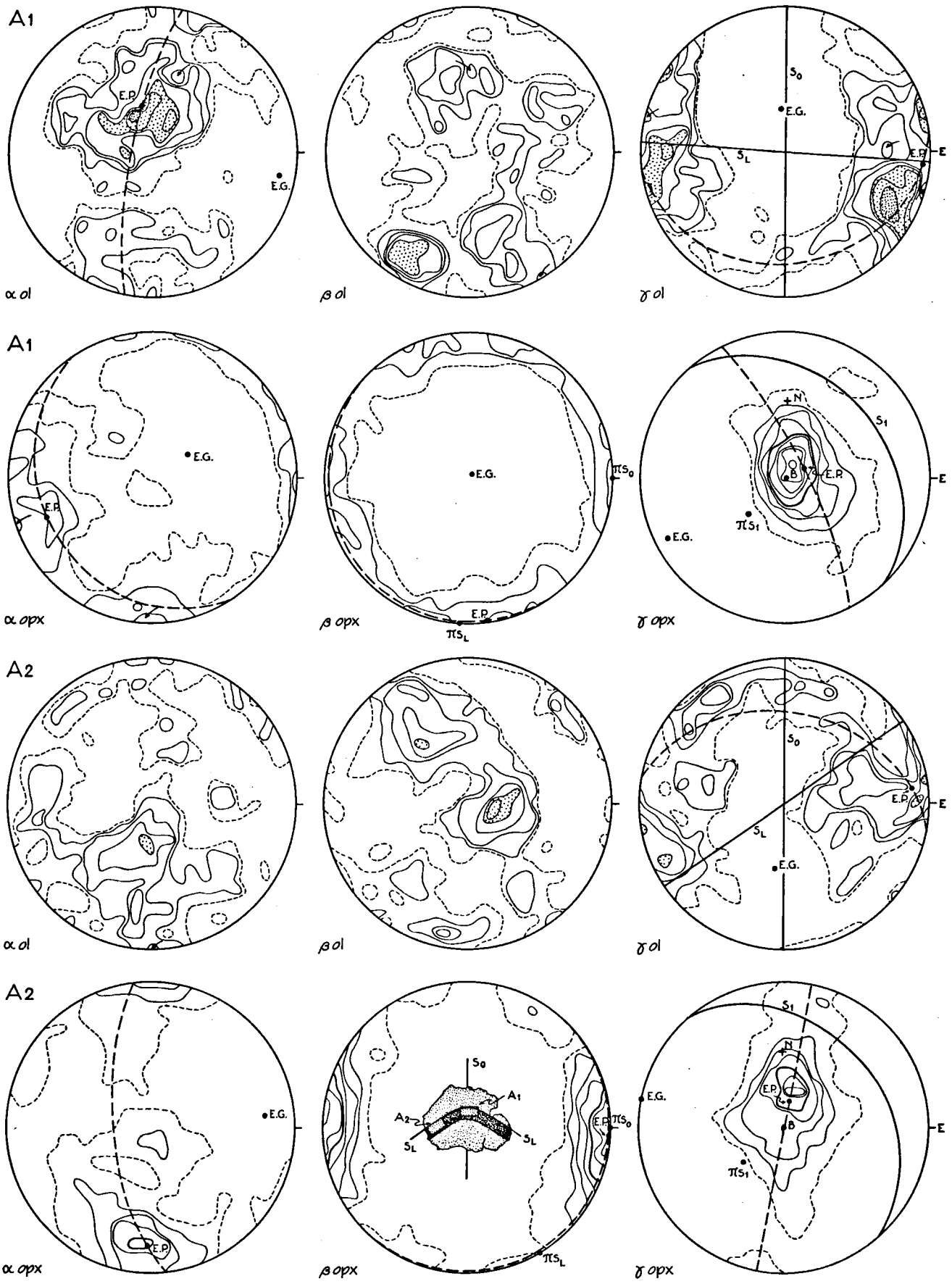


Fig. 24. Folded spinel-amphibole-peridotite AR41; projection at right angles to fold axis — olivine from section A1: $N = 200$, $A = 0.04$; orthopyroxene from section A1: $N = 200$, $A = 0.025$; olivine from section A2: $N = 200$, $A = 0.04$; orthopyroxene from section A2: $N = 200$, $A = 0.025$.

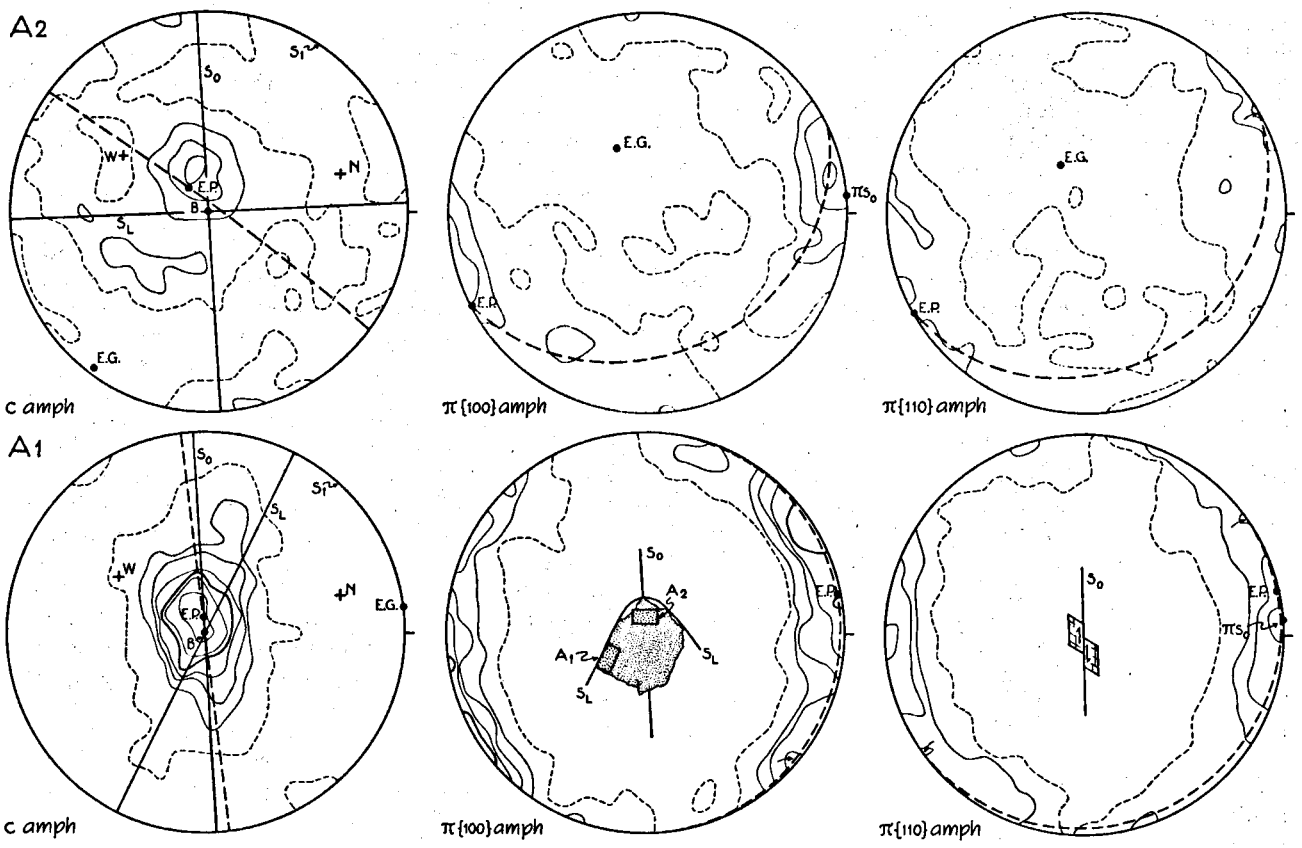


Fig. 25. Folded spinel-amphibole-peridotite AR42; projection at right angles to fold axis — amphibole from section A2: $N = 100$, $A = 0.04$; amphibole from section A1: $N = 100$, $A = 0.04$.

The olivine diagrams of section AR41-A2 show less definite patterns. $\gamma_{OL}$ still possesses the strongest orientation of the three axes; a point-maximum ($k = 0.9$) that may tend to one or more great-circle girdles, is present. E.P. is again near $\pi S_0$, but E.G. lies at the other side of B as compared to its position in AR41-A1. $\alpha_{OL}$ and $\beta_{OL}$ together occupy a broad girdle along $S_0$, and the main $\alpha_{OL}$-concentration seems to be near E.G. of $\gamma_{OL}$. However, more detailed inferences are impossible because of the low degree of preferred orientation.

Orthopyroxene. A very strong point-maximum of $\gamma_{OPX}$ ($k = 3.8$) close to the fold axis dominates the orthopyroxene fabric of AR41-A1. The great-circle drawn around E.G. is not in agreement with the girdle-like extension along $S_0$ of the point-maximum in the fabric diagram. This divergence may be caused by the fact that the distribution of the $\gamma_{OPX}$-axes in AR41-A1 is more complex than the model distribution, to which the calculations apply, viz. a point-maximum in combination with a single great-circle girdle. Apart from the distinct elongation of the maximum along $S_0$, there are indications in the configuration of the lower contours for a second girdle roughly along $S_L$. The $\beta_{OPX}$-diagram suggests a similar interpretation: a perfect great-circle girdle around B displays two regions of higher concentrations, one near $\pi S_0$, the other near $\pi S_L$. The position of E.P. does not appear to have much significance here. The $\alpha_{OPX}$-pattern, although less distinct than $\beta_{OPX}$, also exhibits a great-circle girdle approximately around B, with maximum concentrations near $\pi S_0$ and $\pi S_L$.

Section AR41-A2, where $S_L$ and $S_0$ enclose a smaller angle, shows a different fabric pattern, with $\beta_{OPX}$ now more strongly oriented than $\gamma_{OPX}$. Again, there is a discrepancy between the calculated $\gamma_{OPX}$-girdle and the conspicuous elongation along $S_0$ of the $\gamma_{OPX}$-maximum ($k = 3.1$) in the diagram. The reason is probably the same as in AR41-A1, viz. the simultaneous existence of two $\gamma_{OPX}$-girdles, one along $S_0$, and another a weak, incomplete $\gamma_{OPX}$-girdle along $S_L$. The $\beta_{OPX}$-point-maximum ($k = 3.8$) is centered at $\pi S_0$; it tends to develop into a girdle around B. Some preference for a spread towards $\pi S_L$ may be present. The $\alpha_{OPX}$-girdle lies near $S_0$, and there is a maximum at right angles to the maxima of $\beta_{OPX}$ and $\gamma_{OPX}$.

*Specimen AR42: folded spinel-amphibole- to chlorite-peridotite* (*Fig. 25*). — The locality of AR42 is only 30 m north of the outcrop of AR41, and the $S_L/S_0$-folds exposed here are similar to the folds described above. However, the fold axes plunge gently to moderately NW, and in addition a mineral lineation parallel to the fold axes produced by amphibole prisms, can be observed. The hand-specimen was taken from the hinge of a fold like that shown in Plate II, c. No distinct axial-plane schistosity is visible. The $S_1$-cleavage planes are closely

spaced; their attitude is perpendicular to the fold axis B. Again, the fabric diagrams are drawn in a projection at right angles to the fold axis.
Petrographically, AR42 is a heavily serpentinized spinel-amphibole-peridotite containing a few relicts of clinopyroxene, amphibole having been the most resistant to serpentinization. A large proportion of the spinel-amphibole-aggregates have been altered into chlorite. In a section perpendicular to $S_0$ and parallel to B, elongation of the olivine and amphibole crystals along the fold axis is conspicuous.

Amphibole. In accordance with the direction of the observed mineral lineation, the *c*-axes of amphibole in section AR42-A2 (from the crest of the fold) are concentrated near the fold axis B. However, their concentration is rather weak ($k = 1.2$) and there is no indication of a significant extension along the great-circle around E.G. Poles to {100} possess a slightly stronger degree of preferred orientation ($k = 1.5$); their maximum is found near $\pi S_0$, with an additional incomplete girdle, the axis of which is near the fold axis. Roughly the same girdle is occupied by $\pi$ {110}, and E.P. of $\pi$ {110} is very close to E.P. of $\pi$ {100}.
The other section (AR42-A1) displays a much more distinct $c_{AMPH}$-pattern. The centre of the maximum ($k = 3.3$) is close to B, and E.G. is near $\pi S_0$. Although the most distinct spread of $c_{AMPH}$ is within $S_0$, an additional extension of the maximum along $S_L$ can be observed. Both $\pi${100} and $\pi${110} occupy girdles around the fold axis, with maximum concentrations near $\pi S_0$. Especially $\pi${110} possesses a distinct maximum there.

*Discussion.* — From the diagrams of AR41 and AR42 it appears that the Alpine cleavage $S_1$ did not influence the fabric. The orientation of the analysed minerals is to a large extent related to the fold geometry, i.e. the significant features of the fabric diagrams correlate with the fold axis and the axial plane. This implies that the observed fabric patterns are of metamorphic origin.
The *orthopyroxenes* of AR41 have a strong point-maximum of their *c*-axes ($k = 3.1$—$3.8$) parallel to the fold axis, with development of a partial great-circle girdle along the axial plane, although there are vestiges of an older girdle parallel to the layering plane. In the fold limb, $\beta_{OPX}$ possesses a strong maximum perpendicular to the axial plane, whereas in the crest it develops into a complete great-circle girdle around the fold axis, with maxima perpendicular to both $S_L$ and $S_0$. $\alpha_{OPX}$ spreads along a great-circle around B in the crest, in the limb it rather spreads within the axial plane. The degree of preferred orientation of $\alpha_{OPX}$ is weaker than of the two other axes of the indicatrix; the maxima lie at right angles to the $\beta_{OPX}$- and $\gamma_{OPX}$-maxima.
*Olivine* possesses a much weaker orientation than orthopyroxene. The existence of a $\gamma_{OL}$-maximum ($k = 0.9$—$1.5$) perpendicular to the axial plane was established. No preferred orientation of a crystal axis parallel to the fold axis was found.

The field relations leave little doubt that the folds from which AR42 was taken are of the same generation as the folds at the locality of AR41, although the fold axes are not exactly parallel. In fact, there is a divergence in strike and plunge of the fold axes in the area of the two outcrops, with a preference for moderately north- to northwestward plunging directions.
The *amphibole* *c*-axes are concentrated ($k = 1.2$—$3.3$) parallel to the fold axis and to the mineral lineation, and in the limb a spread within the axial plane is visible. The axis of the $\pi${100}- and $\pi${110}-girdles is the fold axis. In the thin section from the fold crest, $S_0$ is preferably occupied by {100}, in the limb rather by {110}. Tentatively, I suggest that the $\pi${110}-maximum of amphibole at $\pi S_0$, with an asymmetric "tail" like the one in the diagram of the fold limb, might have been brought about by penetrative deformation of a crystalloblastic amphibole fabric with $\pi${100} at $\pi S_0$ and $\pi${110} oriented in two symmetrical maxima at both sides of $\pi${100}, as schematically indicated in Fig. 3, b. To a certain extent, such a fabric is shown by the amphiboles in the fold crest of AR42. Shearing along $S_0$ caused the crystals to break up along their {110}-cleavageplanes into prisms with lozenge-shaped cross-sections. The larger {110}-face may be expected to orient itself along $S_0$. From the asymmetry of the maximum in the present fabric diagram, it appears that the other cleavage is preferably oriented as indicated in the centre, which agrees with the position of the main $\pi${100}-maximum at 30° from the $\pi${110}-maximum. This being so, it seems warranted to derive from the fabric diagram a movement direction in a sense as shown by the barbed arrows. Movement in the opposite sense would be "against the grain", because of the preferred orientation of the {110}-cleavage lying at about 60° to $S_0$.

What is the relation of the metamorphic fabric patterns observed in the folded peridotites to the garnet-peridotite fabrics discussed earlier? At first sight the olivine and orthopyroxene patterns developing in the case of AR41 resemble the garnet-peridotite fabrics, so that one is tempted to postulate a contemporaneous origin for them. However, a marked difference between the orthopyroxene fabrics should not be overlooked: in AR41, the $\gamma_{OPX}$-maxima are more pronounced than in the garnet-peridotite diagrams (in AR41-A1 the orientation of $\gamma_{OPX}$ is even stronger than of $\beta_{OPX}$, which is never the case in the garnet-peridotites), whereas the $\beta_{OPX}$ great-circle girdles are much more complete than in the garnet-peridotites.
Petrographical arguments corroborate the idea that the fabric type developing during $S_L/S_0$-folding is not identical to the garnet-peridotite fabric. Firstly, the folded rocks are spinel-amphibole-peridotites and not garnet-peridotites, so that the folding is more likely to be related to the transformation of garnet-peridotite into spinel-amphibole-peridotite than to the garnet-peridotites themselves. Secondly, the established relation of the amphibole orientation to the $S_L/S_0$-fold

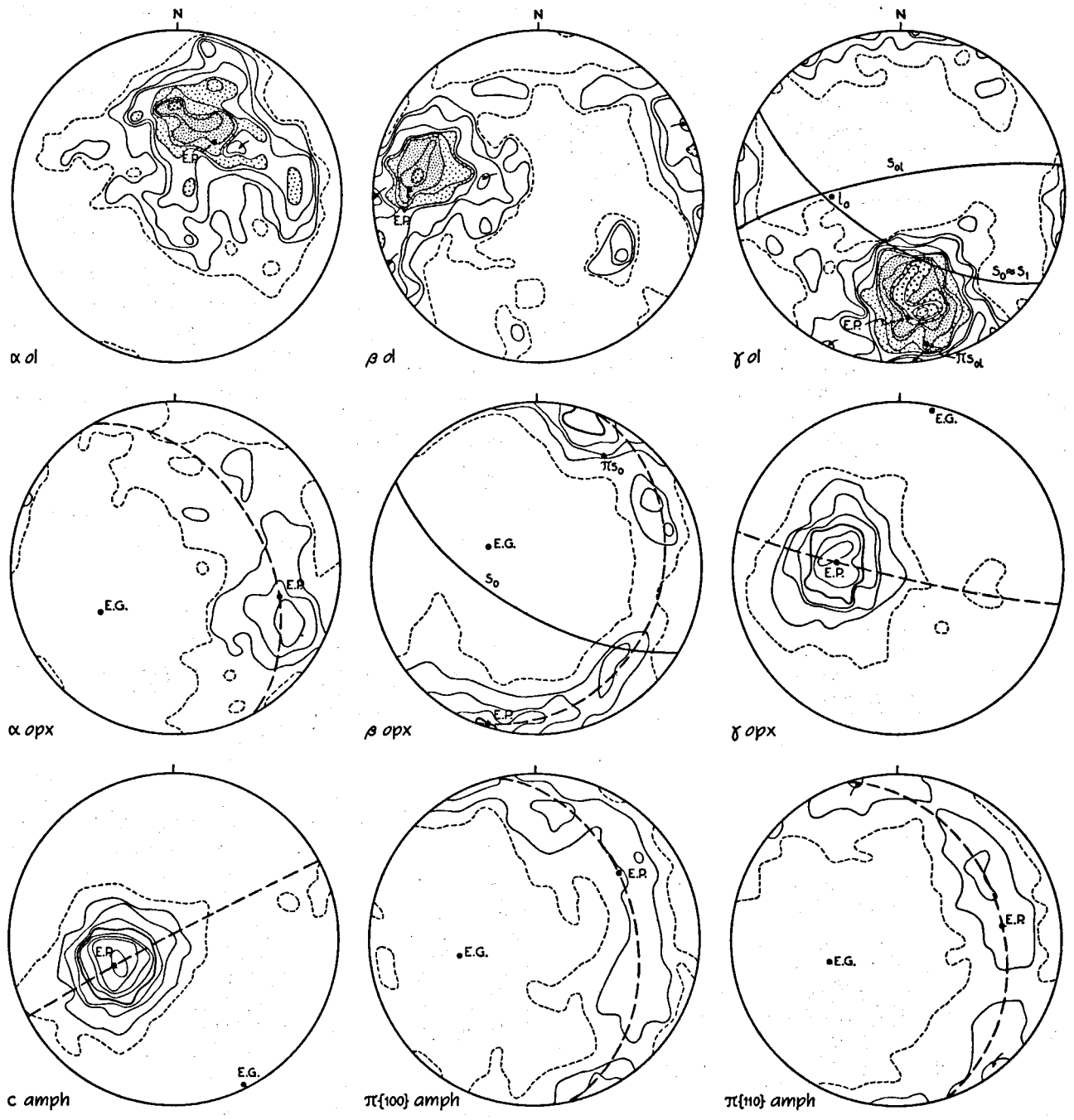


Fig. 26. Chlorite-peridotite AR18 — olivine: $N = 200$, $A = 0.04$; orthopyroxene: $N = 200$, $A = 0.025$; amphibole: $N = 100$, $A = 0.04$.

geometry offers conclusive proof that the fabric is younger than the garnet-peridotite fabric, since amphibole is absent from the garnet-peridotite assemblage. It can be concluded that, with the decomposition of garnet-peridotite into spinel-amphibole-peridotite, an amphibole fabric pattern developed, and that a reorientation of olivine and orthopyroxene took place, especially there where $S_L$ and $S_0$ are not parallel. In the orthopyroxene pattern of AR41, relicts of the garnet-peridotite fabric related to $S_L$ may still be present.

A refined interpretation of the megascopical observations presented on p. 72 is now possible, since there are two $l_0$-lineations of different age, viz. a) clinopyroxene lineations as well as orthopyroxene lineations and lineations due to a preferred elongation of garnets in garnet-peridotites ($l'_0$), and b) amphibole lineations, orthopyroxene lineations in spinel-amphibole-perido-

tites, $S_L/S_0$-fold axes, and δ-lineations on $S_0$ ($1''_0$). In the field their distinction on structural grounds was impossible because $1'_0$ and $1''_0$ are parallel wherever both can be observed, as for instance in partially amphibolized garnet-clinopyroxenites.
We conclude that the garnet-peridotite fabric dependent on $S_L$ and $1'_0$, is transformed into a spinel-amphibole-peridotite fabric related to $S_0$ and $1''_0$, with $1''_0$ parallel to $1'_0$, and $S_0$ generally parallel to $S_L$.

*Specimen AR18: chlorite-peridotite* (*Fig. 26*). — Steeply SSW-dipping to vertical schistosity planes can be observed in the field. Chlorite streaks are parallel to these planes, but no distinct layering is present. On the S-planes a moderately to steeply westward-plunging mineral lineation $l_0$ was noticed. Fabric analyses show that the schistosity planes are $S_0$-planes to which the $S_1$-cleavage is probably parallel.
A qualitative thin-section study of the grain shape reveals a most interesting angular discordance between the elongation of olivine on the one hand and of orthopyroxene and amphibole on the other, the latter parallel to the trace of $S_0$. Dal Vesco (1953, p. 249) probably referred to a similar phenomenon when he reported an angle of about 60° between the crystallographic axes of [ortho]pyroxene and the olivine axes. In Fig. 26 the planes parallel to which olivine ($S_{OL}$) and orthopyroxene and amphibole ($S_0$) are flattened, are drawn as they were determined from thin sections of the analysed hand-specimen. In a section perpendicular to $l_0$, only $S_{OL}$ is clearly visible; there, most orthopyroxene and amphibole grains are nearly equant. It appears in the diagram that $l_0$ lies close to the intersection of $S_{OL}$ and $S_0$.
The rock is a chlorite-peridotite with spinel clouds within amphibole indicating the former presence of clinopyroxene. Chlorite occurs in small aggregates (⌀ 0.5—1 mm), but also dispersed throughout the rock in isolated crystals (Plate VI, a).

Olivine. The orientation is very distinct as compared to most other olivine diagrams. The three axes of the indicatrix display almost perpendicular maxima, with $k = 1.8$ for $\gamma_{OL}$, $k = 1.7$ for $\alpha_{OL}$, and $k = 1.4$ for $\beta_{OL}$. There is no clear tendency to spread along a great-circle girdle in any of the diagrams. E.P. of $\gamma_{OL}$ is 20° from $\pi$ $S_{OL}$, and E.P.s for $\alpha_{OL}$ and $\beta_{OL}$ lie near $S_{OL}$.

Orthopyroxene. $\gamma_{OPX}$ has a very strong point-maximum ($k = 4.1$) with E.P. close to $l_0$. The $\gamma_{OPX}$-axes hardly spread within the $S_0$-plane. $\beta_{OPX}$ shows a well-developed great-circle girdle pattern. The axis of the girdle is near $l_0$, and the main concentration within the girdle is near $\pi S_0$. $\alpha_{OPX}$ also exhibits a great-circle girdle, with its axis near $l_0$. However, the $\alpha_{OPX}$-maximum is almost in $S_0$, and therefore is at right angles to the maxima of $\gamma_{OPX}$ and $\beta_{OPX}$.

Amphibole. The fabric is dominated by an excellent point-maximum ($k = 4.9$) of $c_{AMPH}$ near $l_0$. The lowest contour suggests a slight extension of the maximum along $S_{OL}$. The axes of the $\pi\{100\}$- and $\pi\{110\}$-girdles are also near $l_0$, but within the girdles there are no clear-cut maxima.

*Specimen AR52: chlorite-peridotite* (*Fig. 27*). — This exposure is located only 35 m east of the exposure of AR18 (Enclosure II). $S_L$ can be determined from the occurrence of garnet-clinopyroxenites and their retrogressive products. Locally, $S_L$ is tightly folded with the development of a pronounced axial-plane schistosity $S_0$ (Plate II, d). Generally, $S_L$ and $S_0$ dip moderately to steeply NE (the $S_0$-plane indicated in Fig. 27 was taken from the hand-specimen; its attitude is not very representative of the whole outcrop). Fold axes of $S_L/S_0$-folds, mineral lineations, and δ-lineations on $S_0$, together constitute an $l_0$-lineation that plunges moderately NNW. A fine $l_1$-striation plunging gently to moderately ESE can also be detected on $S_0$, but no distinct $S_1$-cleavage is present.
Petrographically, AR52 is similar to AR18. The former presence of garnet and clinopyroxene could be ascertained with the help of the texture of the spinel relicts. Olivine, orthopyroxene, and amphibole are distinctly flattened parallel to $S_0$.

Olivine. The well-developed $\gamma_{OL}$-maximum ($k = 1.9$) is centered near $\pi S_0$. It tends to spread around $l_0$. $\alpha_{OL}$ and $\beta_{OL}$ roughly follow the $S_0$-plane, with a marked concentration of $\alpha_{OL}$ ($k = 1.6$) plunging N to NE. The orientation of $\beta_{OL}$ is much weaker; the diagram yields no indications for the presence of a maximum within the girdle.

Orthopyroxene. The fabric is controlled by a very strong $\gamma_{OPX}$-maximum ($k = 4.4$) near $l_0$, tending to a partial great-circle girdle approximately along $S_0$. $\beta_{OPX}$ shows a partial girdle around $l_0$, with a definite maximum ($k = 3.2$) at right angles to $S_0$. The $\alpha_{OPX}$-girdle is nearly parallel to the $\beta_{OPX}$-girdle and reaches its maximum concentration 90° away from the $\beta_{OPX}$-maximum.

Amphibole. The *c*-axes concentrate in a point-maximum ($k = 3.2$) with E.P. near $l_0$. There is some spread of $c_{AMPH}$ within $S_0$. $\pi\{100\}_{AMPH}$ and $\pi\{110\}_{AMPH}$ display girdles around $l_0$, both with a conspicuous concentration near $\pi S_0$.

*Specimen AR17: chlorite-peridotite* (*Fig. 28*). — In this outcrop (Plate I, c), which is situated next to the outcrops of AR18 and AR52, the layering plane $S_L$ dips gently NE. It can be recognized by an alternation of layers, rich and poor in chlorite knobs. The knobs are flattened along $S_1$, which dips steeply SSW, and a conspicuous $S_1$-cleavage has been developed. The $l_1$-intersection plunges very gently ESE.
A modal analysis of the moderately serpentinized rock can be found in Table 4, g. Petrographical evidence for the preceding spinel-amphibole-peridotite stage is provided by the presence of spinel relicts within the chlorite aggregates (Plate V, d). Clinopyroxene must have been present in considerable amounts, judging

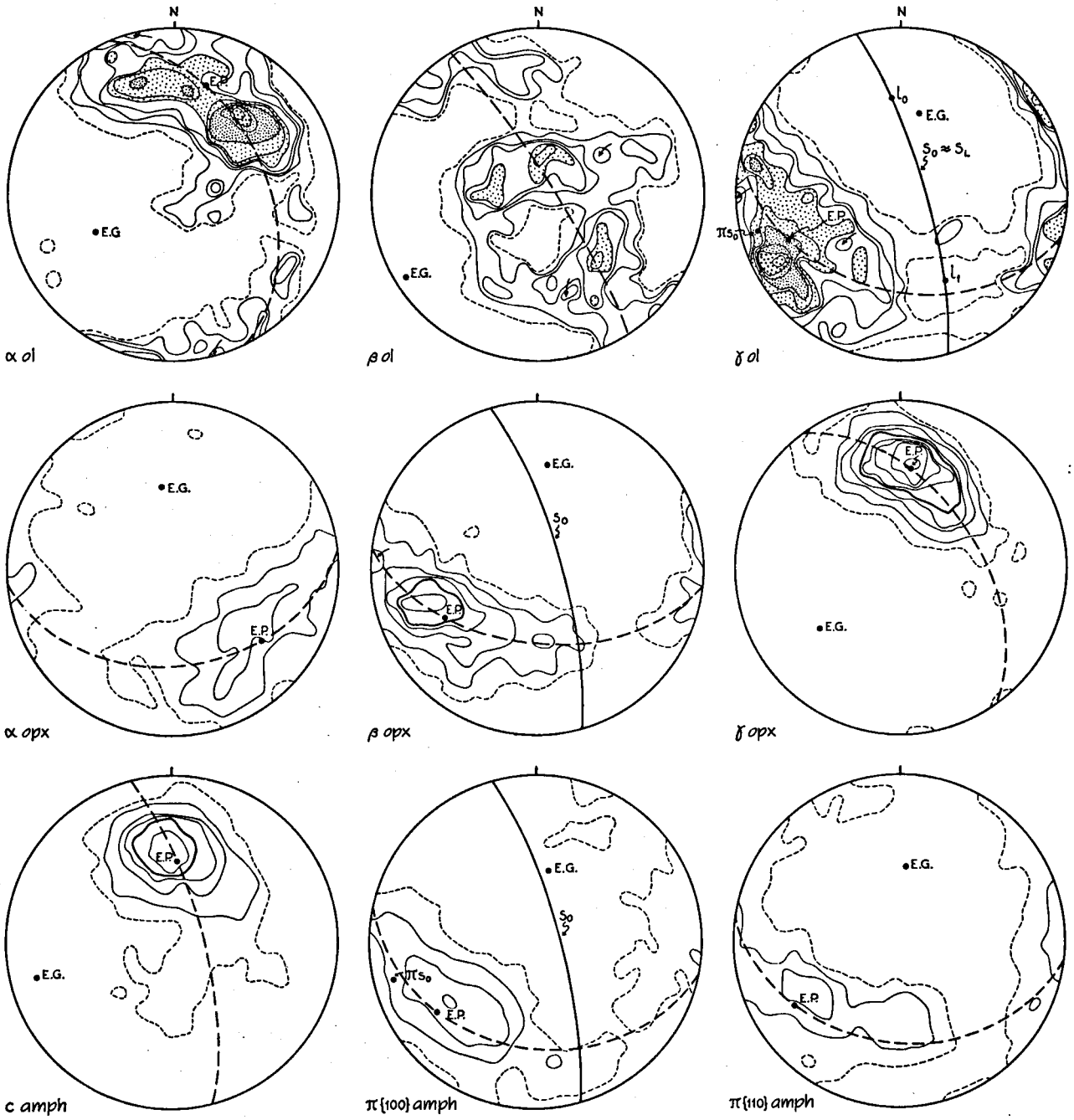


Fig. 27. Chlorite-peridotite AR52 — olivine: $N = 200$, $A = 0.04$; orthopyroxene: $N = 200$, $A = 0.025$; amphibole: $N = 100$, $A = 0.04$.

from the manifold occurrence of amphibole aggregates containing straightly bounded areas with spinel grains and threads (cf. p. 80). Olivine crystals are slightly elongated along $S_L$.

Olivine. The degree of preferred orientation of the three axes of the indicatrix is nearly equal. $\gamma_{OL}$ displays a weak maximum ($k = 0.9$) with E.P. close to $\pi S_L$. A tendency to spread into a great-circle girdle around E.G. exists in the diagram. A $\beta_{OL}$-great-circle girdle can be observed, broadly along $S_L$, with a weak concentration in a gently NNW-plunging direction. The $\alpha_{OL}$-maximum is more or less perpendicular to the $\beta_{OL}$- and $\gamma_{OL}$-concentrations. There is some indication of a girdle-like extension of the $\alpha_{OL}$-maximum perpendicular to $S_L$.

Orthopyroxene. The point-maximum of $\gamma_{OPX}$ ($k = 1.8$) is the most clearly defined feature of the orthopyroxene fabric. E.P. lies in $S_L$ and plunges gently to the north. The fabric diagram does not indicate much of a spread along a great-circle girdle,

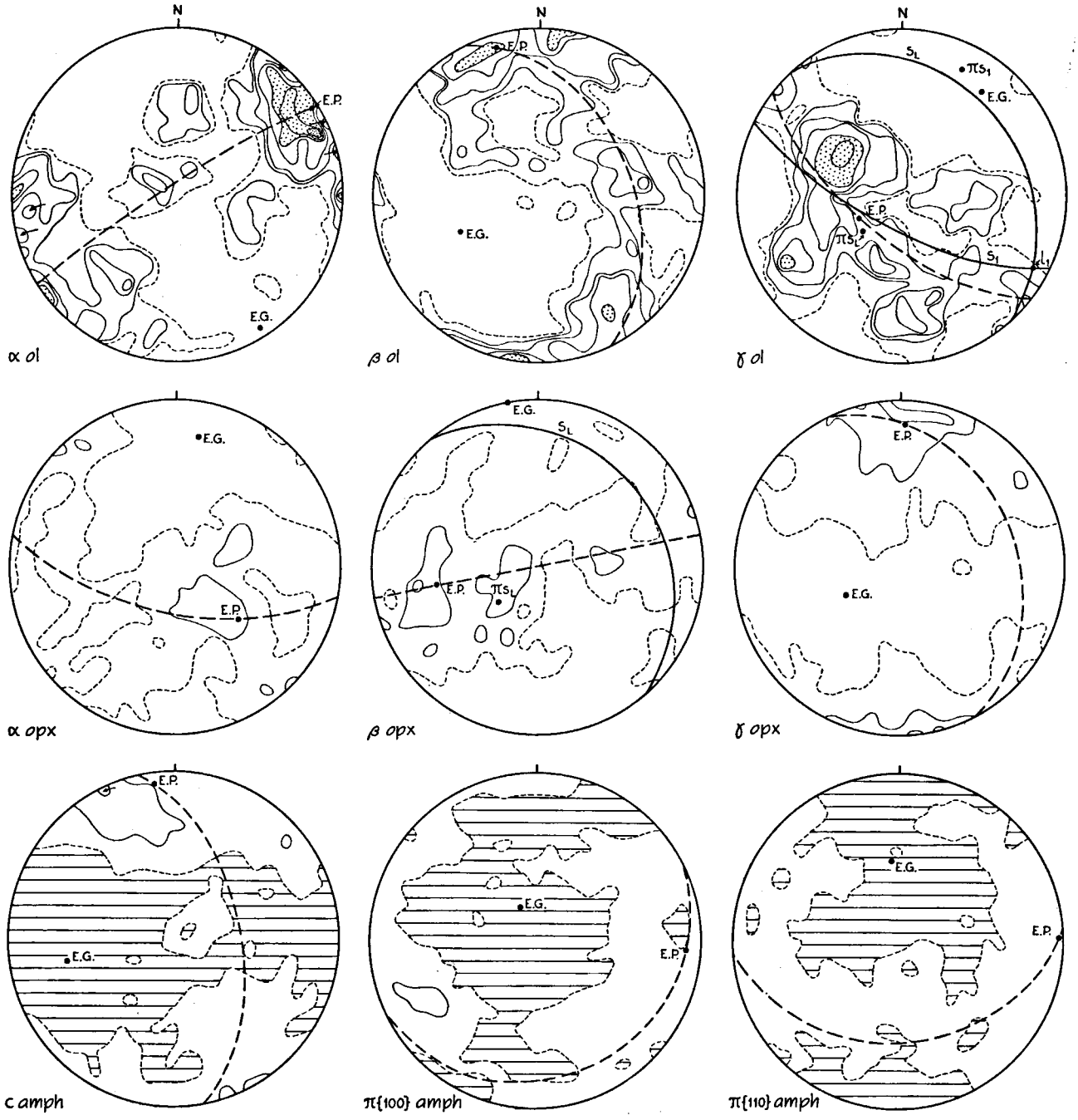


Fig. 28. Chlorite-peridotite AR17 — olivine: $N = 200$, $A = 0.04$; orthopyroxene: $N = 200$, $A = 0.025$; amphibole: $N = 200$, $A = 0.04$.

but it may be considered significant that the calculated great-circle around E.G. is close to $S_L$. $\beta_{OPX}$ and $\alpha_{OPX}$, with $\alpha_{OPX}$ having the weaker orientation of the two, show girdles whose axes lie near E.P. of $\gamma_{OPX}$. The most important $\beta_{OPX}$-concentration appears to be near $\pi S_L$, and E.P. of $\alpha_{OPX}$ is almost at right angles to E.P.s of $\beta_{OPX}$ and $\gamma_{OPX}$.

Amphibole. The *c*-axes exhibit a maximum concentration ($k = 1.1$) in $S_L$. The position of E.P. points to preferred orientations plunging gently to the north. An indistinct partial girdle along $S_L$ may be present. The interpretation of the π{100}- and π{110}-diagrams is difficult because of the very low degree of preferred orientation present (the number of grains measured is twice as large as in the amphibole diagrams of AR18 and AR52). Particularly π{110} may show a great-circle girdle, the axis of which is near the maximum concentration of the *c*-axes.

*Discussion.* — The results obtained from the investigation of specimens AR18, AR52, and AR17 are in

harmony with the conclusions drawn above from the petrofabric analyses of the folds in subarea C. Since in AR52 (Fig. 27) the distribution of the *c*-axes of orthopyroxene and amphibole is solely related to $l_0$ and not to the Alpine $l_1$-lineation, it is evident that the fabrics of these two minerals cannot be of Alpine age. In the light of the foregoing it is logical to consider the amphibole fabric of AR52 as a spinel-amphibole-peridotite fabric. Because of the similarity between the amphibole and orthopyroxene diagrams (cf. $c_{AMPH}$ and $\gamma_{OPX}$ in Fig. 27), the same must hold for the orthopyroxene fabric. Indeed, the presence of a $\gamma_{OPX}$-point-maximum together with a $\beta_{OPX}$-girdle, the $\alpha_{OPX}$-girdle being at right angles to $S_0$ instead of parallel to it, seems to be typical of spinel-amphibole-peridotites rather than of garnet-peridotites. The megascopical identification of the schistosity as $S_0$ is supported by the occurrence of $\beta_{OPX}$-, $\pi$ $\{100\}_{AMPH}$-, and $\pi$ $\{110\}_{AMPH}$-maxima near $\pi S_0$. Because the $\gamma_{OL}$-maximum is perpendicular to $S_0$, with a girdle around $l_0$, the olivine diagrams may also represent spinel-amphibole-peridotite fabric patterns. As in the fold of AR41, the $\alpha_{OL}$-maximum lies near the axis of the $\gamma_{OL}$-girdle.

In AR18 (Fig. 26) the same conformity between the amphibole and orthopyroxene fabrics exists as in AR52. The maxima for $\gamma_{OPX}$ and $c_{AMPH}$ in AR18 are less elongate along great-circle girdles than in AR52, and in AR 18 maximum concentrations within the $\alpha_{OPX}$- and $\beta_{OPX}$-girdles, and in particular within the $\pi\{100\}_{AMPH}$- and $\pi\{110\}_{AMPH}$-girdles, are less distinct than in AR52. But especially on the basis of the orthopyroxene fabric, the schistosity planes observed in the field may be considered as $S_0$-planes. Although a correlation between the olivine fabric and the grain shape is evident in AR18 (Fig. 26), with $\gamma_{OL}$ lying perpendicular to $S_{OL}$, there is a conspicuous dissimilarity with respect to the orthopyroxene and amphibole fabrics in the same rock, so that they cannot be of identical age. If the olivine fabric is younger than the orthopyroxene and amphibole fabrics, the fact that $S_{OL}$ and $S_0$ intersect close to $l_0$ must be due to chance alone, since in that case $l_0$ was already present when $S_{OL}$ originated. It is not quite conceivable that the formation of the olivine fabric (involving a mineral constituting more than 50 % of the rock) would not have obliterated the pronounced schistosity visible in the field. Therefore, it is more logical to suppose the olivine fabric of AR18 to be older than the orthopyroxene and amphibole fabrics. Whether the olivine fabric is a relict garnet-peridotite fabric dependent on $S_L$ cannot be decided, because in the exposure no layering could be observed.

The diagrams for AR17 (Fig. 28) show that the Alpine $S_1$- and $l_1$-structures do not affect the olivine, orthopyroxene, and amphibole fabrics. Again, the similarity between the orientations of $\gamma_{OPX}$ and $c_{AMPH}$ is striking. It can be inferred that $l_0$ plunges gently to the north. The orthopyroxene fabric is of the spinel-amphibole-peridotite type, with a $\gamma_{OPX}$-point-maximum and a $\beta_{OPX}$-girdle. The positions of the $\beta_{OPX}$-maximum and of the $\gamma_{OPX}$- and $c_{AMPH}$-girdles indicate that $S_0$ as determined from the spinel-amphibole-peridotite fabric, is parallel to $S_L$ as observed in the field.

According to the foregoing, the retrogressive metamorphism of the garnet-peridotites into spinel-amphibole-peridotites must be older than the main metamorphism of the surrounding gneisses. The point-maximum of $c_{AMPH}$, which is almost at right angles to the Alpine cleavage $S_1$ in AR17, constitutes conclusive evidence in this respect. However, another possibility might be considered: due to oriented intergrowth with clinopyroxene, the amphibole crystals might have inherited the clinopyroxene orientation of the garnet-peridotites. Obviously, this explanation has only a very limited value, since an important part of the amphibole crystals originated by the decomposition of garnet and the replacement of olivine and orthopyroxene, and since in partially altered garnet-peridotites oriented intergrowths of clinopyroxene and amphibole (with $c_{CPX}/c_{AMPH}$) are scarce anyway as compared to the replacement of clinopyroxene by amphibole of seemingly random orientation (p. 79; Plate IV, d). The hypothesis that the amphibole fabric is controlled to some extent by a pre-existing clinopyroxene fabric, may account for the slight extension of the $c_{AMPH}$-maximum along $S_{OL}(= S_L?)$ in AR18 (Fig. 26), as well as for the spread of the $c_{AMPH}$-axes within $S_L$ in AR42-A1 (Fig. 25).

Summarizing the characteristics of the spinel-amphibole-peridotite fabric and incorporating the data from AR41 and AR42, we can state that orthopyroxene and amphibole show the clearest patterns. The *orthopyroxene* *c*-axes concentrate in a point-maximum ($k$ = 1.8—4.4, average = 3.4) parallel to $l_0$; the maximum may tend to spread along $S_0$. $\beta_{OPX}$ develops into a great-circle girdle around $l_0$, sometimes with a distinct maximum (AR41-A2, AR52; $k$ = 3.2—3.8, average = 3.5) perpendicular to $S_0$, whereas the orientation of $\alpha_{OPX}$, which is always weaker than that of $\beta_{OPX}$ and $\gamma_{OPX}$, seems to be governed by the spatial distribution of the two other axes of the indicatrix. *Amphibole* *c*-axes also exhibit a point-maximum ($k$ = 1.1—4.9, average = 2.7), which is parallel to $l_0$ and in some cases is elongated along $S_0$. Both $\pi\{100\}_{AMPH}$ and $\pi\{110\}_{AMPH}$ display great-circle girdles around $l_0$, within which maxima near $\pi$ $S_0$ may appear (AR42, AR52). For the *olivine* fabric it has been shown that $\gamma_{OL}$ has the strongest orientation, with a point-maximum ($k$ = 0.9—1.9, average = 1.3) perpendicular to $S_0$, except in AR18, where the olivine pattern is related to an older plane, possibly $S_L$. $\alpha_{OL}$ is more distinctly oriented than $\beta_{OL}$; both axes are concentrated in the neighbourhood of $S_0$. It may be significant that E.P. of $\alpha_{OL}$ lies near E.G. of $\gamma_{OL}$, although a correlation between the position of the $\alpha_{OL}$-maximum and $l_0$ does not seem to exist, except perhaps in AR52 (Fig. 27).

According to the refined interpretation of the $l_0$-lineations (p. 113), the amphibole and orthopyroxene lineations are $l''_0$-lineations. The $l''_0$-lineations proved to be parallel to $l'_0$ of the garnet-peridotites: gently

plunging northward in subarea A (AR17, cf. AR37 and AR49), and steeply pitching westward in subarea B (AR18, cf. AR26 and AR50). The $S_0$-planes curve from subarea B to subarea A along with the $l''_0$-lineations, with $S_0$ and $l''_0$ occupying an intermediate position at the exposure of AR52, near the hinge of the synform structure (Enclosure II).
The fact that in general $S_L$ and $S_0$ are parallel, lies at the basis of the assumption made earlier, that the garnet-bearing peridotite zones are parallel not only to the $S_0$-structures, as may be expected, but also to the $S_L$-structures (p. 73).

*Chlorite fabrics.* — It has been demonstrated that in chlorite-peridotites having spinel-amphibole symplektites completely replaced by chlorite crystals, the olivine, orthopyroxene, and amphibole fabrics are still spinel-amphibole-peridotite or perhaps partially even garnet-peridotite fabrics. In the field it could already be ascertained that the *chlorite* orientation must be related to the Alpine cleavage plane $S_1$ (p. 71). Unfortunately, microscopical analysis of the chlorite fabric turned out to yield little additional information, and only one diagram is reproduced here (Fig. 29).
In specimen AR17 (cf. Fig. 28) a weak, though significant, concentration of poles to the basal cleavage {001} of chlorite occurs perpendicular to $S_1$. A similar $\pi$ $\{001\}_{CHL}$-maximum is present near $\pi S_0$ ($= \pi S_1$) in AR18 (cf. Fig. 26).
Diagrams prepared from two thin sections of AR17 (perpendicular to $S_1$ and at right angles to each other) both show a spread of the $\pi$ $\{001\}_{CHL}$-maximum along the perimeter before their rotation into a common plane, so that a reliable determination of the fabric *b*-axis is impossible. The reason why chlorite diagrams prepared from different sections of one hand-specimen do not yield coincident girdle patterns, is in all likelihood related to the difficulties involved in the random sampling of the chlorite crystals. The fact that cleavage planes can only be adjusted on the universal stage if the angle between $\pi$ $\{001\}_{CHL}$ and the plane of the thin section is less than about 45°, causes central positions of $\pi$ $\{001\}_{CHL}$ to be absent from the sample, thus introducing a serious error in the present case, since the degree of preferred orientation of chlorite is generally low. The *Schnitteffekt* also promotes the occurrence of peripheral orientations of $\pi$ $\{001\}_{CHL}$. Its influence is important, because in AR17 we applied pure grain statistics (p. 90) by measuring, within the limits set by the universal stage, all grains within a number of chlorite aggregates containing crystals of various grain sizes. Finally, some deformation of the chlorite crystals may have occurred during the preparation of the thin section, especially within the aggregates.
Therefore, the microscopical fabric analysis of chlorite was abandoned, because it dit not seem to provide more data than had already been gathered in the field, except in the case of the matrix of a chlorite-peridotite-mylonite (see below).

*Specimen AR14: chlorite-peridotite-mylonite* (*Fig. 29*). — The hand-specimen was taken from the narrow peridotite zone between eclogite and gneisses at the southern border of the peridotite lens. The rather fissile peridotites display an E-W striking, nearly vertical schistosity. The S-planes are covered with smeared-out chlorite, so that they are most probably $S_1$-planes.
Detailed petrographical observations on the chlorite-peridotite-mylonite have been presented on p. 84 (see also Plate VI, d). Both the porphyroclasts and the matrix minerals are markedly elongated along $S_1$. A preferred orientation of {001} of chlorite within $S_1$ is already conspicuous under the microscope.

Olivine. Separate diagrams have been constructed for porphyroclasts and matrix. The most prominent feature of the orientation of the *porphyroclasts* is the $\gamma_{OL}$-point-maximum ($k = 1.8$) with E.P. close to $\pi S_1$. A spread along the great-circle around E.G. is hardly visible in the diagram. $\alpha_{OL}$ and $\beta_{OL}$ are concentrated along $S_1$. Particularly the estimated $\beta_{OL}$-great-circle almost coincides with $S_1$. E.P.s of $\alpha_{OL}$ and $\beta_{OL}$ are nearly at right angles to each other.
The orientation of *matrix* olivine is quite different. Here $\alpha_{OL}$ shows the strongest orientation with a point-maximum ($k = 2.4$) at $\pi S_1$. There is a significant extension of the maximum along the great-circle around E.G. $\beta_{OL}$ follows a great-circle girdle along $S_1$, with a maximum concentration close to the axis of the $\alpha_{OL}$-girdle. $\gamma_{OL}$ is weakly oriented along $S_1$.

Chlorite. Measurements of $\pi$ $\{001\}_{CHL}$ were made in two thin sections of AR14. The poles to the planes of the sections ($\pi$A1 and $\pi$B1) are indicated in the diagram. A very strong concentration of $\pi$ $\{001\}_{CHL}$ ($k = 8.2$) can be observed perpendicular to $S_1$. The elongation of the maximum along the great-circle around E.G. is not very distinct. The divergence between the positions of E.G. calculated for the two sections individually may be partially due to sampling errors, since in both cases the estimated girdle-axis approaches the normal to the plane of the section (see above).
Both the chlorite fabric and the fabrics of the two kinds of olivine grains are related to the $S_1$-plane, which is of Alpine age. The petrotectonic behaviour of the olivine porphyroclasts, i.e. the relicts of the rock that was subjected to mylonitization, is clearly different from that of the matrix olivine; the latter seems to have originated by recrystallization during the mylonitization. With some reservations, the Alpine fabric *b*-axis may be supposed to lie near E.G.s of $\pi\{001\}_{CHL}$ and $\alpha_{OL(matrix)}$ as well as near E.P. of $\beta_{OL(matrix)}$. However, its attitude is not in accordance with the expected position of the $l_1$-lineation in this place (Fig. 3, 1; Enclosure II). Unfortunately, no megascopical $l_1$-lineation could be observed, so that the apparent anomaly could still be explained by assuming that the rocks are not entirely in place. Petrofabric analyses of more hand-specimens would

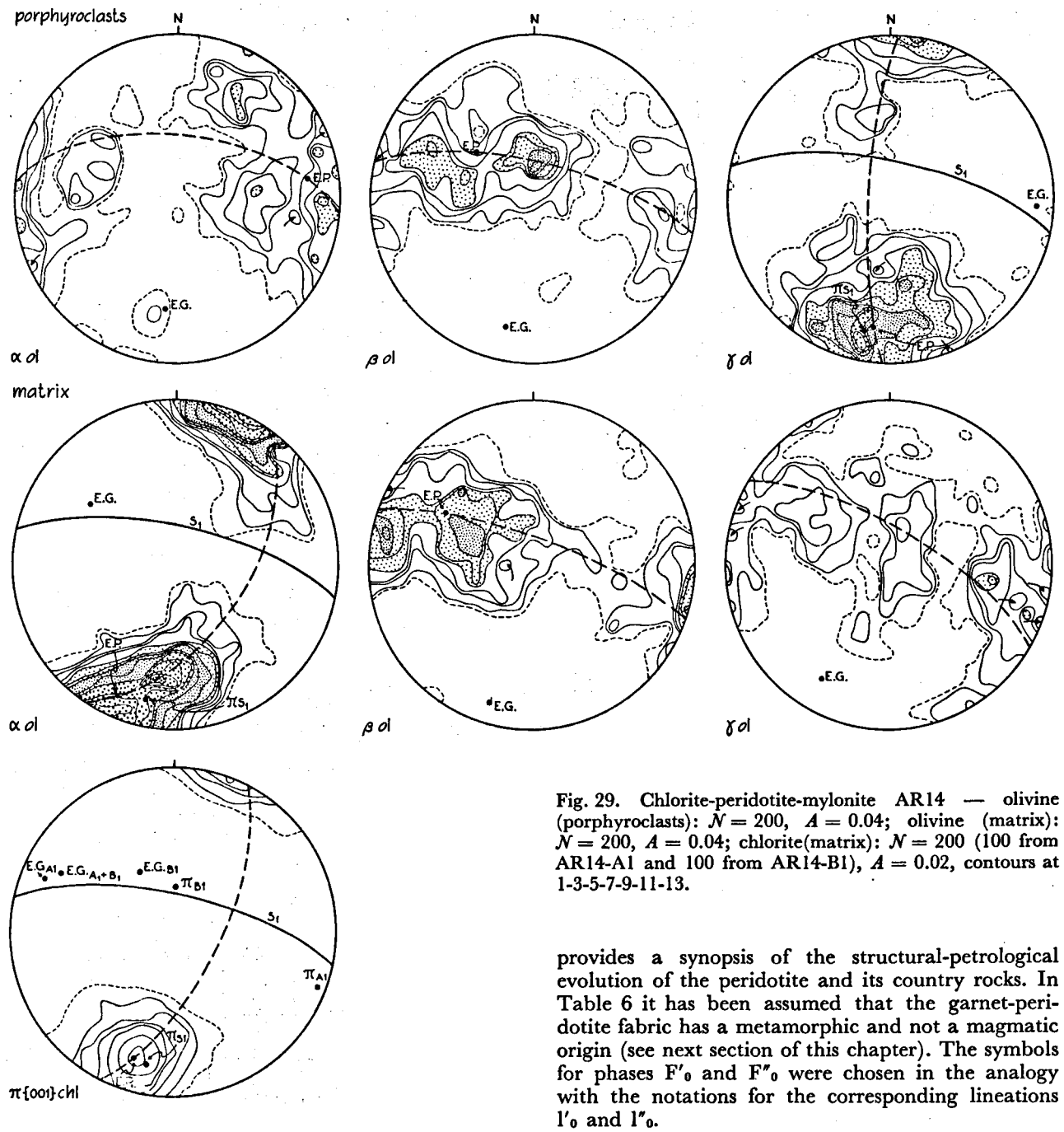


Fig. 29. Chlorite-peridotite-mylonite AR14 — olivine (porphyroclasts): $N = 200$, $A = 0.04$; olivine (matrix): $N = 200$, $A = 0.04$; chlorite(matrix): $N = 200$ (100 from AR14-A1 and 100 from AR14-B1), $A = 0.02$, contours at 1-3-5-7-9-11-13.

be necessary to clarify this point. The question of whether the orientation of the porphyroclasts with $\gamma_{OL}$ at right angles to $S_1$ constitutes an independent mechanism or is simply a relict orientation of a pre-existing spinel-amphibole-peridotite pattern with $\gamma_{OL}$ perpendicular to $S_0$ ($S_0//S_1$), will be discussed in the next section of this chapter.

*Conclusions of the comparative structural-petrological investigation*

Table 6 shows the correlation between the data in Tables 2 and 5 as determined on the basis of the results of the microscopical fabric analysis, and thus provides a synopsis of the structural-petrological evolution of the peridotite and its country rocks. In Table 6 it has been assumed that the garnet-peridotite fabric has a metamorphic and not a magmatic origin (see next section of this chapter). The symbols for phases $F'_0$ and $F''_0$ were chosen in the analogy with the notations for the corresponding lineations $l'_0$ and $l''_0$.

Whether the $S_0$-planes observed in the eclogites are to be correlated with either $S_L$ or $S_0$ in the garnet-peridotite, cannot be decided, because no microscopical fabric analyses of the eclogites were carried out. Since the garnet-peridotite assemblage constitutes an eclogite-facies paragenesis, it is natural to correlate the eclogite-facies paragenesis of the eclogites (pyrope-rich garnet + omphacite; p. 68) with $F'_0$. In the eclogites, the formation of symplektites (clinopyroxene + plagioclase) from the omphacites (and the decomposition of kyanite into spinel, corundum, and plagioclase?) may have taken place under granulite-facies conditions (Vogel, 1967, p. 132), so that a

Table 6. Structural-petrological evolution of the peridotite of Alpe Arami and its country rocks.

| tectonic phase | peridotite | | | | | eclogites | gneisses, etc. |
|---|---|---|---|---|---|---|---|
| | peridotite type | mineral paragenesis | megascopic structures | mineral orientations | metamorphic facies | | |
| ? | ? | titanclinohumite + ....? | ? | ? | ? | | |
| $F'_0$ (pre-Alpine?) | garnet-peridotite | ol + opx + cpx + gar | $S_L, l'_0$ | olivine $\gamma_{ol} \perp S_L$ (k=1.0)<br>orthopyroxene $\beta_{opx} \perp S_L$ (k=2.9)<br>clinopyroxene $c_{cpx} // l'_0$ (k=2.7) | eclogite facies | $S_0$ | ($S_3$ foliation?, bedding?) |
| $F''_0$ (pre-Alpine?) | spinel-amphibole-peridotite | ol + opx + amph + sp (± cpx) | $S_0, l''_0$ | olivine $\gamma_{ol} \perp S_0$ (k=1.3)<br>orthopyroxene $c_{opx} // l'_0$ (k=3.4)<br>amphibole $c_{amph} // l'_0$ (k=2.7) | | | |
| $F''_0$ (pre-Alpine?) | spinel-amphibole-peridotite-mylonite | | $S_m$ | mylonite:<br>olivine: no distinct relation to megascopic structures<br>orthopyroxene: almost no preferred orientation | granulite facies | | |
| $F_1$ (Alpine main phase) | chlorite-peridotite | ol + opx + amph + chl | $S_1, l_1$ | olivine, orthopyroxene, amphibole: orientation unaffected by $F_1$<br>chlorite $\pi\{001\}_{chl} \perp S_1$<br>mylonite:<br>olivine (porphyroclasts) $\gamma_{ol} \perp S_1$ (k=1.8)<br>olivine (matrix) $\alpha_{ol} \perp S_1$ (k=2.4)<br>chlorite (matrix) $\pi\{001\}_{chl} \perp S_1$ (k=8.2) | amphibolite facies | $S_1, l_1$ amphibole | $S_1, l_1$ amphibole, biotite |
| $F_1$ (Alpine main phase) | chlorite-peridotite-mylonite | | | | | | |
| $F_2$ | | | $S_2$ ? | | | | $S_2, l_2$ biotite |
| $F_3$ | | | | | | | $S_3, l_3$ |
| | serpentinite | serpentine, carbonate and talc | vertical, N-S striking talc veins | | greenschist facies | | |

correlation of this possibly first stage of retrogressive metamorphism of the eclogites with $F''_0$ is obvious. The formation of the chlorite-peridotite-mylonite is assumed to have occurred at the end of $F_1$, but an alternative explanation may be that $F_2$ caused the mylonitization.

Some brief remarks may be added here on the deformation of the peridotite. It appeared that the $S_0$-planes related to the $F''_0$-deformation are generally parallel to the $S_L$-planes of the $F'_0$-deformation. Boudinage of hornblendite and of partially amphibolized garnet-pyroxenite, as in Fig. 5, a and b, may have been brought about by $F''_0$. The same parallelism to $S_L$ holds for the $S_m$-planes along which mylonitization of the garnet-peridotite occurred, producing a spinel-amphibole-peridotite paragenesis. Because no typical spinel-amphibole-peridotite fabric developed in the mylonitized zone of AR49 (Fig. 23) and the deformation is of a cataclastic nature, it seems probable that the mylonitization took place somewhat later than the formation of the normal, medium-grained spinel-amphibole-peridotite. The locally curved axial planes of the folds in subarea C (p. 72) also indicate some deformation after the formation of the spinel-amphibole-peridotite fabric and before the Alpine $F_1$-deformation. If we assume that all $S_0$-planes were initially parallel, the occurrence of vertical, N-S striking $S_0$-planes in subarea C in fact requires an additional phase of deformation, i.e. after $F''_0$ and before $F_1$, because it is impossible to bring the $S_0$-planes from subarea C into one plane together with those from subareas A and B, by rotating around the $F_1$-axis at R in Fig. 5, e. The data are too scanty, however, to justify insertion of such a phase in Table 6.

## GENERAL CONSIDERATIONS ON THE PERIDOTITE FABRICS OF ALPE ARAMI

### *Olivine and orthopyroxene fabrics from other regions*

A survey of the petrofabric literature on olivine has been given by Collée (1962). In the brief discussion below, some more recent publications are referred to and attention is also given to orthopyroxene fabrics.

*Magmatic fabrics.* — Jackson (1961) published fabric diagrams for orthopyroxene and olivine from the ultramafic zone of the Stillwater Complex, U.S.A., the magmatic origin of which seems beyond doubt. In fact, Jackson's petrofabric study provides additional evidence for gravity settling of the euhedral orthopyroxene and olivine crystals in a magmatic environment, since the degree of preferred orientation of the grains is directly dependent on the degree of anisotropism of their shape. The orthopyroxene fabrics observed by Jackson, with $\alpha_{OPX}$ (= $b_{OPX}$) at right angles to the layering ($S_L$) and $\gamma_{OPX}$ (= $c_{OPX}$) parallel to $S_L$, are in accordance with the tabular habit of the crystals parallel to $\{010\}_{OPX}$ and their elongation parallel to $c_{OPX}$. Similar orthopyroxene orientations

were recorded by Schmidt (1952) from the pyroxenitic gabbros forming the Merensky Reef of the Bushveld Igneous Complex, South Africa, although additional maxima of $\beta_{OPX}$ perpendicular to $S_L$ were occasionally found. Again, the euhedral to subhedral orthopyroxene crystals are slightly elongated parallel to their *c*-crystallographic axes, and they are mostly flattened parallel to $\{010\}_{OPX}$.

The euhedral olivines from Stillwater are elongated parallel to $c_{OL}$ ($= \beta_{OL}$) and slightly tabular parallel to $\{010\}_{OL}$; the fabric diagrams display $\beta_{OL}$-girdles parallel to $S_L$ and weak concentrations of $\alpha_{OL}$ ($= b_{OL}$) at right angles to $S_L$ (Jackson, *op. cit.*). In other magmatic settings, olivine shows a similar preferred orientation with $\alpha_{OL}$ at right angles to the megascopic foliation, as appears, for instance, from fabric diagrams prepared for olivine phenocrysts in some basalts from New Zealand (Brothers, 1959). In all cases the preferred orientation of $\alpha_{OL}$ is controlled by the tabular habit of the olivine crystals parallel to $\{010\}_{OL}$.

*Lherzolite fabrics.* — Avé Lallemant (1967) demonstrated the tectonic and metamorphic origin of the olivine fabric of the lherzolite of the French Pyrenees: $\alpha_{OL}$ lies in a point-maximum, often extending into a partial or complete girdle, perpendicular to a schistosity ($S_0$) locally constituting the axial plane of an isoclinally folded compositional layering ($S_L$). The $\gamma_{OL}$-axes lie within $S_0$ and are mostly (sub)parallel to the $S_L/S_0$-fold axes. The orientation of orthopyroxene is significantly weaker than the olivine orientation in the same rocks; $\gamma_{OPX}$ displays girdles along $S_0$, in some cases with higher concentrations parallel to the $\gamma_{OL}$-maximum. $\alpha_{OPX}$ may show a maximum near $\pi S_0$; generally, however, $\alpha_{OPX}$ forms a complete girdle whose axis lies parallel to the $\gamma_{OL}$- and $\gamma_{OPX}$-maxima. The $\beta_{OPX}$-diagrams do not indicate much preferred orientation.

The same parallelism of $\gamma_{OL}$ with axes of folding of the peridotite layering was observed by Raleigh (1963, 1965) in a peridotite of lherzolitic mineralogy on Cypress Island, Washington State, U.S.A.

In lherzolitic nodules occurring in a basalt in Auvergne, France, Collée (1962) found that $\alpha_{OL}$ is oriented perpendicular to a plane of tectonic origin ($S_1$) cutting the compositional layering at a wide angle, whereas $\gamma_{OL}$ preferentially lies within $S_1$, often with a pronounced maximum, to which the main $\gamma_{OPX}$-concentration is parallel. $\beta_{OPX}$ and $\alpha_{OPX}$ display great-circle girdles around the $\gamma_{OPX}$- and $\gamma_{OL}$-maxima, and a $\beta_{OPX}$-concentration near $\pi S_1$ may be present. The orthopyroxene orientation seems to be as distinct as the olivine orientation here.

*Chlorite-peridotite fabrics.* — Although the available data prevent extreme generalizations, it may be interesting to note that olivine-schists possibly having a chlorite-peridotite paragenesis (Rost, 1961), from Sunnmøre, Norway, show $\alpha_{OL}$-maxima perpendicular to the schistosity (S) (Ernst, 1935; Lappin, 1967). Furthermore, in peridotites from this region with grains markedly flattened parallel to S, Lappin (*op. cit.*) found a distinct maximum concentration of $\beta_{OL}$ within S, which coincides with the fabric *b*-axis as determined within the sheared gneisses surrounding the peridotites.

*Peridotite-mylonite fabrics.* — In the matrix of the well-known dunite-mylonites of St. Paul's Rocks (Atlantic) Tilley (1947) qualitatively observed a preferred orientation of olivine, with $\alpha_{OL}$ perpendicular to the striping of the matrix. The same olivine orientation was found in finely granulated zones of mylonitic origin cutting across the lherzolite of Lers (Avé Lallemant, 1967). Yoshino (1961), on the other hand, ascertained for olivine porphyroclasts occurring in a clinopyroxene-bearing peridotite-mylonite from the Higashiakaishiyama district, Shikoku, Japan, an orientation with $\gamma_{OL}$ at right angles to the lamination (S) of the rocks. A similar pattern, with $\gamma_{OL}$ perpendicular to S, was observed by Kazakov (1965) for olivine porphyroclasts in a peridotite-mylonite from the Moncha Massif, Kola Peninsula, U.S.S.R.

*Origin of the Alpe Arami fabrics*

To obtain more insight into the origin of the garnet-peridotite fabrics, an additional study was made of a specimen found in the torrent near Gnosca (GN1 in Fig. 2) and almost certainly deriving from the peridotite body near Alpe Arami. $S_L$ is clearly defined in the hand-specimen by a pyroxenite band and by a garnet-rich zone in the peridotite. The garnet-peridotite is partially altered into a spinel-amphibole-peridotite assemblage (Plates III, d and IV, b; Table 4, c) and even some chlorite has developed locally. Several sections were cut at right angles to $S_L$, and most of them show a weak elongation of olivine, ortho- and clinopyroxene, and garnet grains parallel to the trace of $S_L$.

The fabric diagrams (Fig. 30; 905 olivines and 500 orthopyroxenes measured) agree with the garnet-peridotite patterns described above (p. 109). Orthopyroxene displays a strong orientation, with $\beta_{OPX}$ showing a point-maximum ($k = 3.7$) at right angles to $S_L$, tending to a great-circle girdle. $\gamma_{OPX}$ lies in a partial great-circle girdle along $S_L$, with a distinct maximum ($k = 2.9$). The $\alpha_{OPX}$-orientation is weaker, and seems to be controlled by the $\beta_{OPX}$- and $\gamma_{OPX}$-orientations. It can be concluded from the foregoing that in the hand-specimen an $l'_0$-lineation is present parallel to E.P. of $\gamma_{OPX}$ and E.G. of $\beta_{OPX}$.

As usual, $\gamma_{OL}$ exhibits the clearest pattern of the three olivine axes. The maximum concentration of $\gamma_{OL}$ in GN1 ($k = 1.1$) lies near $\pi S_L$, and there is a significant extension along a great-circle girdle around the inferred position of $l'_0$. $\alpha_{OL}$ and $\beta_{OL}$ both occupy broad girdles along $S_L$; E.P. of $\alpha_{OL}$ ($k = 0.8$) is close to E.G. of $\gamma_{OL}$ and is therefore near $l'_0$, so that one would conclude that in the garnet-peridotites $\alpha_{OL}$ parallels $l'_0$. This statement is difficult to reconcile, however, with the data obtained for garnet-peridotite specimen AR26 (Fig. 20), in which $\beta_{OL}$ rather seems to be

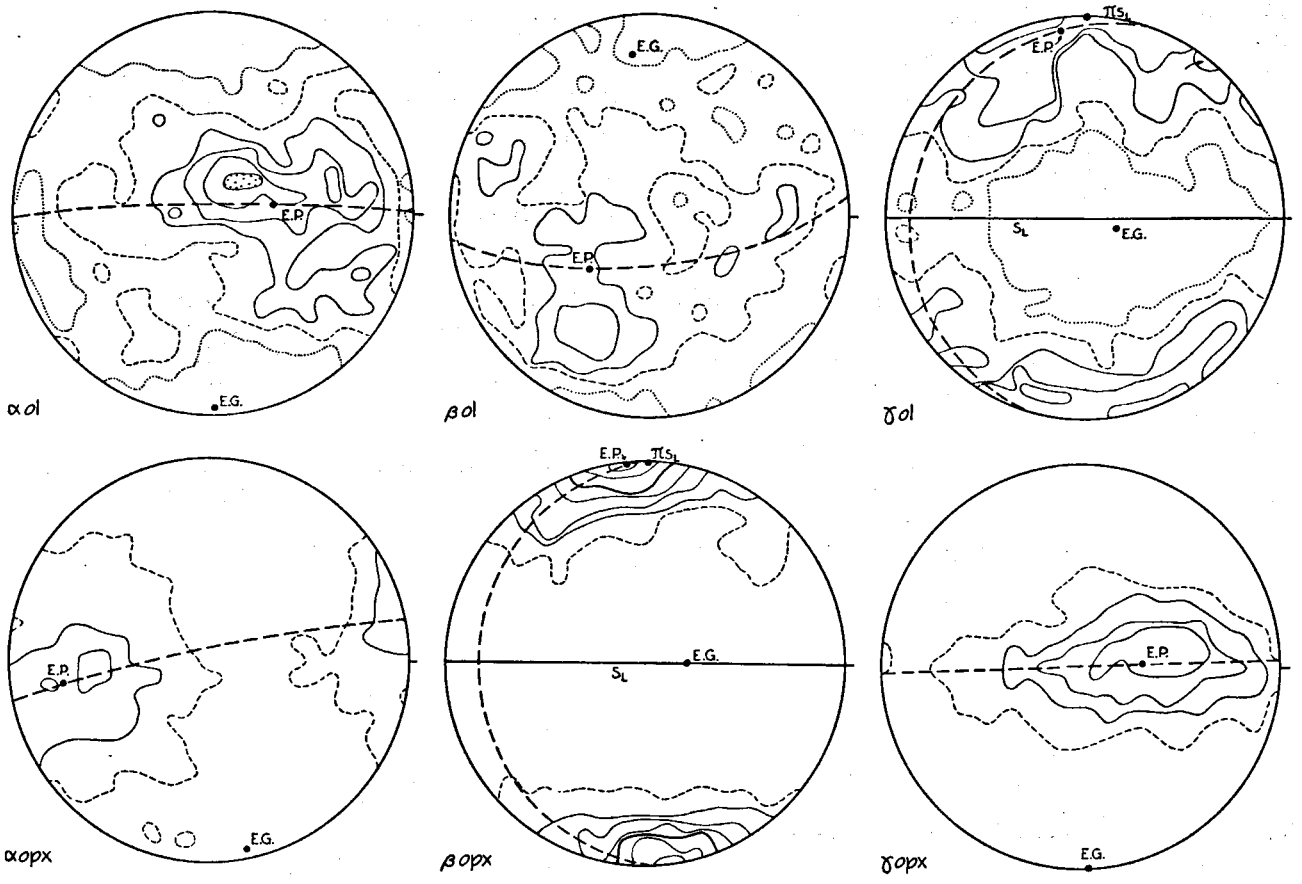


Fig. 30. Garnet-peridotite GN1; projection into plane of thin section GN1-E1 (cf. Fig. 31) — olivine: $N = 905$, $A = 0.039779$, stippled contour at density 0.75; orthopyroxene: $N = 500$, $A = 0.02$.

concentrated parallel to $l'_0$, whereas in the spinel-amphibole-peridotites a parallelism of E.G. of $\gamma_{OL}$ with E.P. of $\alpha_{OL}$, and in some cases even with $l''_0$ (Fig. 27) could be observed. It is therefore possible that the olivine fabric of GN1 was influenced to some extent by the deformation related to the partial alteration of the garnet-peridotite into spinel-amphibole-peridotite.

From the above review of the literature it is evident that both the olivine and the orthopyroxene fabrics of the garnet-peridotite of Alpe Arami differ materially from the orientation patterns to be expected for these minerals in a magmatic environment, so that the garnet-peridotite most likely had a non-magmatic, i.e. a metamorphic origin. Its genesis will be ascribed to a tectonic phase $F'_0$ (Table 6). It follows that the $S_L$-plane acted as a tectonic plane, although it cannot be excluded that the compositional layering itself dates back to an earlier, possibly magmatic stage, before the formation of the garnet-peridotite took place. An additional argument for a tectonic and metamorphic rather than a magmatic origin of the garnet-peridotite is provided by the parallelism of the $l'_0$- and $l''_0$-lineations, since it is much more difficult to see why the magma currents required to explain, for a magmatic genesis, the alignment of the ortho- and clinopyroxene crystals along $l'_0$, are parallel to the $l''_0$-lineations of tectonic origin related to a subsequent metamorphism of these rocks, than to assume two consecutive tectonic phases with parallel *b*-axes. From the structural and petrofabric point of view, to the contrary, there is a close relationship between garnet-peridotite and spinel-amphibole-peridotite, thus indicating that they originated under almost the same conditions and that the interval between their phases of formation ($F'_0$ and $F''_0$) was probably small.

However, it appears that the garnet-peridotite and the spinel-amphibole-peridotite fabrics from Alpe Arami bear no resemblance to previously published peridotite fabrics of metamorphic origin, such as lherzolite and chlorite-peridotite fabrics, since both the orientation patterns and the relative strength of the preferred orientation of olivine and orthopyroxene differ markedly. The olivine fabrics of chlorite-peridotite-mylonite AR14 (Fig. 29), on the other hand, conform to the orientation patterns of the porphyroclasts and the matrix of other peridotite-mylonites, and the orientation of matrix olivine in AR14 also resembles the olivine orientation displayed by the Norwegian chlorite-peridotites (see above).

If it is accepted that the Alpe Arami fabrics are metamorphic in origin, it is nonetheless extremely difficult, if not impossible, to give a satisfactory hypothesis for the exact mechanism of their genesis. Two processes have been proposed by which a preferred orientation of olivine may be brought about in metamorphic rocks (Hartman & den Tex, 1964; Raleigh, 1963): a) recrystallization along with elastic deformation in a non-hydrostatic stress field, and b) plastic deformation.

On the basis of a theory proposed by Kamb, Hartman and den Tex (1964) concluded that an olivine fabric originating by recrystallization of a polycrystalline aggregate which is deformed elastically under uniaxial compression, may show two different types of preferred orientation: with intergranular liquid, the crystals are flattened in a plane at right angles to the unique compression axis ($z$) and $\alpha_{OL}$ tends to be oriented parallel to this axis, although there is no direct relation between the tabular habit ("fabric habit") of the grains and the orientation of $\alpha_{OL}$; without intergranular liquid, the most stable lattice orientation has $\gamma_{OL}$ parallel to $z$, but a preferred dimensional orientation is unlikely to occur. For the case of uniaxial tension, Hartman and den Tex (*op. cit.*) found that the crystals will be elongated parallel to the unique tension axis, with $\gamma_{OL}$ preferentially lying in a great-circle girdle perpendicular to this axis when intergranular solutions are present, whereas in a dry environment the effect of uniaxial tension is the same as for uniaxial compression, i.e. $\gamma_{OL}$ is parallel to the unique tension axis.

Experimental work, mainly on metals, has shown that plastic deformation (cold-working) of mineral aggregates is capable of producing a preferred lattice orientation, and this process may also be held responsible for the occurrence of a preferred orientation of olivine in peridotites (Raleigh, 1963). When one plane in the mineral lattice functions as the slip plane (T) with a slip direction (t), it appears experimentally that upon uniaxial compression, T rotates towards a position perpendicular to the unique compression axis, whereas upon uniaxial tension, t rotates towards the unique tension axis, so that, if T and t of a mineral are known from experiments, predictions can be made as to the preferred orientation to be expected (Raleigh, *op. cit.*). However, complications arise when more than one slip plane is present, and the data obtained from single-crystal experiments cannot be applied to mineral aggregates without some reservations. As a result of the plastic deformation, there will be a direct relation between the lattice orientation and the dimensional orientation of the minerals: the crystals will be flattened parallel to T and elongated along t. Moreover, they will show strain effects such as translation lamellae, kink bands, and undulose extinction. For experimentally deformed *olivine*, the following glide mechanisms were found: T = {100}, t = [010]; T = {110}, {100}, t = [001]; T = {110}, t = [001]; T = {010}, t = [100] (with increasing temperature, the glide systems are active in this order); for *orthopyroxene*: T = {100}, t = [001]; and for *clinopyroxene* (diopside): T = {100}, t = [001] (Raleigh, 1967). Although the experimentally determined conditions cannot simply be extrapolated to rocks deformed by natural forces, Raleigh's results strongly suggest that the manner in which the olivine in such rocks reacted to plastic deformation also depended on external factors such as temperature and possibly confining pressure.

Since the above theoretical and experimental deductions are necessarily simplified models of the more complicated natural processes, it is evident that the reverse procedure, i.e. deduction of the mechanism causing the preferred orientation from the observed rock fabric, is still more speculative, and the following discussion must be regarded in that light.

In agreement with Hartman and den Tex (1964), the orientation of $\gamma_{OL}$ at right angles to $S_1$ for the olivine porphyroclasts in peridotite-mylonite AR14 (Fig. 29) may be explained by selective preservation from cataclasis of grains having $\gamma_{OL}$ (sub)parallel to the axis of major stress, since, if mylonitization is assumed to have started under dry conditions, these orientations are thermodynamically the most stable ones. After crushing of most grains had occurred, the introduction of solutions became possible and prolonged stress not only could induce strain effects in the remaining porphyroclasts, but also favoured the development of a piezocrystalline fabric, in the sense of Hartman and den Tex, due to recrystallization of matrix olivine. The fact that most olivine grains are tabular parallel to $S_1$, irrespective of the orientation of the crystal lattice, and thus show a fabric habit, is an indication for piezocrystallization. The lattice orientation found for matrix olivine is on the whole in accordance with the predictions of Hartman and den Tex: $\alpha_{OL}$ lies perpendicular to $S_1$. The occurrence of the $\beta_{OL}$-maximum within $S_1$ might be explained by considering that the stress field probably was triaxial rather than uniaxial, with $\beta_{OL}$ (= fabric *b*) possibly lying parallel to the direction of maximum tension.

Returning to specimen GN1, we may now try to deduce the mechanism responsible for the preferred orientation of olivine in the garnet-peridotites, on the basis of an axial-distribution analysis (A.D.A.) (Fig. 31). The thin section (GN1-E1) used for A.D.A. was cut parallel to the expected position of the $\gamma_{OL}$-partial great-circle girdle. The fabric diagrams of Fig. 30, which also include measurements from other sections of GN1, are projections into the plane of GN1-E1; it appears that GN1-E1 was cut almost perpendicular to the $l'_0$-lineation. For the A.D.A., only the orientation of $\gamma_{OL}$ with respect to $\pi S_L$ was considered, since a maximum of $\gamma_{OL}$ near $\pi S_L$ is the most strongly and most consistently developed feature of the olivine orientation in the garnet-peridotites; the more $\gamma_{OL}$ approaches $\pi S_L$, the more heavily the olivine grains are shaded (key in Fig. 31).

Although the number of grains used for the A.D.A. is rather small (405 olivine grains were measured in


Fig. 31. Axial-distribution diagram for 405 γ-axes of olivine in thin section GN1-E1 (cf. Fig. 30); numbers to the right of the key-diagram refer to the number of grains contained in each of the three direction-groups.

GN1-E1), the following general statements can be made. The olivine grains show extremely xenomorphic outlines, and there is a slight indication for a preferred elongation of the grains parallel to the trace of $S_L$. However, the preferred orientation of the crystal lattice ($\gamma_{OL}$ perpendicular to $S_L$) does not seem to be directly related to either a particular grain size or a particular habit, because both small and large and both elongated and equant grains are found in all three classes into which the grains were subdivided on the basis of the state of their preferred orientation. Furthermore, there is a distinct clustering in the axial-distribution diagram of grains with a similar degree of preferred orientation of $\gamma_{OL}$.

It may be concluded that the olivine grains in GN1-E1 display a fabric habit that may have been brought about by recrystallization under elastic strain in the presence of an intergranular solution (Hartman & den Tex, 1964). The fabric habit of olivine is even more conspicuous in other peridotite specimens from Alpe Arami, as evidenced by the pronounced flattening of olivine parallel to $S_L$ in garnet-peridotite AR26 (p. 103) and its marked elongation along the $S_L/S_0$-fold axis in spinel-amphibole-peridotite AR41

(p. 109), in both cases independent of the lattice orientation of the olivine grains.
However, a serious objection to the above hypothesis is that the observed preferred lattice orientation of olivine is in contradiction with the theory of Hartman and den Tex. Recrystallization under uniaxial compression in the solid state would indeed give rise to the observed preferred orientation, but in that case the fabric habit of olivine cannot be explained.
On the other hand, plastic deformation of olivine under such conditions that the glide system T = {100} (with t = [010] or t = [001]) could be operative, may have produced the preferred olivine orientation.
A frequently encountered hypothesis for the explanation of olivine fabrics in lherzolites is translation gliding by T = {010} and t = [100]. The fact that lherzolites and garnet-peridotites have different stability fields (Fig. 7) might explain the promotion of another glide system in the latter rocks. However, the olivine grains in GN1 bear almost no signs of mechanical deformation and — as stated before — no direct relation between preferred orientation and elongated habit of the crystals appears to be present.
To surmount these difficulties, I tentatively assume that an initial stage of plastic deformation was succeeded by dimensional piezocrystallization in the sense of Hartman and den Tex (1964). It is conceivable that due to the latter process the strain effects disappeared, aggregates of similarly oriented grains developed by polygonization (Turner & Weiss, 1963), and the tabular habit of the olivine grains parallel to $S_L$ originated.
In view of the experimentally determined glide system for orthopyroxene (T = {100}, t = [001]), the same hypothesis may be applied to the orthopyroxene fabric of GN1. It will be perfectly clear, however, that much work still remains to be done before a really sound explanation for the origin of the peridotite fabrics of Alpe Arami can be given.

CHAPTER VII

## THE RESULTS, CONSIDERED WITHIN THE FRAMEWORK OF THE GEOLOGY OF THE ALPS

The present investigation has shown that the garnet-peridotite of Alpe Arami is a metamorphic rock that originated under eclogite-facies conditions. Two phases of retrogressive metamorphism could be distinguished: an initial phase involving the formation of spinel-amphibole-peridotite, which occurred under granulite-facies conditions, and a subsequent phase during which chlorite-peridotite developed under amphibolite-facies conditions. The second phase of retrogradation of the peridotite was contemporaneous with the main phase of metamorphism of the surrounding gneisses, which is of Alpine age. The interval between the formation of the garnet-peridotite and its first alteration into spinel-amphibole-peridotite was probably small; both phases occurred before the Alpine main phase.
Obviously, these results are more in agreement with the hypothesis of O'Hara and Mercy (1966) than with the theories of Dal Vesco (1953) and Grubenmann (1908) (cf. p. 63). However, not much has been said yet about either the mode of emplacement of the garnet-peridotite or its actual age, i.e. the time of crystallization of the garnet-peridotite minerals.
On the basis of the occurrence of titanclinohumite in the garnet-peridotite and the position of the ultramafic rocks in a Mesozoic *Muldenzone*, it was argued that the garnet-peridotite of Alpe Arami belongs to the Mesozoic ophiolite suite of the Pennine zone of the Alps (p. 88). It was also shown that the mineral paragenesis of the garnet-peridotite of Alpe Arami differs from the mineralogical composition of garnet-bearing peridotites found among the pre-Alpine (Hercynian or older) gneisses of the Southern Alps and the Austro-alpine region, e.g. near Arosio and Alpe Seefeld (p. 87; localities e and f in Fig. 10). Furthermore, the garnet-spinel-peridotite of Alpe Seefeld has an olivine fabric with $\alpha_{OL}$ at right angles to S (Andreatta, 1934) and $\beta_{OL}$ parallel to the fabric *b*-axis (Ladurner, 1956), which is different from the olivine fabrics found in the garnet-peridotite of Alpe Arami.
These observations therefore suggest that before the Alpine orogeny the garnet-peridotite of Alpe Arami was not yet present as a discordant body between the (pre-)Hercynian gneisses of the Alps; they support the hypothesis that the peridotite was folded into its present position during the Alpine orogeny, and more particularly, due to the $F_1$-phase defined in this paper. This leads to the idea that the early history of the garnet-peridotite took place in an environment unlike the present one. It will be clear that the problem of when and where the garnet-peridotite was formed and underwent its initial decomposition into spinel-amphibole-peridotite, cannot be solved satisfactorily by the present structural-petrological analysis.
Two hypotheses concerning the origin of the garnet-peridotite may be considered: a) the rock was tectonically emplaced from a deep level of the pre-Alpine basement of the Alps (lower crust or upper mantle), where it was already present before the beginning of the Alpine orogeny; the garnet-peridotite may in that case even be of Precambrian age; b) not only the emplacement of the garnet-peridotite, but also its formation is related to the Alpine orogeny. Radiometric age determinations may eventually show whether one of these hypotheses is correct. We shall content ourselves here with a few speculations that seem to favour the second hypothesis. The following

is based on a comparison with the results obtained by Bearth (1967) in an adjoining part of the Pennine zone of the Alps.

The region of Zermatt-Saas Fee is well-known for its metamorphic ophiolites (Bearth, 1967; see our Fig. 10). Among them are eclogites showing various stages of retrogressive metamorphism, first into glaucophane-schists, thereafter into garnet-amphibolites, and then into prasinites. Bearth could convincingly demonstrate that the eclogites originated by a metamorphism of basic intrusive and extrusive rocks, such as gabbros and pillow lavas, because the minerals and structures of the preceding magmatic stage were not entirely obliterated by the metamorphism.

The determination of the age of the ophiolites is a complicated problem. We must clearly distinguish between the time of crystallization of the constituent minerals and the moment of emplacement of the rocks. According to an hypothesis put forward by de Roever (1957), some members of the ophiolite suite, such as peridotites and gabbros, may be considered as tectonically emplaced solid fragments of the upper mantle, whereas the volcanic members of the ophiolite association may have originated due to the simultaneous effusion of basic magma.

Bearth (1967) has shown that the zone of Zermatt-Saas Fee consists of a coherent mass of mafic and ultramafic rocks accompanied by only minor quantities of Mesozoic sediments. Although the absence of primary contacts prevents the establishment of clear age-relationships between most of the ophiolites and the sediments, it is evident that the age of the ophiolites, in the sense of the moment of their emplacement, is Alpine, and there can hardly be any doubt that the ophiolites of volcanic origin, such as the pillow lavas, were formed during the Mesozoic, so that the metamorphism that gave rise to the development of the eclogites also must have taken place during the Alpine orogeny (Bearth, *op. cit.*).

However, it should not be concluded from the foregoing that all Alpine ophiolites were subjected to the same degree of metamorphism. In fact, it was demonstrated by Bearth (*op. cit.*, Table 17) that mineral parageneses of various metamorphic grades are present among the ophiolites of the Alps. All parageneses seem to belong to the high-pressure lineage of orogenic metamorphism as defined by den Tex (1965).

Bearth considers the garnet-peridotites and eclogites occurring in the Lepontine gneiss complex as ophiolites that were subjected to a similar metamorphism, albeit of a higher grade, as those in the Zermatt-Saas Fee region. Although the eclogites from Gorduno undoubtedly differ in many respects from the eclogites of Zermatt-Saas Fee, they show a comparable type of high-pressure metamorphism. At first sight, Bearth's hypothesis seems quite attractive. Rocks such as the plagioclase-peridotites present among the ophiolites of Piedmont (p. 88) may represent the primary material from which the garnet-peridotites were formed. Titanclinohumite in the garnet-peridotite may then be viewed as a relict mineral of this previous assemblage. The fact that the occurrence of garnet-peridotites seems to be restricted to the tectonically deepest levels of the Pennine zone of the Alps (the region of the lower Pennine nappes) (localities a, b, and c in Fig. 10) also leads to the supposition that the formation of the garnet-peridotites is in some way related to the Alpine orogeny.

However, in view of the results of the present investigation, this assumption would have the paradoxical consequence that the phases $F'_0$ and $F''_0$ in Table 6 would also be of Alpine age. It is remarkable that Avé Lallemant (1967, p. 54) arrived at a similar conclusion in his study of the lherzolite of the French Pyrenees. More radiometric age determinations are required, however, to prove or disprove the hypothesis that the formation of orogenic peridotites, although antedating the main phase of metamorphism of the rocks into which they were emplaced, may nevertheless be related to the same orogeny.

The formation of the garnet-peridotite of Alpe Arami and its initial retrogressive metamorphism into spinel-amphibole-peridotite being accepted as having taken place during the Alpine orogeny, it has been shown that these phases of metamorphism a) antedated the main phase of metamorphism in the Lepontine gneiss complex, and b) took place when the peridotite was not in its present position. A regional metamorphism with the characteristics of the high-pressure lineage of den Tex (1965) seems to have affected the ophiolites before a metamorphism more akin to den Tex's intermediate-pressure lineage occurred in the Lepontine gneiss complex.

I would tentatively suggest that the garnet-peridotite and the eclogite of Alpe Arami were formed during a first phase of Alpine metamorphism at a deep level in the Pennine eugeosyncline, when the nappes were already piled upon each other. There, the garnet-peridotite underwent its first stage of retrogressive metamorphism into spinel-amphibole-peridotite. Along with eclogite, the peridotite was then thrust as an *Ophiolit-Decke* (Bearth, 1967) into Mesozoic sediments, and was folded between two masses of (pre-)Hercynian gneiss as part of a *Muldenzone*, where the mafic and ultramafic rocks underwent a subsequent stage of retrogradation, spinel-amphibole-peridotite giving rise to chlorite-peridotite, and eclogite to amphibolite, due to the metamorphism that affected the Lepontine gneiss complex. This hypothesis must of course be judged by scientists who are more expert in Alpine geology than the present author.

Leiden, July 1968.

## SAMENVATTING

Bij Alpe Arami, op de waterscheiding tussen het Gordunoen Gnoscadal nabij Bellinzona in het Zwitserse kanton Tessin, is een lensvormig peridotietlichaam ontsloten. De geologische ontwikkeling van de peridotiet van Alpe Arami werd reeds bestudeerd door Grubenmann (1908), Dal Vesco (1953) en O'Hara en Mercy (1966). Zij maakten daarbij gebruik van de „klassieke" methodes van petrografisch, mineralogisch en chemisch onderzoek. In dit proefschrift wordt hetzelfde probleem benaderd met behulp van structureel-petrologische methodes.

Rondom de peridotiet vindt men voornamelijk gneizen. Zij worden gerekend tot de wortelzone van de Penninische dekbladen van de Alpen. Op grond van de structurele studies van Wenk en de absolute-ouderdomsbepalingen van Jäger kan aangenomen worden dat de metamorfose van de gneizen van Alpiene ouderdom is. De belangrijkste fase van deze metamorfose ($F_1$) ging gepaard met de vorming van schistositeitsvlakken ($S_1$) die thans steil naar het zuiden hellen.

In de peridotiet wijzen de omzetting van granaat (die rijk is aan pyroop) in een symplektitische vergroeiing van spinel en amfibool, en de vervanging van deze symplektiet door chlorietkristallen, op de aanwezigheid van drie opeenvolgende mineraalparageneses, nl. een granaatperidotiet-, een spinelamfiboolperidotiet- en een chlorietperidotietparagenese. Titaanklinohumiet is wellicht een relictmineraal uit een nog oudere paragenese. De uit omgezette granaten ontstane chlorietknollen zijn vaak afgeplat volgens vlakken, die evenwijdig zijn aan de $S_1$-vlakken van de omringende gneizen. Het {001}-vlak van chloriet ligt bij voorkeur evenwijdig aan $S_1$; de vorming van chloriet in de peridotiet vond dus waarschijnlijk plaats gedurende de fase $F_1$ van de Alpiene orogenese. $S_1$-vlakken zijn in de peridotiet ook terug te vinden als splijtvlakken. Een oudere structuur is de gelaagdheid ($S_L$), die optreedt tengevolge van kwantitatieve verschillen in de mineralogische samenstelling van de peridotiet. Op de $S_L$-vlakken is soms een mineraallineatie ($l_0$) zichtbaar. In het zuidelijke gedeelte van de lens helt $S_L$ steil naar het zuiden en is dus evenwijdig met $S_1$, waarbij $l_0$ steil naar het westen duikt, terwijl $S_L$ in het noorden meestal zwak tot matig naar het noorden helt, met een naar het noorden duikende $l_0$-lineatie. De peridotiet kan misschien beschouwd worden als een synform met een horizontale tot iets naar het oosten duikende as, die tussen de gneizen ontstaan is door plooiing gedurende de fase $F_1$ (fig. 6, a en b).

Maakselanalyse toonde aan dat de oriëntatie van de indicatrixassen (die overeenkomen met de kristallografische assen) van de mineralen olivijn en orthopyroxeen, in de granaatperidotiet afhankelijk is van de ligging van het $S_L$-vlak: γ-olivijn en β-orthopyroxeen liggen bij voorkeur loodrecht op $S_L$, waarbij de oriëntatie van olivijn duidelijk zwakker is dan die van orthopyroxeen. Bovendien liggen γ-orthopyroxeen en *c*-klinopyroxeen evenwijdig aan $l_0$ ($=l'_0$). De omzetting van granaatperidotiet in spinelamfiboolperidotiet hangt samen met het ontstaan van schistositeitsvlakken ($S_0$) die meestal evenwijdig zijn met de gelaagdheid $S_L$. Op sommige plaatsen komen plooien van $S_L$ voor met $S_0$ als assenvlak. De assen van deze plooien zijn evenwijdig aan de $l_0$-lineaties in de granaatperidotiet. In de spinelamfiboolperidotieten ligt γ-olivijn meestal loodrecht op $S_0$, terwijl γ-orthopyroxeen en *c*-amfibool evenwijdig zijn met $l_0$ ($=l''_0$). De maaksels van olivijn, orthopyroxeen en amfibool zijn niet beïnvloed door de omzetting van spinelamfiboolperidotiet in chlorietperidotiet. Een uitzondering hierop vormt het olivijnmaaksel van een chlorietperidotietmyloniet, afkomstig van de zuidrand van de peridotietlens. De gerekristalliseerde olivijn in de matrix vertoont een duidelijk maaksel, met een maximum van α-olivijn loodrecht op de schistositeit ($= S_1$) van de myloniet.

De oriëntatie van de mineralen in de granaatperidotiet van Alpe Arami kan niet met behulp van een magmatische ontstaanswijze verklaard worden. De granaatperidotiet is derhalve een metamorf gesteente. Mogelijk is het maaksel veroorzaakt door een proces van plastische deformatie, gevolgd door elastische deformatie en rekristallisatie in een niethydrostatisch krachtenveld. Aangezien de $S_L$- en $S_0$-structuren in de peridotiet, en de daarbij behorende lineaties, discordant zijn ten opzichte van de structuren in de omringende gneizen en ouder zijn dan de $F_1$-metamorfose, moeten de vorming van de granaatperidotiet en zijn omzetting in spinelamfiboolperidotiet plaatsgevonden hebben, voordat de peridotiet, gedurende de Alpiene orogenese, in zijn huidige positie terechtkwam. Tabel 6 geeft een schematisch overzicht van de geologische ontwikkeling van de peridotiet van Alpe Arami.

Het structureel-petrologische onderzoek is niet in staat een antwoord te geven op de interessante vraag, wanneer en waar de granaatperidotiet gevormd is. Het is denkbaar dat de granaatperidotiet vóór het begin der Alpiene orogenese reeds als zodanig in de diepte aanwezig was. De schrijver neigt echter tot de opvatting dat ook de granaatperidotiet een produkt der Alpiene orogenese is. Daarbij moet het gesteente ontstaan zijn in een vroeg stadium van deze orogenese, tijdens een fase van hoge-drukmetamorfose, die wellicht gecorreleerd kan worden met een soortgelijke metamorfose in de door Bearth beschreven basische gesteenten nabij Zermatt en Saas Fee.

Enkele algemene aspecten van de methode der maakselanalyse komen ter sprake in hoofdstuk V. Voor de maakselanalyse van tweeassige mineralen is de vijfassige universele draaitafel te verkiezen boven het model met vier assen. Men boekt een aanzienlijke tijdwinst, wanneer men de metingen met behulp van een electronische rekenmachine direct verwerkt tot diagrammen (zie fig. 17, b). Hierbij is men in staat het oppervlak van de gebruikte telcirkel in overeenstemming te brengen met de strooiing van de metingen. Het berekenen van statistische parameters op grond van modelverdelingen maakt een kwantitatieve vergelijking tussen verschillende diagrammen mogelijk.

## REFERENCES

Andreatta, C., 1934. Analisi strutturali di rocce metamorfiche, V. Oliviniti. Period. Min., 5, pp. 237—253.

—, 1936. La formazione gneissico-kinzigitica e le oliviniti di Val d'Ultimo (Alto Adige). Mem. Mus. Stor. Nat. Venezia Tridentina, Anno 6, Vol. 3, pp. 87—245.

Avé Lallemant, H. G., 1967. Structural and petrofabric analysis of an "Alpine-type" peridotite: the lherzolite of the French Pyrenees. Leidse Geol. Med., 42, pp. 1—57.

Bächlin, R., 1937. Geologie und Petrographie des M. Tamaro-Gebietes (südliches Tessin). Schweiz. Min. Petr. Mitt., 17, pp. 1—79.

Bearth, P., 1967. Die Ophiolithe der Zone von Zermatt-Saas Fee. Beitr. Geol. Karte d. Schweiz, N. F., 132, 130 pp.

Berek, M., 1913. Trigonometrische Beziehungen zwischen den Orientierungen der optischen Achsen, der optischen Symmetrieachsen sowie der Polarisationsrichtungen auf beliebigen Flächen zweiachsiger inaktiver Kristalle. N. Jb. Min. Geol. Paläont. Beil. Bd., 35, pp. 221—240.

—, 1923. Neue Wege zur Universalmethode. N. Jb. Min. Geol. Paläont. Beil. Bd., 48, pp. 34—62.

—, 1924. Mikroskopische Mineralbestimmung mit Hilfe der Universaldrehtischmethoden. Berlin, Borntraeger, 168 pp.

Bianconi, F., 1965. Resti fossili in rocce mesometamorfiche della regione del Campolungo. Schweiz. Min. Petr. Mitt., 45, pp. 571—596.

Blattner, P., 1965. Ein anatektisches Gneissmassiv zwischen Valle Bodengo und Valle di Livo (Prov. Sondrio und Como). Schweiz. Min. Petr. Mitt., 45, pp. 973—1071.

Brothers, R. N., 1959. Flow orientation of olivine. Am. Jour. Sci., 257, pp. 574—584.

Carpanese, T., 1933. Contributo alla conoscenza della titanolivina. Period. Min., 4, pp. 339—372.

Chatterjee, N. D., 1961. Aspects of Alpine zonal metamorphism in the Swiss Alps. Nachr. Akad. Wiss. Göttingen, II. Math.-phys. Kl., pp. 59—71.

Chayes, F., 1949. Statistical analysis of three-dimensional fabric diagrams. Chapter 23 in Fairbairn (1949).

Collée, A. L. G., 1962. A fabric study of lherzolites with special reference to ultrabasic nodular inclusions in the lavas of Auvergne (France). Leidse Geol. Med., 28, pp. 1—102.

Cossa, A., 1874. Intorno alla lherzolite di Locana nel Piemonte. Atti R. Accad. Sci. Torino, 9 (1873—74), pp. 545—555.

Dal Vesco, E., 1953. Genesi e metamorfosi delle rocce basiche e ultrabasiche nell'ambiente mesozonale dell' orogene pennidico. Schweiz. Min. Petr. Mitt., 33, pp. 173—480.

Daubrée, A., 1866. Expériences synthétiques relatives aux météorites (Troisième partie). C. R. Acad. Sci. Paris, 62, pp. 660—674.

Deer, W. A., Howie, R. A. & Zussman, J., 1962. Rock-forming minerals, 1: ortho- and ring silicates. London, Longmans, 333 pp.

Dodge, T. A., 1934. The determination of optic angle with the universal stage. Am. Min., 19, pp. 62—75.

Ehlers, E. G., 1966. A simplified method of 2V determination using 3- and 4-axis stages. Min. Mag., 35, pp. 958—962.

—, 1967. On the determination of 2V. Min. Mag., 36, pp. 299—300.

Emmons, R. C., 1943. The universal stage (with five axes of rotation). Mem. Geol. Soc. Am., 8, 205 pp.

Ernst, Th., 1935. Olivinknollen der Basalte als Bruchstücke alter Olivinfelse. Nachr. Ges. Wiss. Göttingen, Math.-phys. Kl., N. F., Fachgr. IV, 1 (1934—40), pp. 147—154.

Essene, E. J. & Fyfe, W. S., 1967. Omphacite in Californian metamorphic rocks. Contr. Min. Petr., 15, pp. 1—23.

Fairbairn, H. W., 1949. Structural petrology of deformed rocks. 2nd ed. Cambridge (Mass.), Addison-Wesley, 344 pp.

Fischer, G., 1960. Über die Auswertung von Gefügediagrammen. Abh. dtsch. Akad. Wiss. Berlin, Kl. III, pp. 283—299.

Fischer, R. A., 1953. Dispersion on a sphere. Proc. R. Soc. London, A, 217, pp. 295—305.

Flinn, D., 1958. On tests of significance of preferred orientation in three-dimensional fabric diagrams. Jour. Geol., 66, pp. 526—539.

—, 1965. On the statistical analysis of axial distribution diagrams. N. Jb. Min. Mh., pp. 54—64.

Friedman, M., 1964. Petrofabric techniques for the determination of principal stress directions in rocks. In: State of stress in the earth's crust, W. R. Judd, ed., Proc. Internat. Conf. Santa Monica, California, 13—14 June 1963, pp. 450—552.

Gnehm, G., 1964. Über ein Pyrop-Vorkommen im Tessin. Aufschluss, 15, pp. 165—166.

Green, D. H. & Ringwood, A. E., 1963. Mineral assemblages in a model mantle composition. Jour. Geophys. Res., 68, pp. 937—945.

—, 1967. The stability fields of aluminous pyroxene peridotite and garnet peridotite and their relevance in Upper Mantle structure. Earth Planet. Sci. Lett., 3, pp. 151—160.

Grubenmann, U., 1908. Der Granatolivinfels des Gordunotales und seine Begleitgesteine. Vjschr. Naturf. Ges. Zürich, 53, pp. 129—156.

—, & Hezner, L., 1916. Zusammenstellung der Resultate über die von 1900—1915 im mineralogisch-petrographischen Institut der Eidg. Techn. Hochschule ausgeführten chemischen Gesteins- und Mineralanalysen. Vjschr. Naturf. Ges. Zürich, 61, pp. 149—203.

Hammer, W., 1899. Olivingesteine aus dem Nonsberg, Sulzberg und Ultenthal. Zeitschr. Naturwiss., 72, pp. 1—48.

Harten, D. van, 1965. On the estimation of relative grain frequencies in heavy mineral slides. Geol. Mijnb., 44, pp. 357—363.

Hartman, P. & den Tex, E., 1964. Piezocrystalline fabrics of olivine in theory and nature. Publ. Dept. Petr. Min. Cryst., University of Leyden, 2nd Ser., 39, 33 pp.

Henry, N. F. M., 1942. Lamellar structure in orthopyroxenes. Min. Mag., 26, pp. 179—189.

Hess, H. H., 1960. Stillwater Igneous Complex, Montana. Mem. Geol. Soc. Am., 80, 230 pp.

Hezner, L., 1909. Der Peridotit von Loderio (Kt. Tessin). Vjschr. Naturf. Ges. Zürich, 54, pp. 244—260.

Higgins, A. K., 1964. Fossil remains in staurolite-kyanite schists of the Bedretto-Mulde Bündnerschiefer. Eclogae Geol. Helv., 57, pp. 151—156.

Hodges, J. L. & Lehmann, E. L., 1964. Basic concepts of probability and statistics. San Francisco, Holden-Day, 375 pp.

Ito, K. & Kennedy, G. C., 1967. Melting and phase relations in a natural peridotite to 40 kilobars. Am. Jour. Sci., 265, pp. 519—538.

Jackson, E. D., 1961. Primary textures and mineral associations in the ultramafic zone of the Stillwater Complex, Montana. U.S. Geol. Surv. Prof. Paper, 358, 106 pp.

Jäger, E., 1962. Rb-Sr age determinations on micas and total rocks from the Alps. Jour. Geophys. Res., 67, pp. 5293—5306.

—, 1965. Rb-Sr age determinations on minerals and rocks from the Alps. Sciences de la Terre, 10, pp. 395—407.

—, 1966. Das Alter von Graniten und Gneisen. Tscherm. Min. Petr. Mitt., 3. F., 11, pp. 304—316.

—, & Faul, H., 1959. Age measurements on some granites and gneisses from the Alps. Bull. Geol. Soc. Am., 70, pp. 1553—1557.

—, Niggli, E. & Wenk, E., 1967. Rb-Sr Altersbestimmungen an Glimmern der Zentralalpen. Beitr. Geol. Karte d. Schweiz, N. F., 134, 67 pp.

Kamb, W. B., 1959. Ice petrofabric observations from Blue Glacier, Washington, in relation to theory and experiment. Jour. Geophys. Res., 64, pp. 1891—1909.

Kazakov, A. N., 1965. Microstructural orientation of olivine in rocks of the supposed upper earth mantle. Zap.

Vsesoyuzn. Min. Obshch., 2nd Ser., 94, pp. 576—580 (in Russian).

Knoblauch, P. & Reinhard, M., 1939. Erläuterungen zum Blatt 516 (Iorio) der Geologischen Atlas der Schweiz 1 : 25 000. Bern, Francke, 88 pp.

Kobe, H., 1956. Geologisch-petrographische Untersuchungen in der Tessiner Wurzelzone zwischen Vergeletto-Onsernone und Valle Maggia. Schweiz. Min. Petr. Mitt., 36, pp. 244—348.

—, 1966. Paragesteinszüge, Struktur und Anatexis im Gebiete zwischen V. Onsernone und V. Maggia (Tessin). Schweiz. Min. Petr. Mitt., 46, pp. 461—472.

Kushiro, I. & Yoder, H. S., 1965. The reactions between forsterite and anorthite at high pressures. Carnegie Inst. Yearb., 64, pp. 89—94.

—, 1966. Anorthite-forsterite and anorthite-enstatite reactions and their bearing on the basalt-eclogite transformation. Jour. Petr., 7, pp. 337—362.

Lacroix, A., 1893. Minéralogie de la France et de ses colonies. T. 1, Fasc. 1, Paris, Baudry et Cie, 304 pp.

—, 1894. Etude minéralogique de la lherzolite des Pyrénées et de ses phénomènes de contact. Nouv. Arch. Mus. Hist. Nat., 3me Sér., 6, pp. 209—308.

Ladurner, J., 1956. Das Verhalten des Olivins als Gefügekorn in einigen Olivingesteinen. Tscherm. Min. Petr. Mitt., 3. F., 5, pp. 21—36.

Lappin, M. A., 1967. Structural and petrofabric studies of the dunites of Almklovdalen, Nordfjord, Norway. In: Wyllie (1967), pp. 183—190.

Legoux, P., 1960. Les péridotites de Conakry et du Kaloum (république de Guinée) et leur serpentinisation. Bull. Soc. Géol. France, 7me Sér., 2, pp. 50—63.

MacGregor, I. D., 1965. Stability fields of spinel and garnet peridotites in the synthetic system $MgO$-$CaO$-$Al_2O_3$-$SiO_2$. Carnegie Inst. Yearb., 64, pp. 126—134.

—, 1967. The use of mafic and ultramafic inclusions in defining the depth of origin of basaltic magmas (abstract). Trans. Am. Geophys. Union, 48, pp. 255—256.

Meixner, H., 1960. Mineralisationen in einem Serpentin der Hohen Tauern (Islitzfall, Venedigergruppe, Osttirol). N. Jb. Min. Abh., 94, pp. 1309—1332.

Mellis, O., 1942. Gefügediagramme in stereographischer Projektion. Tscherm. Min. Petr. Mitt., 53, pp. 330—353.

Mercy, E. L. P. & O'Hara, M. J., 1965. Olivines and orthopyroxenes from garnetiferous peridotites and related rocks. Norsk Geol. Tidsskr., 45, pp. 457—461.

Nickel, E., 1960. Ein fraglicher Belemnit in den Frodaleragneisen vom Lukmanier. Schweiz. Min. Petr. Mitt., 40, pp. 95—113.

Nicolas, A., 1966. Etude pétrochimique des Roches vertes et de leurs minéraux entre Dora Maïra et Grand Paradis (Alpes piémontaises); le complexe Ophiolites-Schistes lustrés. Thèse, Nantes, Faculté des Sciences, 299 pp.

Niggli, E. & Niggli, C. R., 1965. Karten der Verbreitung einiger Mineralien der alpidischen Metamorphose in den Schweizer Alpen (Stilpnomelan, Alkali-Amphibol, Chloritoid, Staurolith, Disthen, Sillimanit). Eclogae Geol. Helv., 58, pp. 335—368.

Noble, D. C., 1964. Mathematical rotation of orientation data. Geol. Soc. Am. Bull., 75, pp. 247—248.

—, & Eberly, S. W., 1964. A digital computer procedure for preparing beta diagrams. Am. Jour. Sci., 262, pp. 1124—1129.

O'Hara, M. J., 1967. Mineral facies in ultrabasic rocks. In: Wyllie (1967), pp. 7—18.

—, & Mercy, E. L. P., 1963. Petrology and petrogenesis of some garnetiferous peridotites.Trans. R. Soc. Edinburgh, 65 (1962—63), pp. 251—314.

—, & Mercy, E. L. P., 1966. Garnet-peridotite and eclogite from Bellinzona, Switzerland. Earth Planet. Sci. Lett., 1, pp. 295—300.

Peters, T., 1963. Mineralogie und Petrographie des Totalpserpentins bei Davos. Schweiz. Min. Petr. Mitt., 43, pp. 529—685.

—, & Niggli, E., 1964. Spinellführende Pyroxenite ("Ariégite") in den Lherzolitkörpern von Lherz und Umgebung (Ariège, Pyrenäen) und der Totalp (Graubünden, Schweiz), ein Vergleich. Schweiz. Min. Petr. Mitt., 44, pp. 513—517.

Phillips, F. C., 1938. Mineral orientation in some olivine-rich rocks from Rum and Skye. Geol. Mag., 75, pp. 130—135.

Quervain, F. de, 1938. Zur Kenntnis des Titanklinohumites (Titanolivin). Schweiz. Min. Petr. Mitt., 18, pp. 591—604.

Raleigh, C. B., 1963. Fabrics of naturally and experimentally deformed olivine. Ph. D. thesis, University of California, Los Angeles, 215 pp.

—, 1965. Structure and petrology of an alpine peridotite on Cypress Island, Washington, U.S.A. Beitr. Min. Petr., 11, pp. 719—741.

—, 1967. Experimental deformation of ultramafic rocks and minerals. In: Wyllie (1967), pp. 191—199.

Ramsay, J. G., 1964. The uses and limitations of beta-diagrams and pi-diagrams in the geometrical analysis of folds. Quart. Jour. Geol. Soc. London, 120, pp. 435—454.

Reinhard, M. & Bernoulli, D., 1964. Erläuterungen zum Blatt 1333 (Tesserete) der Geologischen Atlas der Schweiz 1 : 25 000. Bern, Kümmerly & Frey, 54 pp.

Roever, W. P. de, 1957. Sind die Alpinotypen Peridotitmassen vielleicht tektonisch verfrachtete Bruchstücke der Peridotitschale? Geol. Rundschau, 46, pp. 137—146.

Rosenbusch, H., 1877. Mikroskopische Physiographie der Mineralien und Gesteine, Bd. II, Massige Gesteine. Stuttgart, Schweizerbart, 596 pp.

Rost, F., 1961. Chlorit und Granat in ultrabasischen Gesteinen. Fortschr. Min., 39, pp. 112—126.

—, 1963. Ultrabasite der Kruste und ihr Mineralbestand. N. Jb. Min. Mh., pp. 263—272.

—, & Grigel, W., 1964. Über accessorische Elemente in mitteleuropäischen Eklogiten und ihren Mineralien. Geochim. Cosmochim. Acta, 28, pp. 1933—1951.

Sander, B., Kastler, D. & Ladurner, J., 1954. Zur Korrektur des Schnitteffektes in Gefügediagrammen heterometrischer Körner. Sitz.ber. österr. Akad. Wiss., Math.-naturw. Kl. I, 163, pp. 401—424.

Scheidegger, A. E., 1965. On the statistics of the orientation of bedding planes, grain axes, and similar sedimentological data. U.S. Geol. Surv. Prof. Paper, 525-C, pp 164—167.

Schiener, A., 1950. Neuere Mineralfunde aus den Salzburger Alpen. Tscherm. Min. Petr. Mitt., 3. F., 2 (1951), pp. 143—146.

Schmidt, E. R., 1952. The structure and composition of the Merensky Reef and associated rocks on the Rustenburg Platinum mine. Trans. Geol. Soc. South Africa, 55, pp. 233—279.

Schmidt, W., 1925. Gefügestatistik. Tscherm. Min. Petr. Mitt., N.F., 38, pp. 392—423.

—, 1942. Zur Arbeit Otto Mellis: "Gefügediagramme in stereographischer Projektion". Zentralbl. Min. Geol. Paläont., A, pp. 184—187.

Schrauf, A., 1882. Beiträge zur Kenntniss des Associationskreises der Magnesiasilicate. Zeitschr. Kryst. Min., 6, pp. 321—388.

Schwander, H. & Wenk, E., 1965. Monazit als Kern pleochroitischer Höfe in Biotiten der Tessiner Gneisse. Schweiz. Min. Petr. Mitt., 45, pp. 797—806.

Selby, B., 1964. Girdle distributions on a sphere. Biometrika, 51, pp. 381—392.

Shand, S. J., 1939. On the staining of feldspathoids, and on zonal structure in nepheline. Am. Min., 24, pp. 508—513.

Siemes, H., 1967. Ein Rechenprogramm zur Auswertung von Röntgen-Texturgoniometer-Aufnahmen. N. Jb. Min. Mh., pp. 49—60.

Sobolev, N. V., 1962. Paragenetic types of garnet from ultrabasic rocks and eclogites. Dokl. Akad. Nauk USSR, Earth Sci. Sec., 143, pp. 105—107 (Engl. transl.).

Staub, R., 1951. Über die Beziehungen zwischen Alpen und Apennin und die Gestaltung der alpinen Leitlinien Europas. Eclogae Geol. Helv., 44, pp. 29—130.

Stauffer, M. R., 1966. An empirical-statistical study of three-dimensional fabric diagrams as used in structural analysis. Can. Jour. Earth Sci., 3, pp. 473—498.

Steiger, R. H., 1964. Dating of orogenic phases in the central Alps by K-Ar ages of hornblende. Jour. Geophys. Res., 69, pp. 5407—5421.

Streckeisen, A., Grauert, B. & Peters, T., 1966. Bericht über die Exkursion der Schweiz. Mineralogischen und Petrographischen Gesellschaft ins Silvretta-Kristallin und in den Totalp-Serpentin. Schweiz. Min. Petr. Mitt., 46, pp. 704—722.

Strüver, G., 1874. Sulla peridotite di Baldissero in Piemonte. Atti R. Accad. Sci. Torino, 9 (1873—74), pp. 763—772.

Taylor, W. H. & West, J., 1928. The crystal structure of the chondrodite series. Proc. R. Soc. London, A, 117, pp. 517—532.

—, 1929. The structure of norbergite. Zeitschr. Krist., 70, pp. 461—474.

Tex, E. den, 1965. Metamorphic lineages of orogenic plutonism. Geol. Mijnb., 44, pp. 105—132.

Tilley, C. E., 1947. The dunite-mylonites of St. Paul's Rocks (Atlantic). Am. Jour. Sci., 245, pp. 483—491.

—, 1951. The zoned contact-skarns of the Broadford area, Skye: a study of boron-fluorine metasomatism in dolomites. Min. Mag., 29, pp. 621—666.

Tocher, F. E., 1960. Hornblende orientation. Geol. Mag., 97, pp. 461—465.

Tröger, W. E., 1959. Optische Bestimmung der gesteinsbildenden Minerale. T. 1, Bestimmungstabellen. 3. Aufl., Stuttgart, Schweizerbart, 147 pp.

Turner, F. J. & Weiss, L. E., 1963. Structural analysis of metamorphic tectonites. New York, McGraw-Hill, 545 pp.

Vistelius, A. B., 1966. Structural diagrams. Oxford, Pergamon Press, 178 pp.

Vogel, D. E., 1967. Petrology of an eclogite- and pyrigarnite-bearing polymetamorphic rock complex at Cabo Ortegal, NW Spain. Leidse Geol. Med., 40, pp. 121—213.

Voskresenskaya, V. B., Koval'sky, V. V., Nikishov, K. N. & Parinova, Z. F., 1965. On the occurrence of titaniferous olivine in kimberlites of Siberia. Zap. Vsesoyuzn. Min. Obshch., 2nd Ser., 94, pp. 600—603 (in Russian).

Wang, H. S., 1939. Petrographische Untersuchungen im Gebiet der Zone von Bellinzona. Schweiz. Min. Petr. Mitt., 19, pp. 21—199.

Watson, G. S., 1965. Equatorial distributions on a sphere. Biometrika, 52, pp. 193—201.

—, 1966. The statistics of orientation data. Jour. Geol., 74, pp. 786—797.

Wenk, E., 1953. Prinzipielles zur geologisch-tektonischen Gliederung des Penninikums im zentralen Tessin. Eclogae Geol. Helv., 46, pp. 9—21.

—, 1955. Eine Strukturkarte der Tessineralpen. Schweiz. Min. Petr. Mitt., 35, pp. 311—319.

—, 1956. Die lepontinische Gneissregion und die jungen Granite der Valle della Mera. Eclogae Geol. Helv., 49, pp. 251—265.

—, 1963. Das reaktivierte Grundgebirge der Zentralalpen. Geol. Rundschau, 52, pp. 754—766.

Wenk, H. R. & Trommsdorff, V., 1965. Koordinatentransformation, Mittelbare Orientierung, Nachbarwinkelstatistik. Beitr. Min. Petr., 11, pp. 559—585.

Whitten, E. H. T., 1966. Structural geology of folded rocks. Chicago, Rand McNally & Co., 663 pp.

Winchell, A. N. & Winchell, H., 1951. Elements of optical mineralogy. Pt. 2, descriptions of minerals. 4th. ed., New York, Wiley, 551 pp.

Winchell, H., 1937. A new method of interpretation of petrofabric diagrams. Am. Min., 22, pp. 15—36.

Wyllie, P. J., ed., 1967. Ultramafic and related rocks. New York, Wiley, 464 pp.

Yoder, H. S., 1967. Spilites and serpentinites. Carnegie Inst. Yearb., 65, pp. 269—279.

Yoshino, G., 1961. Structural-petrological studies of peridotite and associated rocks of the Higashi-akaishi-yama District, Shikoku, Japan. Jour. Sci. Hiroshima University, C, 3, pp. 343—402.

# PLATES

## PLATE I

Megascopic structures of the peridotite: $S_L/S_1$-relations.

*a.* Weakly folded pyroxenite layers ($S_L$) in chlorite-peridotite; $S_1$ visible as elongation of chlorite knobs; $S_1$ "refracted" in pyroxenite layers (looking E).

*b.* $S_L$ and $S_1$ in garnet-peridotite (looking W). Locality of hand-specimen AR49.

*c.* $S_L$ and $S_1$ in chlorite-peridotite (looking W). Locality of hand-specimen AR17.

*d.* $S_L$ and $S_1$ in garnet-peridotite with partially kelyphitized garnet (looking W).

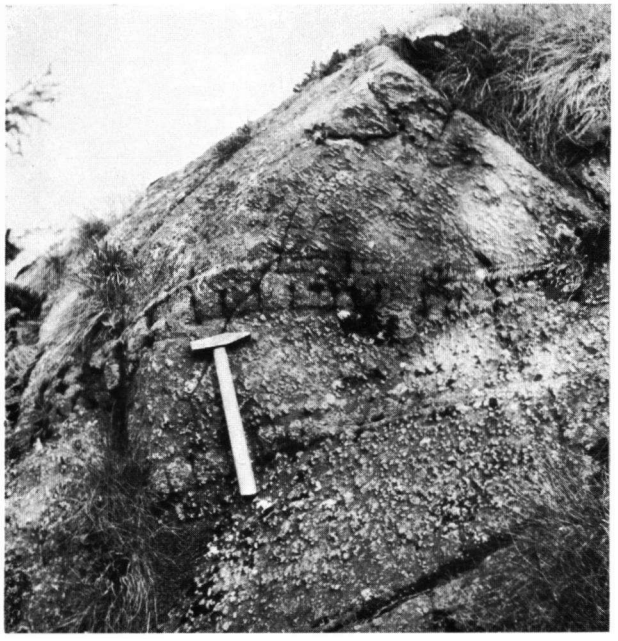

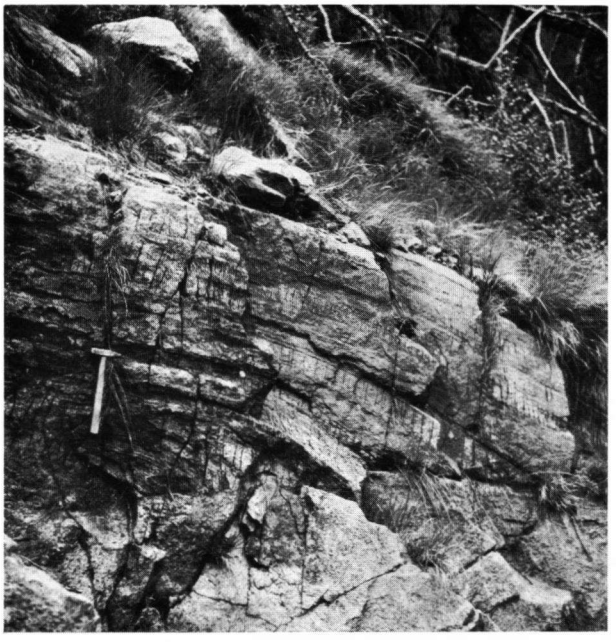

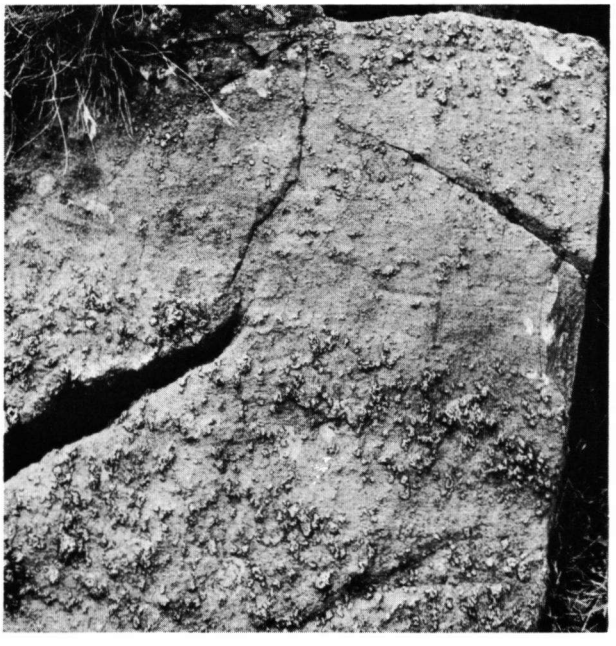

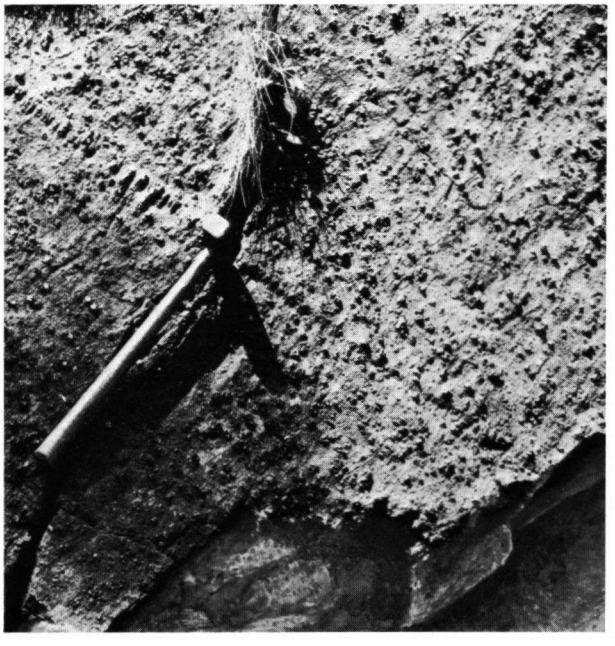

## PLATE II

Megascopic structures of the peridotite: folds.

*a.* $S_L/S_1$-fold of parasitic type. Chlorite knobs flattened parallel to the axial plane.

*b.* $S_L/S_1$-fold in chlorite-peridotite. Hornblendite layer (dark band) fractured in lower limb of fold.

*c.* $S_L/S_0$-folds in spinel-amphibole-peridotite. Locality of hand-specimen AR41.

*d.* $S_L/S_0$-folds in chlorite-peridotite, with development of axial-plane schistosity ($S_0$). Outlined folded layers are partially altered garnet-pyroxenites. Locality of hand-specimen AR52.

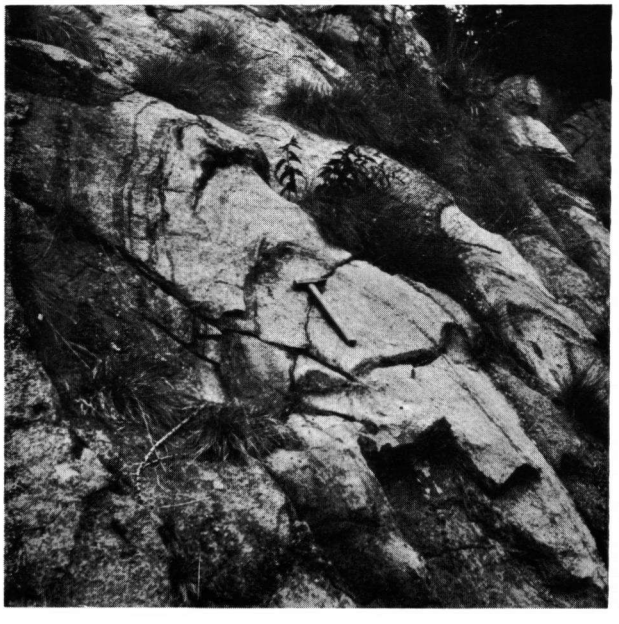

## PLATE III

*a.* Garnet (GA), slightly kelyphitized (dark rim), and dark brown spinel (SP) in garnet-spinel-peridotite of Alpe Seefeld, Ultimo Valley, Alto Adige, northern Italy. Elsewhere in the section similar spinel grains occur as inclusions in garnet.

*b.* Garnet with inclusions of dark brown spinel (dark areas) in garnet- and spinel-bearing serpentinite near Arosio, Ticino, Switzerland.

*c.* Garnet (GA) with kelyphite rim (spinel threads and amphibole). One amphibole crystal (AM) protrudes far into the olivine- and orthopyroxene-bearing matrix of the peridotite. Thin section AR26-Al.

*d.* Garnet (GA), almost completely altered into kelyphite (spinel-amphibole-symplektite). Symplektitization started not only externally but also around an olivine inclusion (OL), causing the development of an orthopyroxene rim replacing the enclosed olivine grain near its contact with the symplektite. Thin section GNl-Bl.

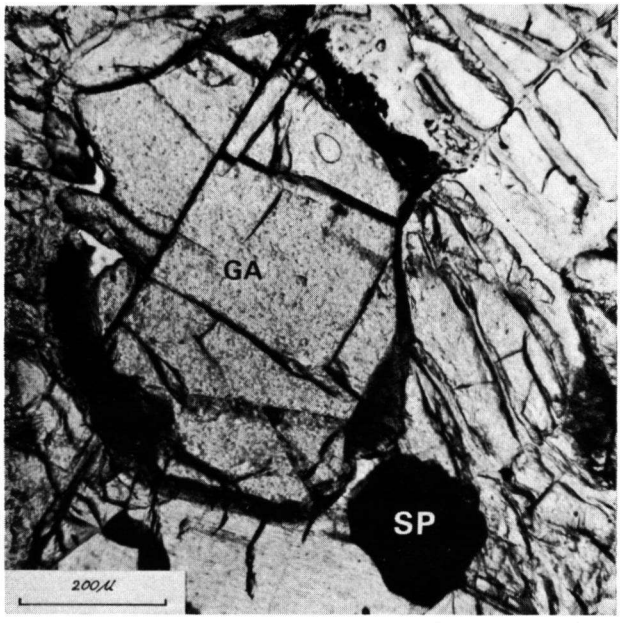
GA
SP
200 µ

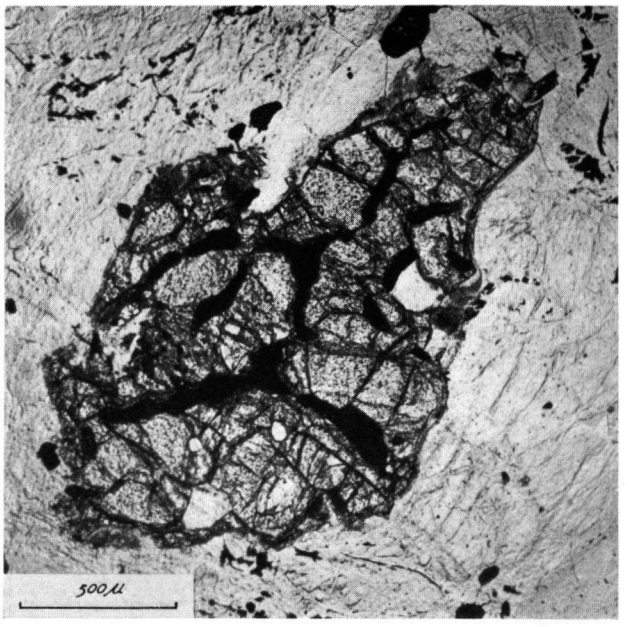
500 µ

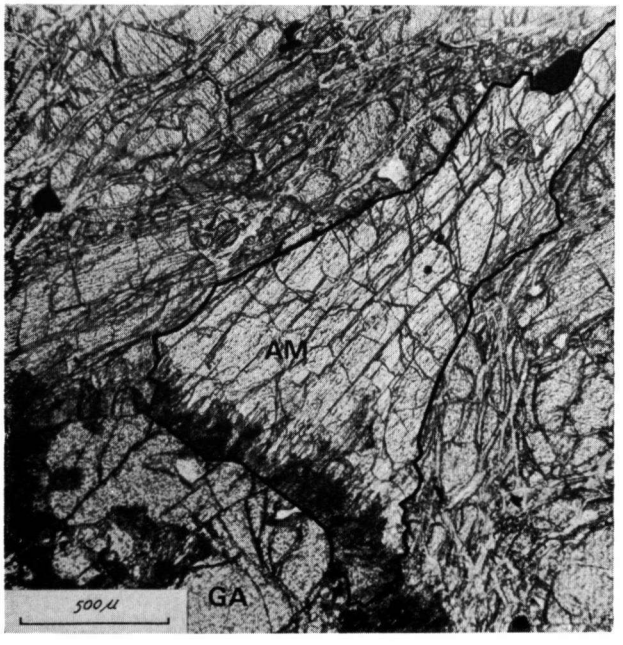
AM
GA
500 µ

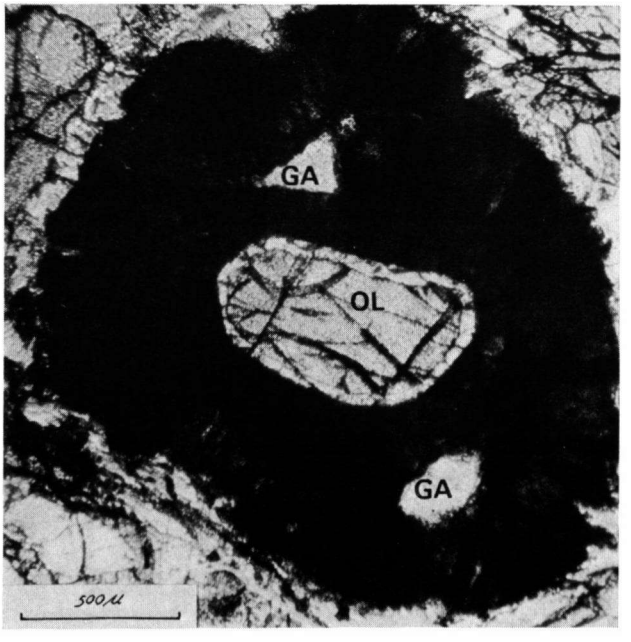
GA
OL
GA
500 µ

## PLATE IV

*a.* Zircon (ZR) in garnet-peridotite. Garnet (GA) is partially altered into spinel-amphibole symplektite (KEL). Thin section GO1-A.

*b.* Olivine (OL) with very irregular grain boundary, in garnet-peridotite. Orthopyroxene (OPX) shows lamellae parallel to {100} and kink bands subparallel to {001}. Crossed nicols. Thin section GN1-B1.

*c.* Orthopyroxene rim (OPX) between kelyphite (KEL) consisting of spinel-amphibole symplektite, and olivine (OL), in garnet-peridotite. Virtually no recrystallization of symplektite. Thin section AR47-A1.

*d.* Decomposition of clinopyroxene (CPX) into amphibole (AM), with separation of tiny spinel threads and grains, in garnet-peridotite. Thin section AR32-A2.

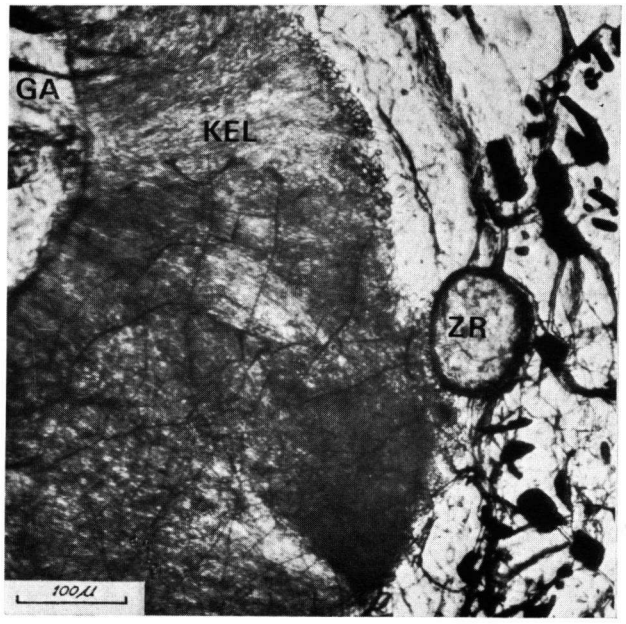
GA
KEL
ZR
100μ

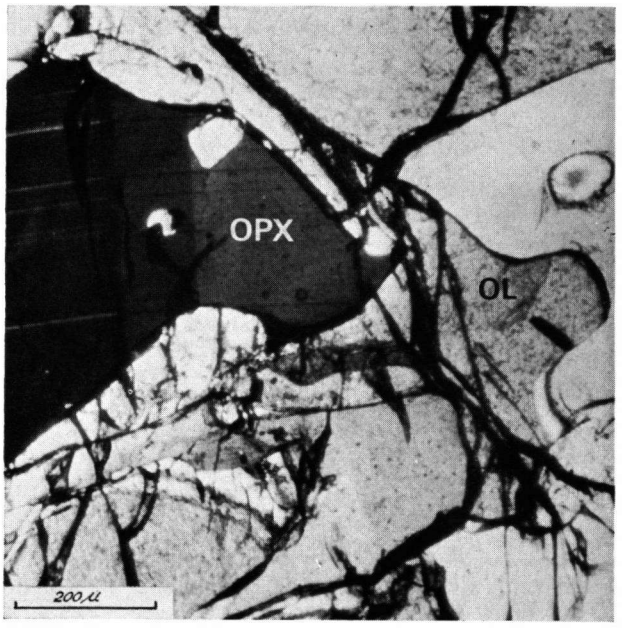
OPX
OL
200μ

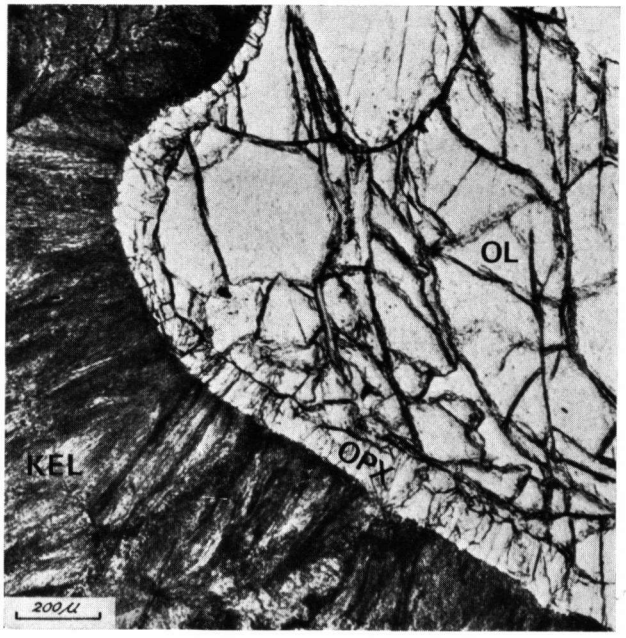
OL
KEL
OPX
200μ

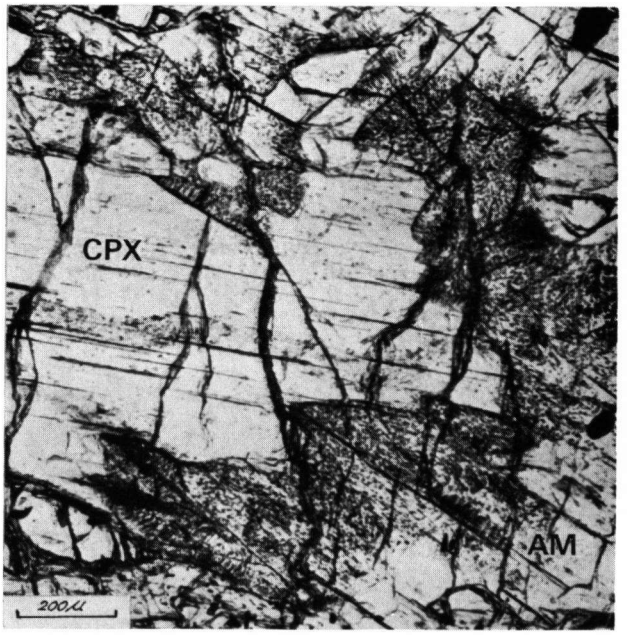
CPX
AM
200μ

## PLATE V

*a.* Spinel dendrites developing during the alteration of clinopyroxene (CPX) into amphibole (AM). Clinopyroxene crystal is the same as in Plate IV, d. Thin section AR32-A2.

*b.* X-ray scanning picture of the Cr-$K_\alpha$ radiation of the area outlined in Plate V, a, determined with the electron microprobe.

*c.* Chlorite with some phlogopite (PHL) developing within radially textured spinel-amphibole symplektite. Spinel-amphibole- to chlorite-peridotite. Thin section AR19.

*d.* Part of a chlorite nodule in chlorite-peridotite. Some chlorite crystals contain carbonate lamellae parallel to their basal cleavage. A relict texture suggesting the former presence of spinel-amphibole symplektite is shown by trails of tiny spinel grains, brown in thin section and perhaps somewhat altered into limonite. Thin section AR17-A2.

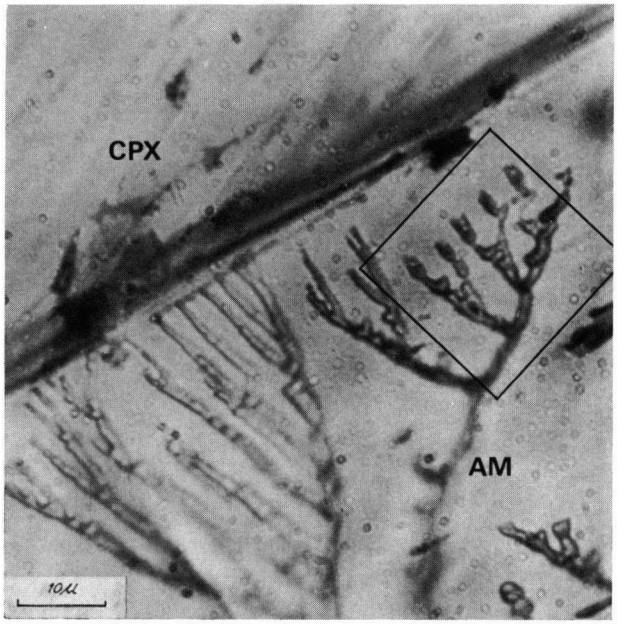
CPX
AM
10µ

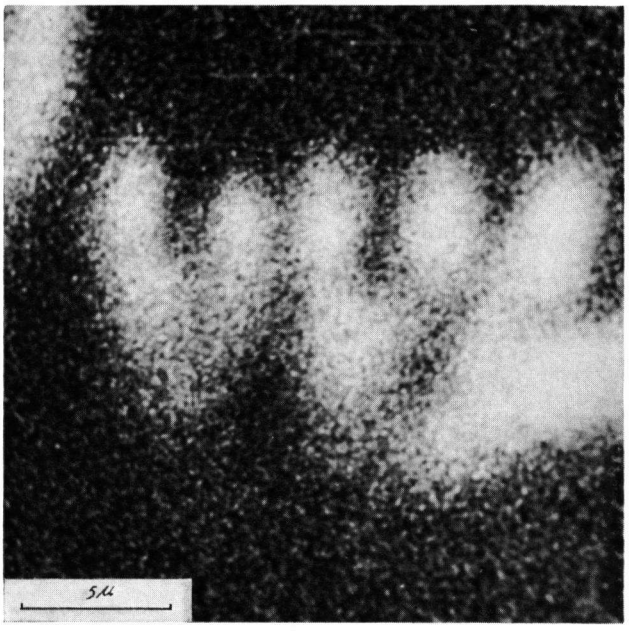
5µ

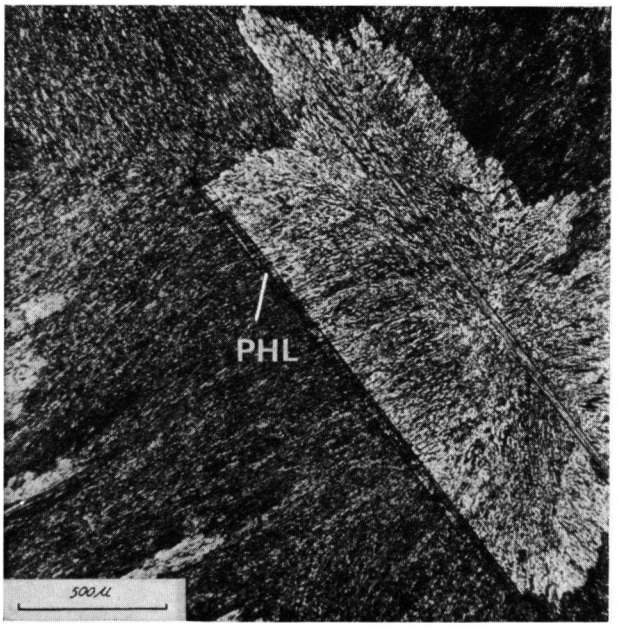
PHL
500µ

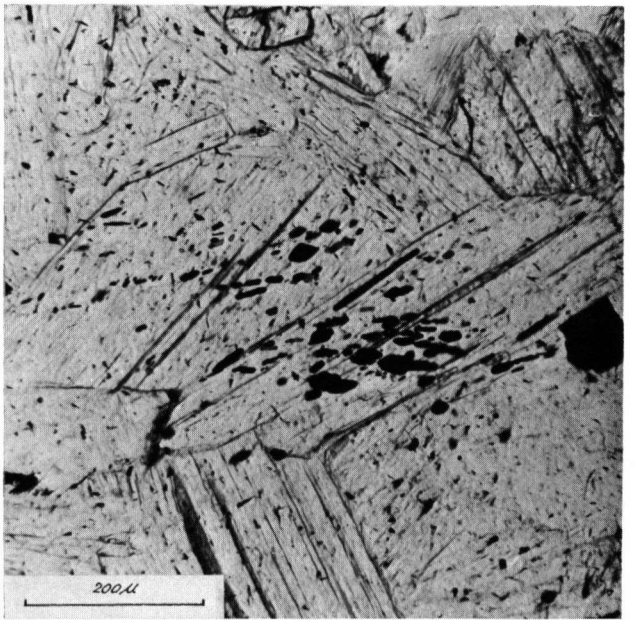
200µ

## PLATE VI

*a.* Isolated chlorite crystal in chlorite-peridotite. Crossed nicols. Thin section AR18-A1.

*b.* Garnet containing inclusion of ilmenohematite intergrown with green spinel (SP), in garnet-rock. Around the inclusion, garnet is altered into green spinel threads lying within rather large amphibole crystals. Thin section AR21.

*c.* Garnet-peridotite with mortar structure and mylonitic band. Crossed nicols. Thin section AR49-A1.

*d.* Chlorite-peridotite-mylonite with olivine porphyroclasts showing deformation lamellae subparallel to {100}. Crossed nicols. Thin section AR14-A1.

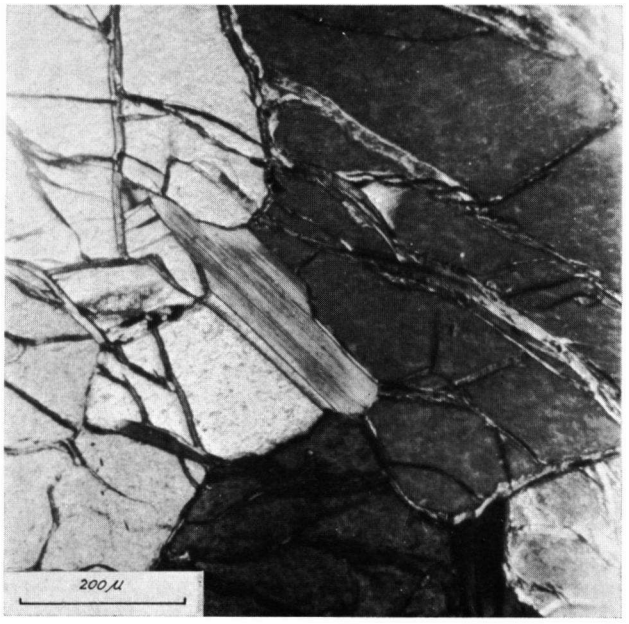
200 μ

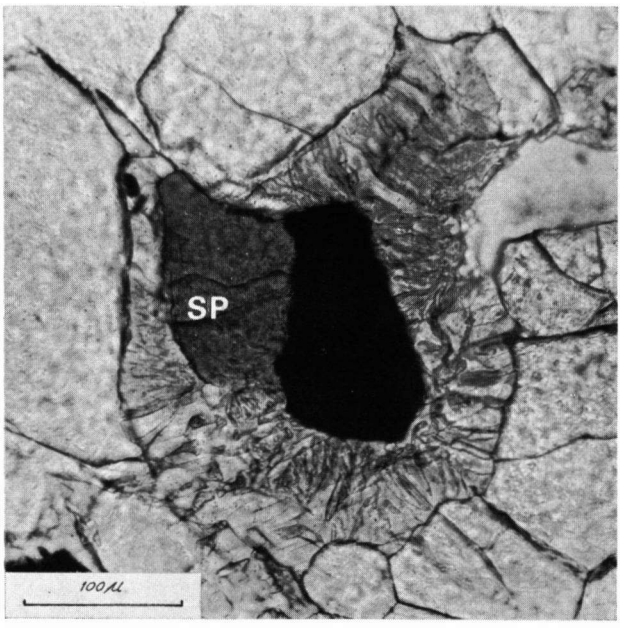
SP
100 μ

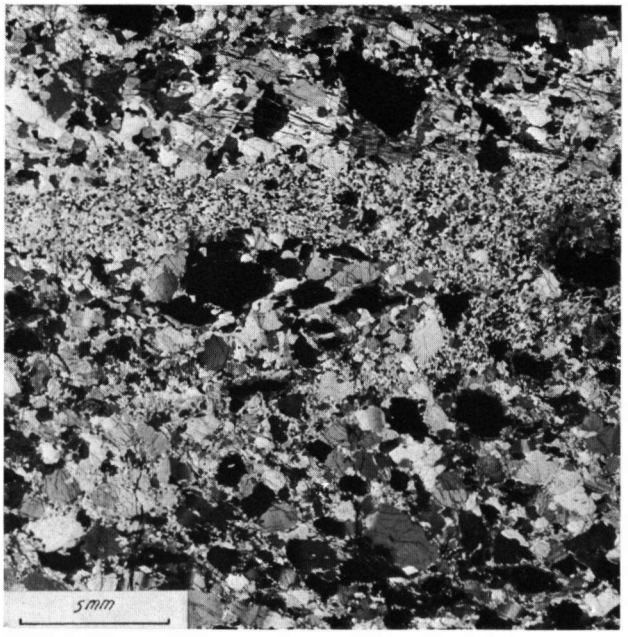
5 mm

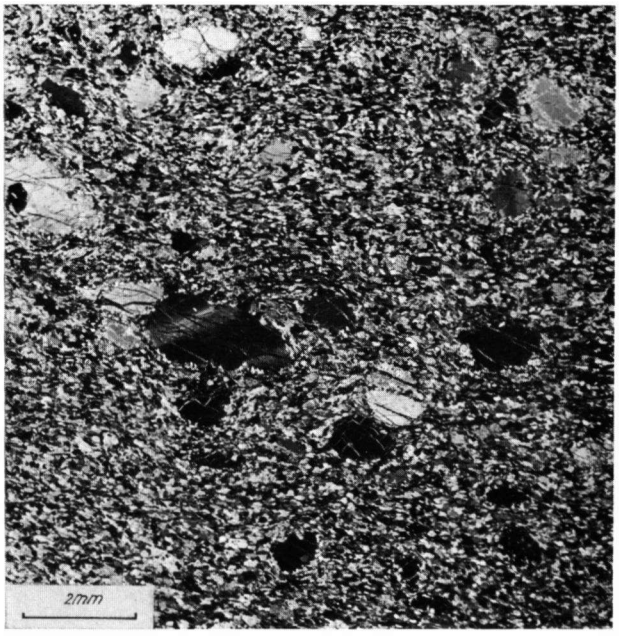
2 mm

# Geological map of the area around Alpe Arami (Gorduno Valley near Bellinzona, Ticino, Switzerland) by J.R. Möckel

July 1966

scale 1:5000

0 0,5 km

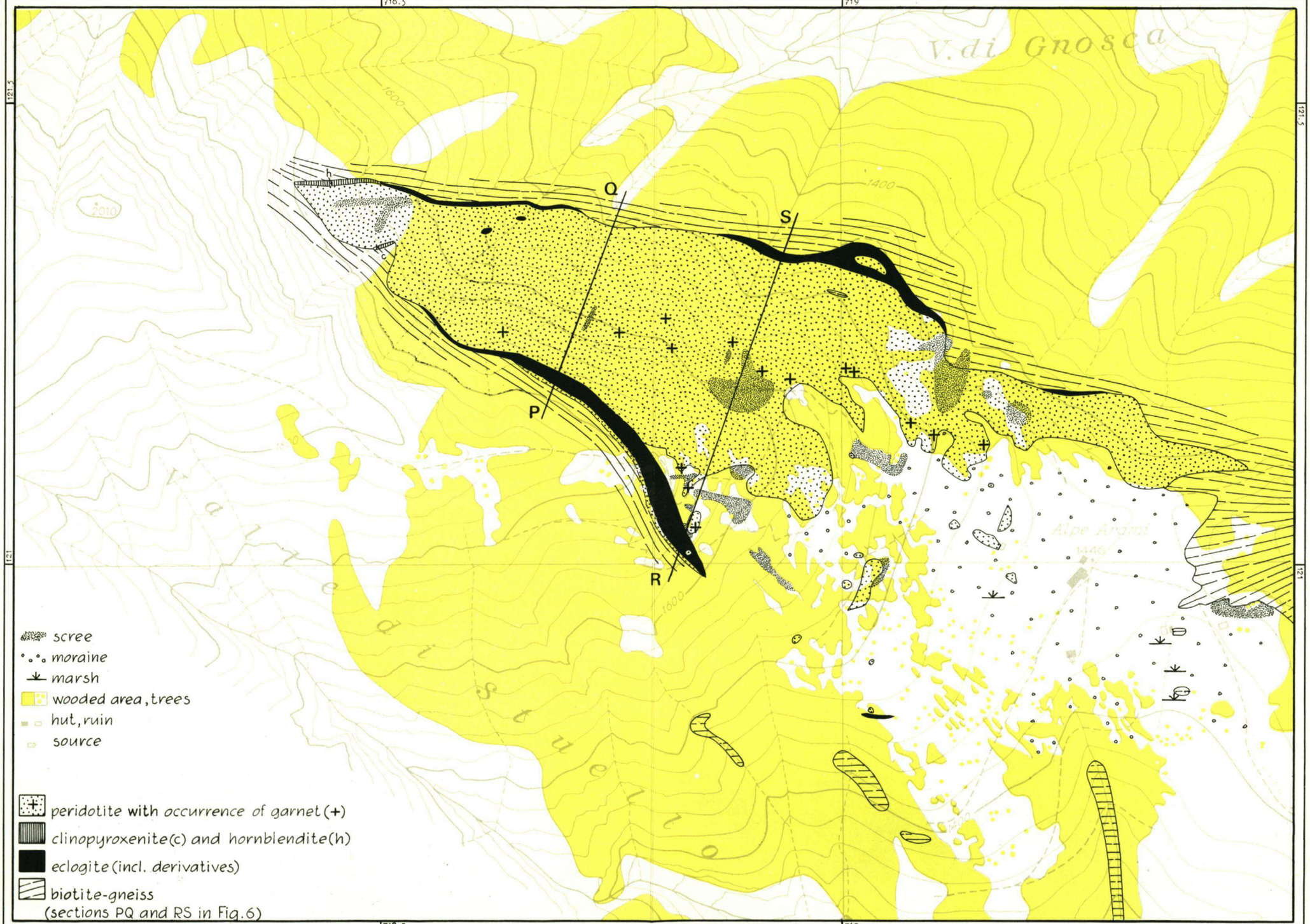

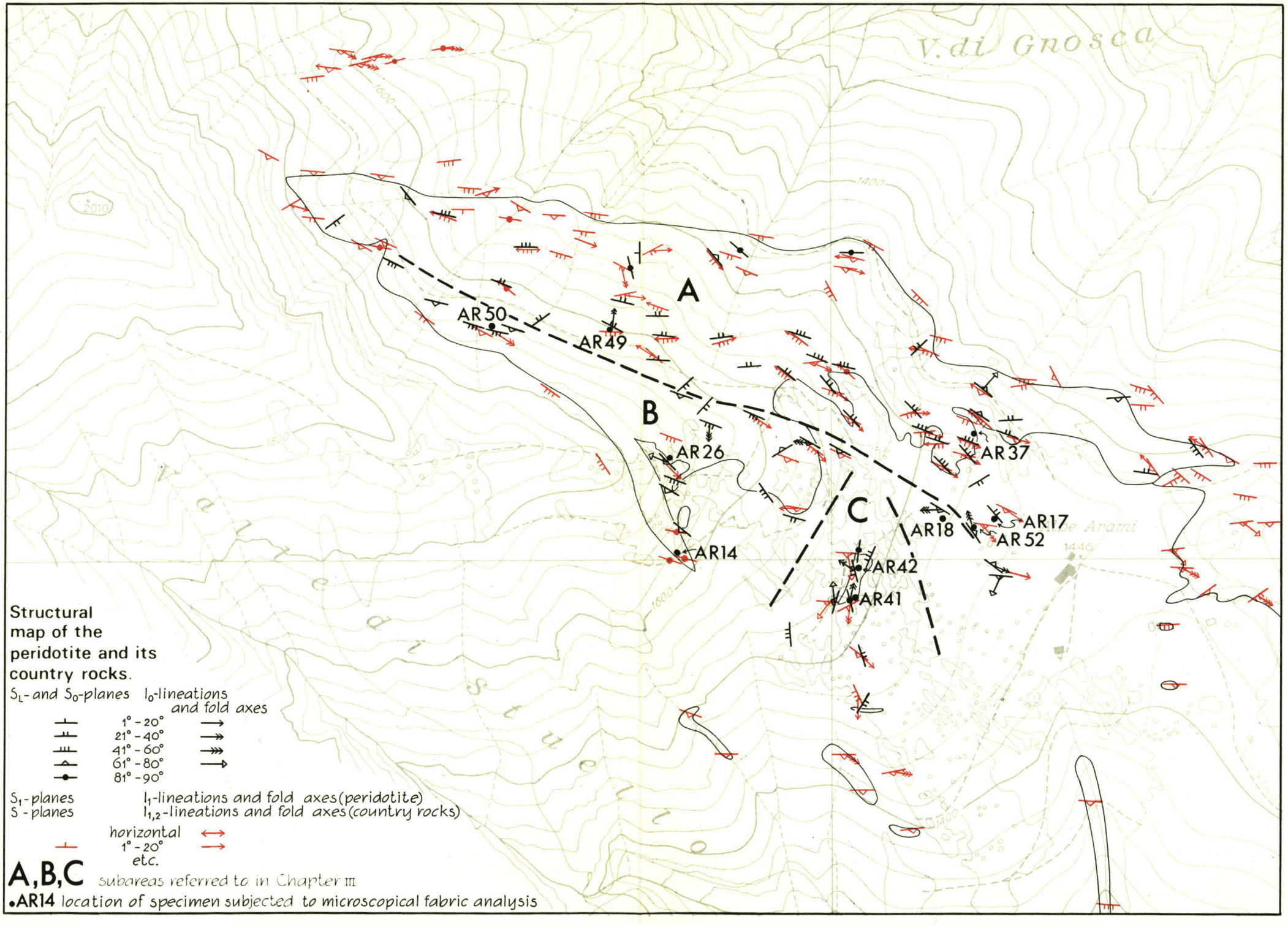
V. di Gnosca
A
B
C
AR50
AR49
AR26
AR14
AR37
AR18
AR17
AR52
AR42
AR41
Structural map of the peridotite and its country rocks.
$S_L$- and $S_0$-planes
$l_0$-lineations and fold axes
1° - 20°
21° - 40°
41° - 60°
61° - 80°
81° - 90°
$S_1$-planes
S -planes
$l_1$-lineations and fold axes (peridotite)
$l_{1,2}$-lineations and fold axes (country rocks)
horizontal
1° - 20°
etc.
A,B,C subareas referred to in Chapter III
•AR14 location of specimen subjected to microscopical fabric analysis